CAROTID PLAQUE VULNERABILITY ASSESSMENT BY MICROSCOPIC MORPHOLOGY ANALYSIS, ULTRASOUND AND 3D MODEL RECONSTRUCTION

A Thesis submitted for the degree of Doctor of Philosophy by

Ahsan Choudhury

Brunel Institute for Bioengineering
Brunel University

January 2012

Author's Declaration

I hereby declare that the work in this thesis has been independently carried out by me. However, inputs were made by other members in the group on certain engineering parts of the project. In specific: the MATLAB programmes used for statistics and analysis was developed by Dr. Hao Gao; the Finite Element based image registration code was developed by Mr. Michael Luppi; and the ex vivo ultrasound scan of CEA specimens was performed jointly with Mr. Warren Hopkins, a superintendent sonographer in Hillingdon Hospital.

I authorize the Brunel University to lend this thesis to other institutions or individuals for the purpose of scholarly research.

Signature

I further authorise the Brunel University to reproduce this thesis by photocopying or by other means, in total or in part, at the request of other institutions or individuals for the purpose of scholarly research.

Signature

Abstract

Research suggests that plaque morphology plays a crucial role in determining plaque vulnerability. However the relationship between plaque morphology and rupture is still not clearly understood due to the limited information of plaque morphology. The aim of this study is to improve our understanding of the relationship between plaque morphology and rupture, and to use this to predict the risk of plaque rupture from the morphology at the molecular level. This can enable the identification of culprit lesions in clinical situations for assessing plaque rupture risk.

Histological assessments were carried out on 18 carotid plaque specimens. The 3-D collagen, lipid and macrophage distributions along the entire length of the plaque were analysed in both ruptured and non-ruptured symptomatic plaques. In addition, plaque morphology on the rupture sites were examined and compared with the surrounding regions. It was found that ruptured plaques had thinner fibrous caps and larger lipid cores compared to non-ruptured plaques. Also, ruptured plaques had lower collagen content compared to non-ruptured plaques, and higher collagen contents upstream compared to downstream region from the plaque throat. At the rupture site there was lower collagen content, and a larger lipid core thickness behind a thin fibrous cap compared with the mean for the longitudinally adjacent and circumferential regions. Macrophage cells were located nearer to the boundary of the luminal wall in ruptured plaques. For both groups, the area occupied by macrophages is greater at the upstream shoulder of the plaque. There is a positive correlation between macrophage area and lipid core area, a negative correlation between macrophage area and collagen content, and between lipid core size and collagen content for both plaque groups.

3D reconstruction of ex-vivo specimens of carotid plaques were carried out by a combined analysis of US imaging and histology. To reconstruct accurate 3D plaque morphology, the non-linear tissue distortion in histological images caused by specimen preparation was corrected by a finite element (FE) based deformable registration procedure. This study shows that it is possible to generate a 3D patient specific plaque model using this method. In addition, the study also quantitatively assesses the tissue distortion caused by histological procedures. It shows that at least 30% tissue shrinkage is expected for plaque tissues.

The histology analysis result was also used to evaluate ultrasound (US) tissue characterization accuracy. An ex-vivo 2D ultrasound scan set-up was used to obtain serial transverse images through an atherosclerotic plaque. The different plaque component region obtained from ultrasound images was compared with the associated histology result and photograph of the sections. Plaque tissue characterisation using ex-vivo US can be performed qualitatively, whereas lipid core assessment from ultrasound scan can be semi-quantitative. This finding combined with the negative correlation between lipid core size and collagen content, suggests the ability of US to indirectly quantify plaque collagen content. This study may serve as a platform for future studies on improving ultrasound tissue characterization, and may also potentially be used in risk assessment of plaque rupture.

Contributions and Outcomes

1. The systematic and detailed assessment of plaque morphology reveals the morphological difference between the ruptured and non-ruptured plaques at different longitudinal locations, and the morphological difference around rupture sites. The main results are:
    - Ruptured plaques have a thinner mean fibrous cap thickness in comparison to non-ruptured plaques
    - Ruptured plaques have a larger mean lipid core size than non-ruptured plaques
    - The collagen content in the fibrous cap of ruptured plaques is comparatively lower than non-ruptured plaques.
    - Plaque morphology at the actual rupture site is significantly different compared to the longitudinally adjacent and circumferential regions

2. 3D distribution of macrophage cells in ruptured and non-ruptured plaques:
    - Ruptured plaques have a higher mean macrophage content overall in comparison to non-ruptured plaques.
    - In ruptured plaques macrophages are localised at a closer proximity to the luminal wall than in non-ruptured plaques where they are found closer to the lipid core
    - The upstream region of maximum stenosis has higher macrophage content than in the downstream region for both ruptured and non-ruptured plaques.

3. Development of a technique for high resolution 3D reconstruction of arterial plaque specimens for stress analysis, by combining histological analysis and ultrasound imaging.

4. Demonstrated that it is feasible to semi-quantify the lipid core of plaques using ex-vivo ultrasound.

Major novelties of the study

1. This was the first study to collect results from histological sections throughout the entire plaque length with small section intervals (<250micron);
2. The study of plaque morphology differences between (a) the ruptured and non-ruptured; (b) different longitudinal locations; (c) rupture sites and surrounding region.
3. Most of the techniques developed in plaque 3D reconstruction were novel.
4. Quantitative assessments of histological processing induced, non-uniform, tissue distortion for different plaque components.
5. Comparison of plaque ultrasound images with tissue distortion corrected histological analysis and section photograph.

Acknowledgements

I would like to express my appreciation to all the people who have helped me during the course of my research. Firstly and most importantly, I owe a debt of gratitude to my supervisor, Dr. Quan Long for his direction, ideas, encouragement, and support throughout my PhD. I have learnt so much from him and his guidance has helped me to cultivate my skills as a researcher. I appreciate all the time and effort he has given to me to enable this work to come to the stage that it has. He has helped me to develop my mind to think critically, as well as my presentation and writing skills. I would also like to give a sincere gratitude to Dr. Ian Kill for his invaluable input. He has always been there for me when I needed help or advice. As well as having an incredible sharp scientific mind, he has an overwhelming level of humour. In addition I would like to thank the consultant vascular surgeon, Dr. Saroj Das of Hillingdon Hospital, for providing the carotid arteries used for the research as well as for all the advice and support he has given me.

Working with my fellow students has made my life in the department much more enjoyable. I would like to thank everyone for their help and friendship (Francesco Clavica, Karnal Patel, Samantha Fernando, Yi Li, and Xiao Yan). However I would like to give a special thank you to Hao Gao who has given me invaluable support for the MATLAB programming and support throughout my research; and to Masoud for his time and effort in helping me to prepare this thesis.

Finally I would also like to give a special thank you to my family who have supported me in everyway possible to complete this research successfully. I am blessed to have wonderful parents whose love and encouragement has guided me throughout my life.

Table of Contents

List of Figures

CHAPTER 4

CHAPTER 5

CHAPTER 6

List of Tables

CHAPTER 6

CHAPTER 7

Abbreviations

2D	2-Dimensional
3D	3-Dimensional
AHA	American Heart Association
APES	3-Aminopropyltriethoxysilane
CAD	Computational Aid Design
CAD	Coronary Artery Disease
CCA	Common Carotid Artery
CEA	Carotid Endarterectomy
CFD	Computational Fluid Dynamics
CT	Computed Tomography
DAB	Diaminobenzidine
EC	Endothelial Cells
ECA	External Carotid Artery
ECM	Extracellular Matrix
ER	Endoplasmic Reticulum
FC	Fibrous Cap
FCT	Fibrous Cap Thickness
FEA	Finite Element Analysis
FEM	Finite Element Method
FGF-2	Fibroblast Growth Factor-2
FSI	Fluid Simulation Interaction
H & E	Hematoxylin & Eosin
HCL	Hydrochloric Acid
HDL	High Density Lipoprotein
HRP	Horseradish Peroxidase
ICA	Internal Carotid Artery
ICAM-1	Intracellular Adhesion Molecule-1
ICH	Immunohistochemistry
IgG	Immunoglobin
IL-1	Interleukin-1
IMS	Industrial Methylated Solution

IMT	Intimal Media Thickness
IVUS	Intra-Vascular Ultrasound
LC	Lipid Core
LDL	Low-Density Lipoprotein
MCP-1	Monocyte Chemotactic Protein-1
M-CSF	Macrophage-Colony Stimulating Factor
mL	Millilitre
MMP	Matrix-Metalloproteinase
MRI	Magnetic Resonance Imaging
MT-MMP	Membrane Type Matrix Metalloproteinase's
NaCl	Sodium Chloride
NCFA	Necrotic Core Fibroatheroma
NO	Nitric Oxide
OCT	Optical Coherence Tomography
OCT	Optical Cutting Temperature
OD	Optical Density
PDGF	Platelet-Derived Growth Factor
PSOCT	Polarization Sensitive Optical Coherence Tomography
PSR	Picrosirius Red
RBC	Red Blood Cell
RBC	Red Blood Cells
SMC	Smooth Muscle Cells
SPIO	Super Paramagnetic Iron Oxide
TBS	Tris Buffered Solution
TF	Tissue Factors
TGF-β	Transforming Growth Factor-Beta
TNF-alpha	Tumour Necrosis Factor-Alpha
TNT	Trinitrotoluene
TOF	Time-of-Flight
tPA	Tissue Plasminogen Activator
uPA	Urokinase Plasminogen Activator
US	Ultrasound
VCAM-1	Vascular Cell Adhesion Molecules-1
VSMC	Vascular Smooth Muscle Cells

Chapter 1

Introduction

1.1 Atherosclerosis

1.1.1 Structure of Healthy Arteries

Arteries are composed of three distinct layers, known as the intima, media, and adventitia. Healthy arteries have a very thin intima layer, which is comprised of an endothelial cell layer and an internal elastic lamina. The internal elastic lamina forms a boundary between the intima and media. In the medial layer there can be found smooth muscle cells and collagen fibres which are found in bundles. The collagen found here is mainly composed of the type VI form, and the region is also heavily interspersed with elastin fibres. A basement membrane – external elastic lamina, forms a distinct boundary between the adventitia and the media. This layer is primarily composed of type III collagen fibres, and ground substances such as fibronectin. Other components found in the adventitia include inflammatory cells, fibroblasts, and nerve bundles. It also contains the vasa vasorum which is a network of blood vessels that supply the artery with oxygen and nutrients.

1.1.2 Atherosclerosis

Atherosclerosis is the name given to a disease that affects arterial blood vessels. "Athera" means porridge in Greek, and this name has been adapted because plaque has a foamy appearance when the diseased artery is placed under a microscope. The “sclerosis” part denotes the hardening. Atherosclerosis is generally referred to as a hardening or furring of the blood vessels, however this is an oversimplification. Atheromas (atheromata or atheromatous plaques) are formed in the vessel wall. In the

later stages it can either reduce or totally restrict the blood flow in the lumen. This process is known as stenosis, and can cause further problems due to rupturing or damage to tissue in the downstream regions. The onset of atherosclerosis can sometimes start in the later years of childhood in certain individuals. It is generally found in most major arteries; however it remains silenced and unnoticed when there is no ischemia symptoms for the patient. It only becomes symptomatic when it starts to interfere with circulatory blood supplies to the heart or brain etc. It is considered to be the major cause of strokes, heart attacks, and various heart diseases. Data obtained from the US (2004) has shown that out of everyone who has atherosclerosis, 65% of men and 47% of women only first realise that they have the disease when they have a heart attack.

1.1.3 Risk Factors

The disease is commonly considered as being a systemic disease that is initiated by certain risk factors. These risk factors can be classified as environmental or genetic. The environmental factors include: infectious agents; lack of exercise; cigarette smoking; and low antioxidant levels etc. The genetic risk factors are more related to certain disorders such as: obesity; diabetes; systemic inflammation; familial history; hypertension; reduced concentration of high-density lipoproteins (HDL); increased concentration of low-density lipoprotein (LDL); sex of the individual (male/female), above the age of 60; depression, increased levels of haemostatic factors and other behavioural traits.

1.2 Atherosclerosis Development Process

In brief, the first steps of atherogenesis are the formation of fatty streaks which are small sub-endothelial deposits of lipids (figure 1.1(a)). The first response to these

deposits is the inflammatory process. Monocytes enter the artery wall from the bloodstream. They then differentiate into macrophages, and then slowly turn into large foam cells. The lesion at this stage appears as a fatty streak (figure 1.1(b)).

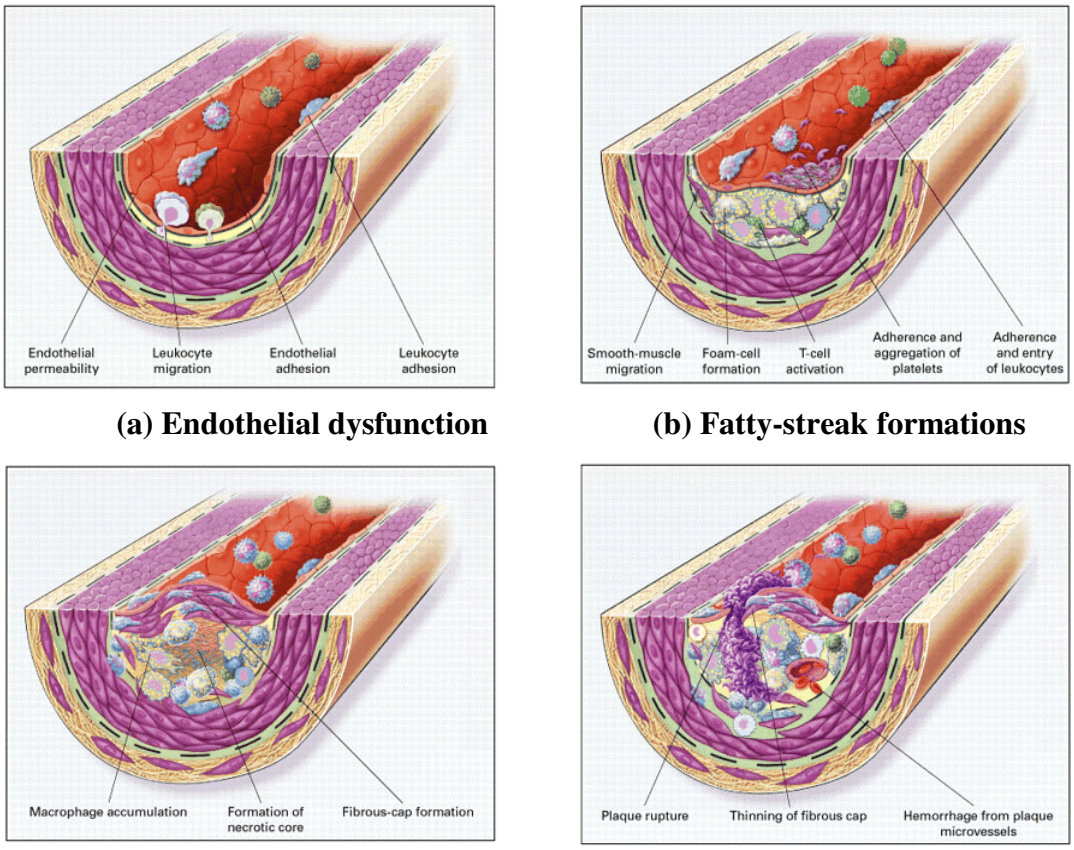

(a) Endothelial dysfunction **(b) Fatty-streak formations**

(c) Advanced, complicated lesion **(d) Unstable fibrous plaques**

Figure 1.1: Major phases of atherogenesis lesion development (Ross R et al 1999)

The composition of fatty streaks is initially lipid-laden monocytes and macrophages (foam cells), together with T-lymphocytes within the arterial wall as in figure 1.1(b). At a later stage, the fatty streaks are joined by various numbers of migratory smooth muscle cells. This is followed by T-cell activation, which is mediated by tumor necrosis factor α (TNF-a), interleukin-2 (IL-2), and granulocyte–macrophage colony-stimulating factor. The third step is foam cell formation, which is regulated by oxidized low-density lipoprotein, macrophage colony-stimulating factor, tumor necrosis factorα, and interleukin-1 (IL-1). The final step involves platelet adherence

and aggregation. This occurs as a result of stimulation from integrins, P-selectin, fibrin, thromboxane A2, and tissue factor, and is accountable for leukocyte adherence.

The progression of fatty streaks allows lesions to develop from an intermediate stage to an advanced level, and is associated with fibrous cap formation near to the walls of the lesion as demonstrated in figure 1.1(c). This occurs in response to an injury and represents a type of healing or fibrous response. The fibrous cap covers a mixture of leukocytes, lipids, and debris, which can cause the formation of a necrotic core. The continuous adhesion and entry by leukocytes causes lesions to expand at their shoulders. Macrophage colony-stimulating factor, monocyte chemotactic protein-1 (MCP-1), and oxidized low-density lipoprotein are principle factors associated with macrophage accumulation. The result of apoptosis and necrosis, increased proteolytic activity, and lipid accumulation is the necrotic core. A number of contributing factors are associated with the formation of the fibrous cap. These include increased activity of platelet-derived growth factor, transforming growth factor ß, interleukin-1, tumor necrosis factor$_\alpha$, and osteopontin.

The rupturing or ulceration of fibrous caps usually occurs in thinning regions that cover advancing lesions. The fibrous cap starts to thin because there is a continuous influx and activation of macrophages (figure 1.1(d)). The macrophages at these sites release matrix-metalloproteinase's (MMP's) and other proteolytic enzymes that act to degrade the matrix. This can then ultimately lead to incidences of haemorrhages from the vasa vasorum or from the lumen, and can cause the formation of a thrombus and occlusion of the artery.

1.3 Vulnerable Plaque

In the past clinicians and researchers have thought that the build up of fatty plaques in arteries that resulted in blockage of vessels to the heart or brain was the main cause of heart attacks and strokes. Over a period of time, the arteries would narrow considerably due to the build-up of plaque to an extent that they become completely blocked or significantly narrowed, blood clot or thrombus. The consequence of this is that the heart is deprived of blood, which then eventually causes a heart attack. However, this is responsible for only 3 out of 10 heart attacks.

Recent research has revealed that significant numbers of people who have heart attacks do not have plaques narrowing the arteries. It is more the case that rupture prone plaques are found located within the artery wall. This may not always result in it bulging out and blocking blood flow through the artery (Kobayashi et al (2009)). It is for this reason that researchers are looking into how inflammation affects arteries, and if it could lead onto a heart attack. Studies have suggested that inflammation can lead towards the development of "soft" or vulnerable plaques (figure 1.2). They also revealed that vulnerable plaques do not contain just debris that block an artery, but also contains numerous cell types which can contribute to the blood clotting process.

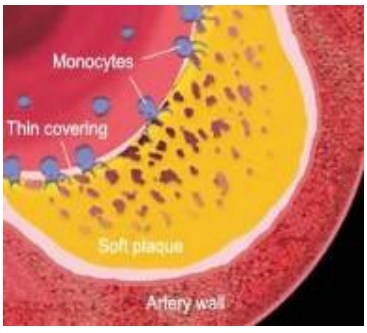

Figure 1.2 Cross-section of the arterial wall highlighting the monocytes, thin covering, and the soft plaque of the vessel

http://health.allrefer.com/health/atherosclerosis-pictures-images.html

Chapter 1 Introduction

The atheromatous plaque has been well described in terms of its progression, and the clinical characterization of the atherosclerotic lesion has also been well documented. However, the vulnerable plaque in terms of its concepts is still a novel area. "Vulnerable plaque" is a term that has been derived from a sub-group that are known as stenotic plaques. They are prone to both rupture and erosion, sometimes causing acute coronary syndromes and sudden cardiac death. Rupture prone plaques have been shown in post-mortem evaluation to have specific characteristics such as thin fibrous caps (<65µm for coronary arteries - Tavora et al 2010), large lipid rich pools, and increased macrophage activity. The cellular mechanisms involved result in the reduction of collagen synthesis, local over expression of collagenases, and apoptosis of smooth muscle cells. The plaque shoulder region has most of these changes. Pro-coagulant factors, especially tissue factors are released when there is a disruption in the fibrous cap integrity. This results in a nidus for thrombus formation, as well as the potential for acute coronary incidents (Prediman K et al 2003). Throughout the vasculature, vulnerable plaques are continuously being ruptured; however, only a minority of plaques proceed to clinical syndromes caused by occlusive thrombus. Research is being carried out to establish the factors involved in determining the rupture induction.

Based on studies of culprit plaques, a criterion set has been developed for defining vulnerable plaques. These are known as the "major criteria" and describe five different plaque types. A higher risk of plaque complications may be implicated if one or more of these factors are present.

- Active inflammation (monocyte/macrophage infiltration)
- Thin cap with large lipid core
- Endothelial denudation with superficial platelet aggregation

- Fissured plaque
- Stenosis >90%

Figure 1.3 shows an example of a cross-section of a plaque consisting of a thin fibrous cap and a large lipid rich core. The histomorphologic features of ruptured plaques are very different to that of intact plaques. For example, ruptured plaques tend to have a relatively larger volume compared to intact plaques. They also have outward (positive) remodelling, a large lipid core which usually consists of more than 40% of the plaque volume, and is composed of free cholesterol crystals, cholesterol esters, and also oxidized lipids impregnated with tissue factors (Prediman K et al 2003). Other histomorphologic features of ruptured plaques include the infiltration of inflammatory cells into the fibrous cap and adventitia (mostly monocytic-macrophages, some activated T cells and mast calls); thin caps depleted of smooth muscle cells and collagen, and also increased neovascularity. The presence of these features in a plaque prior to rupture shows it to be vulnerable to rupturing. The concept of plaque vulnerability has been derived on the basis of this hypothesis (Prediman K et al 2003).

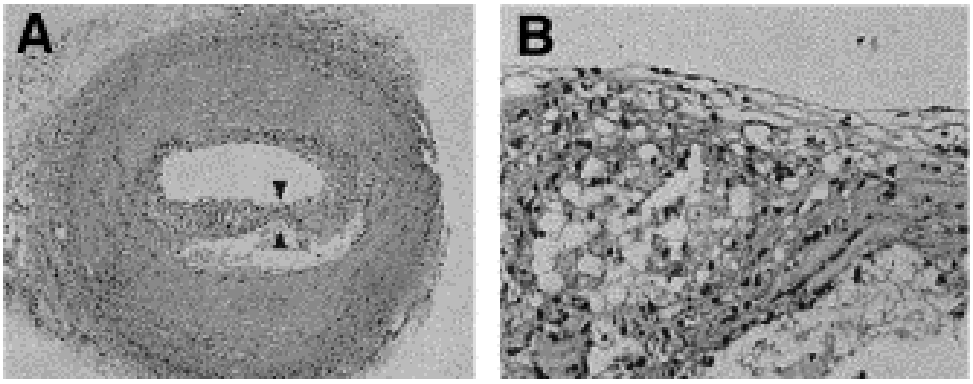

Figure 1.3 (A) Cross-section of an artery demonstrating a thin fibrous cap (indicated by the arrowheads) overlying a crescentic lipid rich core; (B) higher magnification of the margin of the cap and shows the highly dense infiltration of foamy macrophages (Shah et al 2003)

1.4 Clinical Management of a Patient with Arterial Plaque

Due to the difficulty and economical costs of diagnosis of arterial plaque, currently there is no national screening system available to provide an early warning of atherosclerosis development. Most patients who are eventually diagnosed as having arterial plaque often displayed symptoms such as hypertension or neurological symptoms. If the patients' early symptoms are minor and noticed by patients or their medical practitioner, a suitable treatment may prevent a major rupture of the plaque and the consequent stroke or heart attack from occurring. Depending on the severity level of the plaque, drug treatment or eventually surgical treatment such as carotid endarterectomy (CEA) may be introduced to prevent major heart attacks or strokes. As will be described in the following chapters, the assessment of plaque vulnerability and risk of potential rupture is very difficult non-invasively. The inclusion criteria for CEA are still dependent on the degree of stenosis (for asymptomatic patients) and symptoms (for symptomatic patients).

The benefits of CEA in the prevention of a rupture are obviously absolute, but in asymptomatic patients it is not possible to predict. A recent study by Charurvedi et al showed that the NNT (number needed to operate) =22 for 50% to 60% stenosis, ARR of 4.6% over 5 years; while NNT=6.3 for stenosis > 70%, ARR of 16% over 5 years (Chaturvedi et al 2008)). This has significant impact on man power and economical resources. A reliable rupture risk assessment could define CEA efficiency for preventing rupture, and would also reduce unnecessary procedures for low risk patients. This approach could reduce unnecessary surgical risks and reduce the financial burden to the NHS.

1.5 Thesis Structure

The organisation of the thesis can be found as follows:-

- **Chapter 1. Introduction:** Introduces the background of the healthy and diseased arteries, aims, contributions, research outcomes, and the importance of the research
- **Chapter 2. Literature Review:** Provides a literature review which covers the current hypothesis on plaque rupture mechanisms, the status of research in all related areas involving plaque rupture risk assessment, and details of the current knowledge on plaque components. It will also include the techniques required for plaque structure and vulnerability assessments.
- **Chapter 3. Methodology Development:** Provides detailed descriptions of the methods that were applied to the plaque morphology analysis, the image registration procedure, and the plaque tissue characterisation using ultrasound, which are then used in the subsequent chapters.
- **Chapter 4. Plaque Morphology Analysis:** Investigates the morphology of atherosclerotic plaques between ruptured and non-ruptured groups. It assesses plaque features including the fibrous cap and the lipid core, with the central element of the chapter being primarily focused on collagen, the main structural component in an atherosclerotic plaque.
- **Chapter 5. Macrophage Distribution:** Investigates the macrophage cell content and distribution in atherosclerotic plaques comparing ruptured and non-ruptured groups. It also investigates the correlation between macrophage cells and lipid content.
- **Chapter 6. Plaque 3D Reconstruction:** Focuses on the development of a procedure for generating a 3D plaque geometry model based on histological

sections, addressing the problems of **a)** registration of the sections into 3D, and **b)** the structural distortion caused to the histological sections by tissue processing.

- **Chapter 7. Ultrasound Plaque Characterisation:** Evaluates the feasibility of using 2D ultrasound to characterise plaque components via an ex-vivo setup, and by using histological sections of plaque specimens as the "gold standard".
- **Chapter 8. Discussion and Conclusion:** This is the discussion and conclusion for the thesis. Although individual results maybe discussed in each chapter, this chapter provides the general discussions with cross-literature comparisons, covering the whole study area.

Chapter 2

Literature Review on Atherosclerotic Plaques

2.1 Stages of Plaque Progression and Vulnerability

The description of the different stages of plaque progression is best described using the American Heart Association (AHA) classification system which has categorised atherosclerotic lesions into 8 different types. This categorisation has been based upon the plaques structure and composition. There are three papers which describe in detail this classification system (Stary et al 1992, Stary et al 1994, Stary et al 1995). An updated version of this can be found in a fourth paper (Stary et al 2000). To understand the path a lesion may take in its progression, this classification system can be very informative. The figure below (figure 2.1) briefly shows a summary of the categories.

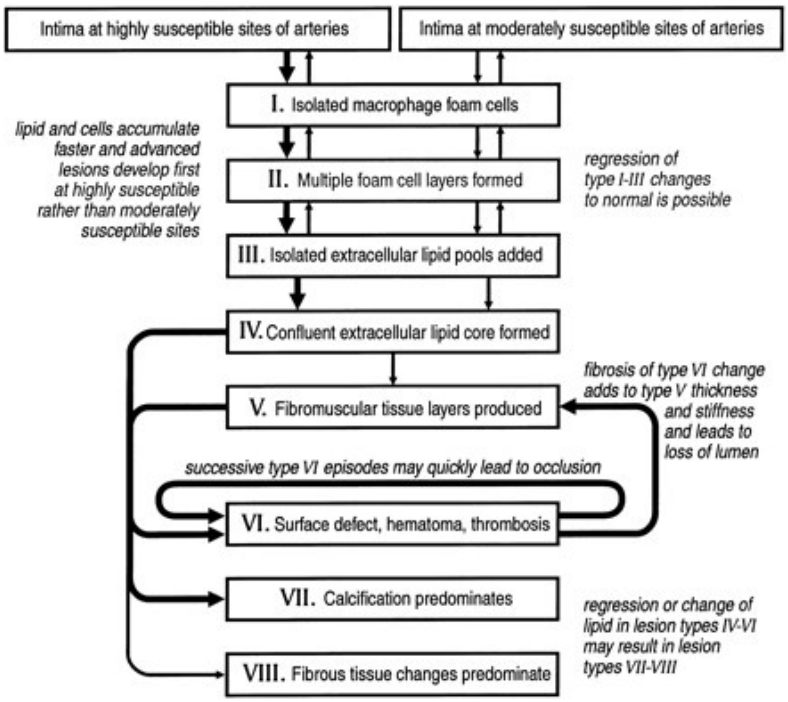

Figure 2.1 Stages of plaque progression (Stary et al 2000)

More detailed description for each stage is summarised in table 2.1.

Lesion type	Characteristics
I	The presence of the first signs of lipid droplets which are usually found located around isolated groups of macrophages
II	"Fatty streaks", increased number of foam cells that are organised to form stratified layers. However, the vast majority of the lipid is contained intracellularly, with only a small amount of extracellular lipid. A certain number of type II lesions stay at this stage for a prolonged period of time, whilst some may progress quickly
III	A stepping stone from the clinically silent type II lesions and the more advanced and dangerous type IV – type VI lesions. The formation of small pools of extracellular lipid amongst the layers of smooth muscle cells
IV	Widespread and highly concentrated accumulations of extracellular lipid. Both the lipid core and fibrous cap can be clearly defined. Type IV lesions can be vey difficult to detect in vivo because they do not obstruct the lumen. However, due to the morphology comprising of a large lipid core and a thin fibrous cap, they are prone to rupture.
V	Depositions of fibrous tissue, especially in the fibrous cap, and in regions where the accumulations of large lipid pools have caused disruptions to the normal arterial structure. They are more stenotic compared with type IV lesions.
VI	Undergone a rupture. Plaques of this nature show disruption of the lumen surface, hematoma or hemorrhage, and thrombosis. They are essentially type IV or V plaques that have had a rupture.
VII	Comprises primarily of calcification, regardless of the presence of a lipid pool.
VIII	Having extensive fibrous tissue with minimal or no lipid. The formation of this type of lesions could have arisen from the reabsorption of the lipid core, or remodelling of a previously formed thrombus.

Table 2.1 Different types of atherosclerotic plaques (Stary et al 2000)

2.2 Morphology of Atherosclerotic Plaque

2.2.1 Macro Level

Numerous distinctive features have been shown in detailed histological assessment of ruptured plaques. A large lipid core (≥30-40% plaque volume) composed of free cholesterol crystals, cholesterol esters, oxidised lipids embedded with tissue factors; a thin fibrous cap depleted of smooth muscle cells and collagen; outward (positive) remodelling; infiltration of inflammatory cells into the fibrous cap and adventitia (predominantly monocyte-derived macrophages, activated T cells, dendritic cells and

mast cells); and an increase in adventitial and plaque neovascularity. These phenotypic and morphological features of ruptured plaques are considered to be indications of plaque vulnerability when present in plaques that have not yet ruptured. This forms the basis for the concept of vulnerable plaques.

Fibrous Cap

The fibrous cap is an important morphological feature of atherosclerotic plaques, which functions to maintain a barrier between the lipid rich necrotic core, and the flowing blood in the lumen. It is formed from a layer of fibrous connective tissue, which is thicker and less cellular than the normal intima. It is infiltrated by the migration and proliferation of macrophages, smooth muscle cells (SMC), foam cells, and lymphocytes, which contributes to its formation (Ross R et al 1990). It is primarily composed of the structural molecules, collagen and elastin.

The fibrous cap contributes towards luminal encroachment (stenosis), which is used in current clinical practices as an indicator for surgical intervention. Although studies have shown the benefits of surgery in patients with high-grade stenosis (70-99%), its benefit in patients with moderate stenosis (30-70%) is less clearly known (Li et al 2006). Outward expansive remodelling in plaques can increase plaque size without compensatory narrowing of the lumen (Ivan et al 2002), causing potentially vulnerable plaques to be underestimated in terms of size and therefore vulnerability. This has led to investigators focusing efforts on the importance of the fibrous cap in relation to a rupture event. Yonetsu et al (2011) have shown, using OCT, that ruptured coronary plaques have thinner fibrous caps than non-ruptured plaques. Studies have shown that plaque with thin fibrous caps have higher peak stress levels than plaques with thicker fibrous caps. A slight decrease in fibrous cap thickness can significantly

elevate stress levels on the fibrous cap, and making it vulnerable to rupture (Gao et al 2008). Synetos et al (2009) demonstrated, using optical coherence tomography (OCT), that lesions in proximal segments of coronary arteries have thinner fibrous caps (49±20μ) than lesions that are located in distal segments (70±32μm) of the arteries (p=<0.05). Plaque rupture was found in 75% of proximal lesions, compared with 42.3% in the distal lesions (p=<0.05). The study showed that the thickness of fibrous caps has important implications with regard to plaque rupture. This finding is in concordance with a recent study carried out by Cicha et al (2010) which demonstrated that upstream regions, which are associated with cap thinning by proteolytic enzymes, are predominant sites of rupture. Other studies have shown the importance of the fibrous cap in relation to rupture (Redgrave J et al (2008) and Yonetsu T et al (2011)), who investigated critical cap thickness resulting in increased likelihood of a rupture.

The fibrous cap of atherosclerotic carotid plaques is an absolutely crucial determining feature of plaque rupture. The importance of the fibrous cap in relation to rupture has attracted large amounts of research investigating this not only as a parameter to assess rupture risk, but as a dynamic parameter in this complex disease. However, despite its importance, there is still a lack of understanding of the detailed systematic assessment of fibrous cap morphology in carotid plaques, and how this can influence plaque rupture. Improving our knowledge on fibrous cap morphology in a systematic way, and in its relationship with other plaque components, may help us to improve the risk assessment of plaque rupture and its etiology.

Chapter 2 Literature Review

Lipid Core

The lipid core is an important morphological component of atherosclerotic plaques as it can determine the vulnerability of a plaque to rupture. It is a necrotic acellular entity composed of free cholesterol, cholesterol crystals, and cholesterol esters which have originated from lipids that have either infiltrated the arterial wall, or lipids that have been derived from the death by apoptosis or necrosis of foam cells, predominantly macrophages. In the early stages of lesion development, fatty streaks are formed in the intima; this then progresses to develop into lipid–rich necrotic cores that can be found in advanced atherosclerotic plaques. Lipid cores are therefore involved in the entire period of plaque evolution, from the initial fatty streak stage to plaque rupture (Guyton et al 1996). Investigating the lipid-rich core in relation to plaque rupture is a crucial area for investigators as it can help improve our understanding of both plaque development, and risk assessment of plaque rupture.

Studies have shown that large eccentric lipid cores in plaques can be a mechanical disadvantage as it can contribute to plaque instability by redistributing circumferential stress to the shoulder regions, where nearly 60% of all plaque ruptures tend to occur (Huang H et al 2001). Gao et al (2008) demonstrated that increases in lipid core size correspondingly increased plaque stress levels, a notable factor in triggering fibrous cap rupture. Yehuda et al (2011) showed that exposing monocytes to lipid extracts in vitro promoted the expression of proinflammatory factors in human monocytes and macrophages. This may suggest that larger sized lipid cores in plaques may have increased proinflammatory factors, which in turn may increase plaque vulnerability. Discriminating between plaques with large lipid cores and smaller ones has therefore been of paramount importance in assessing a patients risk to rupture. Meese et al

(2008) demonstrated that it is possible to discriminate lipid-rich from non-lipid rich plaques using a clinical catheter based near-infrared (NIR) spectroscopy.

Studies have highlighted the importance of the lipid core in relation to plaque rupture. However, there is still a lack of knowledge regarding the detailed assessment of the morphology of the lipid core and its influence on other plaque components, which are also considered important in plaque rupture. Understanding these relationships may help in improving the risk assessment of plaque rupture.

2.2.2 Molecular Level

Inflammation

The morphology of atherosclerotic plaques is dynamically influenced by the molecular processes that occur within arterial walls. These molecular processes are a result of inflammatory activities which regulate variations in plaque morphology and cause certain plaques to be more prone to rupture than others. Inflammatory cells are predominately located adjacent to sites of fibrous cap rupture and around lipid cores (Shah PK et al 2007). Inflammatory cells are recruited into atherosclerotic plaques by cell adhesion molecules such as vascular cell adhesion molecules (VCAM)-1, and cytokines such as monocyte chemoattractant protein (MCP)-1, IL-8, and eotaxin (Libby P et al 2002). Once inflammatory cells are inside arterial walls they are retained and activated through the activity of other cytokines such as macrophage colony stimulating factor (M-CSF). Another mode of entry for inflammatory cells into plaques may be through adventitial walls or the plaque neo-vasculature, which is enhanced in atherosclerosis (Kolodgie FD et al 2003). Zalewski et al (2005) demonstrated a link between lipoproteins and inflammation through the enzyme Lp-PLA2 (lipoprotein associated phospholipase A2). The majority of studies found in

literature demonstrated that the primary immuno-inflammatory cells implicated in atherothrombosis are monocyte-derived macrophages and T-lymphocytes. There are some recent studies that suggest a potential role for mast cells in the pathogenesis of atherosclerosis and plaque instability (Kovanen PT et al 2007). Taranto et al (2010) demonstrated differences in gene expression profiles of atherosclerotic plaques compared with healthy control subjects. The study found that 42 genes were differently expressed, 13 genes were up-regulated, whilst 29 were down-regulated in plaque tissue. The study supports the notion that inflammation plays a key role in determining plaque morphology. Kitakaze et al (2009) demonstrated the association of inflammation with plaque morphology by showing that the inflammatory molecule, tumour necrosis factor-α (TNF-α), found in atherosclerotic lesions, up-regulated RAGE expression. RAGE encodes for a trans-membrane receptor that mediates responses to cell danger and stress, in addition to activating programmes responsible for acute and chronic inflammation, and therefore may promote atherogenesis. It can therefore be seen that inflammatory molecules play an important role in altering plaque morphology, and can determine the progression and vulnerability of plaques.

Matrix Metalloproteinase (MMP)

Plaque morphology is greatly influenced by the proteolytic activities of matrix metalloproteinase's (MMP). There are several types of MMP's functioning in plaques, with the primary role of collagen degradation. Since collagen is widely believed to play a structural role in atherosclerotic lesion stability, the study of MMP has been the subject of many investigations to improve our understanding on plaque remodelling, and in the risk assessment of plaque rupture. It is widely believed that MMP's play a crucial role in influencing plaque morphology. Studies have sought to

understand the role of the different types of MMP's in influencing the different morphologies. Djuric et al (2008) investigated the gene expression of MMP-8 in human carotid plaques, and compared the result from stable (fibrolipid) and unstable (complicated) plaques, but could not identify any significant differences between the groups. Barascuk et al (2011) demonstrated a link between MMP-9 and plaque morphology. The study developed an ELISA for the quantification of type III collagen degradation mediated by MMP-9 in urine. The results obtained from the study showed intra- and inter-assay coefficients of variation to be below 10%. The biomarker in the urine level of *ApoE-KO* mice towards the end of the 20 week study increased two-fold (p<0.0001), and were three-fold higher than control mice, and therefore demonstrates the link between MMP and the effect it may have on plaque morphology. Kunte et al (2010) demonstrated how MMP-9 can cause morphological differences in atherosclerotic plaques of patients with symptomatic internal carotid artery (ICA) stenosis. The study showed that plaques obtained from patients with symptomatic carotid stenosis as a result of embolic mechanisms showed higher content of MMP-9 {0.63% (0.42–1.01) vs. 0.25% (0.05–0.45); p=0.007}. Considering a lower MMP-9 content was found in asymptomatic plaques, this finding suggests that MMP-9 may have a role in influencing plaque morphology towards a more rupture prone configuration. Kobayashi et al (2009) demonstrated that MMP-positive macrophages located at the plaque surface may be associated with plaque vulnerability, and when located at the bottom of the intima, may be associated with outward arterial remodelling. The study found that MMP positive-macrophages have the ability to contribute to plaque vulnerability by altering plaque morphology including outward positive remodelling. Although the majority of studies have shown MMP to be present in atherosclerotic lesions, a recent investigation by Baroncini et al

(2011) showed using the carotid plaques from thirty patients, that MMP-9 are present in all stages of atherosclerotic lesion progression. However, MMP-9 measurements in the study were taken from the overall specimen, and not in primary diseased regions.

Macrophage

Macrophage Development

Macrophages are phagocytic cells that are derived from bone-marrow and have key functions for tissue homeostasis. They have an important role in the innate and acquired immune responses (McKnight et al 1998). Macrophage cells found in tissue are derived from circulating blood monocytes which are recruited by constitutive or inflammatory signals. Macrophages have a crucial role in tissue remodelling during development and wound repair. They have the ability to secrete an array of cytokines, growth factors and proteinases, all of which influence the remodelling of the extracellular matrix. They also recruit other cell types such as fibroblasts and smooth muscle cells which are necessary for wound repair.

Apoptotic Macrophages in Plaque Rupture Sites

Macrophage apoptosis in plaque rupture sites is one of a number of cellular events that can contribute to vulnerable plaque formation. It is characterised by certain key features such as inflammation, thinning of a protective collagenous cap, and a lipid rich necrotic core consisting of macrophage debris. Macrophage debris in turn can promote inflammation, plaque instability, and thrombosis. Studies have sought to understand the processes involved in macrophage apoptosis and the effects it may have on plaque development. In advanced plaques, macrophages have been shown to promote tissue repair by scavenging oxidised lipids and producing growth factors that are necessary for promoting smooth muscle cell proliferation and extracellular matrix

synthesis. However, contrary to this, a large body of evidence suggests the role of macrophages as being very important in the pathogenesis of atherosclerosis.

Macrophage cells contain within them an organelle known as the endoplasmic reticulum (ER) which is responsible for lipid synthesis, protein folding, and protein maturation. It is also the major signal transducing organelle that senses and responds to changes in homeostasis. Factors influencing its ability to function optimally are collectively called ER stress. When ER stress occurs in macrophage cells of plaques, it can contribute to macrophage apoptosis and plaque necrosis. Seimon et al (2009) altered a signalling pathway in relation to apoptosis, involving p38 mitogen-activated protein kinases (MAPK). *ApoE-/-* mice deficient in macrophage p38α MAPK on a western diet were found to have a marked increase in macrophage apoptosis and plaque necrosis. Lesions demonstrated significant decreases in collagen content and increased thinning of the fibrous cap. The findings suggest that p38MAPK has an important role in suppressing ER-stress induced macrophage apoptosis. Increased ER stress can severely impair its function in macrophages. During this stage the organelle sends apoptotic signals which cause an increase in macrophage-derived foam cell death resulting in plaques becoming vulnerable. An important component of the ER stress mediated apoptosis pathway is C/EBP homologous protein (CHOP). An investigation by Tsukano et al (2010) showed that large numbers of CHOP-expressing macrophages showed apoptosis in advanced lesions in wild-type mice, whilst only few apoptotic macrophages were observed in CHOP-/- mice, suggesting an important role for ER-stress CHOP pathway in macrophage apoptosis and in plaque instability. Another study performed by Croons et al (2009) also showed that anisomycin, a protein synthesis inhibitor, selectively decreased the macrophage content in rabbit

atherosclerotic plaques by apoptosis. The p38 MAPK plays an important role in anisomycin-induced macrophage death. De Meyer et al (2011) reported that Lithium chloride (LiCl) selectively decreased the macrophage content in rabbit atherosclerotic plaques by inhibiting inositol monophosphatase (IMPase) without affecting the viability or functionality of SMCs and endothelial cells. The study showed evidence for the local administration of an IMPase inhibitor to stabilise atherosclerotic plaques.

2.3 Hypothesis of Plaque Rupture Mechanisms

2.3.1 Effects of Inflammation on Plaque Rupture

Inflammation may cause atherosclerotic plaque development and rupture through many interacting pathways. To validate this hypothesis, extensive researches have been performed by many groups to investigate the link between inflammation and plaque rupture.

Over the past decade the appreciation of the importance of inflammation in atherosclerosis has increased significantly. It was previously considered to be a bland lipid storage disease. However, with considerable advances in basic and experimental sciences, the importance of inflammation and the fundamental cellular and molecular mechanisms that play a role in the development of atherogenesis have been highlighted. Strong evidence for the importance of inflammation in atherosclerosis at both basic and clinical levels has emerged in parallel. Data generated from studies highlight that insights into the link between inflammation and atherosclerosis can generate both predictive and prognostic information which have substantial clinical benefits. Inflammatory processes are not only involved in plaque progression, but also seem to play a critical role in plaque rupture. Fatty acid binding protein 4 (FABP4) are carrier proteins found located along the biological span of membranes in

macrophage cells, and are involved in the movement of fatty acids. A study by Agardh et al (2011) demonstrated that the expression of FABP4 is increased at the mRNA level in unstable carotid plaques compared with stable plaques, suggesting an increased uptake of fatty acids (lipids) by macrophage cells in unstable plaques. In addition, immunohistochemical analyses showed the co-localisation of FABP4 to macrophage populations. The study further highlights the inflammatory role of macrophages on plaque rupture.

Interleukin-17A (IL-17A) functions as a proinflammatory cytokine that responds to the invasion of the immune system by extracellular pathogens, and induces destruction of the pathogen's cellular matrix. It modulates immune cell trafficking and initiates inflammation in immune and infectious diseases. Erbel et al (2011) demonstrated that (IL-17A) expression levels were significantly associated with vulnerable and ruptured plaques (p=0.003). In addition Erbel et al (2011) showed that IL-17A had a negative correlation with a potent anti-inflammatory/atheroprotective cytokine IL-10 (p=0.0006, r=-0.46).

Ionita et al (2009) reported that Myeloid related protein (Mrp)-14, an inflammatory marker associated with myocardial infarction, is strongly associated with the morphological features and the inflammatory status of rupture-prone atherosclerotic plaques. The study used 186 human carotid plaques to quantify levels of Mrp-14 and found that high levels were present in lesions which had large lipid cores, high macrophage content, and low smooth muscle cell and collagen content. Mrp-positive macrophages were present in higher numbers in rupture-prone lesions compared to stable lesions.

Hallow et al (2009) reported on the relationship between the inflammatory process and the mechanical stress of the plaque. The investigation used 2D heterogeneous finite element model to determine the spatial distribution of stress for each histological cross-section studied. The lesions were classified as early, intermediate, advanced, or mature, based on their morphological characteristics, and used immunohistochemistry to determine selected inflammatory markers. The study found a monotonic spatial relationship between mechanical stress and activated NF-κB in all stages of plaque progression, and a progression-dependent relationship between stress and the presence of macrophage and MMP-1 expression.

As many studies have shown, inflammation is unquestionably a fundamental part in plaque rupture process. Studies have therefore attempted to investigate whether inflammation can be detected via alternative parameters that may be associated to inflammation itself, and which maybe easier to detect and quantify. Tang et al (2008) studied the relationship between the degree of MRI-defined inflammation using ultra small super paramagnetic iron oxide particles (USPIO) and the severity of luminal stenosis in plaques of 71 asymptomatic patients. Tang et al (2008) demonstrated that inflammation and degree of stenosis are likely to be independent risk factors to plaque rupture as no relationship was found. This study raises further questions with regards to plaque pathogenesis and rupture, because studies have shown that inflammatory activity is one of the main causes of plaque build-up and causing plaque encroachment and luminal narrowing. However the study (Tang et al 2008) recognized the need for further validation.

2.3.2 Effects of Collagen on Plaque Stability

Changes in plaque collagen content may cause atherosclerotic plaques to become either vulnerable to rupture when there is a deficit or it may lead to arterial stenosis when there is an excess amount of collagen. To validate this hypothesis many studies have been carried out to investigate the role of collagen in plaque and its link to the rupturing process.

The main effect of collagen on plaque stability is by varying the strength of the fibrous cap. Plaque instability is mainly caused by the proteolysis of the collagen present in the fibrous cap, as a result of the enzymatic actions of metalloproteinase's, which are released by cells such as macrophages that are present in the lesions (Aikawa et al 1998).

Numerous studies have shown the effect of collagen changes on the stability of atherosclerotic plaques. In addition, the causes for these changes have also been the subject of many researches. Angiotensin II is a hormone that causes blood vessels to constrict (vasoconstriction), and blood pressure to increase. It acts through two different types of receptors, AT1 and AT2, and are integral proteins spanning the membrane. When angiotensin II binds to the type 1 receptor, it can have a significant role in atherogenesis and collagen synthesis. However, a study by Dandapat et al (2008) investigated the effects of up-regulating angiotensin II type 2 receptors in arteries by injecting LDLR knockout mice with adeno-associated virus type 2. The study found that the over-expression of angiotensin II type 2 receptor reduced enhanced collagen accumulation, and MMP expression. Hector et al (2010) demonstrated that differences in collagen cross-links in plaques may adversely affect the tensile strength of plaques, and may be linked to plaque stability in vulnerable

plaques. Formation of covalent intermolecular cross-links pyridinoline (Pyd) and deoxypyridinoline (Dpd) affect collagen maturation in plaques. The study demonstrated that greater collagen deposition, increased presence of CD68 positive cells, and an increased Pyd: Dpd ratios are found in plaques compared with normal vascular tissue. Cheng et al (2009) demonstrated that administering Angiotensin II into carotid arteries of ApoE KO mice's, induces the expression of an active form of MMP-8 and MMP-13 in macrophage cells, triggering the destabilisation of plaques which have a vulnerable macrophage rich phenotype. This occurs as a result of a relative decrease in plaque stabilising collagen, and increasing the activity of collagenases. The study therefore showed the effect of decreased collagen on the stability of plaques.

2.3.3 Effects of Wall Stress On Plaque Rupture

High mechanical stresses may influence atherosclerotic plaques to rupture due to the effects of the pulsatile blood pressure and flow. An extremely high local stress may induce the fibrous cap of a plaque to rupture directly. Extensive studies have been carried out to support the hypothesis that stress levels may influence the risk of plaque rupture. This section will highlight the research that has been performed to support the hypothesis.

Wall Stress and Strain

Biomechanical studies on the development and progression of atherosclerosis have been widely performed from a hemodynamic point of view. The vast majority of studies show that stress induced by blood flow on arterial walls has an important role towards initiation and progression of the disease. The development of stress exerted by blood pressure on arterial walls is a crucial factor for the disease. The progression

of the disease may be affected if the wall stress is too high. High levels of stress acting plaque can result in disruption.

To understand the effect that mechanical forces can have on an atherosclerotic plaque, a review of the principles of material properties and the physical laws, which define the interaction between opposing forces in a cylindrical vessel such as a blood vessel would be helpful (Lee et al 1994). Stress is defined by the forces acting on a surface divided by the size of the surface; stress can act on a vessel wall in all directions including radially, circumferentially and longitudinally. Normal stress can be defined as perpendicular forces acting on the vessel wall such as that applied by blood pressure. Parallel forces acting on the endothelial cell layer results in shear stress. When there is a given radial pressure within a vessel, a compensatory circumferential tension results. The tendency to rupture of thin walled vessels like in a vulnerable carotid plaque is explained by plaque stress analysis. The complex geometries of an atherosclerotic vessel have many other factors that needs to be considered, however, the principle concept remains the same: a high circumferential stress in a thin fibrous cap of the atheromatous plaque can cause mechanical failure of the plaque.

Strain can be defined by the amount of deformation a structure undergoes as a result of an applied external force, normalised to its length. Changes in the length of the material are reflected by strain, and are expressed as a fraction or a percentage of the initial length. Materials stiffness is characterised by the ratio between the stress applied and the reflecting strain that is observed. This is usually expressed by the elastic or Young's modulus (E). $\boldsymbol{E}$ **= stress/strain**

When the elastic modulus of structures remains constant over a range of stresses, then a linear elastic behaviour is observed. The material is known as isotropic when the modulus remains constant in all directions. An immediate stress/strain response occurs after a force has been applied to an elastic material. This phenomenon is not observed in biological structures, and is known as viscoelasticity as there is a time response to a given force until a new equilibrium strain has been reached.

A wide variability of the material properties are characterised by vascular structures. 1) They are anisotropic: and are stiffer in their axial and circumferential directions then radial; 2) they have nonlinear elastic properties, becoming stiffer with increasing levels of strain. Due to the complex structure of plaques, researchers make use of a computational structural technique known as finite element (FE) analysis to study the distribution of mechanical forces in atherosclerotic plaques. Complex structures can be evaluated by this technique by dividing it into fractional areas in order to determine regions of maximum stress.

Stress and Plaque Rupture

Mechanical stresses in arteries caused as a result of forces created by pulsating blood flow, play an important role in the atherosclerotic plaque rupture process. Studies have focused their research on improving the understanding of the association of stress to the plaque rupture process. A recent study carried out by Tang et al (2009), demonstrated using in-vivo MRI of carotid plaques from 20 patients, that localized critical stress values had a much better correlation with plaque morphological features that are generally associated with plaque rupture risk, compared to global maximum stress conditions. Richard et al (1989) assessed different geometries of plaques that had caused coronary thrombosis, and showed that there was an increased level of

stress concentration at the edge of the fibrous cap near to the boarder with the normal intima. The study also showed that in cases where the lipid pool was small (<15% of the vessel circumference), the point of maximum stress was located in the centre of the plaque. These results are supported by Cheng et al (1993), which evaluated circumferential stress distribution and magnitude in plaque rupture, by studying lesions from patients who died of acute coronary events and compared them with non-ruptured lesions of individuals who died from other causes. Finite element (FE) model was used to establish that mechanical stresses were higher in regions of rupture then non-ruptured regions. The study also found that the locations of plaque rupture were not always necessarily locations of high mechanical stresses. This suggests that there must be local variations in plaque strength, and that may determine which high stress region ruptures or not. A study carried out by our group (Gao et al (2009) also performed plaque stress analysis by using fluid structure interaction method based on MRI data. They found that wall shear stress distributions were highly associated with the degree of stenosis; however its level of magnitude were much lower than the wall tensile stress in the fibrous cap. Wall tensile stress is higher in the luminal wall compared to the outer wall, with the lowest being in the lipid core region. Local stress concentrations were found to be mostly occurring in the thinner fibrous cap regions located near to the plaque shoulders. Gao et al (2008) also performed a one-way fluid-structure interaction (FSI) simulation on 13 carotid bifurcation cases to demonstrate that stress levels are more sensitive to changes in fibrous cap thickness compared with lipid core volume. A slight decrease in cap thickness can result in a significant increase in stress levels, and therefore increase the likelihood of a rupture. Tang et al (2008) demonstrated that there is an association between biomechanical stresses and ultra small paramagnetic iron oxide (USPIO) enhanced MR-defined inflammation

within carotid plaques. The presence of inflammatory activity in vulnerable plaque has been established by past studies. Therefore, the finding by Tang et al (2008) shows that biomechanical stresses have an important role in influencing vulnerable plaques to rupture.

Mechanical Environment Induced Collagen Remodelling

Blood flow in the lumen of arteries generates a mechanical environment which induces collagen remodelling. Collagen remodelling in the arterial wall is a critical determinant of plaque progression, vascular remodelling, clinical CAD manifestations, and plays an important role in modulating the stability of plaques. This subject has been the focus for many researches to improve the understanding of the pathology of the disease, and to improve the risk assessment of plaque rupture.

A very early research on the topic was performed by Ku et al (1985), which showed that low and oscillating wall shear stress caused as result of blood flow correlates with specific location of intimal thickening. Mechanical strain based remodelling of collagen fibres in plaques was studied by Driessen et al (2004). Driessen et al (2004) demonstrated that fibre alignment is modulated by the principle strain field. Hariton et al (2006) on the other hand suggested that collagen fibre architecture was a consequence of stress. Hariton et al (2007) demonstrated using an iterative finite element based procedure, that human carotid bifurcation, which is subjected to stress due to the complex geometries in the region, modulates collagen fibre direction. The study found a good correlation between the predictive fibre architecture at the cylindrical branches and at the apex of the bifurcation, with histological observations. A study by Christopher J et al (2000) investigated the effects of chronic cyclical mechanical strain on extracellular protein production by cultured vascular smooth

muscle cells (VSM). They found that exposing VSM cells to 5 days of chronic cyclical mechanical strain increased collagen concentrations (+50% $p<0.001$) when compared with cells grown in static conditions. The study also investigated if cyclic mechanical strain resulted in the release of a soluble factor (cytokine) which had the potential to increase extra cellular matrix (ECM) protein production. The culture media on which the VSM cells were embedded in was removed after exposure to chronic mechanical strain and transferred to human VSM cells grown on static plates. The results show that the conditioned media caused a significant increase in the production of collagen proteins. These results suggest that mechanical stress in plaque can cause a marked increase in collagen production. Stone et al (2007) demonstrated that plaque progression is found in sub-segments with low endothelial shear stress (ESS), which are associated with either constrictive or expansive remodelling. Sub-segments with low ESS were found to exhibit plaque progression when compared with sub-segments with moderate/higher ESS (33.3% vs. 7.9%, respectively, $p=0.009$), and constrictive remodelling (44.0% vs. 5.3%, respectively, $p=0.16$). The study shows that mechanical environments which are associated with low endothelial shear stress are responsible for collagen remodelling and plaque progression. However, mechanical environment induced collagen remodelling can also take place as a result of interstitial flow. Interstitial flow is the connective transport of fluid through the tissue extracellular matrix. This type of fluid flow, also known as creeping fluid flow, has been shown to induce the morphology and migration of cells such as fibroblasts, and endothelial cells by modulating the mechanical environment of cells. Shi et al (2011) demonstrated using a conceptual mechanotransduction model that cell surface glycocalyx HSPGs, in the presence of integrin-mediated cell-matrix adhesions and cytoskeleton organisation, are able to detect interstitial flow and

activate the FAK-ERK signalling axix. This activation results in the up-regulation of MMP expression. As mentioned in this review, MMP's play a crucial role in collagen degradation and plaque remodelling.

2.4 Techniques for Plaque Morphology Assessment

2.4.1 Non-Invasive Imaging Techniques

Multi-Spectrum MRI

Multi-spectrum MRI provides a useful non-invasive tool for the study of arterial plaque morphology, and for plaque rupture assessment. The reliable characterization of plaque, especially the different plaque components can be achieved with different MRI scan sequences. It was first introduced in the late 1990's as a research tool (Nelson et al 1995), and has now become a conventional method for monitoring plaque development (Hockings et al 2002). A normal scan of carotid MRI is performed using 3-inch bilateral surface coils (FOV, 10 x 10 cm; slice thickness, 2-3mm). Image acquisition includes 3D TOF MR Angiography. T1-weighted pre- and post-contrast spin echo (T1W1), T2-weighted spin echo imaging (T2W1) and T1-weighted fat saturated spin echo imaging. In sequence images, collagen tissue will appear as high signal intensity, while lipid tissue will appear as a darker contrast. However, the main limitations of using in vivo MRI to assess plaque are: (1) the spatial resolution is not adequate, and (2) the contrast between tissues is not clear. Therefore, it is still difficult to reveal thin fibrous caps with a thickness less than 0.25mm.

MRI can also be used to perform ex-vivo scans to study plaque specimens. Ex-vivo MRI has several advantages over in-vivo MRI as it can achieve a higher resolution

resulting in higher image quality. Ex-vivo MRI can also enable easier tissue characterisation of the different components of plaque (Xie et al 2010).

Ultrasound

Ultrasound (US) has the ability to image large arteries such as the carotid, brachial, iliac, and femoral arteries, by simply placing the ultrasound probe over the region of interest. B-mode ultrasound has the capability to accurately measure the arterial diameter, the thickness of the arterial wall, and can also permit a limited characterisation of plaque morphology. The arterial wall is the most reliable for the IMT measurements, but it does not indicate if the thickening is as a result of intima or media infiltration or hypertrophy. Nevertheless, there are a large number of studies that have demonstrated that the IMT may be a useful marker for cardiovascular disease progression (O'Leary DH et al, Hollander M et al). Doppler ultrasound is able to measure blood-flow velocity, and it can also be used to estimate the degree of luminal stenosis by detecting flow disturbances on the downstream side of large stenoses. The majority of ultrasound probes that are available commercially operate at 3.5-10 MHz. The axial resolution on an ultrasound probe is usually less then 400µm, whilst the lateral resolution is about 600µm (Fayad ZA et al, Landini L et al). However, there has been advancements using radio frequency (RF)-data based algorithms which have enabled the automatic detection of vessel walls. With such algorithms, it has been possible to track the displacement of the vessel wall in time with an error of less than 10µm (Hoeks et al, Hiltawsky et al). Some of the key important advantages of using non-invasive ultrasound are the low economical cost, availability, the lack of side effects, and the short examination times. However, there are still many challenges with regards to coronary ultrasonography including measurement reproducibility problems for some applications. Nederkoorn et al

reported a sensitivity of 87% in diagnosing 70% to 90% stenosis versus <70% stenosis. Current ultrasound tissue characterization of different plaque components is still a developing area, and until now, the results have not been promising. However, non-invasive ultrasound (B-mode, M-mode, and echo-tracking) remains the standard imaging technique for patients that are suspected as having carotid artery disease.

2.4.2 Invasive Imaging Technique

Intra-Vascular Ultrasound (IVUS)

Intravascular ultrasound (IVUS) provides real-time high resolution images of the coronary arteries. It is used as a diagnostic imaging tool to provide an accurate depiction of the morphology of an atherosclerotic plaque with a typical axial resolution of 80-100 microns, while the lateral resolution reaches 200-250 microns in a conventional IVUS system (20-40MHz) (van der Wall et al 2011). Recent developments in the post-processing of the IVUS raw signal have resulted in an enhanced method for defining plaque composition. IVUS is able to assess the severity of stenosis, calculate the vessel diameter, as well as determining the boundaries of the atherosclerotic plaque (McNeil et al 2003). There are numerous studies that can be found in the literature that demonstrates the usefulness of IVUS in evaluating the composition and development of an atheromatous plaque (Furukawa S et al 2011).

Thermal Imaging

Inflammation is one of the most important pathophysiological mechanisms which contribute towards plaque vulnerability, plaque disruption, and increased thrombogenicity (Vaina et al 2005). It is believed that the inflammatory process is associated with the generation of heat, and this has therefore made it possible to use intravascular measurements of temperature using a thermography catheter to quantify

the inflammation process. Ex-vivo studies have been carried out on carotid arteries for the thermal detection of cellular infiltrates in living atherosclerotic plaques (Casscells et al 1996). In a study that was carried using in-vivo experiments on coronary arteries, it was found that atherosclerotic plaques had a significantly higher heterogeneous temperature pattern compared with healthy arteries (Stefanadis C et al 2003, Stefanadis C 2001), which enabled the detection of different locations with an inflammatory reaction. Furthermore, it was found that the temperature difference between plaque and normal healthy vessels was higher in patients who have an adverse outcome (Stefanadis C et al 2003). This second observation lead to the assessment of a cut-off temperature difference value, however, a larger scale study is needed to determine the optimum temperature cut off-level to enable the detection of vulnerable plaques (Madjid M et al 2006).

Optical Imaging

Optical Coherence Tomography (OCT) is an intravascular technique that utilises optical reflections of an infrared light source. From this it can be seen that this imaging modality can be described as being analogous to ultrasound, however the difference being the energy that is transmitted is in the form of infrared light rather than sound waves (Cilingiroglu M et al 2006). The infrared spectrum upon release is reflected from the vascular structures, analysed, and forms a cross-sectional image. The resolution that is attainable using OCT is in the range of 2-20 μm, and is currently the highest among all the imaging modalities available for coronary artery disease assessment. There are a number of factors that can affect the resolution range such as the complexity of the system and its transmission and analytic capabilities. It also depends whether the system is catheter based or not.

Further to the superior resolution that can be achieved using OCT, it also has the technical advantage of not having a transducer within the catheter, which enables the system to be very thin, and also easy to manipulate. Diameters as thin as 0.006 inches have been produced in imaging catheters (Nissen SE et al 2001). Another important advantage of OCT is the high image acquisition speed (4-8 frames per second) that can be achieved. The acquisition rate is almost that of video speed, and it therefore enables image reconstruction, and the analysis process is thus more accurate.

2.4.3 Functional Imaging (Targeted Molecular Imaging)

Nuclear imaging methods are based on non-invasive detection of radioactive radiation from isotopes introduced into the body. If these radionuclides are able to be conjugated with a tracer compound that has functional roles during the atherosclerotic process, functional imaging of atherosclerosis becomes possible.

Due to the non-invasiveness of MRI, plaque progression and regression can be studied in experimental animal models and also in patients with suspected coronary artery disease. McConnell et al (1998) demonstrated lesion regression in cholesterol fed rabbits after withdrawal of the lipid diet. In comparison to these findings, Helft et al (2002) showed that plaque size and lipid core size continued to expand in animals that were continuously being fed high cholesterol diet. Johnstone et al (2002) demonstrated that it is possible to visualise thrombus formation using T2-weighted MRI. This review shows that the use of functional imaging could have many valuable applications for studying atherosclerotic development. An important application with regards to plaque rupture could be the analysis of inflammation. Atherosclerosis and its subsequent plaque rupture are widely recognised as being an inflammatory disease. The ability to visualise this would prove to be a valuable tool in plaque

rupture assessment. Matthias et al (1998) hypothesised that inflammation is reflected by signal changes in contrast enhanced MRI. They found that with the use of contrast media-enhanced MRI, it is possible to visualise the localisation, activity, and extent of inflammation in cardiac tissue. The use of this method may therefore have the possibility of being a powerful non-invasive diagnostic tool in assessing plaque rupture. Currently there are no diagnostic modalities that can detect precursory molecular or cellular events directly. Winter et al (2003) injected intravenously $\alpha_v\beta_3$-targeted paramagnetic nano-particles to specifically detect the neovasculature. They found a 47±5% enhancement in MRI signals for angiogenesis detection. Histology and immunohistochemical verification confirmed the marked proliferation of angiogenic vessels within the aortic adventia, which was coincident with the proliferation among cholesterol fed diets in animal models. In comparison, a few incidences of neovasculature were found in control animals. Functional imaging using this form of molecular approach may provide a method for defining the burden and progression of atherosclerosis in vulnerable patients (Winter et al 2003).

2.4.4 High Resolution Study

Micro-CT

Micro-computed tomography (CT) became an important powerful tool in the laboratory for investigators in recent years due to technical advances that were taking place with regards to increasing computer speed and memory. This enabled micro-CT systems to have the ability to generate thin-section of images of small specimens (Feldkamp LA et al 2004, Müller R et al 2004). The spatial resolution for a typical Micro-CT is approximately 48µm, (Kristanto et al 2011). Early investigators implemented the use of three-dimensional micro-CT, and primarily focused on the technical and methodological aspects of this system, however there have been other

studies which have concentrated on the practical aspects of the technology. Until recently, the technology has been implemented in the visualisation of the vasculature for the following areas: intact isolated rodent organs; myocardial, renal, and hepatic vasculature; and trabecular bone in surgical bone specimens. There are only a limited numbers of studies in the literature implementing the technology for analysing the vulnerability of atherosclerotic plaque rupture. A study by Langheinrich AC et al (2004) investigated the feasibility for analysis of coronary artery wall in autopsy specimens. The purpose of the study was to evaluate the feasibility of micro-computed tomography (CT) for analysis of the coronary wall. They demonstrated that micro-CT is able to provide quantitative information about plaque morphology which can be equivalent to that of histological analysis. A hotelling T^2 test showed significantly smaller values for vessel wall perimeter and lumen area with histology sections ($p<0.001$). However, the use of micro-CT for analysing plaque rupture vulnerability does have limitations. In the study, micro-CT was only able to visualise between structural features that had sufficient contrast material. However, to assess plaque vulnerability, it is important to understand the morphology of the plaque on a cellular level, in which case histology analysis has a clear advantage, nevertheless, it can still prove to be a useful tool when considered to be an additional tool for the ex-vivo assessment of plaque rupture.

Histology

Conventional Wax Histology

The application of histology for the assessment of atherosclerotic carotid plaques is routinely used for research purposes. The application of histology enables researchers to identify and analyse plaque components which are important in the study of plaque

development and vulnerability. Histology can be used to study many aspects of the atherosclerotic plaque including a) parameter size measurement; b) the localisation of specific cells or molecules; c) tissue structure and d) plaque model development for stress analyses purposes etc. A study carried out by Devuyst et al (2005) applied the use of histology to measure the thickness of the fibrous cap at different locations. The results were then compared with ultrasound cap thickness measurements to see the feasibility of ultrasound in distinguishing between symptomatic and asymptomatic plaques. An example of the application of histology for localising cells involved in atherogenesis was demonstrated by Kolodgie et al (2000). The study used antibodies to stain for macrophage cells and caspases 1 and -3 to identify localisation within the plaque. Further, the application of histology can be used to study the structure of plaque tissue to assess for its vulnerability. Whittaker et al (1994) used histology to investigate collagen structure in plaque using circularly polarised light. The study found a progressive increase in the maximum brightness of collagen fibres in the scar tissue (e.g. after a plaque rupture) with time. The study showed that the use of circularly polarised light has the ability to enhance the application of histological assessment of tissue, and is able to provide information regarding the structure and composition of plaque collagen tissue

Frozen Section Procedure (Cryosection)

This is a pathological laboratory technique used to perform rapid microscopic analysis of tissue specimens. This method can be applied to study the carotid arterial plaque and has been used in some studies. Lessner et al (2002) used cryosectioning to section the entire length of the carotid plaque at 140μm intervals. The study found that the growth of lesions are caused by macrophage-derived foam cells, which are derived primarily from the recruitment and proliferation of circulating precursors e.g.

monocytes, rather than from resident macrophages. The technique can also be used to study the distribution of lipid in plaque using Nile Red staining which is not possible using conventional wax histology (Lessner et al 2002). The advantage of using this technique over conventional histology is the rapid preparation time that can be achieved (10 minutes (cryosection) versus 16 hours (conventional histology)). However the quality of the sections in cryosection is by comparison of a much lower quality compared to formalin fixed, wax embedded tissue processing. In addition, it is much more difficult to perform compared to conventional histology, and therefore this technique will not be applied to this study.

Antibody Staining

Immunohistochemistry is the localisation of antigens in tissue sections by the use of labelled antibody as specific reagents through antigen-antibody interactions that are visualised by a marker such as a fluorescent dye, enzyme, radioactive element or colloidal gold. The first pioneers of the technique were by Albert H. Coons and his colleagues (Coon et al 1941). They were the first to be able to label antibodies with a fluorescent dye and use it to identify antigenic sites in tissue sections. Over time the technique of immunohistochemistry has expanded and developed to an advanced level, and the introduction of enzyme labels such as peroxidase and alkaline phosphatise labels have also been discovered, and used to identify immunohistochemical reactions at both light, and electron microscope level. Immunohistochemistry involves specific antigen-antibody reaction, and it therefore has apparent advantages over traditionally used special enzyme staining techniques that are only able to identify a limited number of proteins, enzymes, and tissue structures. Immunohistochemistry has therefore become an important technique, and is widely used in many medical research laboratories, as well as in clinical

diagnostics. There are many immunohistochemical techniques available to use to localise antigens. The selection of a suitable method should be based upon parameters such as the type of specimen under investigation, and the degree of sensitivity required. Yilmaz et al (2006) studied the distribution of immune cells in atherosclerotic carotid plaques. Immunohistochemical analysis was performed using CD34 to visualise the presence of neovascularisation and intraplaque haemorrhages, smooth muscle cells (SMC: actin), macrophages (CD68), T-Cells (CD3), dendritic cells (DC: fascin), and mature dendritic cells (CD83).

2.5 Plaque Vulnerability Assessment

2.5.1 General Structure Assessment

The rupture of an atherosclerotic plaque is widely believed to be associated with plaque morphology, mechanical forces, vessel remodelling, blood conditions (cholesterol, sugar etc.), and lumen surface conditions (inflammation). Studies have highlighted that certain structural characteristics are linked with plaque ruptures; a) a large atheromatous lipid rich core; b) a thin fibrous cap; and c) weakening of the plaque cap. The quantification of plaque size, shape, and components (fibrous, lipid, calcification/inflammation) can be assessed with development in MRI techniques at the macro-scale level (Yuan C et al 2001). Efforts have been made to use ultrasound and intravascular ultrasound to quantify the motion of vessels, the mechanical properties, the structure of vessel walls, and also to predict the location of where a vulnerable plaque may rupture (Ohayon J et al 2001, Pedersen, P. C et al 2003). There are very few reports in the literature on the ability to measure the mechanical properties of plaque components in-vivo, which if possible, would be extremely beneficial (Chandran KB et al 2003).

A Group led by Professor Gillard JH at Cambridge University, have published many studies on assessing vulnerable plaque structure using MRI in recent years (Sadat et al 2011). The other major contributor on this field is a group at Washington University led by Professor Yuan. As pioneers of non-invasive assessment of vulnerable plaques, together, they have contributed the majority of the work in this specific field. By using Professor Yuan's data, Professor Daling Tang's group has performed a series of studies on plaque stress analysis (Yang C et al 2010). Similarly, our group at Brunel University has utilized the data from the group at Cambridge University to study plaque stress distributions for symptomatic and asymptomatic patients (Gao H et al 2009). The major limitation of this kind of study is the limiting spatial resolution of MRI which makes it difficult to reveal the fine details of fibrous cap thickness: one of the most important features of plaque morphology. In terms of stress analysis, the resolution in the longitudinal direction with a slice thickness of 3mm, contributed to the major uncertainty in model generation. Therefore, the result will only provide a general view of plaque stress distribution. The results especially for the stress analysis may not be reliable for reflecting the variations of plaque morphology in fine details.

2.5.2 Lipid Core Size

The size of the lipid core is a fundamental feature in an atherosclerotic plaque which is present from the initial development, to the advanced stages. Lipid cores contain inflammatory cells which release proteins as well as other chemicals that can contribute towards making a plaque highly vulnerable. The size of the lipid core is therefore an important feature to study in the vulnerability assessment of plaque rupture. Lipid cores normally have a large contrasting difference from the surrounding tissue in plaques in both MRI and ultrasound images. Also, due to its

generally large size, the imaging resolution will generate less impact on the assessment accuracy compared with fibrous cap thickness assessments. A study carried out by Ohayon et al (2008) investigated the change in plaque vulnerability as a function of lipid core size and plaque morphology. They found that lipid core thickness is more of a critical determinant to plaque stability rather than the area of the lipid core. The study demonstrated that plaque instability is to be viewed not as a consequence of a single parameter such as cap thickness, but as a combination of cap thickness and lipid core thickness. Associating the lipid core to other factors to determine stability has been an ongoing area of study by many research groups. Wasserman et al (2008) established using MRI that individuals with thickened carotid walls, have plasma total cholesterol more strongly associated with lipid core presence than other established coronary heart disease risk factors. The study showed that plaque vulnerability to rupture may be increased by high total cholesterol content. However, a major draw-back of the study was that individuals with wall thicknesses <1.5mm were excluded from the study because no cores were apparent in thinner walls, and smaller sized cores could be missed, which may result in findings that are not accurate representations of the population. Another study by Ota et al (2009) demonstrated by in vivo 3T MRI that haemorrhages and large lipid rich cores are independently associated with thin or ruptured fibrous caps. This is important in risk assessment of plaque rupture vulnerability because detection of lipid rich cores in plaques using 3T MRI may indicate, based on the results of this finding, that a thin fibrous cap is likely to be present, and therefore increase the likelihood of rupture and subsequent cerebral ischemic attacks.

2.5.3 Collagen Content

In order to assess the strength of the fibrous cap, and also to see the current level of risk that it is at in terms of rupturing, it is important to look at the quality and quantity of collagen present. As previously mentioned in this review, human atherosclerotic plaques mainly consists of collagen types I and III, however when under microscopic analysis, dense type IV collagen depositions can usually be seen. This is in conjunction with a high level of smooth muscle cell localisation. The depletion of collagen in the fibrous cap is the detrimental effect of two factors. It can be firstly due to a high level of inflammatory infiltrates into the fibrous cap and secondly, due to the apoptosis of the collagen-producing smooth muscle cells.

Many studies can be found in the literature that attempt to demonstrate the collagen content in plaque. Some studies have attempted this either using in-vivo (on animal model) or ex-vivo methods. In a relatively recent study, Seemantini K et al (2007) demonstrated that by using polarization sensitive optical coherence tomography (PSOCT) technology, they were able to measure the collagen content in atherosclerotic plaques ex-vivo. They found a high positive correlation between the PSOCT measurements of the birefringence properties of the collagen and the morphometrical measurements of the corresponding locations using picrosirius red staining and found significant result ($r = 0.62$, $p < 0.001$). Rich et al (2005) used a combination of picrosirius red staining, circularly polarised light, and hue analysis to demonstrate in ex-vivo that collectively it is able to provide a powerful tool for the structural analysis of collagen fibres. With further studies using this method, it may be possible to adapt the technique to quantify the collagen content. Using the video CCD system used by Seemantini K et al (2007), it could be used as a tool in plaque vulnerability assessment. An interesting study carried out by Hector et al (2010)

assessed changes in collagen maturation in plaques ex-vivo to determine its stability. The stability of collagen is achieved through the formation of dysfunctional, intermediate cross-links between adjacent collagen fibrils mediated by the action of lysyl oxidase. In vascular tissues they are pyridinium cross-links, pyridinoline (Pyd) and deoxypyridinoline (Dpd). The study determined whether it is possible to identify and measure differences in the mature pyridinium (Pyd and Dpd) cross-links in plaques. They found that there is an increased Pyd: Dpd ratio in plaques versus normal vascular tissue. This observed difference in cross-links in the plaque may adversely affect tensile strength. There have been very few previous studies that have performed this type of research, and therefore may be used to open new doors into plaque vulnerability assessment. Goncalves et al (2008) studied the association between elastin and collagen with levels of the cysteine protease inhibitor cystatin C in human carotid plaques ex-vivo, using densitometry of western blots for cystatin C levels, and colorimetrically the levels of collagen and elastin. They found that there is a positive correlation between cystatin C levels and collagen (r=50, p=0.004) and elastin (r=0.58, p=0.001) levels in plaques. This finding demonstrates that cystatin C may play an important role in maintaining atherosclerotic plaque stability, and may be used in plaque vulnerability assessments. An in-vivo study performed by Megens et al (2007) evaluated the collagen in apolipoprotein E-/- mice. A collagen marker, CNA35, conjugated with fluorescent Oregon green 488 (OG488), was injected intravenously into the mice subject. Two-photon microscopy was then used for imaging. The study found that atherosclerotic plaques in apolipoprotein E-/- mice exhibited large uptake of CNA35/OG488. Histology was used to confirm the affinity of CNA35 for type I, III, and IV collagen in the arteries. Currently, there is no technique available for the non-invasive human study of plaque collagen contents.

2.5.4 Inflammatory Markers (Macrophage)

Inflammation plays an important role in the initiation, development, progression and complications of atherosclerotic vascular disease. It can therefore serve as a marker for plaque vulnerability assessment. An important inflammatory marker in the disease is macrophage cells. Macrophage cells play a key role in plaque rupture, and have therefore been the subject of many researches investigating their roles as markers in plaque vulnerability assessment. A vulnerability assessment study using macrophage cells as inflammatory markers was carried out by Shiomi et al (2001). They introduced a morphometric vulnerability index to quantify the level of plaque vulnerability. It was carried out by calculating the ratio of plaque area occupied by lipid components (macrophage and extracellular lipids) and by fibromuscular components (smooth muscle cells and collagen fibres). Tang et al (2008) demonstrated that there is an association between the degree of MR-defined inflammation, using ultra small super-paramagnetic iron oxide (USPIO) particles, and biomechanical stress, using finite element analysis (FEA) techniques, in carotid atherosclerotic plaques (p=0.009). USPIO particles have been shown to be taken up by macrophage cells 10-100 times more than other cells. However, due to the ethic issues of patient safety, this kind of study was not performed as common. Ogawa et al (2004) investigated the relationship between the uptake of ^{18}F-FDG and macrophages using PET imaging in Watanabe Heritable Hyperlipidemic (WHHL) rabbits. The study found significantly higher accumulation of ^{18}F-FDG in WHHL rabbits than those in the control subjects. In addition they found a strong correlation between ^{18}F-FDG uptake and the number of macrophages in WHHL rabbits (R=0.81). In conclusion the study showed that macrophages are responsible for ^{18}F-FDG accumulation in atherosclerotic lesions. Although this study was performed using

animal models, it formed an important basis for future research on humans. Arauz et al (2007) investigated the detection of carotid plaque inflammation by ^{18}F-FDG and PET, as used in the previous study by Ogawa et al (2004), however on human subjects. Arauz et al (2007) showed that variable degrees of inflammation in carotid plaques could be assessed in vivo by means of 18F-FDG and PET as a strong ^{18}F-FDG uptake was seen in 85% of carotid lesions studied. The study also showed that there was a significant correlation between ^{18}F-FDG uptake and the degree of ICA stenosis detected by angiography. Rudd et al (2007) further validated the potential clinical use of this method by testing the near-term reproducibility of ^{18}F-FDG-PET imaging of atherosclerosis. Rudd et al (2007) showed that spontaneous change in plaque ^{18}F-FDG uptake is low over 2 weeks, and has favourable inter- and intraobserver agreement. Due to the poor spatial resolution, this technique cannot provide the detailed local distribution of macrophages in a plaque, but it can provide background information. These studies show the extensive work carried out on plaque vulnerability assessments using inflammatory markers, and the potential clinical benefit which can be derived from it.

2.5.5 Stress

It is generally believed that maximal stress conditions may have a link to plaque rupture, and can be used for the vulnerability assessment of plaque (Hackett D et al). There are several factors that may influence the stress distributions in an atherosclerotic plaque including a) blood pressure; b) geometry of the plaque and vessel; c) plaque structure; and d) the material properties of the different plaque components. However, currently it is not possible to measure directly, either in vivo / ex-vivo, plaque mechanical stress. The information of plaque stress distribution was generated by a large number of computational studies based on anatomically realistic

model reconstructed from MRI images or histology images. Our research group in Brunel University plays an important role in plaque stress analysis both in-vivo and ex-vivo. Stress analysis based on MRI measured plaque morphology, can provide a guideline for plaque stress distribution in-vivo. However, due to the limited image spatial resolution of MRI, the simulation model can only identify the general features of a plaque. The detailed fibrous cap information, especially local collagen density, is currently not obtainable. One of the major research objectives of this PhD project is to generate plaque geometry at microscopic levels of precision, to assess the accuracy of the results of stress analysis based on MRI images.

2.6 Summary

The literature review has focused largely on the current understanding in plaque morphology, the hypothesis of plaque rupture mechanisms, the application of different techniques to conduct researches, and in plaque vulnerability assessment. It can be briefly summarized as:

- The development of an atherosclerotic plaque is best described by a classification system developed by Stary et al (1992) which categorises lesions into 8 different types; type I to VIII, each varying in its morphology and developmental stage.
- The morphology of atherosclerotic plaques has been extensively studied at both macro-level and at the molecular level.
    - At the macro-level, studies have indicated the important role played by collagen in both plaque growth and in maintaining the structural integrity of the plaque. The fibrous cap which overlays the necrotic core has been widely investigated and has been shown to be infiltrated with inflammatory cells which degrade the collagen making it prone to

rupture. Also at the macro-level, the size of the lipid core has been assessed, and the impact of lipid core to plaque rupture has been studied.

- At the molecular level, complex inflammatory pathways are present which influences both the development and progression of the disease. Extensive research has therefore been performed on inflammatory cells and proteolytic enzymes such as macrophages and MMP's respectively.

- Plaque morphology assessment can be performed either in-vivo or ex-vivo. For in-vivo methods, assessment has been carried out by using high resolution MRI; Ultrasound; Thermal imaging; Optical imaging; Optical coherence tomography; and functional imaging techniques. For the ex-vivo assessment of plaque rupture, studies have been carried out using MRI; 3D Ultrasound; Micro-CT; and by histological methods including conventional waxing and antibody staining techniques.

2.7 Research Hypothesis

The review also raises important fundamental questions and problems. Previous studies assessing plaque morphology at the microscopic level generally focused on a few transverse planes of a plaque specimen. However, the longitudinal variations of the plaque morphology also play an important role in plaque structure integrity. It has also been identified that previous studies were either analysing the collagen, lipid core size, or assessing inflammation of the plaque, but rarely combining these together. The following hypothesis are therefore proposed in the present study;-

1. If differences in plaque morphology are related to rupture vulnerability, then there may be a morphological difference between ruptured and non-ruptured atherosclerotic carotid plaques.
2. If there are differences in blood flow variations between the upstream and downstream regions of a plaque, which can influence gene expression and cellular function, then plaque morphology may vary longitudinal between rupture and non-ruptured plaques.
3. If macrophages in plaques release proteolytic enzymes which act to degrade collagen causing them to be more prone to rupture, and if there are blood flow variations in the upstream and downstream regions, then ruptured plaques may have a higher frequency of macrophages compared to non-ruptured plaques, and there may be variations in the different regions between the two groups.
4. Using ex-vivo ultrasound imaging techniques to scan plaque morphology may improve current risk assessment procedures on plaque rupture.
5. A combination of histology, ultrasound, FEM, and 3D modelling techniques may provide a solution to using high resolution analysis of plaque morphology to improve the clinical assessment of vulnerable plaques.

2.8 Aims and Objectives

A large amount of researches were performed in recent years investigating the mechanisms of rupture in order to derive indices on more accurate predictions of the rupture risk of a specific vulnerable plaque. Morphological studies of vulnerable plaque are the major source of information for our understanding of the problem. However, most plaque morphological studies were based on just several histology sections on plaque regions (Fagerberg et al 2010). There are rarely studies which

systematically analyse the morphological variation of a plaque along its longitudinal length with fine intervals between histology sections (Coombs B et al 2001). Due to the highly heterogenic nature of the distribution of plaque components, the results obtained from these studies may not reflect an accurate account of the plaque's morphology. Furthermore, the links between local biological activities, plaque morphology, and its dynamic environment (stress loading), were generally not included, and which would influence our understanding of rupture mechanisms.

Aim: The primary aim of this study is to therefore improve the understanding of the relationship between plaque morphology and rupture risk. The other aim of this study is to apply the information obtained and the technique developed in the first part to provide a solution using high resolution analysis of the plaque morphology, and to improve the clinical assessment of vulnerable plaques.

The main objectives to achieve the aim can be broken down as the following:

(a) To study plaque morphology at the micro-level and compare the morphology between the ruptured and non-ruptured plaques.

(b) To study the plaque macrophage content to determine its relationship with the morphology and compare between ruptured and non-ruptured plaques.

(c) To combine the findings from the plaque morphology analysis in (a), with the plaque geometry obtained from ultrasound assessment to reconstruct a high resolution patient-specific 3D-plaque model for plaque stress analysis purposes.

(d) To study the feasibility of using ex-vivo 2D ultrasound for plaque tissue characterisation to improve the risk assessment of vulnerable plaques.

Chapter 3

Methodology Development

This chapter will describe and analyse the methods and techniques used to conduct the present study. It will demonstrate in detail the procedure and highlight the scientific background behind it. The following chapters will then focus on the results and the findings of the specific researches, with a brief mentioning of the common methodologies. The techniques that were used for the specific parts of the study will not be introduced in this chapter, but will be described in the relevant chapters.

3.1 Histology

Histology is the study of the microscopic anatomy of cells and tissues of plants and animals, and has its first roots in the seventeenth century. It is carried out by examining a thin slice or section of tissue under a light microscope or electron microscope. The use of histological stains enhances the ability to visualise or differentially identify microscopic structures. Histology is an absolutely crucial tool of biology and medicine. The general steps that are involved in a typical histology process are **1)** chemical fixation with formaldehyde or other chemicals; **2)** tissue processing – dehydration, clearing and infiltration; **3)** wax embedding; **4)** sectioning; and **5)** staining. In the present study only the paraffin wax histology technique will be discussed, with no reference being made to frozen section histology (cryosection).

3.1.1 Tissue Processing

Before histology analysis takes place, the tissue specimen is required to be prepared for the procedure, which includes tissue fixation and dehydration.

Fixation: The specimen is washed thoroughly (approximately 4 times) in saline solution (0.9% NaCl). Samples are then placed and stored for fixation in a 20 ml solution consisting of 3.7% formaldehyde (18ml of distilled water and 2ml of 37% formaldehyde). The specimens are required to be kept in this solution for at least 4 days for full fixation to be completed. Once completed, the specimens can then be stored indefinitely for future uses, and will resist any degree of decomposition. The principle behind tissue fixation is for stabilisation, and is important for this type of anatomical study of biological tissue. To achieve stabilization, the decomposition caused by tissue enzymes (decay) must be arrested. Formaldehyde is a chemical fixative whereby 4% formaldehyde gas is dissolved in water or a buffer. This moderately toxic agent immediately starts to penetrate the tissue in the specimen and forms cross-link bonds between proteins, and inhibit enzymatic degradation. In addition, the cross-links between proteins harden the tissue. The problems that can be associated with formalin-fixation are the delay in the fixation, and the variations in the duration of the fixation. However, these can be resolved by starting the fixation immediately after surgical removal of the tissue (<30 minutes).

After removal from the formaldehyde solution, the specimen is then gently placed onto a clean ceramic tile to allow it to air dry for approximately 5 minutes. The fine edge of a scalpel is then placed on to the surface of a special tissue marking dye and then used to literally touch the surface on the specimen. Three of these tissue marking dye lines are made on the same specimen, in order to maintain the 3D orientation for each transversal 2D sections.

The specimen is then cut into 5mm segments along the longitudinal direction. Photographs of the specimen were taken on each end of the segment with the tissue

marking dyes. Each of the 5mm segments are then placed into tissue processing cassettes (figure 3.1(a)), and labelled with a block number to maintain the correct longitudinal sequence. The cassettes are then placed into a jar of saline (NaCl 0.9%), and transported to the tissue processor (figure 3.1(b)). This is an automated process to replace the water in the tissue by liquid paraffin wax. During the tissue process, the tissue processing cassettes are immersed in a series of progressively higher concentrated solutions of ethanol (IMS), to dehydrate the tissue, followed by xylene, and then finally hot liquid paraffin wax. A normal procedure can be as follows:

START: Histoclear → 70% IMS → 95% IMS → 100% IMS → 100% IMS → 100% IMS Histoclear → Liquid Paraffin Wax: **END**

This procedure takes overnight to be fully completed. During this 12 to 16 hour process, the liquid paraffin wax will replace the water in the tissue, turning it from an originally soft, moist tissue, into a sample that is homogeneous with paraffin wax. This enables a scaffold to form within the tissue at the cellular and extracellular matrix level, and therefore allows the sample to be sectioned into thin slices. Inadequate tissue dehydration prior to paraffin wax embedding may cause problems during the scaffold formation, which can be resolved by preparing the solutions freshly on a regular basis, depending on the volume of tissue processed. Generally, 10% shrinkage of the tissue volume can be expected after the dehydration process. The degree of shrinkage is different between different tissues. A post-processing image registration technique developed in this study known as finite element modelling may partially correct this non-linear structure distortion. Chapter 6 will provide a detailed description of the method.

(a) Tissue processing cassettes

(b) Tissue processor

Figure 3.1 Image of the (a) tissue processing cassettes containing segments of tissue which are then placed in to the (b) tissue processer

3.1.2 Wax Embedding

After the dehydration process, the histology cassettes (figure 3.1(a)) containing the specimens are removed from the tissue processor (figure 3.1(b)). They are then placed directly into the wax dispenser, which holds the molten wax at a thermostatically controlled temperature to perform the wax embedding. This wax dispenser would have been previously switched on, and left for approximately an hour so that the wax is in a molten form. A wax mould, filled two thirds with liquid wax is used. The specimen from the cassette is removed and then slowly placed into the wax mould containing the liquid wax, and at the same time, maintaining the correct orientation as shown in figure 3.2. Once it has slightly cooled (this is known when a thin skin is formed on top of the liquid wax), and the specimen is fixed at its location, the wax mould is then filled with liquid paraffin wax, and covered with the lid of the cassette. Further liquid paraffin wax is then poured on top of the lid of the processing cassette. It is then placed on a cold tray to cool and solidify, and then placed overnight in a cold room.

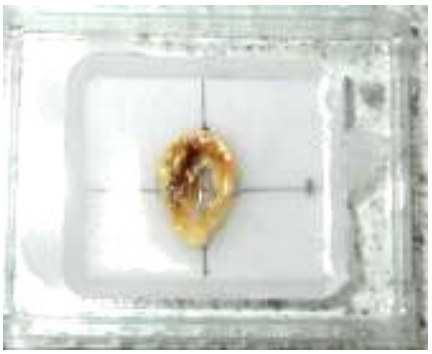

Figure 3.2 Specimen embedded in liquid paraffin wax

3.1.3 Sectioning

A bucket filled with ice is used to transport the wax blocks from the cold room to the microtome. The wax blocks are kept face down on the ice to maximise cooling. A sharp blade or scalpel is used to remove the wax surrounding the internal perimeter of the wax mould, to enable the histology cassette with the attached wax block containing the specimen to be removed from the metal wax mould easily. Once the wax mould has been detached, the wax block that is attached to the cassette is cut into a shape where there is no unnecessary wax surrounding the specimen. The wax block is usually cut into a diamond shape. This is done to prolong the life of the blade on the microtome. Once cut, the wax blocks are placed face down on the ice tray for cooling, ready to be sectioned.

Sectioning Procedure:

1. The wax block is carefully secured onto the microtome. The cutting thickness is initially set at 30 microns so that the excess wax can be quickly removed. After removal of the excess wax, the specimen is reached. This is known once sections of tissue start to appear in the wax strips. The sectioning thickness on the microtome is then reset to 6 microns.

2. The wax block is then sectioned by generating a ribbon which contains 5 tissue sections that are each attached to one another. The ribbon is gently placed using a set of tweezers in to a water bath. It is then separated into its individual components using the tweezers. APES coated microscope slides are used to gently pick up the individual segments and are then kept aside.
3. The microtome is then reset to cut at a thickness of 30 microns, and is applied to the subsequent 30 sections. This segment of tissue is discarded, and the microtome is then reset to section at 6μm thicknesses to enable the subsequent ribbon (containing the 5 sections) to be generated.
4. Steps 2 to 3 were repeated until the end of the wax block was reached.

This procedure will provide 5 sections representing the same longitudinal location (or a station) with a 0.9mm interval between the stations. To perform high resolution tissue analysis for certain cases, the length of the tissue segment that is discarded, was reduced to obtain tissue sections at shorter longitudinal intervals along the length of the plaque for detailed analysis of the specimen. The slide is then labelled and placed onto the hotplate for drying. For the 5 sections, one was stained using hematoxylin and eosin (H&E) for general morphological analysis; two were stained with picrosirius red and counter-stained with hematoxylin for collagen analysis; the forth was stained with CD68 for macrophage analysis, and the fifth section was reserved for future use. The figure below (figure 3.3) shows the microtome that was used for this investigation.

Water Bath Condition

Paraffin wax sections cut using the microtome were floated onto a warm water bath set at a temperature of 37ºC to allow it to stretch and remove any creases. An aim of

the present study is to detect fibrous cap rupture at specific sections, it is therefore important to ensure that a fissured fibrous cap is not caused by histology processing (or artefact). The control of the water bath condition for the stretching is crucial to avoid any of these artefacts. Initially, to provide an optimum stretch of the section, a water bath mixed with alcohol was used. However, this resulted in large amounts of collagen fibre damage. When the alcohol was removed from the liquid in the water bath, there was no further damage. The other possible factor which may cause over stretching or damage of the section is the water bath temperature. To ensure the water bath temperature was calibrated correctly, a test was performed to validate this, and it was found to be reliable. In addition, the test results also showed that paraffin wax sections will not overstretch unless the water bath temperature is above 60ºC. Further details of which can be found in the appendix (2.0).

Figure 3.3 Image of a microtome

3.1.4 Apes Coating Slides

To prevent histology sections from washing-off the microscope slides, due to the harsh treatments that are encountered during the staining process, the microscope glass slides are coated with 3-AMINO PROPYL TRIETHOXYSILANE (APES) to make it positively charged and adhesive to the tissue sections (figure 3.4). To perform

this procedure the microscope slides are placed in a rack (approximately 50 at a time) and are immersed in a series of 4 solutions.

- 90% IMS for 5 minutes
- 3% 3-AMINOPROPYLTRIETHOXYSILANE for 30 seconds
- Acetone for 1 minutes
- Distilled Water for 1 minutes

3.1.5 Staining Protocols of Paraffin Wax Sections

A rehydration process is required to be performed before staining the sections. The different IMS solutions used require constant changing to enable the quality of the solutions to be kept at an optimum level, to ensure the rehydration and dehydration process are carried out effectively. If a stain is constantly used to stain tissue, particles of artefacts may remain afloat within the staining solution and cause disruption to the final image quality. To prevent this from occurring, stains are filtered through a special filtering system so that the quality is maintained. Staining can be carried out on sections that have been processed by chemical fixation. The aim of the staining procedure is to reveal the cellular components, and the counter-stains are used to provide contrast.

Hematoxylin and Eosin (H&E) Staining

The hematoxylin and eosin staining process is composed of two parts. Firstly, the hematoxylin component colours the basophilic structures with a blue-purple hue. The basophilic structures are usually structures that consist of nucleic acids, such as ribosome's, chromatin rich nucleus, and the cytoplasmic regions rich in RNA. The molecular structure of a hematoxylin molecule is shown below in figure 3.4.

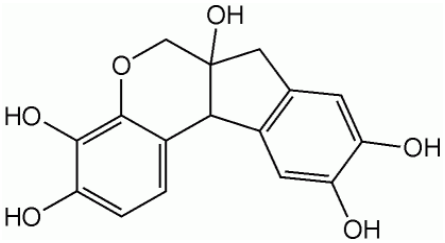

Figure 3.4 Molecular structure of a hematoxylin molecule

The alcohol-based acidic eosin component colours the eosinophillic structures bright pink. Eosinophillic structures are generally composed of intracellular and extracellular proteins. Examples of eosinophillic structures include Lewy bodies and Mallory bodies. Lewy bodies are abnormal aggregates of protein that develop inside nerve cells in Parkinson's diseases (PD) and Alzheimer's disease (AD), and some other disorders. Mallory bodies are inclusions found in the cytoplasm of liver cells and are classically found in people suffering from alcoholic liver disease. The majority of cellular cytoplasm is composed of an eosinophillic nature. Red blood cells for example are stained intensely red. Structures do not necessarily have to be either acidic or basic to be termed basophilic or eosinophillic. The terminology used is based upon the affinity to the dyes. The molecular structure of an eosin molecule is shown below in figure 3.5.

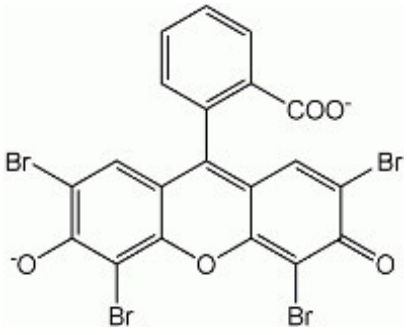

Figure 3.5 Structure of an eosin molecule

Staining Procedure:

1. **Pre-processing:** The slides containing the paraffin sections were firstly placed in a slide holder (glass or metal). The slide holder is then immersed in xylene for 10 minute to deparaffinise the sections.
2. **Re-hydration:** The slides need to be re-hydrated, and are placed in 100% IMS for 5 minutes, 90% for IMS 2 minutes, and 70% for IMS 2 minutes.
3. **Hematoxylin staining:** The slides are placed in distilled or de-ionised water for 5 minutes, and then in Hematoxylin for 5 minutes. Following this, the slides are then immersed in acid alcohol for 2-3 seconds to differentiate the tissue section from its background by removing any hematoxylin from the slide adhesive to produce a clear transparent background. The slide holder containing the sections is then run in cold water for 5-10 minutes until the sections were blued, and to allow the stain to develop.
4. **Eosin staining:** Sections are then counter-stained with eosin for 2 minutes.
5. **Dehydration:** The section finally has to be dehydrated in 90% IMS for 1 minute, 100% IMS for 1 minute, and then 2 changes of xylene for 2 minute and 7 minutes respectively for clearing.
6. **Applying cover-slip:** A drop of a xylene based mounting medium is placed onto the slide using a pipette, and is performed without leaving any air bubbles. The cover slip is then gently placed onto the slide. The xylene based mounting medium is allowed to spread beneath the cover slip, covering the entire tissue section.

Van Gieson

Van Gieson stain is composed of a mixture of picric acid and acid fuchsin. This staining method is used for the differential staining of collagen and other connective

tissues. It was first discovered by Ira Van Gieson. The formula for making the Van Gieson stain is by adding 100mL of saturated aqueous solution of picric acid to 5mL of 1% aqueous solution of acid fuchsin. When acid fuchsin is used in conjunction with picric acid, it produces the Van Gieson stain which demonstrates the collagen fibres in a red colouring.

General Procedure:

After the conventional deparaffinise and re-hydration steps as described in the H & E staining:

3. **H-stain:** The slides are immersed in 0.1M HCL for 1 minute and then in the Hematoxylin stain for 20 minutes followed by a wash in cold running water for a further 5 minutes.
4. **Van Gieson:** The sections are then placed in de-ionised water and then stained with Van Gieson for 5 minutes. Following this, the sections are washed in a beaker of solution that contains water and a few drops of 0.1 HCL. The sections are then rinsed in 90% alcohol for 3 minutes before it is dehydrated.

It is then followed by the conventional steps of dehydration and cover-slip application as described in the H & E staining procedure.

Picrosirius Red with Hematoxylin

Picrosirius red staining is another method to reveal collagen structure in tissue. Viewed under polarised light microscopy, the picrosirius red staining provides an improved differentiation of collagen structure from the other structures. In addition, it can provide collagen fibre orientations. In certain cases, it can distinguish between the different types of collagen. Picrosirius red staining was first discovered in 1979 by L.

C. U. Junqueira (Junqueira et al 1979). It is a strong anionic dye which reacts with collagen via its sulphonic acid groups, the basic groups present in the collagen molecule. Picrosirius red is an elongated molecule that attaches to the collagen fibres in a way that enables their long axis to be parallel. It is this basis of a parallel relationship that results in its birefringence properties. Studies (Junqueira et al 1979) have shown that there is an increase of at least 700% in the light intensity due to the birefringence of the collagen stained by picrosirius red, when compared to control slides that have only been stained with saturated picric acid.

The staining procedure is similar to the H & E staining for steps 1, 2 (re-dehydration) and steps 5 and 6. The difference in the Van Gieson procedure is;

3. The slides are placed into the picrosirius red stain for 1 hour, before being rinsed in cold running water for 2 minutes.
4. It is then counterstained with hematoxylin for 1.5 minutes. The slides are rinsed in cold running water for 5 minutes, and then immediately immersed in acid alcohol for 3 seconds, before being placed in cold running water for a further 4 minutes.

To reveal the fibrous structure of collagen, sections stained with picrosirius red are required to be examined under polarised light microscopy (see section below).

Polarised Light Microscopy

Light is an electromagnetic radiation with its electric and magnetic components oscillating at right angles to each other, and also in the perpendicular direction of its wave propagation. When the directions of oscillation are brought into order, the light is defined as being of a polarised nature. A linear polarizer is a device that operates by dichroism. Apart from the components laying on the direction of the smallest

absorption, the linear polarizer absorbs to a much greater degree all the components of the electric wave field. As a result of this, only one direction of oscillation passes through it, and the light that emerges from the polarizer is known as linearly polarized.

A microscope equipped with a pair of special lens, which is able to reveal the presence of collagen, is called a polarised light microscope. The lens at the bottom is called a polarizer and the second lens is called an analyser (figure 3.12). The polarizer and analyser are arranged with their polarizing axis to be perpendicular. Therefore, no light can be seen from analyser if there is nothing in between them.

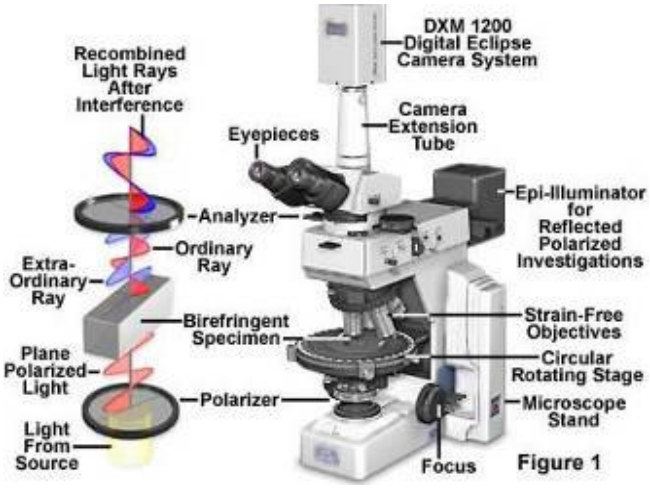

Figure 3.6 Configuration of a light polarizing microscope

The microscope slides stained by picrosirius red was placed on the circular rotating stage between the two lenses, and subjected to polarised light. The birefringence properties of the stained collagen fibres changes the electric oscillation angle, which results in enhanced light passing through the analyser, and an enhanced structure being seen.

The image is captured digitally on a SP-300 Olympus camera. By adjusting the slides orientation, tissues with birefringence properties such as collagen structures were

visible. Figure 3.7 shows a histological transverse cross-section stained with picrosirius-red under a normal microscopy set up (a), with the corresponding image captured as a polarised light image (b). This birefringence behaviour confirms the presence of normal non-degraded collagen.

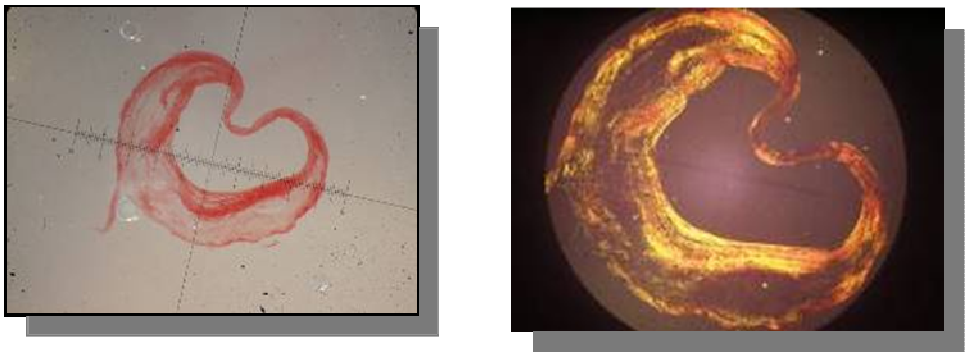

(a) **(b)**

Figure 3.7 Panel (a) picrosirius red stained transverse cross-section of an atherosclerotic plaque; panel (b) the corresponding image captured under polarised light

3.1.6 Staining Protocols of Immunohistochemistry

In comparison to conventional histology analysis which reveals the general tissue structures, immunohistochemistry or IHC is able to provide the distributions of a specific type of tissue component in the section accurately. IHC is a process in which antigens are localised on cells of a tissue section using the principles of antibodies binding specifically to antigens in biological tissues. The procedure is used in basic research to understand the distribution and localisation of biomarkers and differentially expressed proteins in different parts of a biological tissue. The antibody-antigen interaction can be visualised in a number of ways. One of the ways is when the antibody is conjugated to an enzyme such as a peroxidase. This enzyme can catalyse a colour producing reaction that enables the site of the antibody-antigen reaction to be visualised. Alternatively, the antibody can be conjugated to a fluorophore such as fluorescein.

Antibodies used to detect specific antigens can be either of two types; polyclonal or monoclonal. Monoclonal antibodies have a greater degree of specificity in the antigens that they bind. Polyclonal antibodies are generated by injecting animals with a peptide (Ag). After this has been injected, it results in the stimulation of a secondary immune-response which causes an array of antibodies to be produced. This is then isolated from the whole serum. From this it can be seen that polyclonal antibodies are a heterogeneous mix that are able to recognise a wide variety of epitopes. Antibodies can also be categorised into two different types; primary or secondary reagents. Primary antibodies are generated against an antigen of interest and are in most cases un-conjugated or unlabelled. Secondary antibodies are generated against primary antibodies. The concentration of the protein can be measured by densitometry analysis where the intensity of the staining is correlated with the amount of the protein of interest.

The immunohistochemical detection of antigens in tissue can be carried out using either the direct method or the indirect method. In both cases, many antigens need to be unmasked as it can make the difference between whether staining takes place or not. The direct method is a one-step staining method, and is carried out using a labelled antibody (e.g. FITC conjugated antiserum), which reacts directly with the antigen of interest in the tissue sections as shown in figure 3.8. The direct method only requires the use of a single antibody and is therefore very simple to implement. However, the quality of the result can be reduced by the lack of sensitivity due to low signal amplification, and it is therefore not commonly used in laboratory practices.

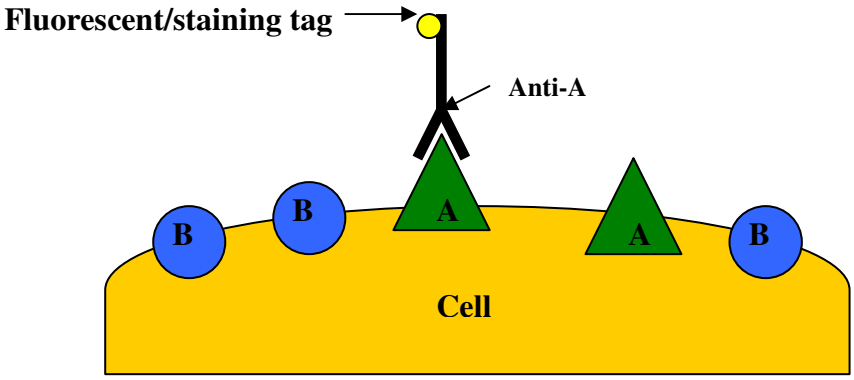

Figure 3.8: Demonstrates the detection of tissue antigen using the direct method

The indirect method involves an unlabelled primary antibody (first layer) which binds to the tissue antigen, and then a secondary labelled antibody (second layer) which binds with the primary antibody (first layer) as shown in figure 3.9. Compared with the direct method, the in-direct method is more sensitive due to the signal amplification caused by numerous secondary antibody reactions with different antigenic sites that are found on the primary antibody. The secondary antibody or the second layer is usually labelled with a fluorescent dye or an enzyme. Most commonly, the secondary antibody is conjugated with a Streptavidin-horseradish peroxidase. This enzyme reacts with 3, 3'-Diaminobenzidine also known as DAB to produce a brown colouring wherever the primary-secondary antibody interaction has taken place. Another advantage of the indirect method is that only a small number of standard conjugated secondary antibodies are needed to be generated. For example, a secondary antibody that has been labelled, and has been raised against rabbit IgG can be used with any primary antibody that has been isolated from rabbit. The direct method, however, requires custom made labelled antibodies for every antigen of interest and is less cost effective.

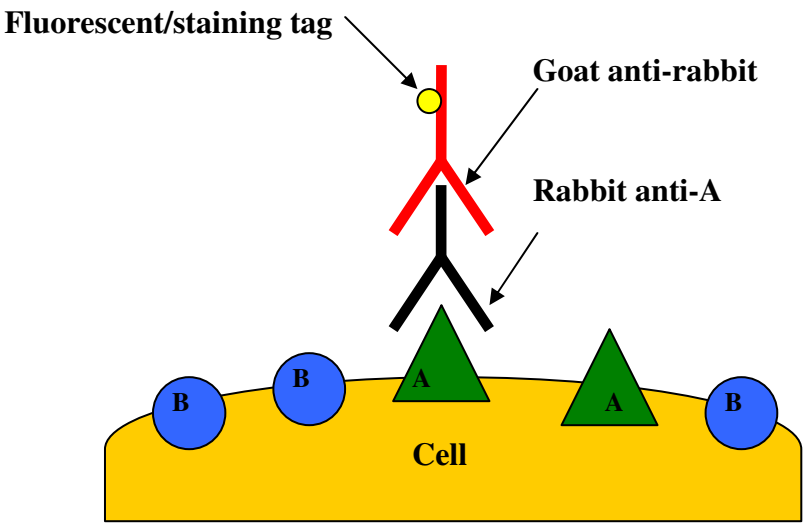

Figure 3.9 Demonstrates the detection of tissue antigen using the indirect method

Based on the scientific background for the two methods and its associated benefits, the present investigation used the indirect method for the analysis, as it has a higher level of sensitivity.

Macrophage Antibody Staining

Immunohistochemical techniques are used in this study to investigate the distribution of macrophages in advanced plaque. Intra-plaque macrophages are normally derived from blood-monocytes. Blood monocytes are young cells that have migratory, chemotactic, pinocytic and phagocytic activities. They also possess receptors for IgG Fc domains (FcR) and iC3b complement. Upon migration into tissues, monocytes undergo a process of differentiation to become multi-functional tissue macrophages.

For research purposes, it is important to differentiate cells of the monocyte/macrophage lineage. There are a wide range of human antibodies that are available to localize the different sub-population of macrophages in tissues of human origin (Waldo et al 2008). Some important antibodies available for staining human macrophage include AIF-1, CD163, CD68, Clone YTH 8.18, Clone MAC387, Clone

RFD7, Clones PM-2K, X-4 and X-14. Each antibody stains for a specific lineage of differentiated monocyte/macrophage cells. For example the CD163 antibody is a membrane glycoprotein on human monocytes and macrophages which is expressed in the intermediate and late phases of inflammation. The antigen is also a member of the scavenger receptor family. Clone YTH 8.18 is reactive with all tissue macrophages, binding to a cytoplasmic epitope. In peripheral blood the antibody stains all granulocytes and around 50% of monocytes, however it does not stain osteoclasts or Langerhans cells.

For this study, CD68 antibodies are used to stain for the macrophage lineages found in human atherosclerotic plaques. The CD68 macrophage antibody used in this study is a 110-kd transmembrane glycoprotein of unknown function, and which is highly expressed by human monocytes and tissue macrophages. This macrophage marker is also expressed in monocytes and epidermal dendritic cells. It is a selective marker for human myeloid cells. The CD68 antibody is also a haematopoietic differentiation marker of the monocyte-macrophage lineage. Further to this, it is a specific oxidised-low density lipoprotein (Ox-LDL) binding protein in human monocyte-derived macrophages.

Prior to the CD68 macrophage antibody staining, the paraffin histology section is required to be subjected to a proteinase K treatment procedure. This is because during tissue fixation, using the formaldehyde solution, protein cross-links are formed that mask the antigenic sites in the tissue. Therefore any immunohistochemical detection of certain proteins would result in weak or false negative staining. The proteinase K solution breaks the protein cross-links, and exposes the antigens and epitopes in fixed

tissues resulting in the enhancement of the staining intensity of antibodies. After this step has been carried out, the following step can then be performed.

Endogenous peroxidise activity was neutralised by using the Novocastra Peroxidase Block. This was followed by the application of the Novocastra Protein Block to reduce the non-specific binding of primary and polymer. The section was subsequently incubated with the optimally diluted primary antibody (CD68). The Novocastra Post Primary Block was used to enhance the penetration of the subsequent polymer reagent. The Novolink Polymer recognises both mouse and rabbit immunoglobulin's, it detects any tissue bound primary antibody. Sections were then further incubated with the substrate /chromogen, 3, 3'-diaminobenzidine (DAB), prepared from Novocastra DAB Chromogen and Novolink DAB Substrate Buffer (Polymer). The reaction with the peroxidase produces a visible brown precipitate at the antigen site of the macrophage as shown in figure 3.11. The sections were then counter-stained with Novocastra Hematoxylin and coverslipped.

The following steps were carried out for the CD68 macrophage antibody staining:-

1. Sections cut and mounted onto slides coated with a tissue adhesive (APES)
2. Sections were de-paraffinised in xylene
3. Sections rehydrated through graded alcohol
4. Slides washed in running tap water
5. Antigen retrieval
6. Slides washed in de-ionised water
7. Endogenous peroxidase neutralised using peroxidase block (5 minutes)
8. Washed in TBS for 2 x 5 minutes
9. Incubated with protein block for 5 minutes

10. Washed in TBS for 2 x 5 minutes

11. Incubated with optimally diluted primary antibody (15 minutes)

12. Washed in TBS for 5 minutes

13. Incubated with Post Primary Block for 35 minutes

14. Washed in TBS for 2 x 5 minutes

15. Incubated with Novolink^{TM} Polymer for 35 minutes

16. Washed in TBS for 2 x 5 minutes with gentle rocking

17. Peroxidase activity developed with **DAB working solution** for 5 minutes

18. Slides rinsed in water

19. Sections counterstained with hematoxylin

20. Slides rinsed in water for 5 minutes

21. Sections were dehydrated, cleared, and mounted.

3, 3'-Diaminobenzidine (DAB) Solution

A key stage during the CD68 staining procedure is the DAB working solution preparation. Since DAB is a major step in the protocol to produce the brown colour and in the final staining quality; it is therefore mentioned here the detailed steps involved in generating the solution and its chemical composition.

3, 3'-Diaminobenzidine (DAB) is an organic compound and is a derivative of benzidine. Benzidine is a precursor to polybenzimidazole fibre. It is a water soluble tetra hydrochloride, and is therefore suitable for used during immunohistochemical staining of nucleic acids and proteins. This chemical compound is formulated by reacting 3, 3'-dichlorobenzidine and ammonia with a copper catalyst at high temperature and pressure, followed by acidic workup. The resulting chemical compound is shown in figure 3.10. 50ul of DAB chromogen was added to 1ml of

NovolinkTM DAB Substrate Buffer (Polymer), and was used within 6 hours of preparation. The final step is the visible appearance of a brown precipitate at the antigen site caused by the reaction of the peroxidase with the 3, 3'-Diaminobenzidine (DAB) (figure 3.11).

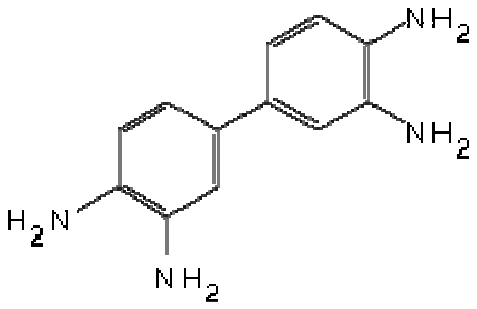

Figure 3.10: The molecular structure of 3, 3'-diaminobenzidine

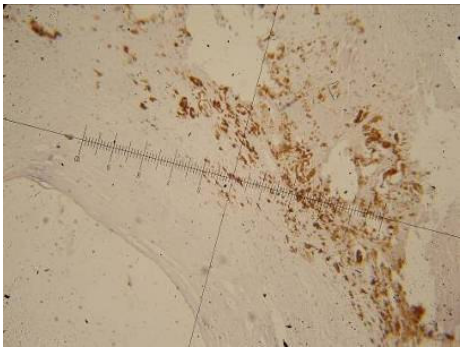

Figure 3.11 Visible brown precipitate at the antigen site caused by the reaction of the peroxidase with the 3, 3'-diaminobenzidine (DAB)

3.2 Land Mark System Maintaining 3D Orientation of Histology Sections

A major objective of this study is to reveal the 3D distribution of collagen and macrophage throughout the arterial plaque. Although histology sections provide high resolution images of the plaque structure in the transverse plane, the 3D relationship between the sections are lost during the processing. This is the major hurdle of applying the 2D histological images to reconstruct 3D tissue structure. By analysing

the histological procedure, there are several main steps which will contribute to the problem listed:

1. To perform tissue processing, specimens are cut into 5mm segments and placed into histology cassette holders, and then placed into a tissue processor for processing. During tissue processing, the 5mm segments are subjected to physical movements within the histology cassette holders, resulting in the downstream/upstream sides of the segments being difficult to distinguish. In addition, non-uniform tissue shrinkage also occurs during tissue processing. The final result of this is that the 3D relationship between the segments is lost, making 3D reconstruction virtually impossible.
2. There are further problems when placing segments into wax moulds for embedding into the paraffin wax, as the circumferential orientation relationship between tissue segments is lost.
3. During sectioning, the relationship between the circumferential orientations for subsequent tissue sections is also lost.

In the present study, we therefore developed a procedure to address the above identified problems to generate an accurate reconstruction of a 3D plaque model. The following sets out the procedure that was used to achieve this.

1. The 3D orientation of the vessel is maintained by applying tissue marking dye along the longitudinal direction of the plaque as demonstrated in figure 3.12, to provide coordinate links for each segments.
2. The carotid artery is cut into 5mm segments, with photographs being taken on both sides of each segment. The segments were then put into histology cassette holders for tissue processing.

3. Before the segments were embedded into liquid paraffin wax and allowed to set, a paper with a cross marked in the centre is placed at the bottom of the wax mould to enable the cut segment to be accurately positioned
4. The line marked by the tissue marking dye on the cut segment is aligned at zero degree to a reference point on the grid (figure 3.12).
5. After the wax embedding procedure, the wax block is sculptured into a triangular shape, with one corner being aligned to the reference point on the grid.
6. Sections are then cut at 6µm thickness and placed on an APES coated microscope slide.
7. Using a glass inscriber, a cross is inscribed onto the microscope slide at the corner used for the reference point. The reference point is used as a guide to maintain the 3D vessel orientation (figure 3.12)

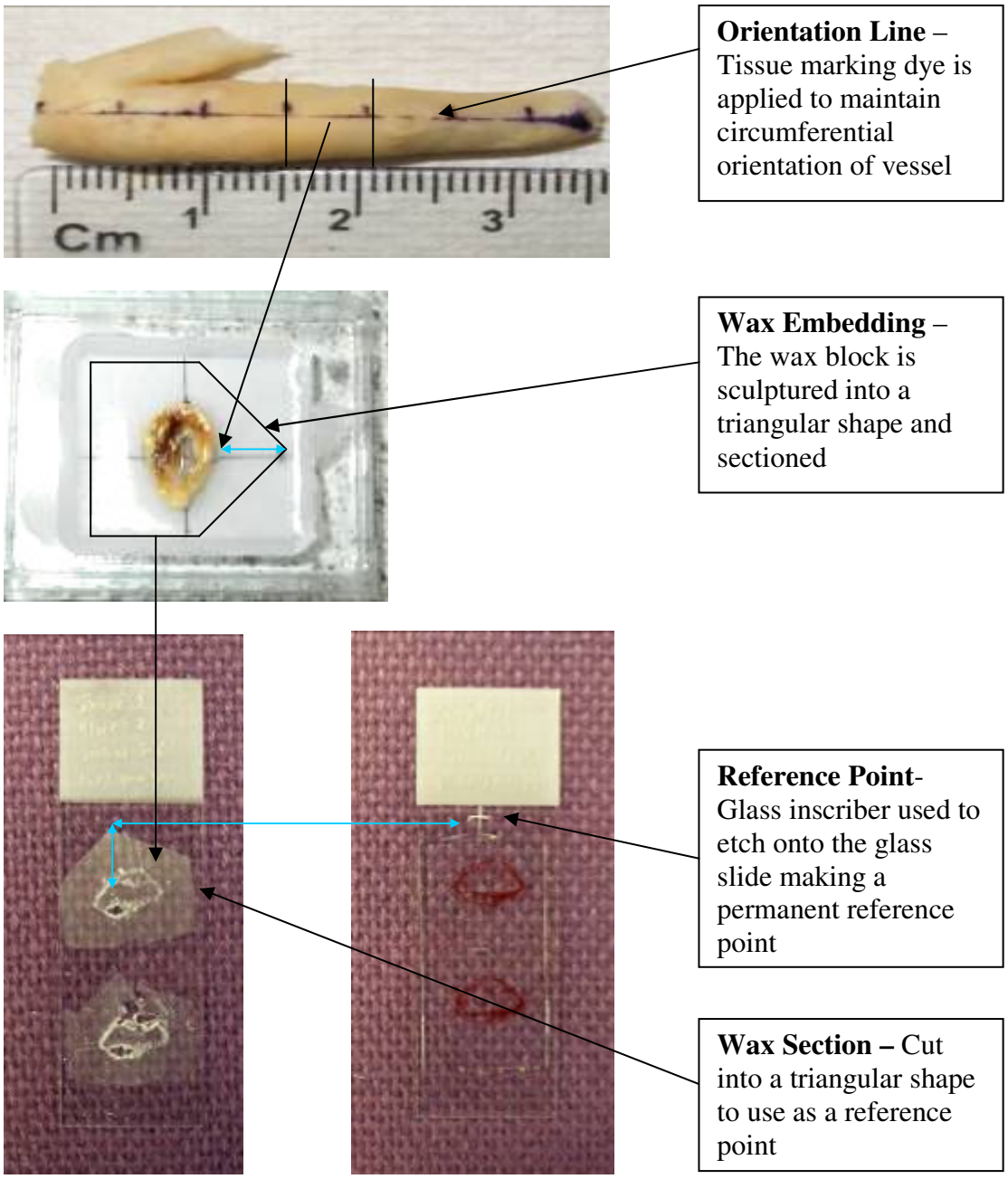

Figure 3.12 Demonstrates the method used to maintain the 3D orientation of the sections

The triangular shaped paraffin wax section is used as a reference point to inscribe the cross onto the microscope slide. This procedure is carried out because the use of xylene during the staining procedure, removes the paraffin wax that surrounds the tissue from the glass slide, and this would consequently remove the reference point

used for the orientation purpose. Making a mark on the microscope slide using a glass inscriber maintains the reference point permanently (figure 3.12).

3.3 Histology Image Restoration Based on Finite Element Method

After aligning the 2D sections into a 3D stack, it would then be possible to create a 3D geometry of the plaque. However, to perform an accurate 3D reconstruction, another major problem is required to be overcome. The plaques structure is subjected to distortions caused as a result of the dehydration process during tissue processing. These distortions are non-uniform and tissue dependent. A finite element method (FEM) based image registration procedure was adopted to correct the distortions to its original geometries before tissue processing in the 2D histological slides. The basic registration procedure is as follows:

1. An ultrasound scan of the specimen is performed before histological analysis to provide accurate outer and inner boundary of the specimen.
2. Histology sections are correlated to the corresponding ultrasound images by using the land mark system developed in the previous section (figure 3.12).
3. The 2D section images are segmented into different regions for the plaque components, such as collagen, lipid, calcifications, and intermediate (mixture of fibrous tissue and lipid).
4. FEM meshes are generated in the 2D section images, and are assigned different mechanical material properties for the different regions.
5. A starting point is required to be found on both inner and outer walls of the artery (plaque) for both ultrasound and 2D section image for each section based on certain landmarks. The outer wall contour is then uniformly divided

into 500 points and inner wall contour into 200 points, on both ultrasound and histology images.

6. The corresponding boundary points from the histology image are mapped to the ultrasound image, resulting in the distorted boundaries of the histology image being extended to the original position, as measured by the ultrasound scan. Following the point movement of the boundary, the internal points are moved to a new position based on the FEM simulation and the assigned mechanical material property (the Young's Modulus and Poisson's Ratio). The final location of the plaque components should be near to their original locations before it was subjected to distortions during tissue processing.

The FEM technical part of the procedure was developed by a colleague in the research group, Mr. Michael Luppy. As a joint developer, I contributed the biological part of work, and applied the procedure to analyses the assessment of the histology distortion on the plaque specimen.

3.4 3D Reconstruction in SolidWorks™

The following steps are involved in the 3D reconstruction of the carotid plaque vessel using the computational aid design (CAD) software SOLIDWORKS™.

Assign z-value for each 2D histology image: The required number of parallel planes is created using the segmented images, and the distance between them is required to correspond with the axial coordinate of the ultrasound section using the software 4Dview. For example, if the first US image was taken at the coordinate z = 3 mm, and the second at the coordinate z = 5.6 mm, the distance from the plane 1 and the plane 2 in the SolidWorks model is required to be d = 5.6 – 3 = 2.6 mm.

Segmentation of 2D images: The in-plane 2D geometry of each section is drawn on the correspondent plane. Using the macro-files written automatically in Matlab 7.0, the manually marked points created during the segmentation process are plotted on to the sketch. The reference point is not plotted, but is used to assure the alignment of all the 2D slices by translating the points from each section according to the reference point, and is in the coordinate (0,0,z).

Increasing wall thickness for adventitia layer to be included: During the endarterectomy surgery, only the intima and the media tunicae are excised from the carotid artery of the patient, however for simulation purposes the adventitia tunica needs to be incorporated into the model, and therefore the thickness of the artery wall is artificially increased to include this layer to be used in the CFD (Computation Fluid Dynamics) and the stress/strain analysis. The thickness of the arterial wall is required to be at least 1 or 1.2mm in the model.

Vessel extension to build bifurcation: Geometrical extension is applied to the model on the internal carotid artery (ICA), external carotid artery (ECA), and common carotid artery (CCA). The CCA is elongated by 2cm, the ICA by 1.8cm, and the ECA is artificially generated as it is not present in the specimen. The procedure is carried out to enable fluid dynamic simulations to be possible in future studies.

3D surface lofting: The 3D geometry is reconstructed using the 2D images stack. Loft functions available in SolidWorks™ are used to generate the arterial wall; the luminal and the lipid-core 3D geometry. The geometries of the lumen and lipid-core are very complex, and can be difficult to understand during the generation of the loft geometries. In addition, abrupt changes in the curvature angles could be generated due to inaccurate geometry coordinates, resulting in a geometry that is difficult to

mesh in AnsysWorkbench. In these circumstances, a manual correction of the 2D geometry was required to make meshing of the 3D model possible.

Minor modification on 2D images: The 2D-slices were corrected if the surface lofting was not possible to generate, or the geometry of the lumen and lipid was irregular. This could have led to problems during the CFD simulation and in the FEM during the meshing. Minor changes were made to the 2D sections, till the 3D geometry was considered to accurately replicate in-vivo vessel geometries. Meshing or computational problems were less likely to occur if the surface of the lipid and lumen was smooth. Abrupt changes between the geometry of two subsequent 2D sections creates computational problems during the FEM simulations, therefore modifications were made to the geometries in the stack to elude any problems in generating the mesh in the FEM simulation, and computational errors in the CFD analysis.

3.5 Plaque Morphology Assessment

3.5.1 Collagen Distribution Analysis

The quantification of the collagen content, and the thickness of the fibrous cap and lipid core were measured using an in-house designed programme using the MATLAB software package. For each subsequent transverse section where there was the presence of a plaque, manually placed points were marked circumferentially on the fibrous cap. The software then placed a set number of line profiles (approximately 20) perpendicularly to the fibrous cap as shown in figure 3.13. To remove elements of bias during the placing of the line profiles, the software is used to perform this action automatically. Along the line profile, a manually placed point was first marked on the fibrous cap-lumen boundary; a second point was marked on the fibrous cap-lipid core boundary, and a third point was then place on the lipid core-outer wall boundary as

indicated by the red circles shown in figure 3.13. The pre-defined calibration of the scale using a special graticule enabled the software to automatically measure the distance between the manually placed points. Using this method we were able to measure the fibrous cap thickness, and the lipid core thickness. The collagen content was quantified by calculating the pixel intensity level of each individual pixel along the perpendicularly placed line profile. This enabled us to correlate the data with the corresponding image on a micro-level to define a collagen threshold level. The non-collagen material was calculated and used to give us an overall percentage of the collagen content in the specified region. This method was applied at 15 and 20 equally distributed regions of the fibrous cap, and was applied to all the cross-sections throughout the longitudinal length of the plaque.

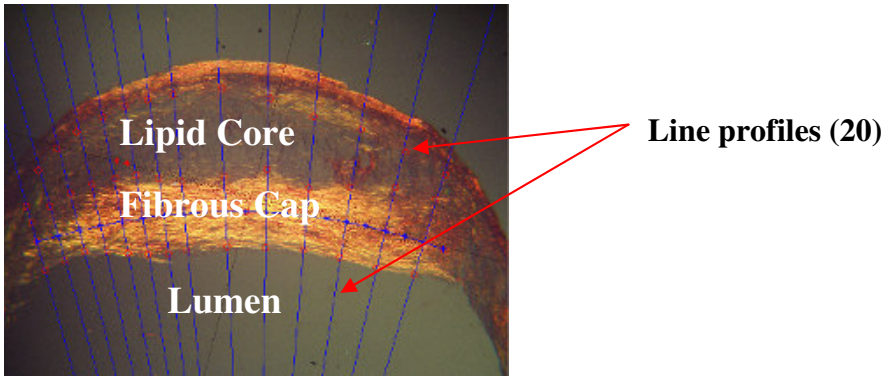

Figure 3.13 Image showing perpendicularly placed lines (software generated) on the atherosclerotic plaque to measure a) the collagen content; b) the fibrous cap thickness; and c) the lipid core thickness

3.5.2 Measurement of the Collagen Content in the Upstream, Throat, & Downstream Regions of the Fibrous Cap

For each plaque specimen, the mean collagen content was first calculated using the 20 perpendicularly placed lines across the fibrous cap for each transverse section. All transverse sections upstream, within (maximum stenosis), and downstream of the

maximal degree of stenosis were classified as upstream, throat and downstream regions respectively as shown in figure 4.3.

3.6 Macrophage Distribution Analysis (Area)

The images of the anti-CD68 stained transverse section were first digitized using a digital camera (Olympus SP350) at a magnification of 40X. Images were uploaded onto an in-house designed programme using the MATLAB software package. The following components were segmented for our study purposes; a) the outer wall; b) the luminal wall; and c) the macrophage aggregation areas. Segmentation was carried out by visual interpretation by marking the boundary of the individual components with manually placed points (figure 3.14). Each point configures to a set co-ordinate, and the combination of points would define the component segmented with reference to size and location, and is electronically stored in file.

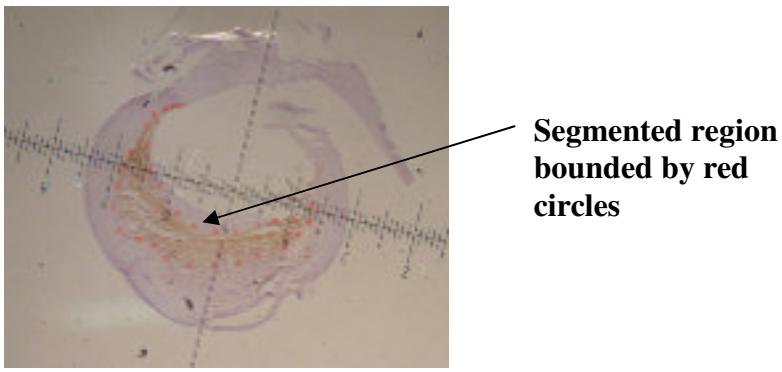

Figure 3.14 Section of an atherosclerotic vessel showing the segmented macrophage (CD68) stained region bounded by the red circles

3.7 Data Analysis

We used the non-parametric unpaired Mann-Whitney U test for the comparison of two independent random samples (x and y). We used this statistical hypothesis test because it enables the assessment of whether one of two samples of independent observations tends to have a larger value than the other. p=0.05 (two-tailed) was set

as the lowest level of significance to justify a claim of a statistically significant effect.

It is defined as:

$$U = n_1 n_2 + \frac{n_2(n_2+1)}{2} - \sum_{i=n_2+1}^{n2} R_i$$

- where samples of size n1 and n2 are pooled and Ri are the ranks

3.8 Summary

In this chapter the following techniques shown in the table below were described in detail, and will be used in the chapters shown, highlighted by the red mark.

TECHNIQUES	CHAPTERS OF THE THESIS						
	1	2	3	4	5	6	7
Histology				*	*	*	*
Immunohistochemistry					*		
Land mark system for maintaining the 3D orientation				*	*	*	
Histology image restoration based on finite element method						*	
3D reconstruction of the plaque model in solid works						*	
Plaque morphology assessment				*			
Macrophage distribution analysis					*		

Table 3.1 Summary of the techniques described and the chapters of this thesis that it will be implemented in

Chapter 3 Methodology Development

Table 3.1 provides a summary of the techniques used for the individual chapters of this thesis. It shows that certain techniques were used in multiple chapters such as histology, whilst other techniques such as immunohistochemistry were specific for individual-chapters.

Chapter 4

Atherosclerotic Plaque Morphology Analysis with Emphasis on Collagen

4.1 Introduction

Collagen is the primary structural component in the fibrous cap of plaques and gives it its biomechanical strength. The collagen content in the fibrous cap is important in the vulnerability assessment of plaque rupture as it plays a crucial role in the mechanical stability of the plaque. Further to this, the stability of the plaque is also in part dependent on the thickness of the fibrous cap, and is an important parameter in plaque vulnerability assessments. Fibrous caps that are considered to be thin (<75μm) in coronary arteries are more prone to rupture compared with fibrous caps that are thick. This is because of the high mechanical stresses normally occurring in regions of the cap that are considered to be thin. These biomechanical forces can render a cap susceptible to rupture. The size of the lipid core is also important in plaque rupture as studies have shown that a large lipid core which is separated from the lumen by a thin cap is more at risk from rupture.

This chapter will quantify the 3-D collagen distribution along the entire length of the plaque for both ruptured and non-ruptured groups of symptomatic patients in detail. It will also correlate these results with the fibrous cap thickness and the lipid core thickness to improve on the current understanding of these relationships, including the risk assessment of plaque rupture. It will also look at the inter-relationship between collagen content, fibrous cap thickness, and the lipid core size in detail using histological techniques and analyse the data into ruptured and non-ruptured patient

groups to help understand the reasons why certain plaques rupture whilst others remain stable. Furthermore, a detailed examination of the plaque morphology at the rupture sites and their adjacent regions will be performed to provide a clear picture of specific ruptures. The carotid plaque specimens were sectioned at 0.5 mm intervals throughout the plaque which produced a large number of sections. This enabled us to have a more comprehensive understanding of plaque vulnerability.

4.2 Method

4.2.1 Carotid Arterial Plaque Specimen

A total of 18 patients were recruited for the study. The research protocol was approved by local ethics committee.

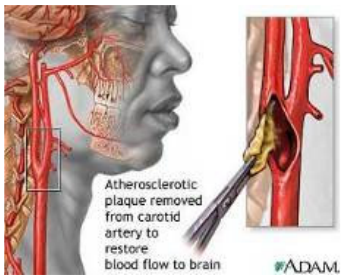

Figure 4.1: Location of the carotid artery and a plaque being removed from within the artery (www.adam.com)

Specimens were obtained after a surgical procedure known as a carotid endarterectomy (CEA) as shown in figure 4.1. During this procedure the surgeon makes an incision through the adventitial layer and excises the intima and media layers which contains the plaque tissue, however the adventitial layer is maintained. After removal of the plaque tissue, a patch is used to regenerate the arterial lumen by sewing a patch onto the adventitia. The plaque specimen that is removed may be circumferentially intact as shown in chapter 6 in figure 6.16(b) or opened as in figure 6.16(a). The removed specimen consists of a small section of the CCA, ICA and ECA. The specimen is immediately collected from the operating room and immersed

in saline (0.9% sodium chloride - NaCl). It is then subjected to a longitudinal 2D ultrasound scan using an in-house designed mechanical arm. After scanning, the specimen is rinsed with saline to remove any traces of blood, and is then placed into a solution containing 2ml formaldehyde and 18ml distilled water, producing a 3.7% concentration of formaldehyde solution.

4.2.2 Histology Processing

Conventional histology processing described in chapter (3) was performed on each specimen which included **(a)** tissue fixation; **(b)** marking on the outer wall with tissue marking dye; **(c)** cutting the specimen into 5mm length longitudinal segments and placing it into histology cassettes for tissue processing; **(d)** wax imbedding; **(e)** sectioning and attaching the sections to APES coated slides. Van Gieson and Picrosirius red with H&E staining were used to provide collagen information. For each section the following histological variables were evaluated: **1)** collagen content; **2)** lipid core thickness; and **3)** mean minimum fibrous cap thickness. Histological variables were calculated using an in-house designed program based on MATLAB.

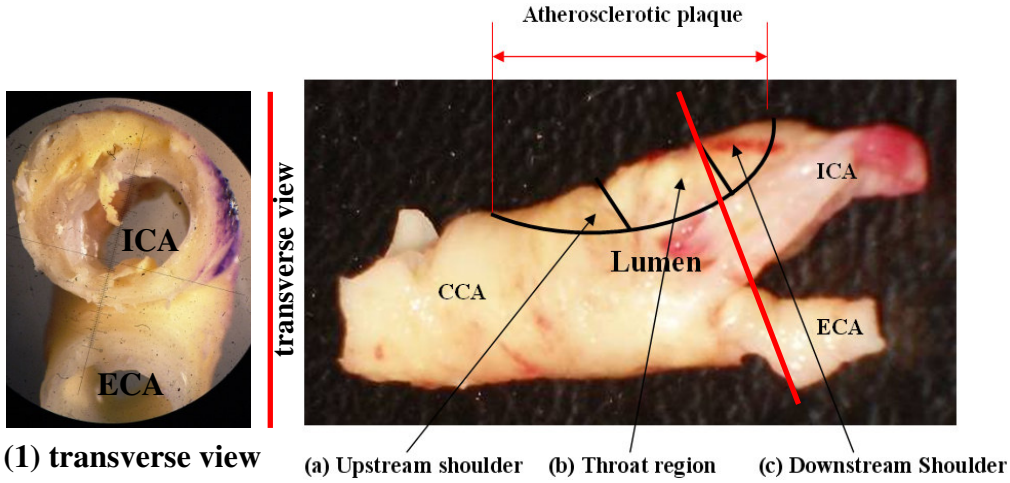

Figure 4.2 Demonstrates the three plaque regions; (a) upstream shoulder; (b) throat region; (c) the downstream shoulder region; and (1) transverse view

Figure 4.2 demonstrates a CEA specimen used for the study and highlights the CCA, ICA, and the ECA. The atherosclerotic plaque usually develops in the region shown by the curve, and is divided into three longitudinal regions; **1)** upstream shoulder; **2)** throat region; and **3)** the downstream shoulder. The remaining regions are plaque free

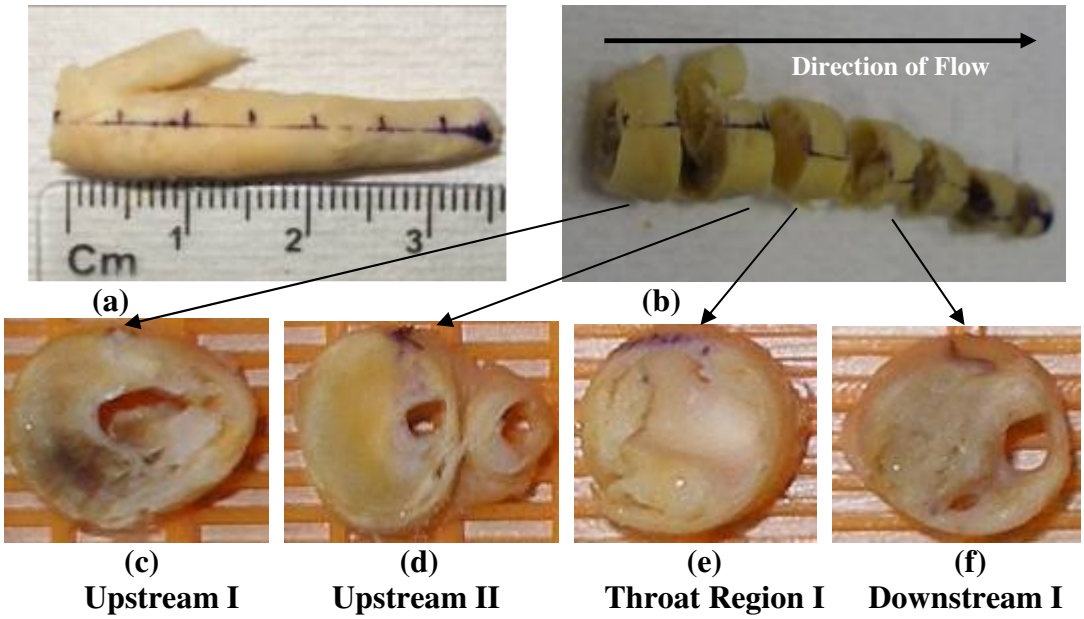

Figure 4.3 Longitudinally marked tissue to maintain the correct orientation, and the segmented regions demonstrating the upstream shoulder, throat, and the downstream shoulder regions of an atherosclerotic plaque

Figure 4.3 (a) shows a CEA specimen that has been marked with a longitudinal line with an axial line marked every 5mm using tissue marking dye. This is performed to maintain the correct 3D orientation of the plaque. Figure 4.3 (b) shows the same specimen cut into 5mm segments to enable it to be placed into histology cassettes for tissue processing. Figure 4.3 (c) to (f) shows in transverse view the upstream, throat, and downstream regions respectively. A clear difference can be seen with regards to the degree of plaque build up between the upstream, throat, and downstream regions. The luminal area in the upstream region is relatively larger in the CCA, and becomes smaller when approaching the throat. The lumen has completely disappeared in the

throat region. This is further enhanced by the buckling of the arterial wall that takes place due to the non-pressure conditions within the lumen as a result of the lack of blood flow. The lumen reappears again in the downstream region.

As described in figure 4.3, carotid endarectomy specimens were segmented into blocks and grouped into the following categories **a)** upstream; **b)** throat region (maximum degree of stenosis); **c)** downstream 1; and **d)** downstream 2.

- The upstream region was defined by the part of the plaque that occurs in the region before the maximum stenosis in the throat.
- The throat region was defined where the bulk of the plaque was found and has the smallest lumen area.
- The downstream region was defined by the part of the plaque that occurred downstream of the throat.

In addition plaque specimens were categorised into two groups: **a)** ruptured; **b)** non-ruptured. The ruptured and non-ruptured specimens are defined as:

- Ruptured plaques were defined by the presence of a clear break or opening in the fibrous cap between the lipid core and the lumen (figure 4.4). The term plaque rupture is used as an alternative to the older usage of plaque ulceration.

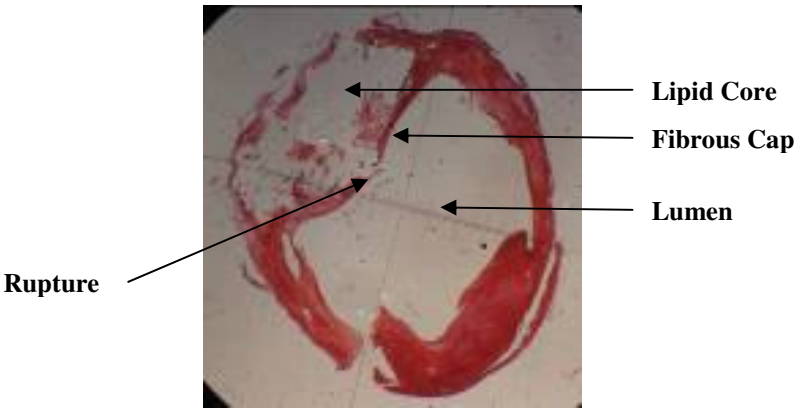

Figure 4.4 Picrosirius-red stained histological transverse section demonstrating a ruptured plaque

- Non-ruptured plaques were defined by a continuous fibrous cap without any breaks, and which completely separated the lipid from the lumen (figure 4.5).

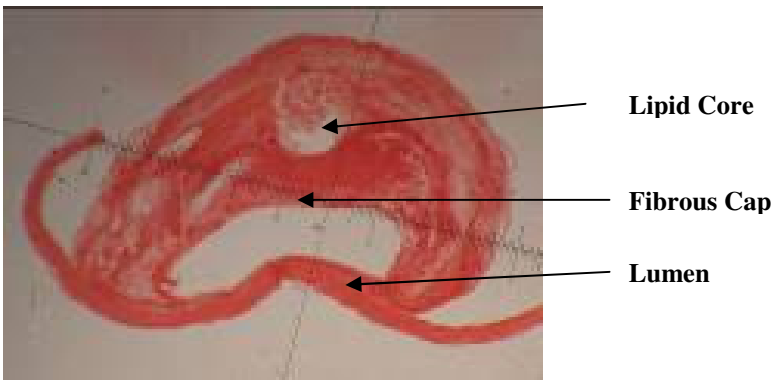

Figure 4.5 Picrosirius-red stained histological transverse section demonstrating a non-ruptured plaque

4.3 Results and Analysis

4.3.1 Differences in Plaque Morphology between Ruptured and Non-Ruptured Groups

4.3.1.1 Mean Collagen Content

Sample Number	Group 1 (n=10) (ruptured)*	Group II (n=8) (non-ruptured)*
1	25.49	41.71
2	45.36	51.10
3	50.96	42.81
4	51.59	35.47
5	47.20	65.64
6	60.38	44.95
7	27.45	52.40
8	41.13	60.41
9	22.43	-
10	29.11	-
(Mean±SD)	**40.1±13.11**	**49.31±10.09**

Table 4.1 Mean collagen % in ruptured and non-ruptured plaques

*All figures are in percentages (%) – collagen area in the fibrous cap / (total collagen area + non collagen area in fibrous cap) * 100 = collagen area (%)

The mean collagen content in both ruptured (n=10) and non-ruptured (n=8) plaque groups was investigated. For the ruptured plaque group, a mean collagen content of 40.11±13.11% was found, compared with 49.31±10.09% for the non-ruptured group (figure 4.6). The overall Mean±SD result and the individual results for the specimens are shown in table 4.1. A graphical representation of the overall mean result is shown in figure 4.6. A statistical analysis using the unpaired Mann-Whitney test (two-tailed) was carried out, and which showed that the result did not reach statistical significance (p=0.08). This however may be due to the small sample size that was used.

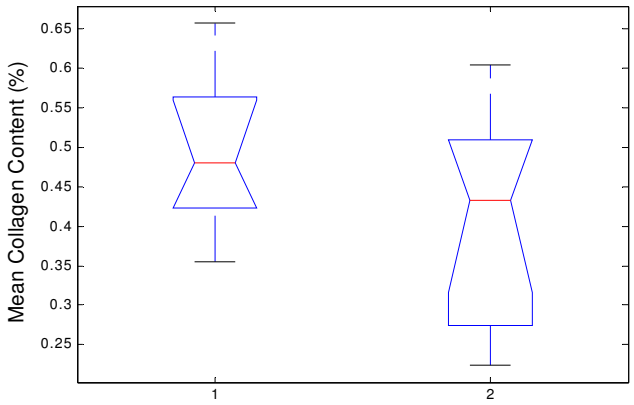

1= non-ruptured; 2= ruptured

Figure 4.6 Comparison of the mean collagen % in ruptured and non-ruptured plaques; Mann-Whitney Test (two-tailed); unpaired

4.3.1.2 Minimum Fibrous Cap Thickness

The mean minimum (the mean of the smallest fc thickness in each section for all specimens in the group) fibrous cap (fc) thickness for the ruptured and non-ruptured plaques was found to be 302.64±97.08 and 417.52±139.74µm respectively. The minimum fibrous cap thickness was assessed by measuring the thickness at the thinnest point for all the sections in each specimen, and then calculating the mean value. A statistical analysis using the unpaired Mann-Whitney test (two-tailed) was carried out which showed the result reached statistical significance (p=0.03).

Sample Number	Group 1 (n=10) (ruptured)	Group II (n=8) (non-ruptured)
1	265.73	382.87
2	121.87	533.99
3	359.02	435.60
4	245.80	587.50
5	252.95	425.90
6	396.30	491.79
7	283.30	353.05
8	304.60	129.48
9	483.30	-
10	313.49	-
(Mean±SD)	**302.64±97.08**	**417.52±139.74**

Table 4.2 Mean minimum fibrous cap thickness

*All figures are in micrometer; **Mann-Whitney test: *p*=0.03, two-tailed**

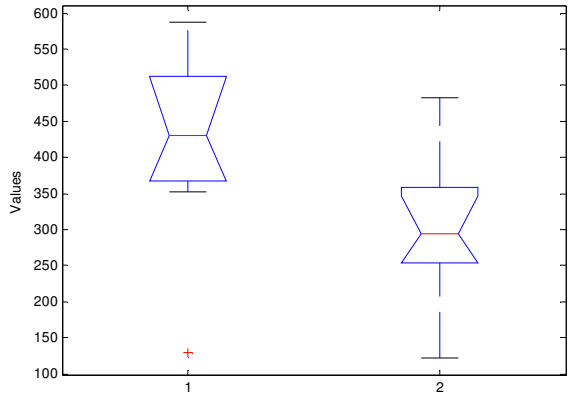

1= non-ruptured; 2= ruptured

Figure 4.7 Comparison of the mean fibrous cap thickness in ruptured and non-ruptured plaques

4.3.1.3 Lipid Core Thickness

An analysis of the lipid core thickness in the central region for both ruptured (n=10), and non-ruptured (n=8) plaques was performed. For ruptured plaques, the mean lipid core thickness in the central region was 904.31±377.04µm, and for the non-ruptured plaques it was found to be 548.62±207.56µm (table 4.3). A statistical analysis using the unpaired Mann-Whitney Test (two-tailed) was carried out which showed the result to be significant (*p*=0.02).

Sample Number	Group 1 (n=10) (ruptured)	Group II (n=8) (non-ruptured)
1	917.48	738.99
2	1183.38	937.76
3	840.90	586.40
4	690.37	511.17
5	1880.97	302.44
6	706.05	528.85
7	693.23	371.57
8	690.23	411.74
9	708.02	-
10	732.48	-
(Mean±SD)	**904.31±377.04**	**548.62±207.56**

Table 4.3 Mean lipid core thickness in ruptured and non-ruptured plaques

*All figures are micrometer; **Mann-Whitney Test; two tailed; unpaired**

Figure 4.8 shows a graphical representation (box-plot) of the data in table 4.3, showing the mean lipid core thickness in ruptured and non-ruptured plaques. The difference between the two patient groups can be seen (p=0.02)

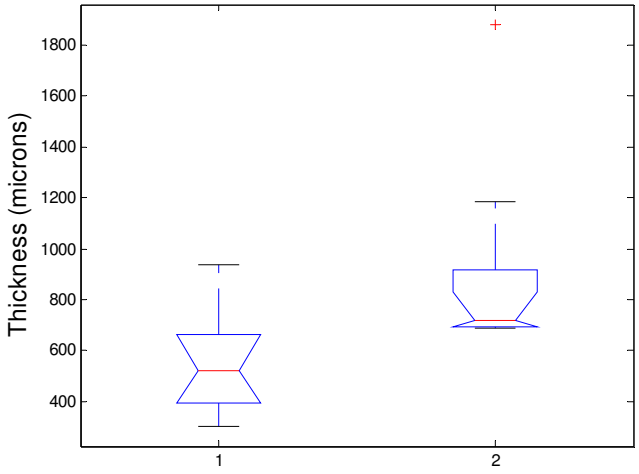

1= non-ruptured; 2= ruptured

Figure 4.8 Comparison of the lipid core thickness in ruptured and non ruptured plaques

4.3.2 Longitudinal Assessment

4.3.2.1 Longitudinal Distributions of Collagen Density

Table 4.4 compares the collagen density in the fibrous cap between ruptured and non-ruptured groups for the upstream, throat, and downstream regions of maximum stenosis. The table details the results for each individual sample, the overall results for the group, and a comparison between the groups. The mean values are presented in a graph format in figure 4.9 to show the trends, and the comparison between the longitudinal variation in the collagen density for ruptured and non-ruptured plaques.

	COLLAGEN DENSITY IN THE FIBROUS CAP OF RUPTURED AND NON-RUPTURED PLAQUES					
Sample number	**Upstream**		**Throat**		**Downstream**	
	Ruptured	**Non-ruptured**	**Ruptured**	**Non-ruptured**	**Ruptured**	**Non-ruptured**
1	56.58	40.7	32.09	66.42	45.59	47.47
2	59.66	44.93	56.39	43.52	35.05	39.46
3	62.44	36.76	34.2	64.63	39.55	74.3
4	78.62	17.76	43.8	55.8	41.13	33.75
5	55.26	49.37	54.45	83.81	50.93	68.16
6	40.94	93.04	34.14	94.69	36.78	72.54
7	51.56	34.39	31.81	46.5	43.76	44.59
8	53.43	47.99	44.63	59.32	59.09	43.45
9	51.7	n/a	34.85	n/a	32.88	n/a
10	31.6	n/a	76.83	n/a	42.18	n/a
Mean ±S.D	**54.18 ±12.48**	**45.62 ±21.63**	**44.32 ±14.56**	**64.34 ±17.54**	**42.69 ±7.81**	**52.97 ±16.09**
	***P*=0.067599**		***P*=0.01554**		***P*=0.20307**	
***P*=<0.05**	Not significant		significant		Not significant	

Table 4.4 Comparisons between ruptured and non-ruptured plaques for collagen density in the fibrous cap in the upstream, throat, and downstream regions. Statistical Test: Mann-Whitney Test; two-tailed; unpaired

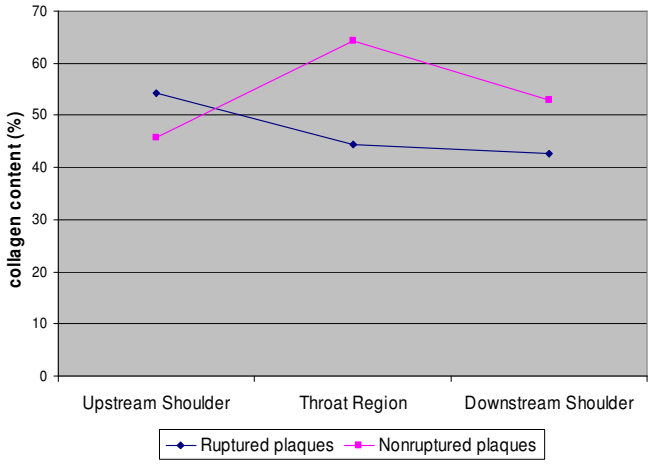

Figure 4.9 Comparison of the longitudinal collagen content in ruptured (n=10) and non-ruptured plaques (n=8)

In the upstream, throat, and downstream shoulder regions of the ruptured plaque group (n=10), the collagen density was 54.18%±12.48, 44.32%±14.56, and 42.69%±7.81 respectively. For the non-ruptured plaque group (n=8), it was 45.62%±21.63, 64.34%±17.54, and 52.97%±16.09 respectively for the upstream, throat, and downstream regions. Figure 4.9 shows that the collagen density in ruptured plaques gradually decreases longitudinally in the downstream direction, whilst the collagen density in the non-ruptured plaque group shows an increase from the upstream shoulder to the throat region, and a decline towards the downstream region, with the peak highest collagen content being in the throat region. Comparisons between the different regions for ruptured and non-ruptured plaque groups yielded some significant results. The difference in the collagen density between ruptured and non ruptured plaques for the upstream and downstream shoulder regions did not reach statistical significance, p=0.067, and p=0.203 respectively (Mann-Whitney Test; two-tailed; unpaired). However, the results for the collagen content difference in the throat region for ruptured and non-ruptured plaques was found to be statistically significant (p=0.015). For ruptured plaques the mean

value for all the regions (upstream, throat, and downstream shoulder) was 47.06%±6.22, and for non-ruptured plaques it was 54.31%±9.43.

4.3.2.2 Cross Comparisons and Statistic Analysis

Table 4.5 compares the overall collagen content for all the non-ruptured plaques studied (n=8) between **a)** the upstream and throat region (p= 0.04); **b)** the throat and the downstream region (p= 0.28); and **c)** the upstream and the downstream region (p= 0.57), and shows the significance level between the different regions.

Upstream Shoulder	*Throat Region*	*Downstream Shoulder*	*Significant*
45.61±21.63	**64.34±17.54**	**52.97±16.09**	**(p=<0.05)**
Upstream Shoulder	**Throat Region**	**-**	***p*= 0.04**
-	**Throat Region**	**Downstream Shoulder**	***p*= 0.28**
Upstream Shoulder	**-**	**Downstream Shoulder**	***p*= 0.57**

Table 4.5 Difference between the collagen contents for the different longitudinal plaque regions in the non-ruptured plaque group

Table 4.6 compares the overall collagen content for all the ruptured plaques studied (n=10) between **a)** the upstream and throat region (p=0.12); **b)** the throat and the downstream region (p=0.73); and **c)** the upstream and the downstream region (p=0.03), and shows the significance level between the different regions.

Upstream Shoulder	*Throat Region*	*Downstream Shoulder*	*Significant*
54.18±12.48	**44.32±14.56**	**42.69±7.81**	**(p=<0.05)**
Upstream Shoulder	**Throat region**	**-**	***p*= 0.12**
-	**Throat region**	**Downstream Shoulder**	***p*= 0.73**
Upstream Shoulder	**-**	**Downstream Shoulder**	***p*= 0.03**

Table 4.6 Difference between the collagen contents for the different longitudinal plaque regions in the ruptured plaque group

4.3.2.3 Case Study of the 3D Collagen Density Distribution

Figure 4.10 shows two cases studies that demonstrate the longitudinal collagen distribution pattern for a ruptured plaque (figure 4.10 (a)), and a non-ruptured plaque (figure 4.10 (b)).

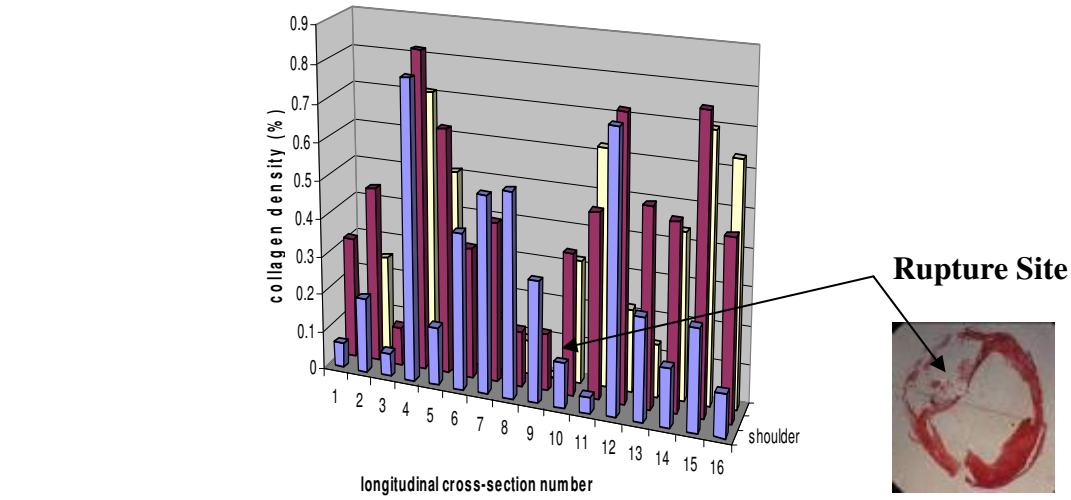

(a)

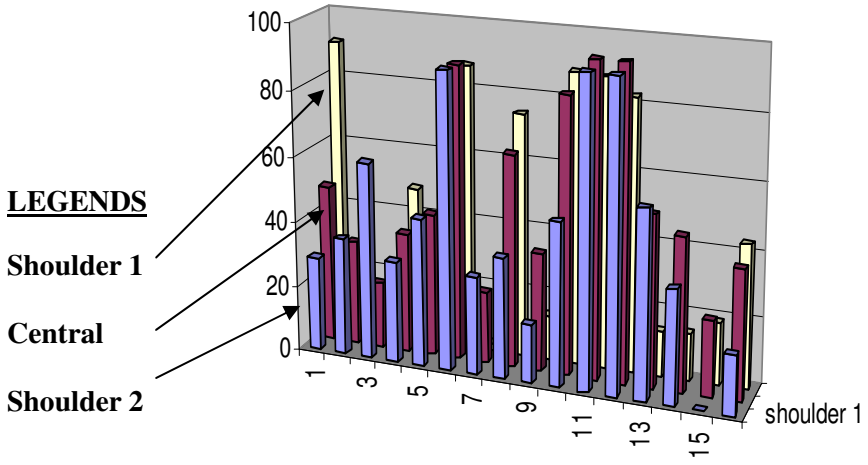

Figure 4.10 Demonstrates the longitudinal distribution of collagen in an (a) ruptured and (b) non-ruptured atherosclerotic plaque

For the ruptured case (4.10(a)), the collagen content in the upstream/downstream and throat regions of the plaque showed large degrees of variations. The upstream and downstream regions have higher collagen content compared with the central region of the plaque. At the throat region (section 10), the collagen content is low. Histological

assessment confirms that this region was also the site for a rupture. Figure 4.10 (b) shows the 3D collagen distribution in a non-ruptured plaque. It can be seen that the collagen content in the throat region is relatively higher compared with both the upstream and downstream regions.

4.3.2.4 Fibrous Cap Thickness for the Different Groups

Table 4.7 compares the fibrous cap thickness of ruptured and non-ruptured plaques in the upstream, throat, and downstream regions.

	FIBROUS CAP THICKNESS OF RUPTURED AND NON-RUPTURED PLAQUES					
Sample number	**upstream**		**throat**		**downstream**	
	ruptured	**Non-ruptured**	**ruptured**	**Non-ruptured**	**ruptured**	**Non-ruptured**
1	324.32	475.55	382.22	316.75	429.6	298.45
2	228.67	235.71	218.94	215.8	191.81	455.28
3	135.25	310.73	316.94	423.87	400.72	319.49
4	160.97	488.23	239.82	478.5	243.1	307.65
5	124.56	347.34	339.14	453.28	137.27	221.14
6	250.23	222.77	281.11	471.15	417.73	364.18
7	157.12	285.69	205.98	369.56	161.67	353.95
8	267.36	428.56	143.27	391.44	312.7	343.34
9	179.75	-	348.15	-	432.18	-
10	214.37	-	270.75	-	351.73	-
Mean ±S.D	**204.26 ±64.13**	**349.32 ±104.18**	**274.63 ±73.99**	**309.04 ±89.20**	**307.85 ±115.98**	**332.93 ±66.55**
	***P*=0.0043878**		***P*=0.01554**		***P*=0.82856**	
***P*=<0.05**	significant		significant		Not significant	

Table 4.7 Comparison of the fibrous cap thickness in the upstream, throat, and downstream regions for ruptured and non-ruptured plaques (Statistical Test Used: Mann-Whitney Test; two-tailed; unpaired)

In the upstream region, there was a significant difference (p=0.004) between the ruptured plaque group which had a thinner fibrous cap (204.26±26μm), compared to the non-ruptured plaque group (349.32±104.18μm). A significant difference

(p=0.01554) was also found in the throat region where the ruptured plaque group had a thinner fibrous cap (274.63±73.99µm) compared with the non-ruptured plaque group (309.04±89.20µm). However no significant difference (p=0.82856) was found in the downstream region between ruptured and non-ruptured plaque groups, although a trend was found where the ruptured group had a thinner overall cap thickness (307.85±115.98 µm) compared with the non-ruptured group (332.93±66.55µm) (figure 4.11). A study carried out by our group (Gao et al 2008) showed that a slight decrease in fibrous cap thickness can cause a significant increase in the stress levels acting on the cap surface. High levels of stress acting on the fibrous cap can cause rupture which may explain in part why certain plaques rupture whilst others remain stable.

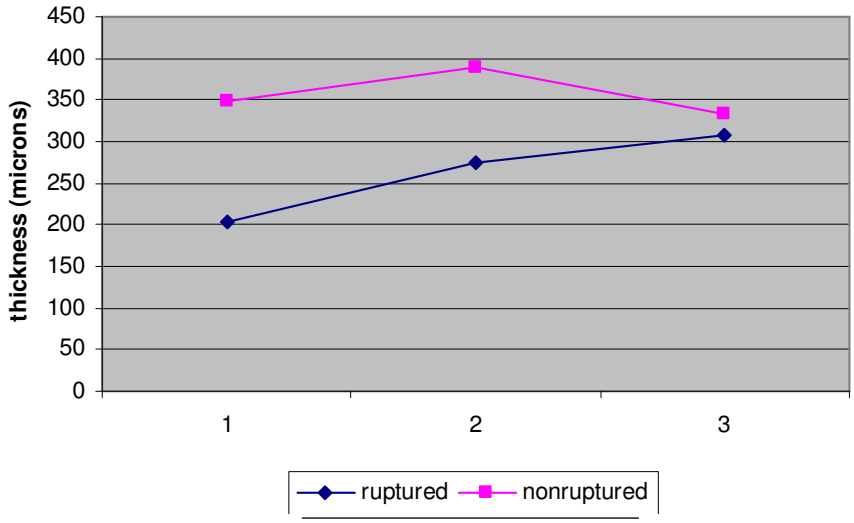

Figure 4.11: Graph comparing the longitudinal fibrous cap thickness between; 1) upstream; 2) throat; and 3) downstream regions for ruptured and non-ruptured plaque groups

4.3.2.5 Lipid Core Thickness for the Different Groups

Table 4.8 compares the mean lipid core thickness for the ruptured and non-ruptured plaque groups in the upstream, throat, and downstream regions of the plaque.

	LIPID CORE THICKNESS OF RUPTURED AND NON-RUPTURED PLAQUES					
Sample number	**upstream**		**throat**		**downstream**	
	ruptured	**Non-ruptured**	**ruptured**	**Non-ruptured**	**ruptured**	**Non-ruptured**
1	766.16	696.87	1363.84	1078.39	731.39	866.35
2	798.65	703.13	1683.51	1314.01	814.61	827.85
3	666.89	559.99	1272.29	790.31	845.16	527.15
4	763.93	565.72	906.7	856.61	777.71	408.88
5	1110.23	415.17	2133.58	624.88	1082.28	377.65
6	629.98	437.04	1266.54	1180.83	850.78	735.28
7	671.21	605.32	1015.14	662.73	539.96	476.42
8	619.88	519.28	992.5	967.59	577.94	655.92
9	936.41	-	1156.26	-	610.76	-
10	603.67	-	1045.1	-	849.28	-
Mean ±S.D	**756.70 ±160.81**	**562.82 ±106.23**	**1283.55 ±374.35**	**934.42 ±245.85**	**767.99 ±161.47**	**609.44 ±189.03**
	***P*=0.008547**		***P*=0.043421**		***P*=0.12199**	
***P*=<0.05**	significant		significant		Not significant	

Table 4.8: Comparison of the Lipid Core Thickness in the Upstream, Throat, and Downstream Regions for Ruptured and Non-Ruptured Plaques (Statistical Test Used: Mann-Whitney Test; two-tailed; unpaired)

The result shows that in the upstream region, the ruptured plaque group had a significantly larger lipid core thickness (756.70±160.81μm) compared with the non-ruptured plaque group (562.82±106.23 μm) (p=0.008547). Also in the throat region, the lipid core continued to have a significantly larger thickness in the ruptured plaque group (1283.55±374.35 μm) compared with the non-ruptured plaque group (934.42±245.85μm) (p=0.043421). In the downstream region, the lipid core thickness in ruptured plaques was greater (767.99±161.47μm) than the non-ruptured plaque

group (609.44±189.03μm), however the difference was found to be not significant (p=0.12199). These results demonstrate a significant morphological difference that exists between ruptured and non-ruptured plaques.

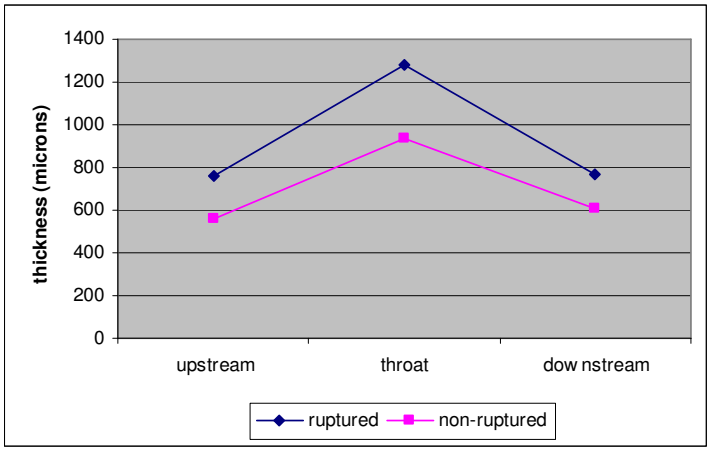

Figure 4.12 Comparison of the longitudinal lipid core thickness between the upstream; throat; and downstream regions for ruptured and non-ruptured plaque groups

Figure 4.12 shows the results from table 4.8 which clearly shows the difference in the lipid core thickness in the upstream, throat, and downstream regions for the ruptured (blue coloured line) and non-ruptured (pink coloured line) plaque groups. Both groups have larger lipid cores in the throat region compared with the upstream and downstream regions, however it can be seen that the lipid core size for the non-ruptured group is proportionally smaller compared with the lipid core size in the ruptured group.

4.4 Morphology Analysis for the Plaque Rupture Site

The purpose of this part of the study is to investigate the morphological characteristics of the rupture site and compare them to the surrounding region in carotid plaques of symptomatic patients. Pathological studies have established that a large lipid rich necrotic core is an important feature of vulnerable atherosclerotic

plaques. Studies have also shown that collagen degradation can lead to weakening of the fibrous cap. Closer examination and investigation of the plaque structure at the rupture site will add valuable information to the understanding of rupture conditions.

4.4.1 Definition of Fibrous Cap Rupture

Defining the presence of a plaque rupture based on histology evidence and interpreting it correctly is an important procedure. Evidence of a break in the continuity of the fibrous cap is usually the first sign of a rupture. However, there is also the possibility that this disruption may have been caused by artefacts during histology analysis. Therefore, further evidence needs to be considered to decide whether a rupture is genuine. Firstly, the appearance of blood cells around the location of the rupture, as shown in figure 4.13. Secondly, examining transverse-sections upstream and downstream to the rupture site as demonstrated in figure 4.13. Investigating histology sections at the upstream and downstream sites to the rupture locations can enable the observation of gradual changes to the plaque structure around the rupture site. On the contrary, artefacts such as a break in the luminal wall as shown in figure 4.14 would not have this characteristic. It is also important to note that in many of the sections, breaks in the luminal wall were caused as a result of surgical procedures during the excision of the plaque.

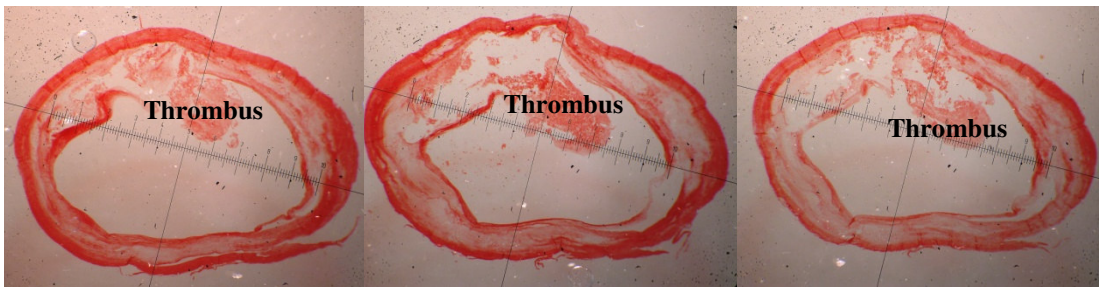

Figure 4.13 Series of transverse sections demonstrating fibrous cap rupture, thrombus and erythrocytes in the lesion, used to distinguish post-mortem artefact from an actual rupture

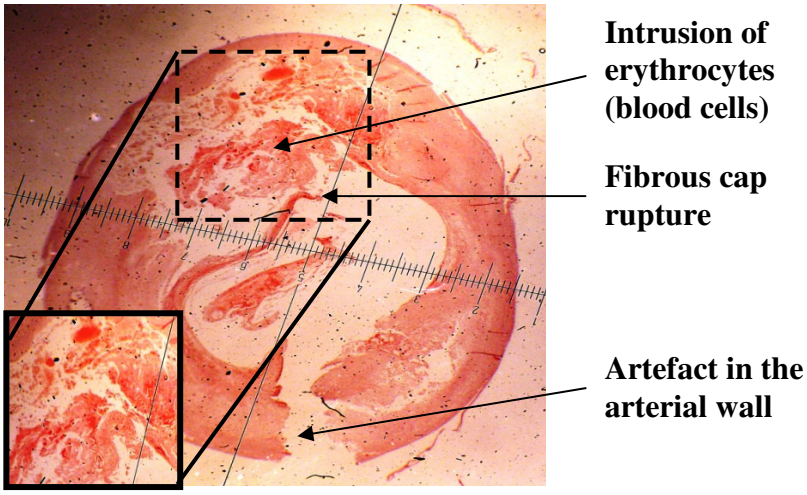

Figure 4.14 Demonstrates an artefact to the arterial wall caused during post-mortem processing; and the intrusion of erythrocytes (inset)

Figure 4.15 (below) shows the six specimens used for the study all with a clear sign of fibrous cap rupture. It can be seen that at sites where there are breaks in the fibrous cap, a thin fibrous cap is present in the adjacent regions. In addition, it can also be seen that directly behind the break in the fibrous caps of all the specimens, the largest lipid core is present.

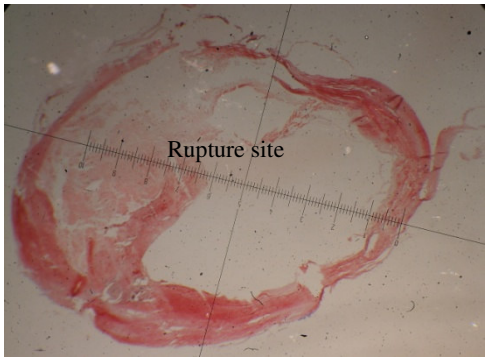

sample 1 (2)

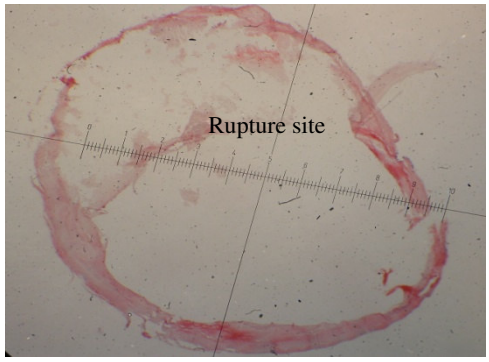

sample 2 (3)

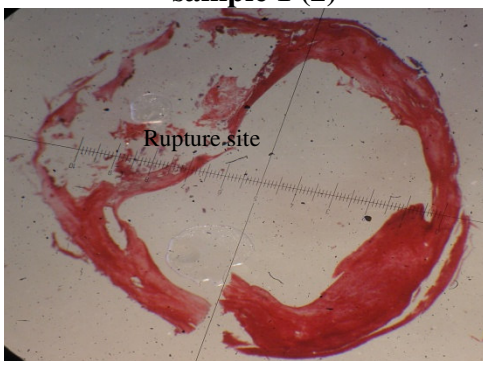

sample 3 (7)

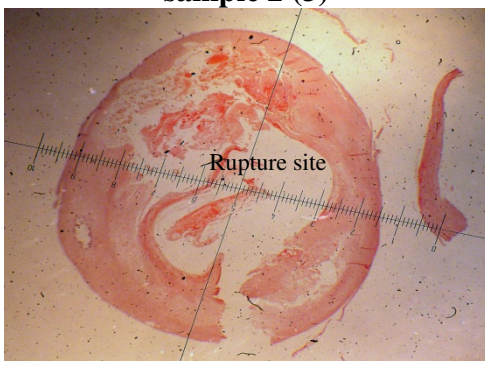

sample 4 (12)

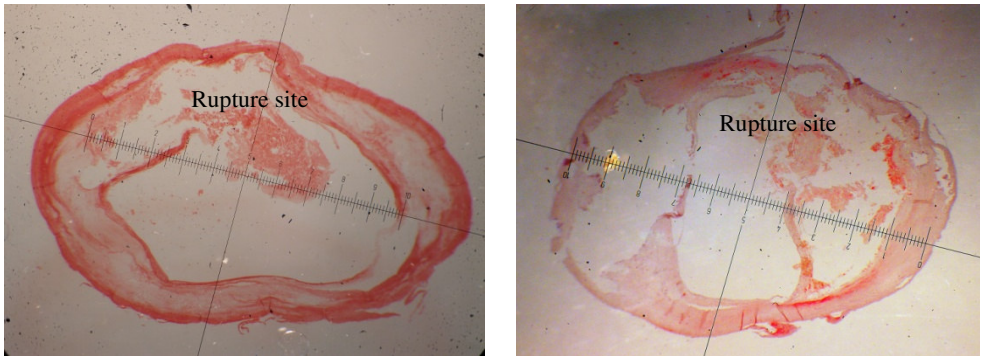

sample 5 (21) **sample 6 (6)**

Figure 4.15 Histology cross-sections of the rupture sites for all the specimens

Figure 4.16 shows the six specimens stained with picrosirius red and viewed under polarised light microscopy. The birefringence is representative of collagen fibres. These confirm the fibrous cap at the rupture site. The perpendicular lines present in sample 1 (2) are points where the parameters were measured, and were carried out for all the specimens. The value indicated by (n) is the section number in which the fibrous cap rupture was observed. Figure 4.16 shows that most (5 in 6 or 83%) rupture occurred on the upstream region of the plaque. For sample 1, 2, 3, 4, and 6 the rupture was located in section number 2, 3, 7, 12, and 6 respectively, which are all at the beginning of the plaque. For sample 5, the rupture was observed further down the plaque in section number (21), on the downstream side. This finding is in concordance to a study carried out by Fagerberg et al (2010), which also found that most rupture occurred on the upstream side of the plaque.

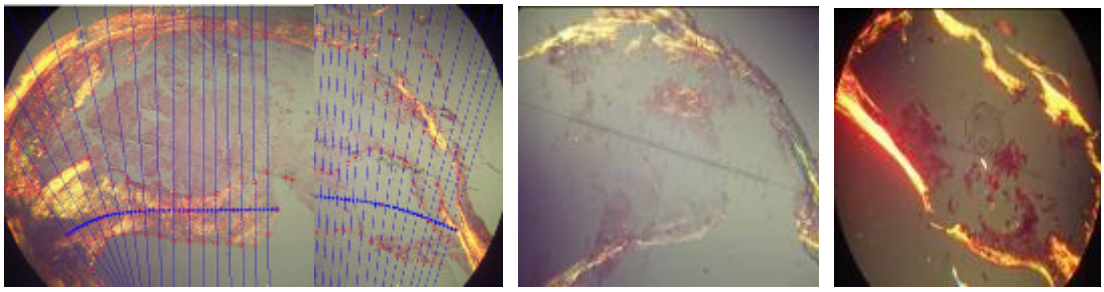

Sample 1 (2) **Sample 2 (3)** **Sample 3 (7)**

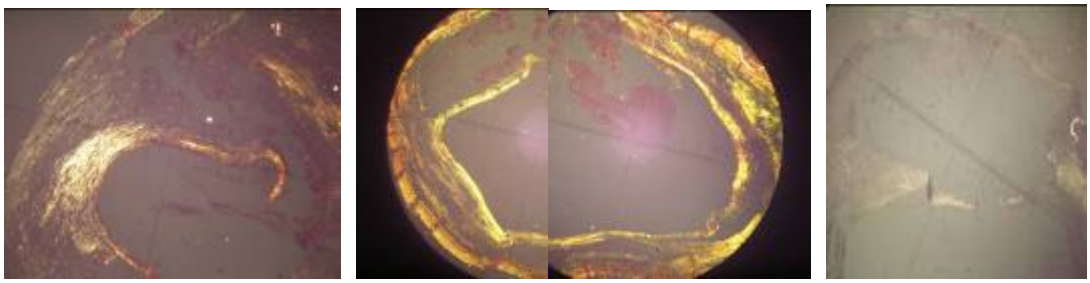

Sample 4 (12) **Sample 5 (21)** **Sample 6 (6)**

Figure 4.16 Picrosirius red stained cross-sections of the histology cross-sections shown in figure 4.15; (n) indicates the section number

4.4.2 Rupture Site versus Adjacent Region in Circumferential Direction

Sample Number	Collagen Content At Rupture Site (%)	Average In The Region (Circu.)	Fibrous Cap Thickness At Rupture Site (μm)	Average In The Region (Circu.)	Lipid Core Thickness At Rupture Site (μm)	Average In The Region (Circ.)
1 (2)	3.77	15.54	854.16	850.59	2000.13	1279.91
2 (3)	11.1	22.46	150.09	311.32	2073.6	1836.24
3 (7)	18.98	40.22	218.16	434.51	2067.55	1545.78
4 (12)	17.71	47.09	177.59	331.3	1829.38	1189.94
5 (21)	28.48	76.82	328.9	558.65	2156.9	1764.64
6 (6)	10.34	24.4	345.78	645.89	2147.19	1618.73
	15.06 ±8.58	**37.76 ±22.47**	**345.78 ±261.38**	**522.04 ±206.43**	**2045.79 ±120.66**	**1539.21 ±258.70**
***P*= <0.05**	***P*= 0.041126**		***P*= 0.17965**		***P*= 0.004329**	

Table 4.9 The collagen content (%), the fibrous cap thickness (μm), and the lipid core thickness (μm) at the rupture site and the average value in the circumferential adjacent region (Circu)

Table 4.9 shows that the mean collagen content in the adjacent region of the rupture site for all the specimens was found to be 15.06±8.58%, compared with 37.76±22.47% for the surrounding regions (p=0.04). This result is in concordance with the findings of (Lendon CL et al 1991) which demonstrates that collagen degradation at rupture sites can weaken the structure and make it more prone to

rupture. There is also a significant difference between the lipid core size behind the rupture site (2045.79±120.66μm), and the lipid core size in the surrounding region (1539.21±258.70μm) where fibrous cap rupture is not present (p=0.004). Studies have shown that atheroma vulnerability to rupture is increased in the presence of a large lipid core (Wasserman et al 2008). However, no significant difference was found between the fibrous caps thicknesses at the adjacent site to the rupture (345.78±261.38μm) compared with the mean value for the relative surrounding region (522.04±206.43μm). Although a trend can be seen from the results which is in line with other studies (Redgrave et al 2008), the finding was not significant (p=0.17965). This however may be due to the small sample size used, and therefore larger studies are warranted to confirm this result.

4.4.3 Rupture Site versus Adjacent Region in Longitudinal Direction

To obtain a better understanding of the rupture conditions this part of the study will investigate the collagen content as a percentage of total collagen and non-collagenous elements in the fibrous cap, and the fibrous cap and lipid core thickness (μm) at a region located 0.5mm directly upstream and downstream of the rupture site. Analysis was performed on the six (6) ruptured specimens used to study the parameters in the adjacent region of the rupture site (table 4.10).

Figure 4.17 shows the longitudinal view of an atherosclerotic plaque highlighting the lumen; the lipid core; the fibrous cap; and the rupture site (n). The figure also shows the upstream (n-1) and the downstream (n+1) transverse cross-sections taken 0.5mm from the rupture site. Measurements of the parameters were performed at the same circumferential location to the rupture site to maintain consistency.

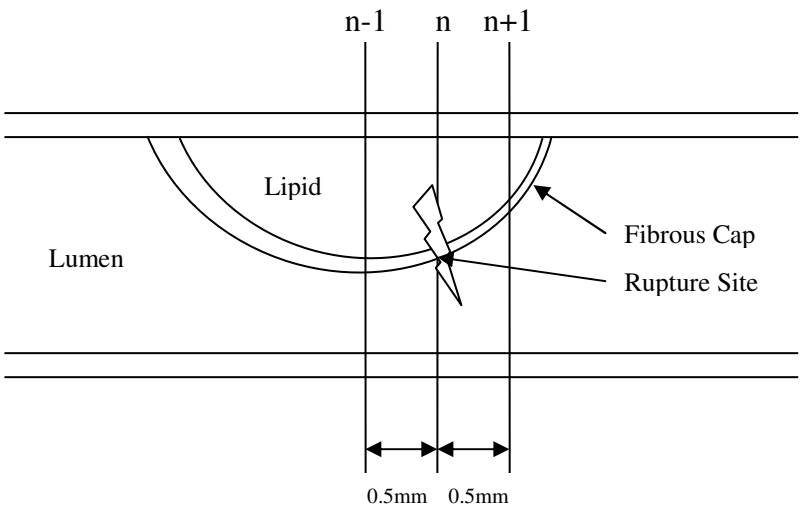

Figure 4.17 Longitudinal locations of the transverse sections (TS) used for the upstream (n-1); and downstream (n+1) in relation to the plaque rupture site (n)

Table 4.10 shows a comparison for the collagen content (%), the fibrous cap thickness (μm), and the lipid core thickness (μm) at the rupture site and at the adjacent region in the longitudinal direction.

	COLLAGEN CONTENT (%)			FIBROUS CAP THICKNESS(μM)			LIPID CORE THICKNESS (μM)		
Sample number	**rupture site (n)**	**n-1**	**n+1**	**rupture site (n)**	**n-1**	**n+1**	**rupture site (n)**	**n-1**	**n+1**
1 (2)	3.77	0	4.53	854.16	1036.53	997.65	2000.13	420.5	1683.45
2 (3)	11.1	65.28	18.62	150.09	258.51	266.24	2073.6	1878.89	357.98
3 (7)	18.98	100	11.76	218.16	355.76	118.13	2067.55	924.65	1458.35
4 (12)	17.71	32.2	52.05	177.59	469.25	630.17	1829.38	783.36	727.19
5 (21)	28.48	97.39	43.48	328.9	345.63	259.54	2156.9	2676.46	2026.9
6 (6)	10.34	26.62	39.93	345.78	489.52	387.45	2147.19	739.28	987.38
Mean	**15.06**	**53.58**	**28.40**	**345.78**	**492.53**	**443.20**	**2045.79**	**1237.19**	**1206.88**
S.D	**8.58**	**34.72**	**19.30**	**261.38**	**279.83**	**321.31**	**120.66**	**860.44**	**626.37**
***P*=<0.05**	***P*=0.008**			***P*=0.13203**			***P*=0.093074**		
	***P*=0.24026**			***P*=0.58874**			***P*=0.008658**		

Table 4.10 Comparison of collagen content (%), the fibrous cap thickness (μm), and the lipid core thickness (μm) in the rupture site and adjacent region in longitudinal direction

It can be seen that the mean collagen content for the rupture site is 15.06±8.58%. In the region directly upstream to the rupture site (n-1) it is 53.58±34.72% (p=0.008),

and in downstream region (n+1) it is 28.40±19.30% (p=0.24026). The results show that the rupture site generally has a lower collagen content compared with the upstream and downstream regions. The result in the upstream region was found to be significantly higher compared to the rupture site indicating an abrupt decrease in the collagen contents.

The mean fibrous cap thickness for all the specimens at the rupture site was found to be 345.78±261.38µm. In the region upstream to the rupture site (n-1) it was 492.53±279.83µm (p=13203), and in the downstream region it was 443.20±321.31µm (p=0.58874). The results indicate that the rupture site generally has a thinner cap thickness compared to the upstream and downstream regions. This result is in concordance with a study carried out by Li et al (2006) which demonstrated, using a flow-structure model, that there is an increase in plaque stress in arteries with a thin fibrous cap. The presence of a moderate stenosis (30% to 70%) with a thin fibrous cap is indicative of a high risk for plaque rupture. Another study by Imoto et al (2005) showed that there was an inverse relationship between surface equivalent stress and the thickness of the fibrous cap.

The mean lipid core thickness for all the specimens at the rupture site was found to be 2045.79±120.66µm. In the region 0.5mm directly upstream from this site (n-1) it was 1237.19±860.44 (p=0.093074), and in the region 0.5mm downstream (n+1) it was 1206.88±626.37µm (p=0.008658). The results indicate that the lipid core thickness at the rupture site is generally larger than in the region directly upstream and downstream to the site. Studies have shown that the presence of a large lipid core increases the risks of plaque rupture. A study by Falk et al (1995) concluded that the major determinants of vulnerability of a plaque to rupture are the size and consistency

of the atheromatous core as well as the thickness of the fibrous cap covering the core. This finding supports the results obtained in the present study and shows that abrupt longitudinal changes in lipid core thickness at the rupture site can influence plaques to rupture.

4.4.4 Correlation between Lipid Core Thickness and Cap Collagen Content

Large lipid cores in plaques are the result of increased macrophage activity which engulfs lipid molecules to form foam cells. These foam cells eventually die and leave behind debris and lipid that contributes to the formation of the lipid core (Ball et al 1995). Macrophage cells also release proteolytic enzymes which degrade collagen in fibrous caps, weakening it to make it more prone to rupture. Investigating the lipid core may therefore enable the indirect assessment of the collagen contents in fibrous caps, and enable the risk assessment of plaque rupture. Differences in the correlation of these parameters between ruptured and non-ruptured plaques may suggest other mechanisms that may be involved in plaque rupture. Current imaging modalities are not able to assess plaque collagen, unless molecular imaging technology is used, however the lipid core of plaques can be observed and measured using imaging modalities such as MRI and ultrasound (Trivedi et al 2004, Honda et al 2004).

The results of this investigation can be seen in table 4.11 which shows that for ruptured plaques the lipid core thickness and fibrous cap collagen content was 904.31±377.04μm and 40.11±13.11% respectively, and was found to be negatively correlated (r= -0.73). For non-ruptured plaques the lipid core thickness and fibrous cap collagen content was 548.62±207.56μm and 49.31±10% respectively, and were also shown to be negatively correlated (r= -0.84) – (two-tailed).

	Ruptured Plaques		Non-Ruptured Plaques	
Sample number	**Lipid Core Thickness (µm)**	**Fibrous Cap Collagen Content (%)**	**Lipid Core Thickness (µm)**	**Fibrous Cap Collagen Content (%)**
1	1183.38	25.49	738.99	41.71
2	708.02	45.36	411.74	51.10
3	693.23	50.96	511.17	42.81
4	690.23	51.59	937.76	35.47
5	706.05	47.20	371.57	65.64
6	690.37	60.38	528.85	44.95
7	917.48	27.45	586.40	52.40
8	732.48	41.13	302.44	60.41
9	1880.97	22.43	-	-
10	840.90	29.11	-	-
Mean±SD	**904.31±377.04**	**40.11±13.11**	**548.62±207.56**	**49.31±10.09**
Correlation	**r= -0.73**		**r= -0.84**	

Table 4.11: Correlation between lipid core thickness (µm) and fibrous cap collagen content (%) in ruptured (n=10) and non-ruptured (n=8) carotid plaques

From figure 4.18 it can be clearly seen that for both ruptured (left panel) and non-ruptured (right panel) plaque groups there is a correlation between lipid core thickness and collagen content. An increase in lipid core thickness was correlated with a decrease in fibrous cap collagen content in most of the samples investigated. However, the results indicate that the strength of the correlation was stronger for the non-ruptured plaque group compared with the ruptured plaque group, r=-0.84 and r=-0.73 respectively.

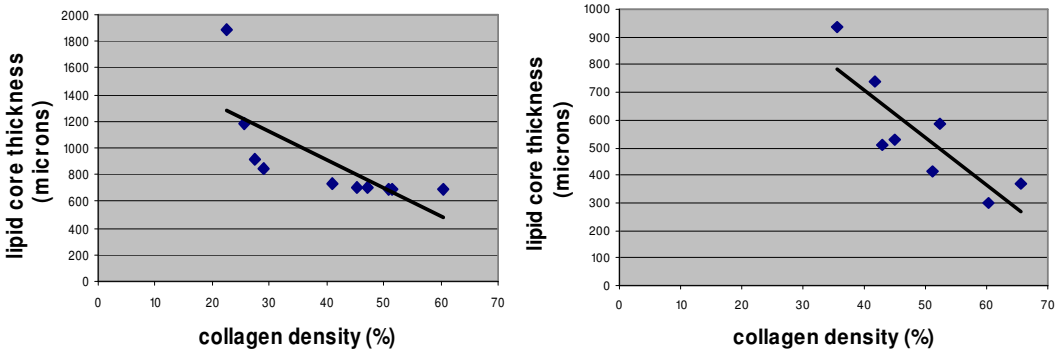

Left panel; ruptured group

Right panel; non-ruptured group

Figure 4.18: Correlation between lipid core thickness and cap collagen content in ruptured plaques (left panel), and non-ruptured plaques (right panel)

4.4.5 Data Measurement Reproducibility Study

To study the reproducibility of the data, intra-observer variability tests were carried out to measure the thickness of the fibrous cap using the method described and were found to be **0.09±0.02%.** The data for the 4 tests is summarised in Table 4.12. The measurement of the fibrous cap thickness was repeated by the observer over a time period range (1 week), and demonstrated the following values.

Test Number	Range	Agreement, % (Mean±SD)
1	0.09-0.13	0.10±0.02
2	0.06-0.13	0.09±0.03
3	0.02-0.08	0.06±0.02
4	0.59-0.10	0.09±0.02
Error Margin (mean value)		**0.09±0.02**

Table 4.12 Reproducibility of the Data

*All figures are in percentage (%)

4.5 Summary

In this chapter, the micro-level structure of arterial plaque was studied. In general, it was found that ruptured plaques have a thinner cap thickness, a lower density of collagen in the cap region and a larger lipid core compared with non-ruptured plaque. Longitudinally, the collagen content decreased from the upstream, plaque throat, to the downstream region for the ruptured group, while for non-ruptured group it was lower, high and low respectively. For fibrous cap thickness, an opposite (compared with collagen contents) trend was found for the ruptured group where the cap thickness increased from the upstream, throat to the downstream region. In the non-ruptured group, the upstream and downstream have similar cap thickness but a thicker cap can be found in the throat region. For both groups, larger lipid core can be found in the throat region. At the rupture site itself, a significantly lower collagen density

and larger lipid core can be found compared with the average value for transverse sections. The collagen content is also significantly lower at the rupture site compared with the immediate up- and down-stream sections. A thinner fibrous cap and larger lipid core can also found in the rupture site but the difference between this and the up- and down-stream sections was not significant. Based on the above study, it seems that local collagen fibrous density is a significant factor in plaque rupture dynamics.

It is believed that the extent of macrophage cell infiltration into the arterial lesion can be indicative of the quality of type I collagen in the plaque. This is because proteolytic enzymes such as the matrix metalloproteinase's are released by the macrophages cells, which play a dominant role in collagen degradation. In the next chapter, the macrophage distribution will be analysed for the same group of patients.

Discussion

A **detailed discussion** of this chapter (4) has been presented in **chapter 8** of this thesis. It has not been included here as the overall findings of this chapter have been integrated with the findings from the other chapters in this thesis.

Chapter 5

Macrophage Distribution in Atherosclerotic Plaques

5.1 Introduction

Figure 5.1 illustrates the general understanding of the process of infiltration of macrophage cells (average size 20 to 50 µm) into plaques. It is a recognisable feature of atherosclerosis and is known to weaken the structural integrity of the fibrous cap rendering it susceptible to rupture (Tearney et al 2003). Macrophage cells release proteolytic enzymes that degrade tissue debris and structural components such as collagen, which are neutralized and removed by a process known as phagocytosis. Macrophages play an important role in all stages of the developmental process of an atherosclerotic plaque. Resident macrophages in plaque tissue are subject to variations in their morphology, and are able to undertake a wide variety of physiological functions.

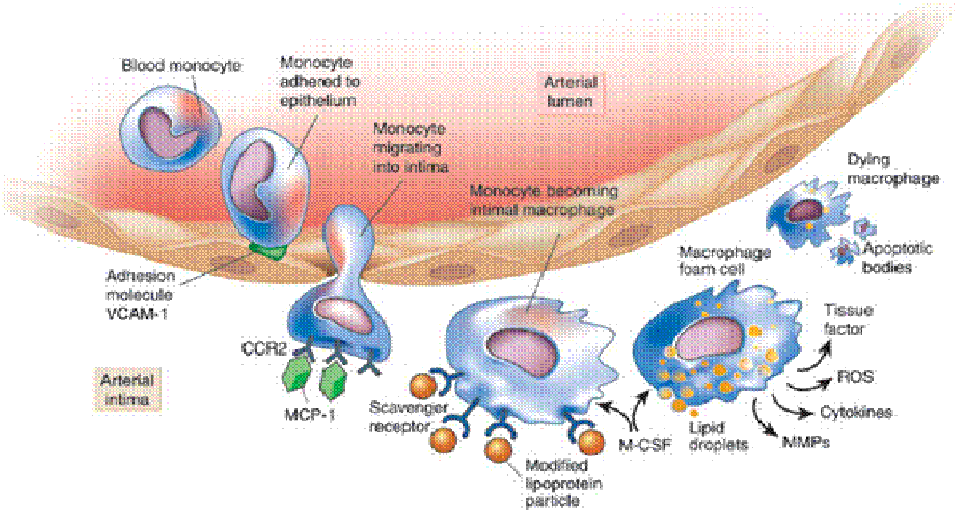

Figure 5.1 – The atherogenesis process (taken from Netters Illustrated Human pathology, Elsevier, 2005)

Associated with the collagen distribution study described in the previous chapter (4), the 3D macrophage distribution along advanced plaques will be studied in high

resolution. For the plaque morphology analysis described in the previous chapter (chapter 4), 19 cases were investigated; however for the present study only 11 plaque specimens will be studied. The reason for this is because antibody staining at high resolution along the longitudinal length of the plaque will be performed, which is very time-consuming. In addition, certain samples used in the previous chapter (4) were not suitable for analysis using immunohistochemistry. Cross-sections with 500μm intervals will be obtained from the histology analysis. For some cases, the intervals between cross-sections were reduced to 250μm to provide a more detailed evaluation of macrophage content. Plaques were obtained from symptomatic patients and classified into ruptured and non-ruptured groups. Since macrophages and low density lipoprotein (LDL) share a close relationship in the development of atherosclerosis, the present study will also assess the correlation between macrophage and lipid contents. Furthermore, macrophages are known to degrade collagen through the secretion of proteolytic enzymes such as MMP's and destabilise the plaque. This study will therefore also investigate the relationship between the macrophage content and the collagen content to improve our understanding of the risk assessment and mechanisms behind plaque rupturing.

5.2 Method

5.2.1 Tissue Specimens and Immunohistochemistry Staining

Histology sections generated from the morphology study were used for the present chapter. The protocol for immunohistochemistry analysis described in chapter 3 was used for the macrophage (CD68) staining. Figure 5.2 is an example of the staining which highlights the brown precipitate at the antigen site of the macrophage cells caused by the reaction between the peroxidase (enzyme) and the 3, 3'-Diaminobenzidine (DAB)-(substrate).

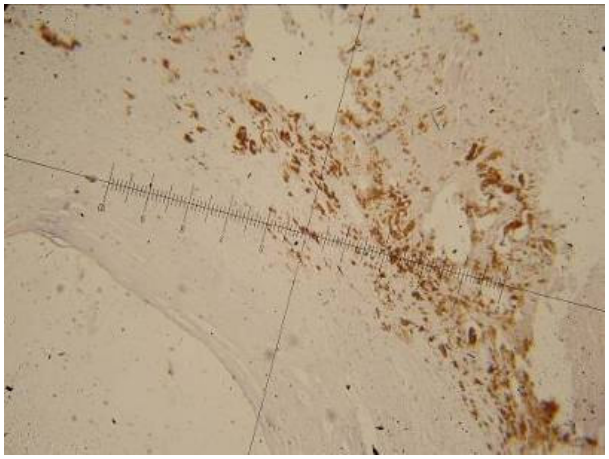

Figure 5.2 Visible brown precipitate at the antigen site caused by the reaction of the peroxidase with the 3, 3'-diaminobenzidine (DAB)

5.2.2 Quantification of Immunostained Cells (Macrophage CD68)

Digital images of the upstream and downstream plaque cross-sections were captured with a CCD-camera (Olympus SP350) at a magnification of 40X. For each analysis, the regions containing the immunostained cells were marked with a boundary by visual interpretation as shown in figure 5.3. The area occupied by the macrophage region was calculated for the sections in the upstream and downstream of the plaque for both ruptured and non-ruptured plaques. Details of the macrophage distribution analysis (area) can be found in the methodology chapter (section 3.6)

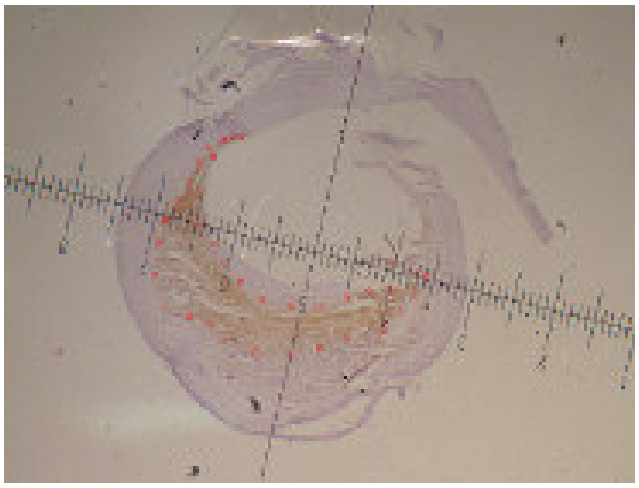

Figure 5.3 Transverse section of an atherosclerotic plaque showing the boundary of the macrophage (CD68) region stained in brown

5.2.3 3D Reconstruction of Macrophage Distribution in Carotid Plaque

A clear view of the variation in the macrophage distribution along the longitudinal length of the advancing plaque can be ideally represented by reconstructing the macrophage distribution in three-dimension (3D). The procedure described in Chapter 3 on 3D plaque morphology reconstruction was followed to generate the 3D macrophage distributions.

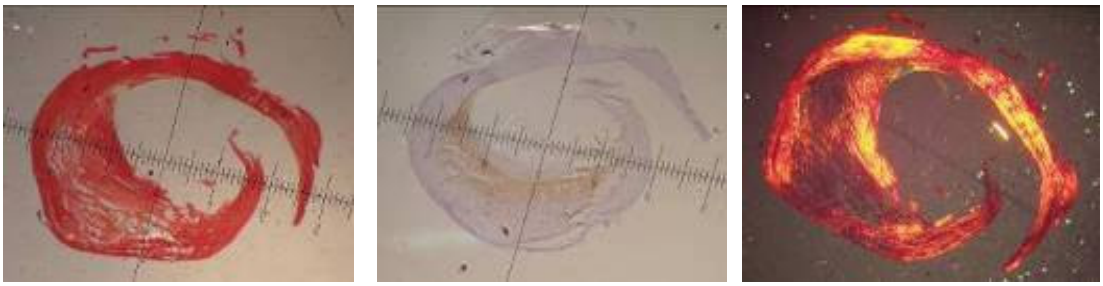

(a) **(b)** **(c)**

Figure 5.4 Transverse section of a plaque stained with (a) picrosirius red staining; (b) anti-CD68 macrophage antibody staining; and (c) viewed under polarized light

Figure 5.4 demonstrates a transverse section located 4.5mm downstream of the carotid bifurcation and displays a large necrotic core separated from the lumen by a thin fibrous cap, highly infiltrated with macrophages.

5.2.4 Statistical Analysis

All values are reported as mean values. A value of $p<0.05$ was considered statistically significant. The non-parametric unpaired Mann-Whitney Test (two-tailed) was used to compare numerical data for the immunostained cells between upstream and downstream regions, and between ruptured and non-ruptured plaques. In addition the Pearsons Product-Moment Correlation Coefficient was used to measure the

significance of the relationship between the lipid core and macrophage area for ruptured and non-ruptured plaque groups.

5.3 Results

	n=11
Average Age (years)	69
Male	6 (58%)
Female	5 (42%)
Asymptomatic	1 (9%)
Symptomatic	10 (91%)

Table 5.1 Patient data for the samples used for the study; *Values are absolute number (n) and percentage (%)*

5.3.1 Longitudinal Macrophage Content for Different Plaque Groups

Macrophage Composition between Upstream and Downstream Sites of Maximum Stenosis in Ruptured and Non-Ruptured Plaques

Figure 5.5 demonstrates one case of a series of transverse sections taken at high resolution (250µm intervals) highlighting the CD68-stained area. An in-house designed programme developed using MATLAB was used to calculate the area of the CD68-stained area. The results for all cases studied are shown in table 5.2.

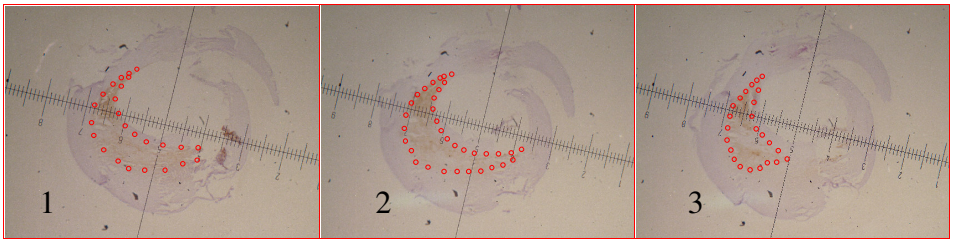

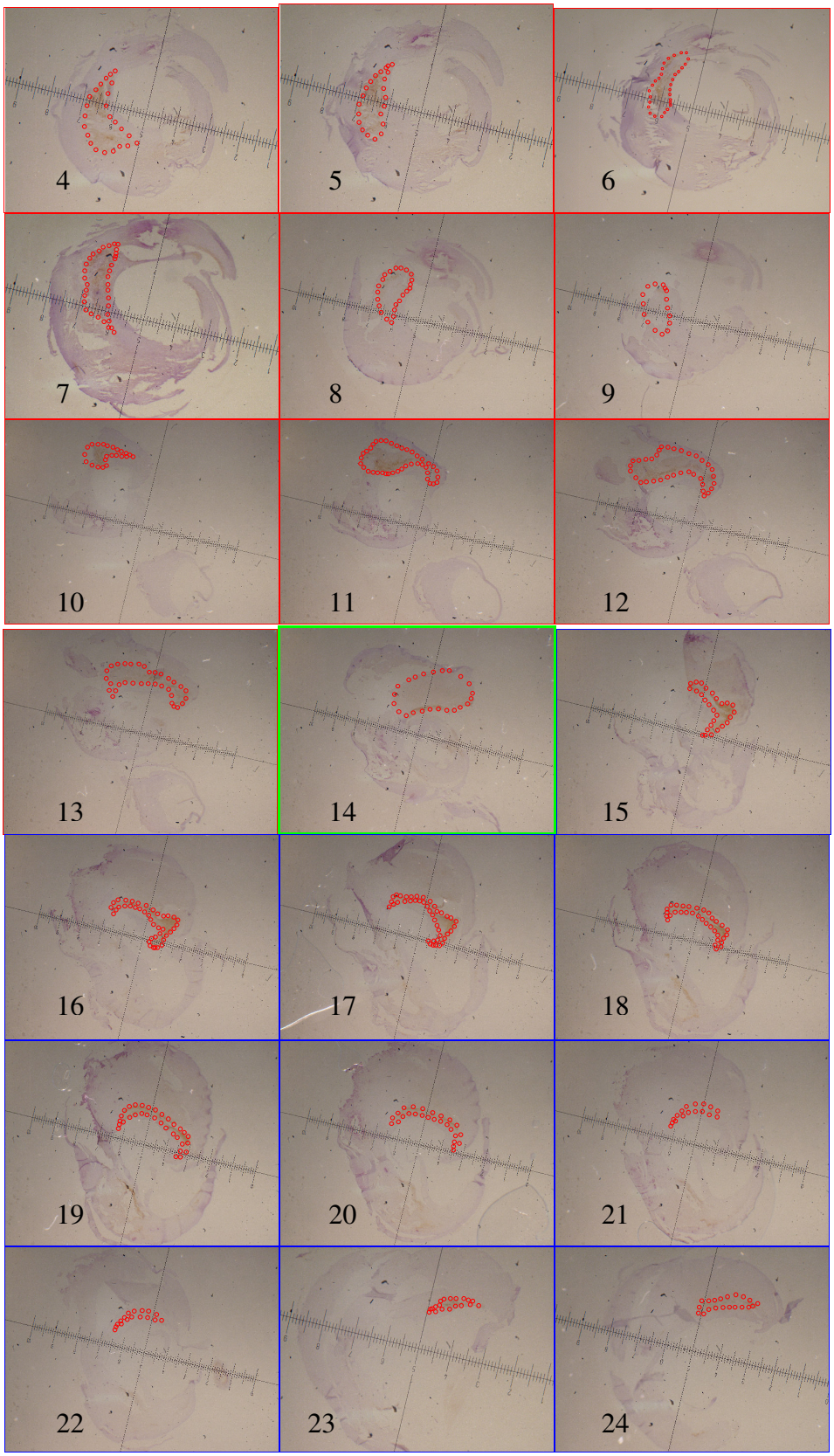
4
5
6
7
8
9
10
11
12
13
14
15
16
17
18
19
20
21
22
23
24

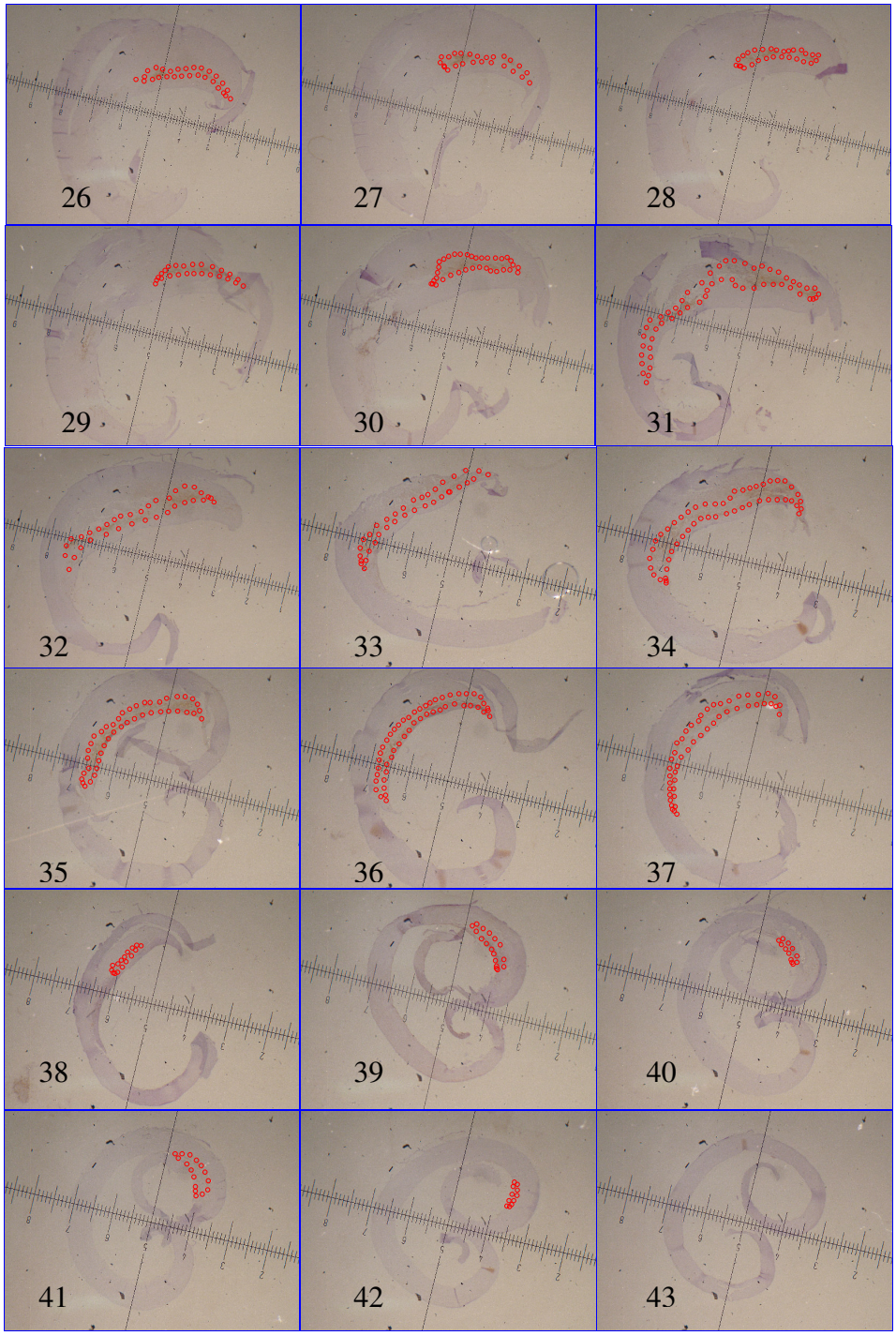

Figure 5.5: series of 6-microns thick sections stained with CD68 macrophage antibody (brown colouring). Sections 1-13 (red boarder) are in the upstream region of the maximum stenosis. Section 14 (green boarder) shows the maximum stenosis and sections 15-43 (blue boarder) are in the downstream region of the maximum stenosis

Figure 5.5 demonstrates a series of transverse sections (1 to 43) from a ruptured plaque which has been stained with anti-CD68 antibodies and counterstained with hematoxylin. The specimens were divided transversely at the point of the maximum stenosis, and from this point the sections were collated from the upstream and downstream regions. Sections 1-13 show the upstream sections (section number indicated on lower left corner of image). Section 14 shows the maximum stenosis, and sections 15-43 show the sections in the downstream region. The brown staining seen in the plaque sections highlights the localisation of CD68 positive stained cells. It can be seen from visual observation that in the transverse sections upstream of maximum stenosis (1-13), there is comparatively a higher amount of brown staining than in the transverse sections found in the downstream of maximum stenosis (15-43). This observation was found in the majority of cases that were studied (91%).

	Macrophage Stained Area (mm^2)			
	Upstream		**Downstream**	
Sample	**Ruptured**	**Non-ruptured**	**Ruptured**	**Non-ruptured**
1	6.34	5.3	5.35	3.43
2	5.63	4.54	3.15	4.34
3	7.37	5.45	3.44	3.23
4	5.11	4.7	4.32	5.32
5	7.57	5.2	4.23	2.92
6	-	4.14	-	3.74
Mean±SD	**6.40±1.07**	**4.89±0.51**	**4.10±0.86**	**3.83±0.88**
	***p*=0.03**		***p*=0.66**	

Table 5.2: Comparison of the macrophage content in the upstream and downstream region of maximum stenosis between ruptured and non-ruptured plaques

Table 5.2 shows the comparison for the CD68-stained area (mm^2) between ruptured and non-ruptured plaques in the upstream and downstream sites of maximum stenosis, measured using the MATLAB software package (see section 3.6 and 5.2.2

for details). In the upstream region, ruptured plaques were found to have a significantly higher mean CD68 macrophage area compared to the non-ruptured plaques (p=0.03). In the downstream region, ruptured plaques showed a trend towards a higher macrophage area than the non-ruptured plaques, which was not significant (p=0.66).

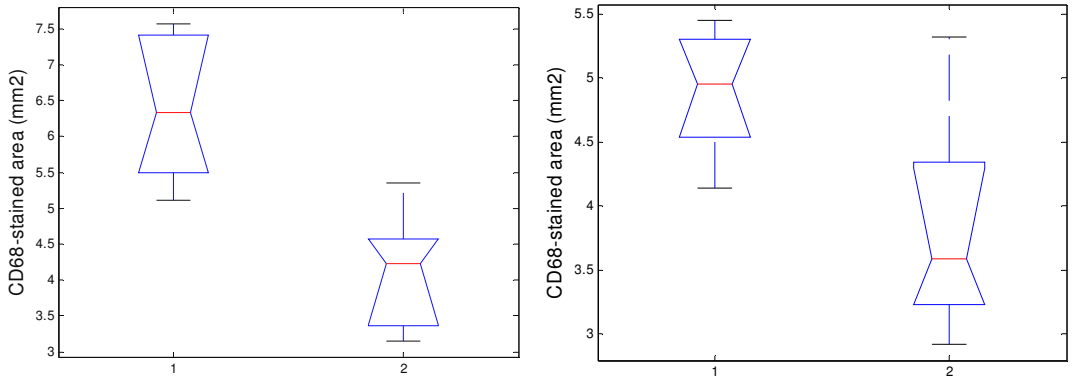

(a) **Upstream** **Downstream** **(b) Upstream** **Downstream**

Figure 5.6: Macrophage content and distribution in 11 symptomatic carotid atherosclerotic plaques in upstream and downstream regions. (a) ruptured (n=5); and (b) non-ruptured (n=6)

Figure 5.6 shows the macrophage content and distribution in the upstream and downstream regions of maximum stenosis in the ruptured plaque (a) and in the non-ruptured plaque group (b). It can be seen from panel (a) that in the ruptured plaque group (n=5), the mean CD68-stained area in the upstream region is significantly higher than in the downstream region (p=0.02), 6.40±1.07mm^2 and 4.10±0.86mm^2 respectively. In the non-ruptured plaque group (n=6), there was also non-significant higher incidence of CD68-staining (mm^2) in the upstream region compared with the downstream region, 4.89±0.51mm^2 and 3.83±0.88mm^2 respectively (p=0.06). The results of the present study are in concordance with an investigation carried out by Fagerberg et al (2010). Their results showed that compared with the downstream region, the upstream region of the stenosis had higher incidence of severe lesion and

more macrophages. Additionally to the study of Fagerberg et al (2010), the present study distinguishes between plaques which have ruptured and plaques that have remained stable. The interval between cross-sections in the present study was also significantly lower than the previous study (Fagerberg et al 2010), where only a limited number of transverse sections in the upstream and downstream sites of maximum stenosis were analysed. The present study however, analyzed transverse sections for CD68-stained areas at high resolution (250µm intervals). As macrophage content and distribution varies considerably along the longitudinal length of the plaque as a result of differing stress distribution regions across the surface of the plaque (Howarth et al 2007), it is important to analyze the macrophage content at high resolution to take into account fluctuations that may be present between transverse sections to obtain accurate and meaningful results.

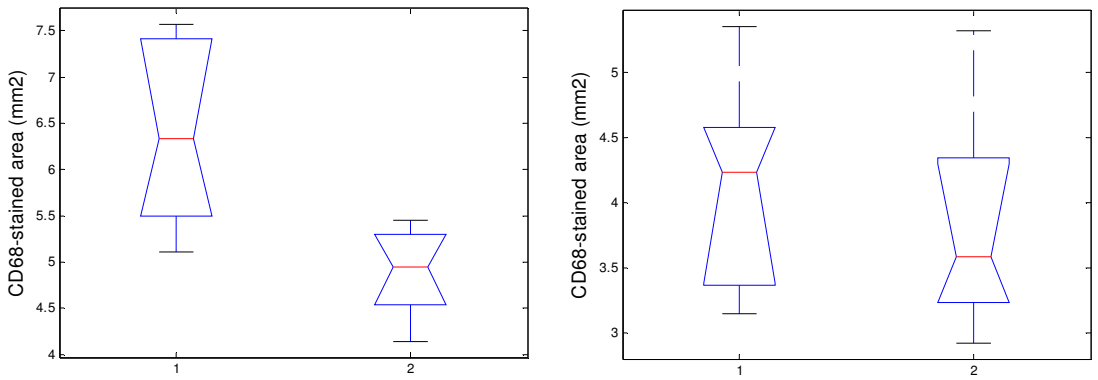

Figure 5.7: Graph comparing (a) upstream and (b) downstream macrophage content between ruptured (n=5) and non-ruptured (n=6) plaque groups

Figure 5.7 compares the CD68-stained area in the upstream (a) and downstream (b) regions of the maximum stenosis between ruptured (n=5) and non-ruptured (n=6) plaque groups. It can be seen from panel (a) that in the upstream region of maximum stenosis, the ruptured plaque group has significantly larger CD68-stained areas

(6.40±1.07mm^2) than in the non-ruptured plaque groups (4.89±0.51mm^2), p=0.03. Larger areas of CD68-stained cells in the ruptured plaque group was also found downstream of maximum stenosis compared with the non-ruptured plaque group; 4.10±0.86mm^2 and 3.83±0.88 respectively, however this result did not reach statistical significance (p=0.66).

5.3.2 Case Study of 3D Macrophage Distribution in Ruptured and Non-Ruptured Atherosclerotic plaques

An analysis of 3 ruptured and 4 non-ruptured carotid plaques to assess the variability of the macrophage distribution in the two plaque groups (ruptured and non-ruptured) was carried out. 3D reconstruction of the macrophage distribution was performed on 7 cases, 4 of the cases are presented in figure 5.8(a)-(b), and 5.10(a)-(b). Based on observations of the 2-D cross sections, it was found that macrophage stained regions were at a closer proximity to the luminal wall in ruptured plaques compared with non-ruptured plaques. This is demonstrated in figure 5.9(a) where the macrophage region (brown line) is further away from the luminal wall compared with figure 5.9(b), where the macrophage region is bordering the luminal wall.

Figures 5.9(c) and 5.9(d) demonstrate 2D views taken from the 3-D plaque model of non-ruptured and ruptured plaques (figure 5.8(a) and 5.8(b)). It can be seen that in the ruptured plaque (figure 5.9(b)); the macrophage stained region (coloured brown) is in close proximity to the luminal wall (coloured orange). Whilst the macrophage stained region in the non-ruptured plaque is relatively further in distance from the luminal wall. Figure 5.10 below shows further examples of the results that were obtained.

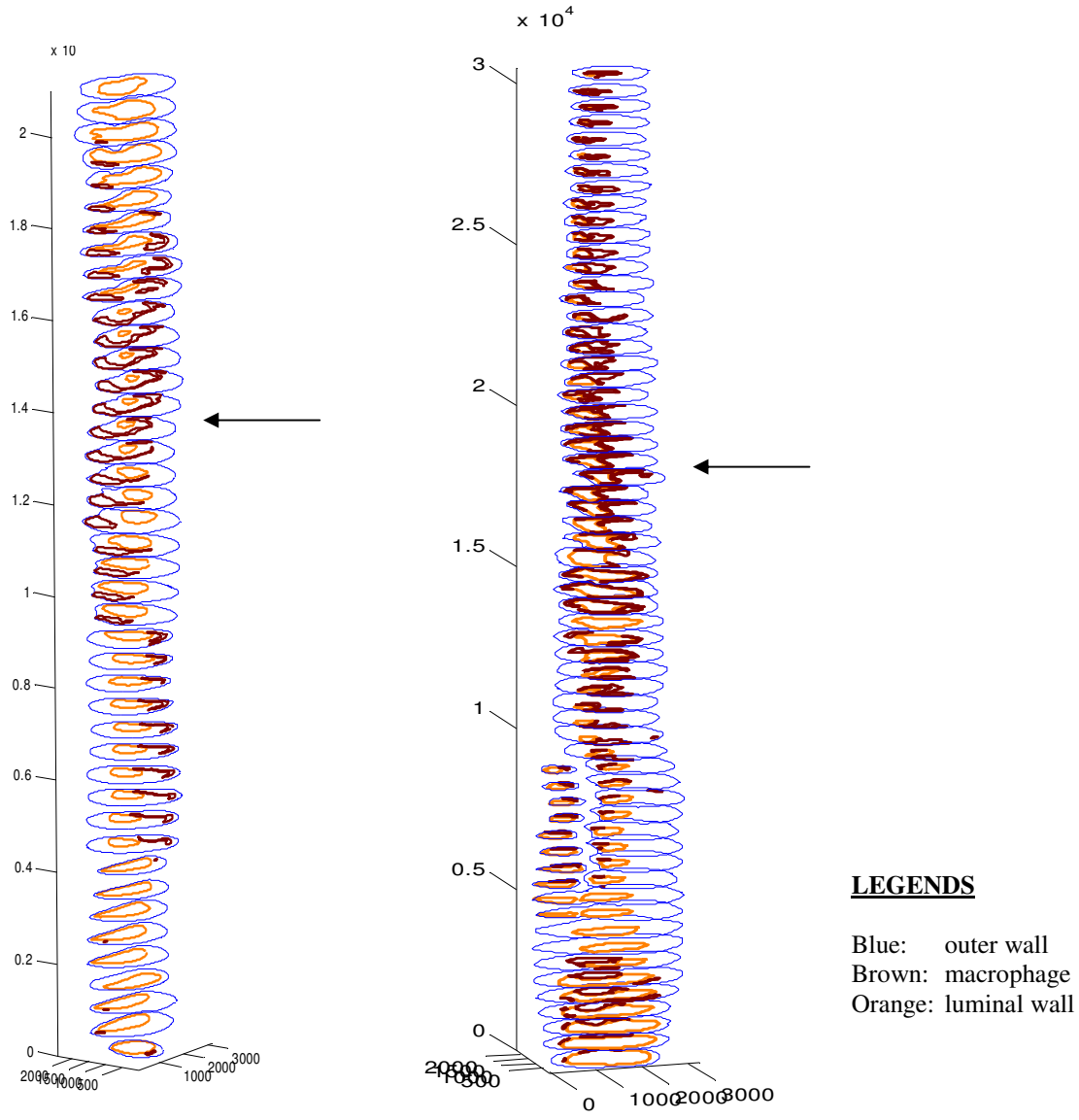

(a) Non-Ruptured Plaque **(b) Ruptured Plaque**

Figure 5.8: 3D-reconstruction of a carotid endarterectomy specimen demonstrating the distribution of the macrophage stained regions. Panel (a) demonstrates a non-ruptured plaque and panel (b) a ruptured plaque

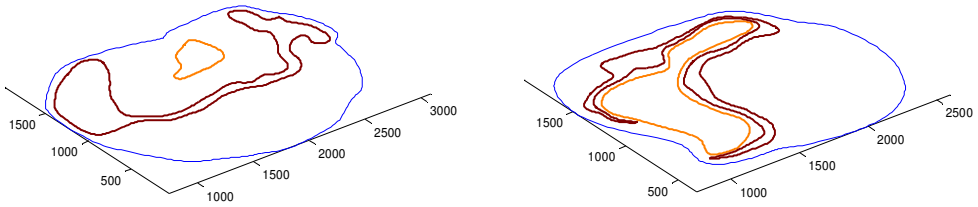

(a) (b)

Figure 5.9: 2-D plain sections taken from (a) non-ruptured plaque, and (b) ruptured plaque. Arrows on figure 5.8(a) and (b) indicate location of the 2-D sections relative to the plaque. Legends are the same as figure 5.8

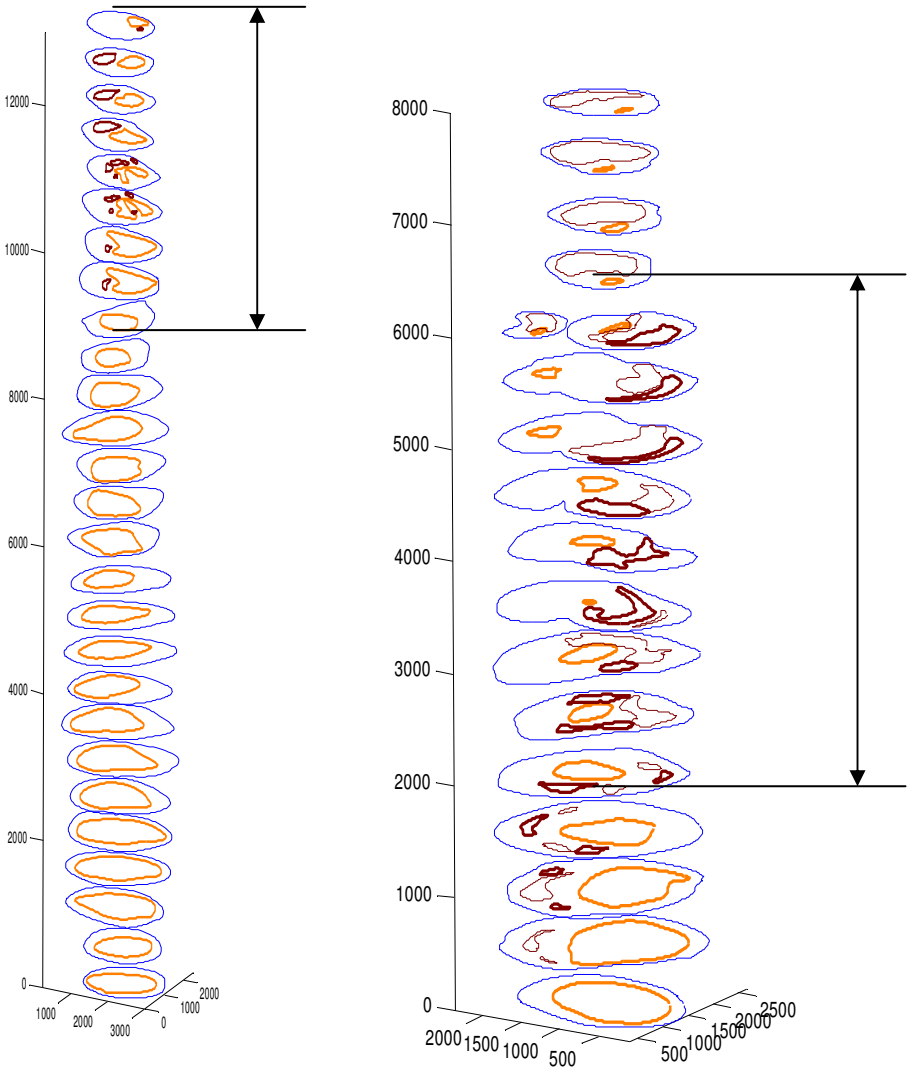

(a) Non-Ruptured Plaque **(b) Ruptured Plaque**

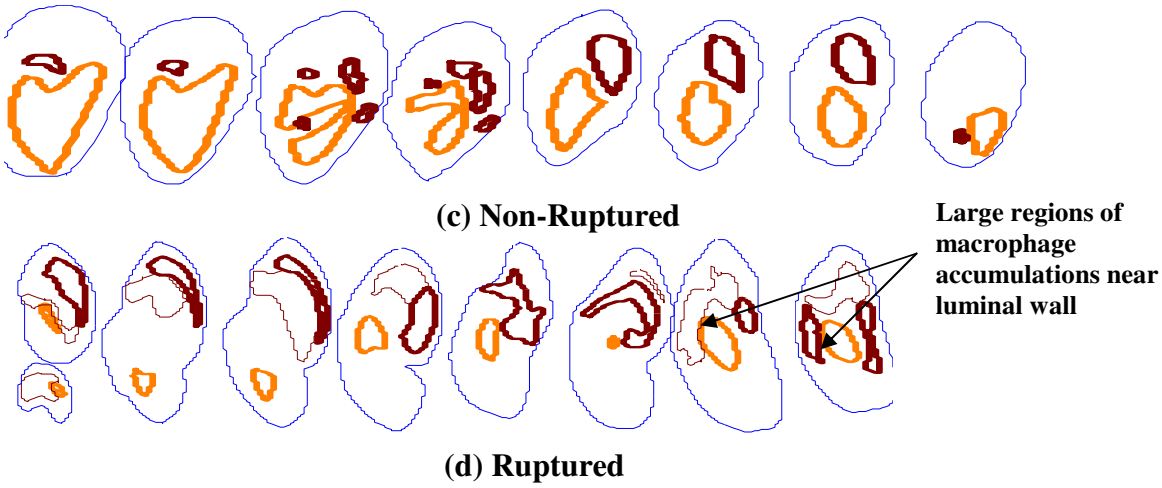

Figure 5.10: 3-D reconstruction of a non-ruptured plaque (a) and ruptured plaque (b), highlighting macrophage distributions (brown). Region marked with arrows are highlighted in 2-D cross-sectional in figure (c) and (d) respectively. Legends are the same as figure 5.8

Figure 5.10(a) (page-123) shows a 3-D reconstruction of a non-ruptured plaque highlighting the lumen (orange), the outer wall (blue), and the macrophage region (brown). It can be seen by visual observation that compared with the ruptured plaque (5.10(b) page-123); the non-ruptured plaque has less macrophage covered regions. In addition, it was found that the macrophage regions were smaller and further in distance from the lumen compared with the ruptured plaque as can be seen from figures 5.10(c) and 5.10(d). Although only a comparatively small sample was studied, the results obtained are in concordance with the studies carried out by Hussain et al (1999) which demonstrated that macrophage accumulation within the cap of carotid plaques is associated with plaque instability and rupture. In relation to the present study, macrophage accumulations in ruptured plaques were found nearer to the lumen and therefore also within the cap region. The results demonstrate that there is a difference in the macrophage accumulation size and distribution between ruptured and non-ruptured plaques. This difference may be due to the influence of biochemical factors including chemokines which have the ability to induce directed chemotaxis in

nearby responsive macrophage cells. Differences in these biochemical factors may result in certain plaques being more prone to rupture than others.

5.3.3 The Relationship between Macrophages and Lipid

The present study has shown that the majority of disrupted plaques have a necrotic core occupying a larger overall volume compared with plaques without disruptions. Further, it has been shown that they have thinner fibrous caps, and a higher accumulation of macrophage cells than intact plaques. They also have an accumulation of lipid filled macrophages at their edges (Lendon CL et al 1991). A study by Ivan et al (2002) showed that macrophages are a prominent feature of the edges of plaques (neo-intima and adventitia), which may suggest that plaques undergo expansive remodelling (outward). It further suggests that the edges of plaques are the most active sites for plaque growth. Ivan et al (2002) demonstrated that macrophage rich lesion of ApoE KO mice had significantly higher levels of expansive remodelling than macrophage-poor wild type mice. Expansive remodelling may be as a result of macrophages in the arterial wall secreting enzymes such as MMPs that degrade matrix components.

The growth of the plaque occurs as lipids accumulate at the expense of matrix proteins and smooth muscle cells. The oxidation of plaque lipids can further enhance connective tissue degradation by activating macrophage cells, and in stimulating the production of matrix metalloproteinase's (MMP). It can therefore be seen that the disruption of plaque is a result of connective tissue degradation which is a process influenced by the plaques lipid content and macrophage activity. Differences in the distribution of macrophages around the necrotic core between ruptured and non-

ruptured plaques may determine whether it influences non-ruptured plaques to become ruptured plaques.

As mentioned the aim of this part of the study is to establish differences in the macrophage content, and distribution between ruptured and non-ruptured plaques, to establish an increased understanding of why certain plaques fissure and others do not. To further enhance this understanding this part of the study will also aim to identify the association of macrophages in relation to the necrotic lipid core in ruptured and non-ruptured atherosclerotic plaques to help determine any differences which may influence plaque stability.

Table 5.3 shows the mean necrotic lipid core cross-sectional area for all the cross-sections in each specimen for the ruptured and non-ruptured plaque groups. It also shows the corresponding mean cross-sectional area occupied by macrophage cells for all the cross-section of the same specimens (correlation results are shown in table 5.4 and 5.5). It can be seen from these findings that the mean necrotic lipid core area for the ruptured plaque group was 8.58±1.67mm^2 and for the non-ruptured plaque group it was 6.43±1.23mm^2 (p=0.03). The mean macrophage area was evaluated for the same specimens and was 3.18±0.83mm^2 and 2.65±1.09mm^2 for ruptured and non-ruptured plaques respectively (p=0.24675). Although the difference was not statistically significant, a trend was observed. The results for the differences in these parameters between the upstream and downstream regions of the plaque are detailed in table 5.6.

	NECROTIC LIPID CORE AREA		MEAN MACROPHAGE AREA	
Number	**Ruptured**	**Non-Ruptured**	**Ruptured**	**Non-Ruptured**
1	7.24	5.55	2.915	2.05
2	9.45	4.82	3.115	1.36
3	10.52	6.27	4.6	2.26
4	9.22	7.18	2.745	3.075
5	6.47	8.33	2.5	4.55
6		6.44		2.59
Mean±SD	**8.58±1.67mm^2**	**6.43±1.23mm^2**	**3.18±0.83mm^2**	**2.65±1.09mm^2**
***P*=<0.05**	***P*=0.03**		***P*=0.24675**	

Table 5.3 Mean lipid core and macrophage area in all the transverse section studied for ruptured and non-ruptured plaques

Table 5.4 and 5.5 shows the descriptive statistics for the ruptured (table 5.4) and the non-ruptured (table 5.5) plaques. The results show that there is a strong positive correlation between the lipid core and macrophage area in ruptured plaques (r=0.76) and non-ruptured plaques (r=0.98).

Variable	Mean	StDev	Variance	Sum	Min	Max	Range	Correlation
Lipid Core	8.58	1.67	2.23556	42.9	6.47	10.5	4.05	r=0.76
Macrophage	3.18	2.65	0.54847	15.88	2.5	4.6	2.1	

Table 5.4: Descriptive statistics for ruptured plaques (n=5). All figures in mm^2

Variable	Mean	StDev	Variance	Sum	Min	Max	Range	Correlation
Lipid Core	6.43	1.23	1.260780	38.59	4.82	8.33	3.51	r=0.98
Macrophage	2.65	1.09	0.995064	15.89	1.36	4.55	3.19	

Table 5.5: Descriptive statistics for non-ruptured plaques (n=6). All figures in mm^2

Table 5.6 shows the relationship between the lipid core size (microns) and the macrophage area (mm^2), and also shows a comparison between the ruptured (n=5) and non-ruptured (n=6) plaques in the upstream and downstream regions. The results

were also presented in a graphical format for a clearer understanding of the correlation between the two parameters as shown in Figures 5.11 and 5.12. To confirm the significance of the correlations, a test was carried out to determine the probability that the correlations did not occur by chance.

	LIPID CORE SIZE (MICRONS^2)				MACROPHAGE AREA (MM^2)			
	Upstream		Downstream		Upstream		Downstream	
	Ruptured	Non-ruptured	Ruptured	Non-ruptured	Ruptured	Non-ruptured	Ruptured	Non-ruptured
1	896.65	704.09	668.74	609.15	6.34	5.3	5.35	3.43
2	1009.49	797.77	1141.57	704.71	5.63	4.54	3.15	4.34
3	912.36	842.85	672.88	483.01	7.37	5.45	3.44	3.23
4	598.55	547.55	604.68	498.4	5.11	4.7	4.32	5.32
5	549.84	822.21	875.55	712.81	7.57	5.2	4.23	2.92
6	-	-	-	-	-	4.14	-	3.74
	793.38 ±205.42	**742.89 ±121.41**	**792.68 ±220.03**	**601.62 ±109.28**	**6.40 ±1.07**	**4.89 ±0.51**	**4.10 ±0.86**	**3.83 ±0.88**

Table 5.6: Relationship between lipid core size and macrophage area in ruptured and non-ruptured plaques in the upstream and downstream regions

Testing the Significance of the Correlation (r)

The significance of the correlation was tested to determine the probability that the observed correlation did not occur by chance. A critical value table was used to determine the intersection value of the alpha level (0.05). For the ruptured group (n=5) the degree of freedom (d.f) was N-2= 3, and the r value was 0.76 which is below the value of the intersection (0.878). Therefore there is no statistically significant relationship between the lipid core and macrophage area for this group. For the non-ruptured group (n=6), degree of freedom (d.f) was N-2= 4, and the r value was 0.98 which is above the intersection value (0.811), and therefore there is a statistically significant relationship between the two parameters for this group.

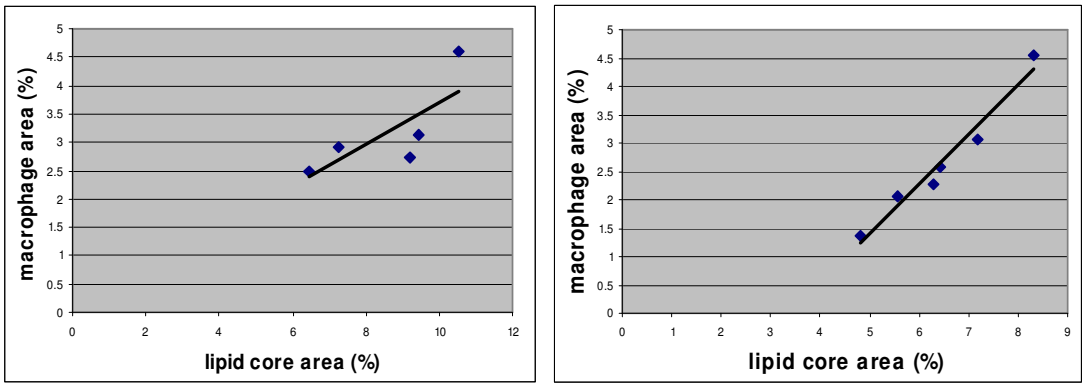

Panel A – ruptured plaque **Panel B – non-ruptured plaque**

Figure 5.11 Panel (A) shows the correlation between the mean lipid core area and the mean macrophage area for the ruptured plaque group n=5 r=0.76; and the non-ruptured plaque group (n=6) r=0.98 (Panel B)

Figure 5.11 shows the correlation between the area occupied by the lipid rich necrotic core and the macrophage cells for each plaque specimen in ruptured (Panel A) and non-ruptured (Panel B) plaques. It can be seen that all analysed specimens demonstrated a clear direct proportional relationship between the two parameters. The correlation coefficient (r) for the ruptured group was r= 0.76 and for the non-ruptured plaque group it was r= 0.98. Although these values represent a strong correlation between the two parameters, the difference in the strength of the correlation between the two groups is not easy to explain. The findings from these results are in agreement with the study carried out by Marie-Louise M et al (2002) which demonstrated that the amount of plaque lipid was greater in plaques with higher macrophage density. Other studies also demonstrated that lipid and macrophage rich plaques were found to be more prone to rupture and cause myocardial infarction in coronary arteries (De Boer OJ et al 2000 and Falk E et al 1995). However, the present study is the first to demonstrate the differences in the correlation between lipid and macrophage area in

ruptured and non-ruptured carotid plaques, and the first to perform the investigation at high resolution along the longitudinal aspect of the plaques.

Figure 5.12 and 5.13 show the longitudinal relationship between the lipid core size (microns) and the macrophage area (mm^2) in the upstream and downstream regions for the ruptured plaque (figure 5.12) and the non-ruptured (figure 5.13) plaque groups. It can be seen from both graphs that as the lipid core decreases in size as it progresses from the upstream to the downstream region, the area occupied by the macrophage cells also decreases proportionally in the same regions.

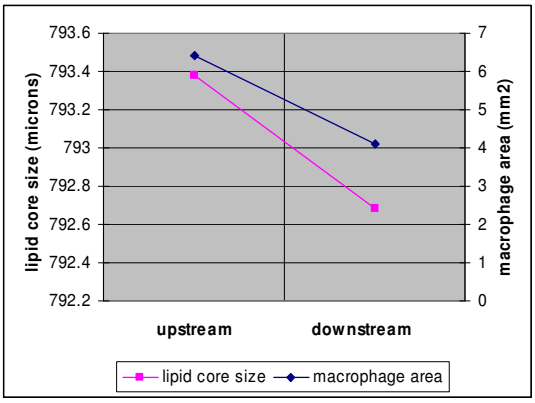

Figure 5.12 Graph showing the longitudinal relationship between the mean lipid core size (µm) and the mean macrophage area (mm^2) in the upstream and downstream regions for the ruptured plaque group (n=5)

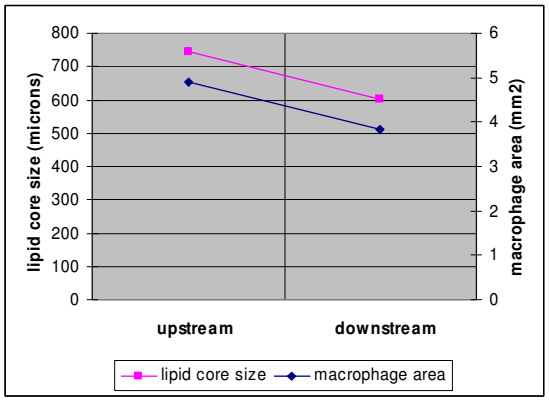

Figure 5.13 Graph showing the longitudinal relationship between the mean lipid core size (µm) and the mean macrophage area (mm^2) in the upstream and downstream regions for the non-ruptured plaque group (n=6)

5.3.4 Relationship between Macrophage and Collagen Content

The integrity of the fibrous cap in an atherosclerotic plaque, and therefore its mechanical strength against rupture depends critically on the collagen content of the fibrous cap. This aspect of plaque structure is dependent on a balance between the synthesis and degradation of the macromolecules that form the extracellular matrix of the fibrous cap, principally interstitial forms of collagen which are derived from the arterial smooth muscle cells. The degradation of collagen is dependent on the presence of macrophages. Macrophages secrete proteolytic enzymes which can act to degrade collagen, and contribute to the weakening of the fibrous cap. It can therefore be seen that macrophages have a critical influence on the stability of the atherosclerotic plaque. This part of the study aimed to detect any differences in the correlation between the macrophage and collagen content in ruptured and non-ruptured plaques.

Table 5.7 shows the mean collagen density (ratio of collagen and non-collagen material, expressed as a percentage), and the mean macrophage area for all the transverse sections for each specimen in ruptured and non-ruptured plaques. For the ruptured plaque group (n=5), the mean collagen was 32.37±10.20% and the mean macrophage area in each transverse section was 3.18±0.83mm^2. In comparison with the non-ruptured plaque group (n=6), the mean collagen content was higher at 52.89±8.80%, and the mean macrophage area was lower at 2.65±1.09mm^2. From this result it can be seen that in the ruptured plaque group (post-rupture), a higher macrophage area was associated with lower collagen content, compared with the non-ruptured plaque group, where a lower macrophage area correlated with higher collagen content. This result indicates an important role played by macrophage cells in influencing the collagen content of the fibrous cap in atherosclerotic carotid

plaques. Furthermore, the results highlight that ruptured and non-ruptured plaques have different mean macrophage areas which results in different mean quantities of collagen in the fibrous cap.

	Mean Collagen Content		Mean Macrophage Area	
Number	**Ruptured**	**Non-Ruptured**	**Ruptured**	**Non-Ruptured**
1	27.45	60.41	2.915	2.05
2	25.49	65.64	3.115	1.36
3	22.43	52.4	4.6	2.26
4	41.13	44.95	2.745	3.075
5	45.36	42.81	2.5	4.55
6	**-**	51.1	**-**	2.59
Mean±SD	**32.37±10.20%**	**52.89±8.80%**	**3.18±0.83mm^2**	**2.65±1.09mm^2**
***P*=<0.05**	***P*=0.03**		***P*=0.24675**	

Table 5.7 Mean collagen content and mean macrophage area for all transverse sections in each specimen for ruptured (n=5) and non-ruptured (n=6) plaques

Figure 5.14 shows the correlation between the mean macrophage area (mm^2) in each transverse cross-section and the mean collagen content (%) in the fibrous cap in the ruptured (a) and non-ruptured (b) plaque groups. It can be seen that both plaque groups have good correlation between the two parameters. The significance of the correlations was tested to determine the probability that the observed correlation did not occur by chance. The test showed that both correlations were significant (p=<0.05). However, it can also be seen that the non-ruptured group has a stronger correlation coefficient (r= 0.96), compared with the ruptured group (r=0.86). If the presence of macrophage cells was the only contributing factor in causing fibrous cap rupture, then it would be expected that the ruptured group would have a higher correlation coefficient (r) compared with the non-ruptured group. However this is not the case based on the present results and it is suspected that other important factors or mechanisms may be present to form a combination in addition to the influence of

macrophage cells that is critical in contributing towards plaque rupture. Studies using larger numbers of samples are warranted to improve the statistical validity of the present findings.

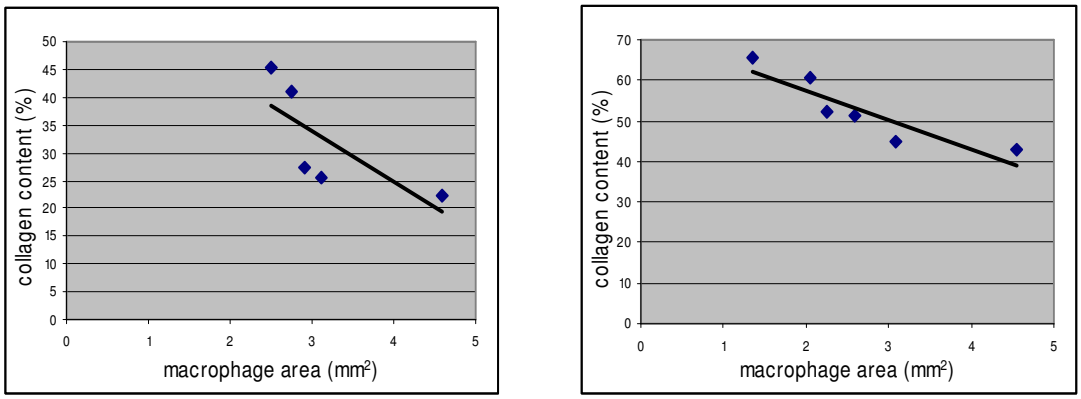

(a) **(b)**

Figure 5.14 Scatter plot showing the correlation between the mean macrophage area (mm^2) and the collagen content (%) for each specimen in (a) ruptured (r=0.86) and (b) non-ruptured plaque groups (r=0.96)

Standard Control

To verify the antibody staining technique, and to prove the stained brown coloured region were macrophage cells, a carefully designed experiment was performed. Briefly, two tests were carried out, (a) and (b). Both tests followed the step-by-step procedure described in chapter 3 (section 3.1.6). Test (a) followed the normal protocol (steps 1 to 21); test (b) followed the same steps minus the incubation with the primary antibody (step 11). This step was substituted by incubating the section with TBS solution. Figure 5.15(a) and (b) show the results for test (b) and test (a) respectively. It can be seen from figure 5.15(a) that there is no brown stained region. In the corresponding section (figure 5.15(b)), there is positive brown staining indicating that the brown coloured regions are macrophage cells.

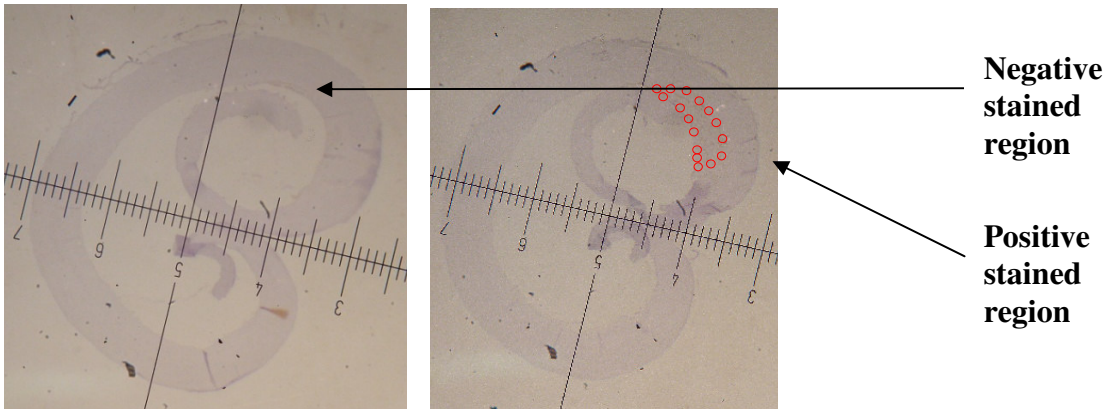

Figure 5.15 Panel (a) shows a cross-section with negative staining, and panel (b) shows the corresponding positive stained section incubated with CD68 primary antibody indicated by the brown colouring

5.4 Discussion

The major contributions of this part of the study can be summarized as: **1)** macrophages occupy a larger area upstream of the plaque throat compared with the downstream region in both ruptured and non-ruptured plaque groups; **2)** In both upstream and downstream regions, the ruptured plaque group has a higher macrophage area (mm^2) in each transverse section compared with the non-ruptured plaque group; **3)** macrophage stained regions are found distributed at closer proximity to the luminal wall in ruptured plaques compared with non-ruptured plaques, where macrophage stained regions are distributed further away from the luminal wall boundary; **4)** the area occupied by macrophage cells is directly proportional to the size of the lipid rich necrotic core and the collagen content.

The presence of immune cells in atherosclerotic plaques has been shown to be a major contributing factor for both the progression and destabilisation of the disease, which can lead towards plaque rupture and acute ischemic syndromes (Chi Z et al 2007). In a recent study, it has been suggested that hemodynamic factors might contribute to the

recruitment of circulating immune cells into the atheroma and therefore might be an important player in the destabilisation of vulnerable plaques (Fagerberg et al 2010). In the present study, we investigated in transverse sections of carotid plaque the macrophage composition of the upstream and the downstream regions, to determine if different flow conditions in these regions may affect the local inflammatory response, measured by the macrophage content. In addition, we aimed to determine any differences in this between ruptured and non-ruptured plaques that may open pathways to understanding the rupturing mechanism.

There is a significant difference in the flow conditions at the upstream and downstream regions of atherosclerotic plaques (figure 5.5(a)). On the upstream side approaching the throat, there is an increase in the flow velocity due to luminal narrowing, and as a result, there is a high wall shear stress based on mass conservation law. In contrast, on the downstream side, there is an abrupt increase in the cross sectional area that causes separation of the flow from the downstream arterial wall, resulting in flow reversal, vortices, or possibly oscillatory flow. These different types of hemodynamic conditions may induce different configurations of arterial wall remodelling. Plaque rupture is more common on the upstream side, either at the lateral plaque shoulder or at the midcap region during exertion (Burke et al, 1999). Rupturing is less common in the downstream region where there is predominant plaque growth (Smedby et al, 1997). It was reported in a recent study that high shear stress may contribute to plaque rupture at the upstream side, and that low shear stress may be responsible for the growth of the plaque at the downstream side (Slager et al 2005). A 20 case stress analysis study of in-vivo carotid plaque carried out in our group showed that extremely high wall tensile stress is more likely to occur upstream of a plaque. If the degree of stenosis of 60% is set as a critical

value, 6 out of 7 cases in our study have maximum wall tensile stress occurring upstream (Gao H. PhD thesis). The present study shows that not only are upstream regions of plaque more likely to have higher wall tensile stress, it also has higher contents of macrophage accumulation which will further weaken the local structure and make it prone to rupture. By using ultra-small super-paramagnetic iron oxide (USPIO)-enhanced MRI, Howarth et al (2007) demonstrated that there is a correlation between areas of high stress and macrophage accumulation in carotid plaques.

The structural integrity of the fibrous cap of the plaque and hence its vulnerability to rupture depends largely on its content of fibrillar interstitial collagen. A large number of studies have focused on proteinases that may degrade interstitial collagen. A specialised pathway exists for degrading macromolecules of the extracellular matrix which include a group of proteolytic enzymes known as matrix metalloproteinase's (MMP). Interstitial collagenases are involved in the initial stages of collagen degradation by cleaving the triple-helical fibrils of interstitial collagen types I, II, and III at a single site (Gly775-Leu/IIe776), resulting in fragments that are three quarter and one quarter length (Mitchel et al 196l). This process ultimately weakens the fibrous cap of the plaque and makes it prone to rupture. These proteinases are largely secreted by inflammatory cells including macrophages.

Since macrophage cells are generally found accumulated on the boundary of lipid cores, it is interesting to study the quantitative correlation between the **macrophage area and the lipid core size for both plaque groups**. It was found that there was a direct proportional relationship between the area of the lipid core and the area occupied by the macrophage cells in both plaque groups. A large lipid core correlated

with a large accumulation of macrophage cells. The investigation also found that there was a difference between the plaque groups in relation to the significance of the correlation between the parameters. The non-ruptured plaque group has a significant correlation (r=0.98) between the parameters, compared with the ruptured plaque group, which was found not to have a significant correlation (r=0.76). It is not clearly known why there is this difference. It may be due to the ruptured plaques being at advanced stages of the atherosclerosis development process, and as a result there could be other factors playing a role in the pathology of the disease progression, other than influences from the lipid core alone which would have a more primary role in non-ruptured plaques. Although there is no measurement of MMP activity in this study, it does show that high levels of macrophage cell accumulations are associated with low collagen content. This indirectly suggests that the release of proteolytic enzymes such as MMP by macrophages causes the degradation of collagen, and therefore demonstrates the role of macrophage cells in plaque structure stability.

Combined analysis of chapters 4 and 5

In relation to the results in chapter 4, it was found that for both ruptured and non-ruptured plaque groups, a higher macrophage content in the upstream region correlated with a thinner fibrous cap, compared with the downstream region where the lower macrophage content correlated with a thicker fibrous cap. Furthermore, decreases in the macrophage content from the upstream to the downstream region were also found to be correlated with a decrease in the collagen density in the same regions for both plaque groups. As it is widely known that macrophage release proteolytic enzymes such as MMP can degrade collagen (Deguchi et al 2005), it provides an indirect link for the role of macrophages in collagen degradation in the

fibrous cap. Fagerberg et al (2010) has shown that the vast majority of plaque ruptures occur at upstream regions, and therefore these findings, which have categorised plaques into up/downstream regions, and ruptured/non-ruptured plaque groups, may help in the biological understanding of rupture mechanisms. It may also help in understanding the effects of different hemodynamic conditions on the development of an atherosclerotic plaque, and in the risk assessment of plaque rupture.

Figure 5.16 summarises the results from chapters 4 and 5 for the lipid core size, the fibrous cap thickness, the collagen content, and the macrophage area in ruptured (red crosses) and non-ruptured (blue crosses) plaques, and it has therefore been presented here at the end of both chapters (4 & 5). It provides a cross-group comparison of the ruptured and non-ruptured plaque (horizontally presented) for the upstream region; the downstream region; and the throat region. It also presents the longitudinal variations of the parameters (vertically presented).

	Lipid Core Size			Fibrous Cap Thickness			Collagen Contents			Macrophage Area		
Upstream	++	+	non-s, non-s	+	++ ++	sig, sig	++	+	non-s, sig	++ +	++	non-s, sig
	sig			sig			non-s			sig		
Downstream	++	+₊		+++	++ +		+	+		+₊	+	
	non-s			non-s			non-s			non-s		
Throat	+++	++		+₊	++		+	++		n/a	n/a	
	sig			sig			sig					

Figure 5.16: Summary of the morphology analysis results from Chapters 4, 5. Keys: Red = ruptured group results; Blue= non-ruptured group results; Sig=Significant; non-s=Non-Significant; High=++; medium=+₊; Low=+

Chapter 6

3D Reconstruction of an Arterial Plaque by the Combination of Histology and Ultrasound

6.1 Introduction

The 3D reconstruction of a realistic plaque model would provide not only an opportunity for detailed examination of the plaque status but, more importantly, models for further study such as computational stress analysis and correlation of biological activities to elucidate rupture mechanisms. Analysing plaque geometries obtained from medical imaging has proven difficult to reveal the fine details of tissue structure changes due to the limited spatial resolution of images. This PhD project is part of a larger study of plaque rupture risk in our research group which involves plaque stress analysis and ultrasound assessment of plaque vulnerability. It would be beneficial for the overall research if the 3D representation of plaques could be generated at microscopic levels of accuracy, based on histology section images, to be used to perform plaque stress analysis and subsequent correlation of results with histology findings. In this chapter, the work that has been carried out to reconstruct 3D plaque geometry from histological images will be presented, as well as an assessment on tissue distortion caused by the histological procedures.

Histology sections of plaque specimens can provide not only high resolution images of the plaque (resolution at micron-level), but also accurate tissue definitions of different components of the plaque. Furthermore, important plaque features including the lipid core, and the fibrous cap etc can be easily identified. Histology sections can also reveal other information such as the localisation of specific cell types, which can

be used to further refine the 3D plaque model. Structural information such as collagen and elastin density can be revealed, which is important when constructing a model for stress analysis as varying tissue properties can affect the results.

Histological images have been used for analyzing plaque rupture in recent years in a 2D manor (Schulte-Altedorneburg G et al 2000). However, there are many potential problems of advancing the technique into 3D plaque reconstruction. The major problems are (a) registration of the sections in 3D; (b) distortions of the structure during tissue processing.

The aim of this part of the study is to develop a procedure for generating a 3D plaque geometry model based on histology sections, and address the problems listed above. The procedure will be performed on one case. In addition it also quantifies the tissue distortion that occurs in the plaque tissue as a result of the histology procedure, which will be investigated in 3 cases.

6.2 Method

To reconstruct the plaque as a 3D image, the most important and difficult step is to correct the tissue distortion and generate accurate 2D transverse images. In general, to recover image distortion, a set of rules needs to be defined so that every pixel in the source image will follow the rule and be mapped to a target image. In this study, an ex-vivo ultrasound scan on the carotid endarectomy (CEA) specimen was applied to provide plaque specimen 3D geometry information before distortion. Ultrasound scans may not be adequate to provide accurate plaque tissue characterisation within a plaque; however it is able to provide information such as the location of the luminal

and outer walls of the plaque. Regardless of the type of structural distortion that may be induced by tissue processing, the wall points on the specimen should remain on the walls after histology processing, although the internal point location may change. Therefore, by mapping the wall points on the histology section image (source image), to the corresponding wall points obtained from the ultrasound images (target image), the movement of the internal points can be predicted based on the mechanical stress balance equations according to the predefined tissue material mechanical property for each plaque component. Finite element simulation will be used to solve the stress balance equations and predict the internal point movement to recover the image distortion.

To perform a recovery process based on this procedure, there are several objectives that need to be achieved. They are as follows:

a) Register every histology section to the images from the US scan in the longitudinal direction and transverse planes;

b) Segment the images of the histology sections into regions of different plaque components, and assign different mechanical properties to the different tissue types;

c) Generate luminal and outer wall contour points mapping relationship between source and target images;

d) Run the FEM simulation on the source image to move the points on the walls to the mapping location in the target image. The movement of the internal points will define the FEM simulation.

For step (c), specific landmarks are required to be identified on the corresponding source and target images on the luminal and outer walls to define the starting points of the luminal and outer wall contours. Also, it is necessary to uniformly separate the wall contours into a fixed numbers of point for both source and target images to enable each contour point on the source image to be matched to a corresponding point on the target image. The following section will describe the procedure in further detail. In addition to plaque geometry 3D reconstruction, the present study will also describe the methodology for the quantitative assessment of tissue distortion caused by histological processing. The specimen used is a carotid endarectomy which was collected from Hillingdon hospital immediately after surgical procedure. The specimen has >90% blockage and is from an elderly patient. The collection procedure was approved by the local ethics committee.

6.2.1 Ex-Vivo Ultrasound Scan of Plaque Specimen

Carotid endarectomy (CEA) was performed on patients with carotid plaques, and the excised specimen collected the same day, providing fresh samples for analysis. The samples were rinsed thoroughly in saline (0.9% NaCl) and then subjected to an ex-vivo US scan.

Mechanical Arm: The ex-vivo scan set-up using the mechanical arm is an in-house designed equipment that enables the 2D ultrasound probe to travel along a rail at a controllable and consistent velocity. The CEA specimens were immersed in a container filled with distilled water (figure 6.1). The ultrasound probe is attached to the mechanical arm (actuate) and is lowered into the water and positioned directly above the beginning of the CEA specimen. The probe travels on a rail that is driven by a step motor and is connected to a computer that regulates the motion. As it travels

along the rail it collates a series of 2D plane images. The accuracy of the probe movement is 8µm/step.

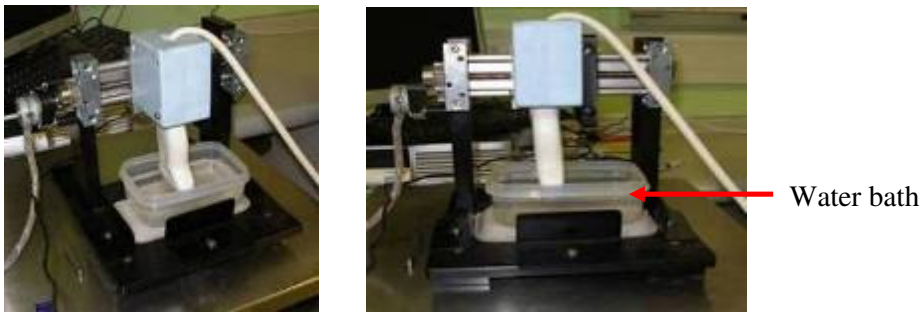

(a) (b)

Figure 6.1 (a) side view and (b) anterior view of the mechanical arm

Figures 6.1 shows photographs of the mechanical arm used to perform the 2D ultrasound scan. Panel (a) shows the side-view, and panel (b) shows the anterior-view of the mechanical arm. The ultrasound probe is mounted on a rail and is immersed in the container (figure 6.1) containing the specimen to be scanned. During the experiment, the probe moves at a constant speed which enables the US system to record a sequence of 2D transverse images covering the entire longitudinal length of the specimen as shown in figure 6.2. After the 2D ultrasound scan using the mechanical arm, the specimens were subsequently subjected to histology analysis.

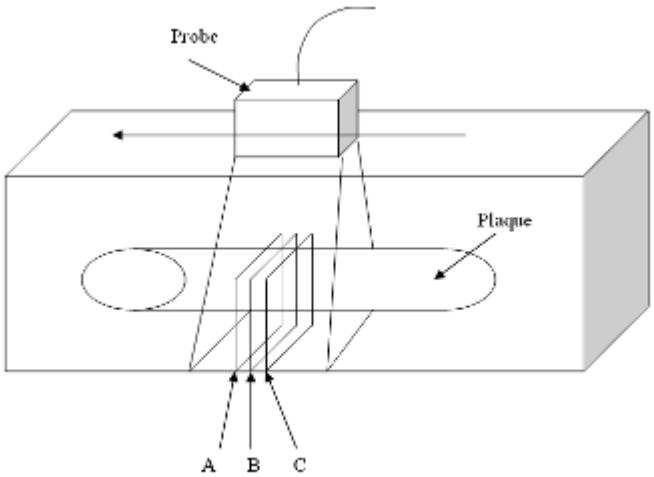

Figure 6.2 Diagram to show the probe movement including the ultrasound scan plane, perpendicular to the image plane

6.2.2 Histology Analysis

The standard histology procedure described in section 3.1, and the 3D specimen marking system described in section 3.2 were applied to the specimen. Histology sections with a longitudinal interval of 0.25mm were obtained throughout the specimen. Sections were stained using picrosirius red and H & E.

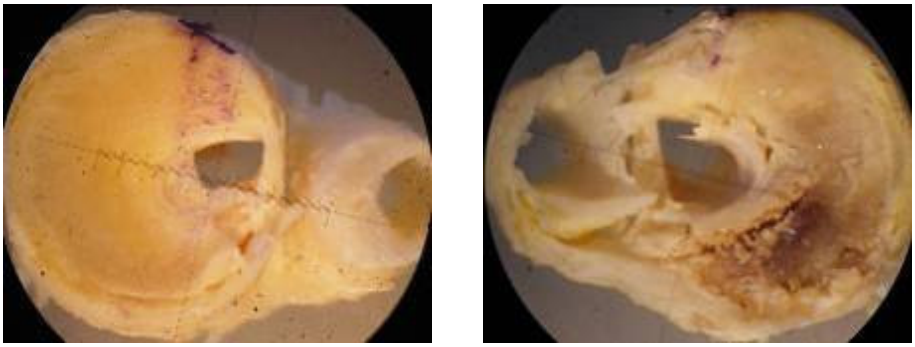

(a) **(b)**

Figure 6.3: Photograph of the right side of a 5mm segment (a); and the left side of the same segment (b)

6.2.3 Registration of Histology Sections to the US Scan Images

(a) Longitudinal Alignment: The histology sections have a thickness of 6-microns, whilst the US images are much thicker. It was therefore necessary to perform a registration process to align each histology section to the corresponding US images.

Basic landmarks that can be used:

- US images from both ends of the specimen should be the same as the images obtained of the corresponding sections.
- US images of the bifurcation apex should be the same as the histology image at the same apex position.

Chapter 6 Plaque 3D Reconstruction

To precisely correlate each histological transverse-section to the corresponding ultrasound cross-section was an almost impossible task. It must be noted that during the tissue processing, all the blocks did not contract in length in similar ways. During the histology procedure, transverse-sections were cut from each block every 225µm in the longitudinal axis; however, this distance would not reflect the actual distance between each subsequent 2D section because the sectioning was performed after the tissue processing stage which results in tissue shrinkage. It can therefore be seen that the distance between the histology sections can only be used as a guide to match the ultrasound images to the corresponding histology sections. The longitudinal length of each block cut from the CEA specimen before subjecting it to tissue processing was measured (figure 6.4). Based on the total number of histology sections that were generated from each block through sectioning (Table 6.1), and assuming that the longitudinal shrinkage as a result of tissue processing in each block was constant, it was possible to determine accurately the distance between subsequent sections.

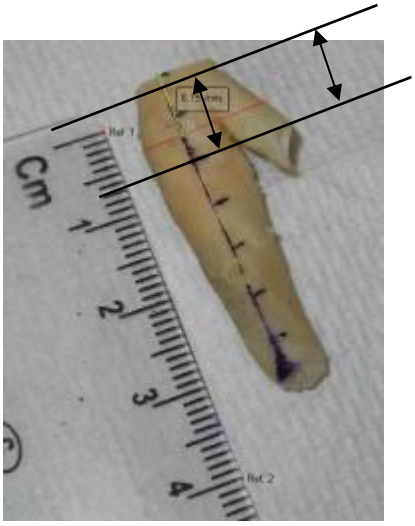

Figure 6.4 Image showing the distance of the bifurcation from the beginning of the specimen –*identified using the assistance of ultrasound images

The first section was placed by assuming that the first histology section corresponded to the ultrasound section that was furthest from the bifurcation (figure 6.4). Starting from this section we collated all the other sections knowing that each block was 5mm in length, and the corresponding numbers of histology sections for each block (Table 6.1). The longitudinal location of each 2D transverse image can be obtained by the image number.

Block No	From section No	To section No	Total slices for the block
1	1	9	9
2	10	21	12
3	22	32	11
4	33	44	12
5	45	54	10
6	55	65	11
7	66	72	7
			Total of 72 sections

Table 6.1: Total numbers of histology sections generated from each tissue block

(b) Circumferential Registration

Identification of a landmark on the microscope slide provided a guide to achieve circumferential alignment for each section. Rigid rotation was applied to achieve circumferential orientation. This involved orientating the histology section to the same alignment as the corresponding ultrasound image. An in-house designed programme was used for the purpose. Ultrasound images were adjusted accordingly to align them with the histology cross-section using the imaging software Paintbrush (figure 6.5).

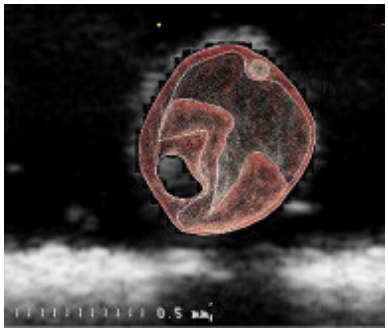

Figure 6.5: A registered histology section that has been circumferentially aligned with the corresponding ultrasound section

2) Image Resizing: This step is performed to resize the images to a suitable size using a program developed in MATLAB 7.0. The resizing of the images was performed in two steps: 1) the histology cross-section images were adjusted to a size of 573 x 430 pixels in width and height, and 2) the corresponding ultrasound images were then resized to fit the histology cross-section image.

6.2.4 Segmentation of the Histology Images and Different Mechanical Properties of Different Plaque Components

Segmentation of the Plaque Components: Using the same procedure described in section 6.2.5 (below), the inner plaque components which could be recognised in the source image were segmented (figure 6.6). The components that were segmented include the lipid-rich core, the mixed region, which is a combination of fibrous and lipid tissues, and the calcified region, which is identified during the sectioning process, characterised by its hard nature and the damage it causes to the fibrous tissue in its immediate surrounding region, which can be recognized in the histology sections. The commands for ANSYS to draw the geometry of the plaques components were recorded automatically in a macro file and performed for the outer and luminal walls.

(a) (b) (c)

Figure 6.6 Segmentation of the (a) semi-lipid tissue; (b) the calcified region; and (c) the lipid tissue open segmentation

6.2.5 Generation of Luminal and Outer Wall Contour Points Mapping Relationship between the Pair of Histology and Ultrasound Images

Images of histological sections were manually segmented on the outer wall and the luminal wall by a series of points using a programme in Matlab 7.0. A contour was generated to represent each wall by passing through the points. The starting point of the contour had to be at a recognisable landmark on the boundaries. The contours were then interpolated into a certain number of uniformly distanced points, i.e. 200 points for luminal wall which has a small perimeter or 500 points on an outer wall contour which has a larger perimeter.

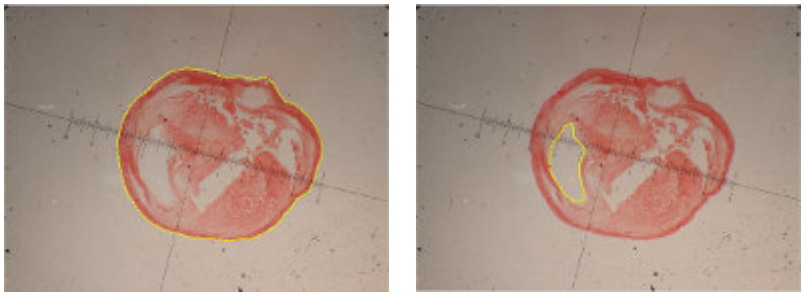

(a) (b)

Figure 6.7 The boundary of the (a) wall source; and (b) the luminal wall

Starting from the same recognisable landmarks on the walls found on the histology image (figure 6.7), the luminal and outer walls on the corresponding ultrasound image (target image) were also manually segmented and represented by contours. The same numbers of points used for the outer wall and luminal wall in the histology image are

used to mark the ultrasound image (figure 6.8). This enabled us to see any link between the two sets of points in the images. It is important to note here that the definition of the inner luminal wall location is difficult for this case since the ultrasound scan was performed when there was no luminal pressure being applied. As a consequence, the lumen contracted into a very small region (the small dark region at the lower left of the vessel).

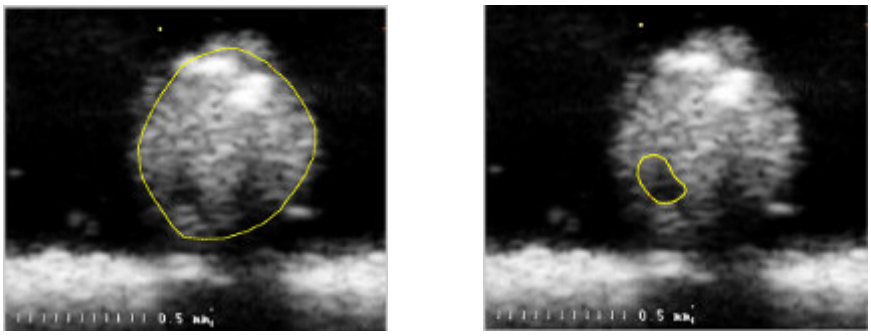

(a) **(b)**

Figure 6.8 Images showing (a) the boundary of the outer wall target, and (b) the boundary of the luminal wall target

The Displacement Vector for each set of boundary points (the contour points as described above) was calculated by mapping the point from the source image to the corresponding point on the target image as shown in figures 6.9. The vectors were eventually used as boundary conditions in the following FEM simulations.

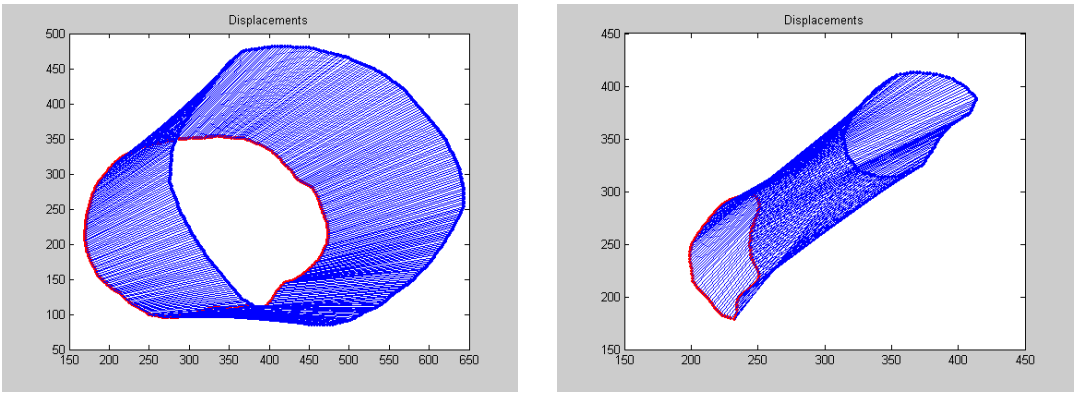

(a) **(b)**

Figure 6.9 Images demonstrating (a) the displacement vector of the wall, and (b) the displacement vector of the luminal wall

6.2.6 FEM Simulation of Non-Linear In-Plane Registration

The segmented images (both source and target) were inputted into ANSYS 11 to build the numerical mesh with planar elements (PLANE182). It is assumed the plaque components have linear, elastic material property for simplicity. The plaque is subdivided into four different regions such as fibrous region; lipid core region; mixed region (content fragmented collagen and lipid); and calcification region. The material properties assigned for each region are presented in table 6.2 based on published literature (Baldewsing et al 2005). Parameters that were assessed were Young's modulus and Poisson's ratio. Young's modulus is a measure of the stiffness of an isotropic elastic material, whilst Poisson's ratio is the ratio of the fraction of expansion divided by the fraction of compression.

	Fibrous Area	**Lipid Core**	**Mixed Region**	**Calcification**
E [MPa]	10^6	10^3	10^4	10^9
ν	0.5	0.3	0.3	0.5

Table 6.2 Material properties applied to the different plaque components

Since there are no measured material properties for the specimens, to assess the reliability of the assumed material property to the simulation result, a sensitivity test was performed and is explained in detail in the appendix section. This was carried out to evaluate the changes that may occur to the results if the material properties for one or more of the plaques components were altered. It has not been included here as it does not directly support the objectives of this study.

The calculated displacement vector was applied to each contour points of the histology image on the outer and luminal walls as a loading condition for FEM simulation. The result of this procedure is that the shape of the histology image

moulded to the shape of the ultrasound image. With the correct numerical mesh and predefined material properties on each mesh point, and the boundary loading condition, the FEM simulation is able to provide definition of mechanical stress, strain and displacement for each internal mesh point. It is the displacement of the internal mesh points that we require for the image registration purpose.

Mapping of the Registered Image: Two (2) text files were extracted using the post processor ANSYS 11, one (1) containing coordinates of every node of the mesh in the FEM model, and one (1) containing the displacement that every node encounters after elastic deformation. This enabled every pixel in the original image to be moved to the predicted position after elastic deformation. This process is the remapping of the histology image on to the new registered image which finalises the 2D-2D registration process and can be seen in figure 6.10 – panel B. After this procedure the registered image is matched with the US image (Figure 6.10 – Panel D). It can be seen in figure 6.10 - panel C and D how the different plaque components move according to the solution of the FEM model.

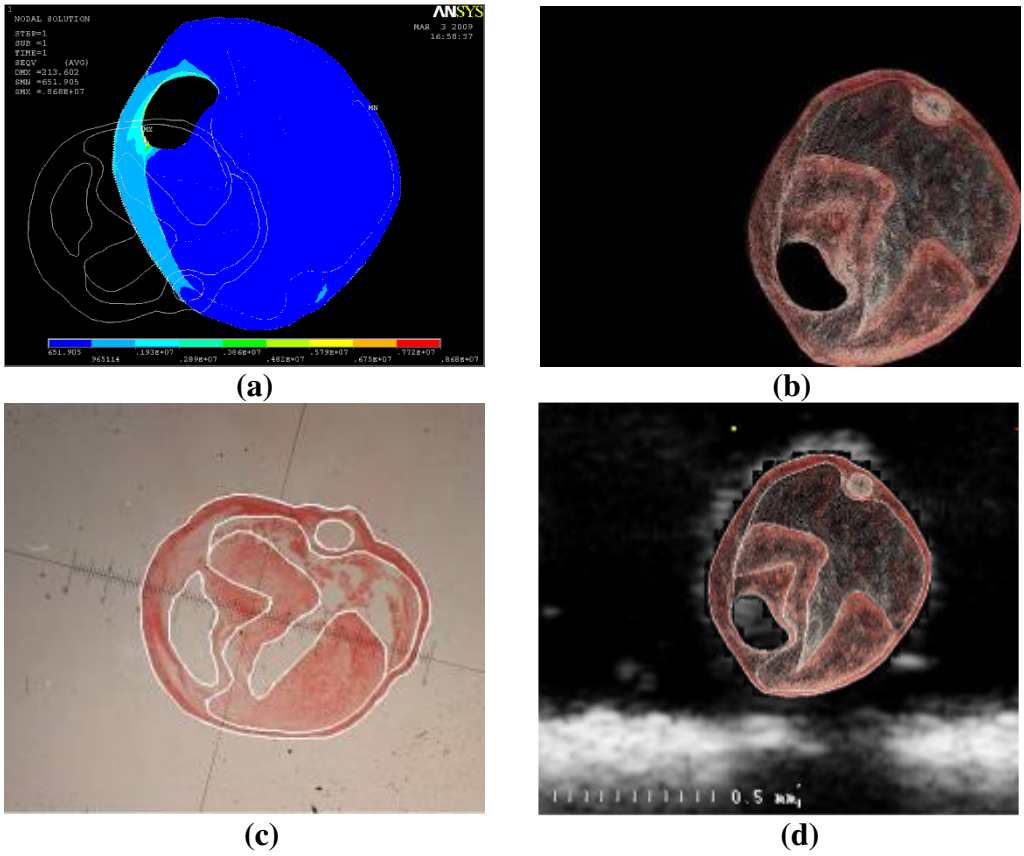

(a) (b)

(c) (d)

Figure 6.10 Images demonstrating the (a) solution of the FEM model; (b) the mapped image; (c) the source image segmentation; and (d) the target image segmentation

After the 2D in-plane registration, the sequence of histology images can then be stacked according to the axial coordinate assigned above to build the 3D model. The procedure described in section 3.4 is used to reconstruct the 3D model of the plaque.

6.3 Results

Registered Images Used For 3D Plaque Reconstruction

If z = 0 was the axial coordinate of the first ultrasound section, 72 sections were extracted for the specimen and their z coordinates are shown in table 6.3.

1	2	3	4	5	6	7	8	9	10	11	12	13	14	15	16	17	18	19	20
0	0.6	1.2	1.8	2.4	3.0	3.6	4.2	4.8	5.3	5.7	6.1	6.5	6.9	7.3	7.7	8.1	8.5	8.9	9.3
21	**22**	**23**	**24**	**25**	**26**	**27**	**28**	**29**	**30**	**31**	**32**	**33**	**34**	**35**	**36**	**37**	**38**	**39**	**40**
9.7	10	10.5	11	11.5	12	12.5	13	13.5	14	14.5	15	15.3	15.7	16.1	16.5	16.9	17.3	17.7	18.1
41	**42**	**43**	**44**	**45**	**46**	**47**	**48**	**49**	**50**	**51**	**52**	**53**	**54**	**55**	**56**	**57**	**58**	**59**	**60**
18.5	18.9	19.3	19.7	20.2	20.7	21.2	21.7	22.2	22.7	23.2	23.7	24.2	24.7	25	25.5	26	26.5	27	27.5
61	**62**	**63**	**64**	**65**	**66**	**67**	**68**	**69**	**70**	**71**	**72**								
28	28.5	29	29.5	30	35.6	31.2	31.8	32.4	33.0	33.6	34								

Table 6.3 Axial coordinate z [mm] of ultrasound sections from number 1 to 72

The above coordinates (table 6.3) were used in the SolidWorks software to construct the stack of 2D sections. This formed the basis for the skeleton of the 3D geometry of the carotid artery. For the purpose of the 3D reconstruction, only 15 out of the total 72 sections were used to avoid over definition of the surface details which can cause problems with surface generation. The sections chosen were: 1, 5, 9, 14, 18, 23, 29, 35, 41, 47, 51, 57, 62, 65, and 70. The figure below (figure 6.11) demonstrates the results showing the sections that were used in the reconstruction of the model using the SolidWorks software. The first (1) column is the histology sections stained with picrosirius red and captured using optical microscopy. The second (2) column shows the same section captured using polarised light. Due to the limited low magnification that was possible using our set-up for polarised light microscopy, more than one image is used in certain cases to represent the same section. It can be clearly seen that with the use of polarised light, the ability to characterise the tissue in the plaque improves vastly. The third (3) column shows the corresponding ultrasound image, and the last column (4) shows the results of FEM registration. During the registration procedure, histology sections were matched to the corresponding ultrasound sections. The registered images in the fourth (4) column were used for the reconstruction of the 3D plaque model. Please note that in the third column, the luminal wall is difficult to identify because of the lack of luminal pressure when the ultrasound (US) scan was performed.

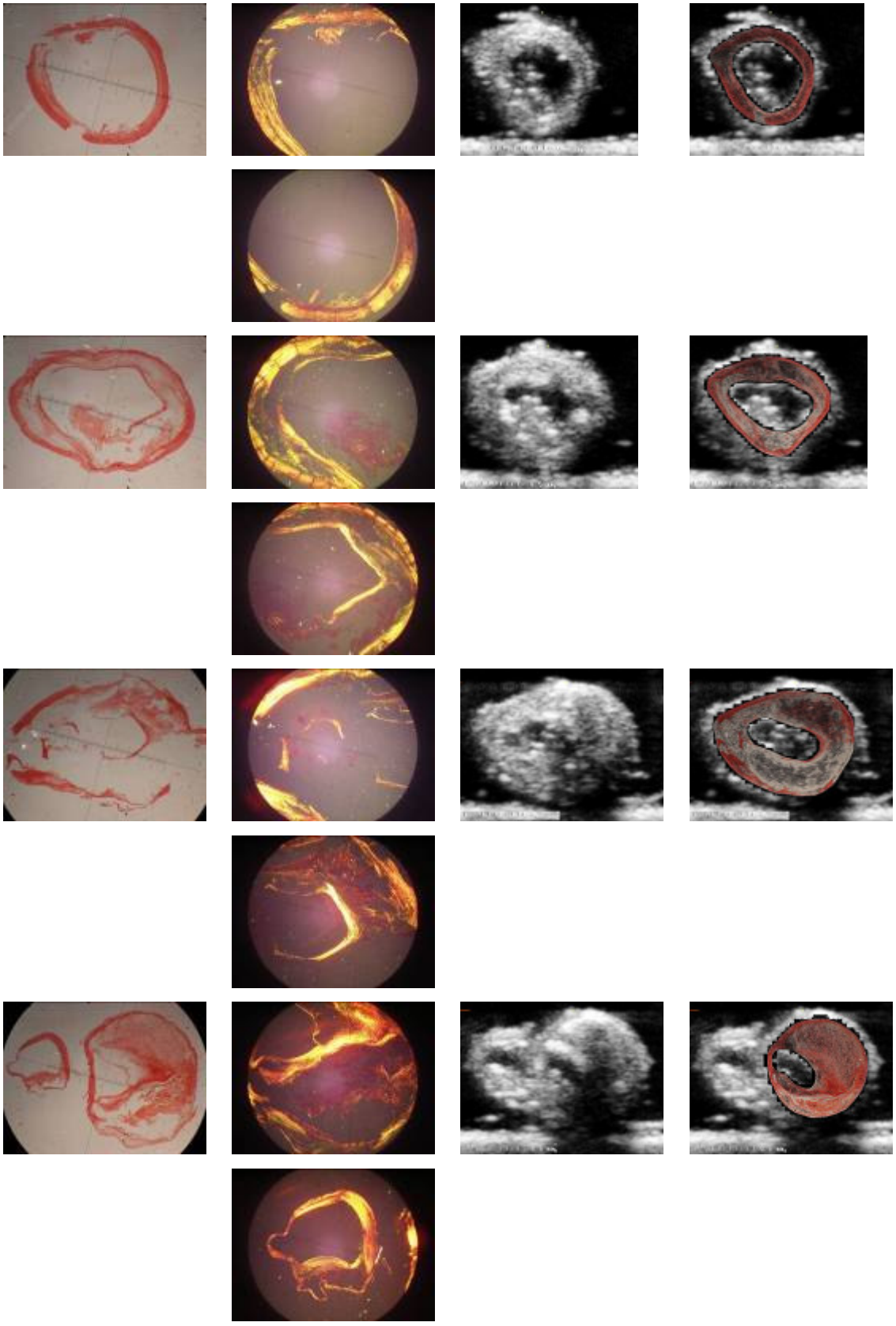

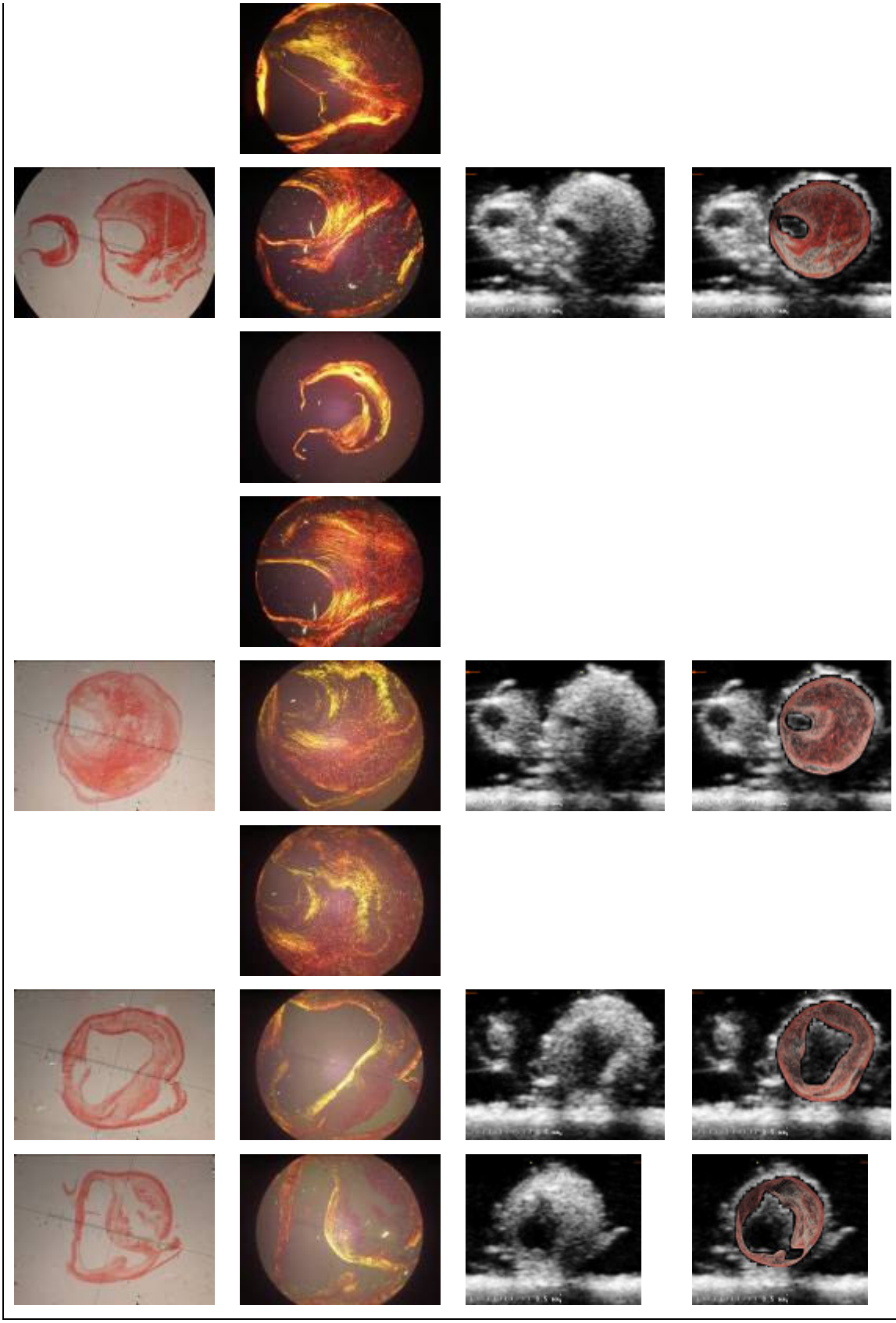

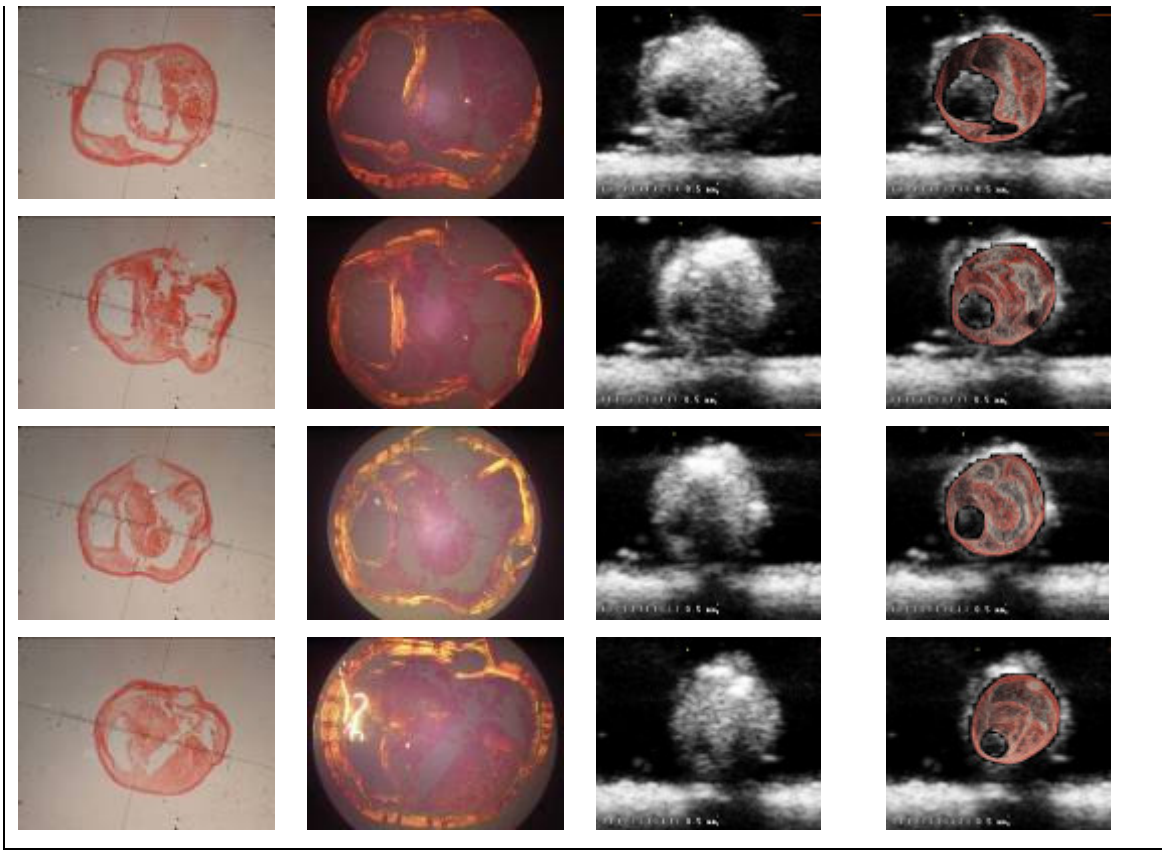

Figure 6.11: Images used for the 3D reconstruction; First column: H&E stained histology section *(3X magnification)*; second column: polarized light microscopy image of collagen *(40X magnification)*; third column: associated US image; fourth column: co-registrated results

6.3.1 3D Reconstruction Results

Figure 6.12 shows a series of histological transverse section of the plaque shown in figure 6.15, generated after in-plane FEM registration. The registered histology sections (panel 1-11) clearly show the gradual narrowing of the lumen and its changing plaque composition progressing over the series of transverse sections.

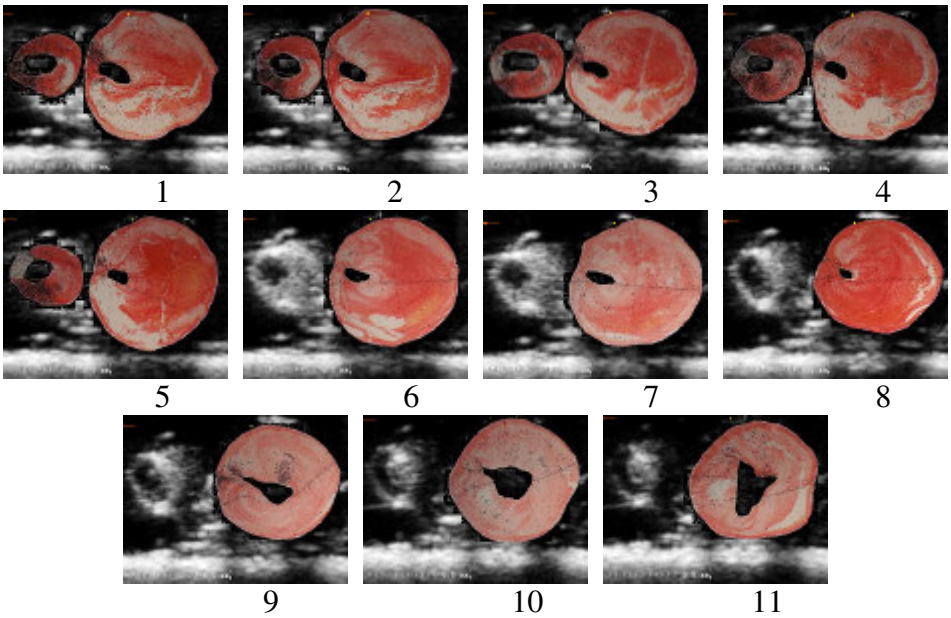

Figure 6.12 Examples of plaque histological images after FEM registration. Panels 1 to 11 represent a sequence in the plaque marked region (A) in figure 6.14

Figure 6.13 shows the 3D reconstruction of the CEA model after the in-plane FEM and axial registration was carried out. Figure 6.13 (a) shows the 3D reconstruction of the specimen. Figure 6.13 (b) shows the 3D reconstruction after extensions of CCA, ICA and ECA beyond plaque regions in order to build an entire carotid bifurcation which can be used for fluid dynamic simulation purposes. Figure 6.13 (c) shows the plaque reconstruction after lofting has taken place using SolidWorks to generate the surface of the outer wall, the lumen, and the lipid core boundary.

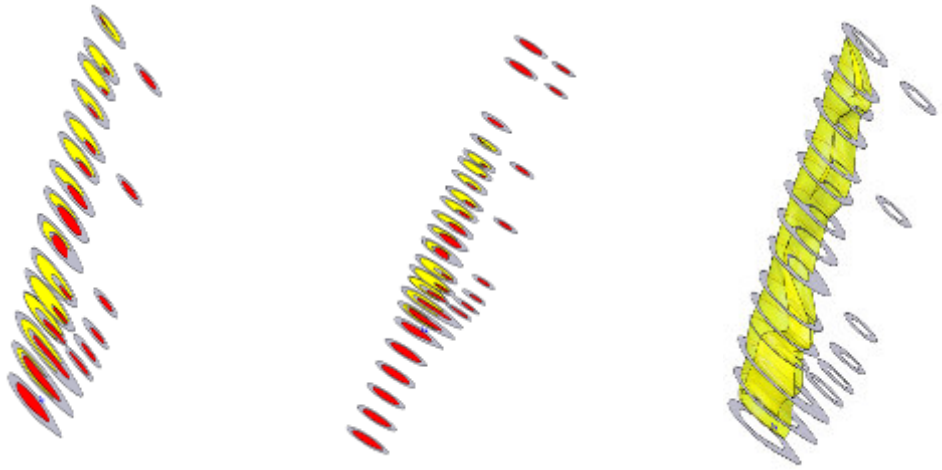

(a) (b) (c)

Figure 6.13 Panel (a) shows the 3D reconstruction of the CEA model. Panel (b) shows the geometrical extension to the ICA, ECA, and CCA for fluid dynamic simulations. Panel (c) shows the surface of the outer wall, the lumen, and the lipid core boundary. (Red: lumen, yellow: lipid core, grey: arterial wall)

Figure 6.14 (a) demonstrates the 2D registered histology images of a plaque stacked according to the axial coordinates. Figure 6.14 (b) shows the same image magnified to highlight clearly plaque geometry and the gradual changes in geometry between subsequent sections. Figure 6.14 (c) shows the reconstructed patient specific 3D plaque.

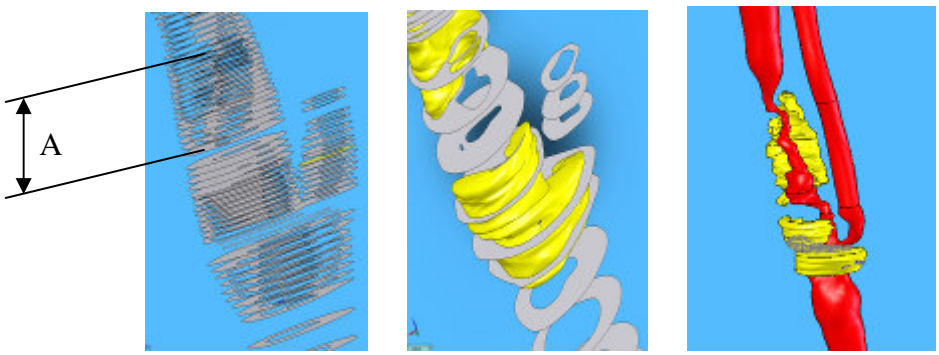

(a) (b) (c)

Figure 6.14 Image showing (a) the 2D registered histological image of a plaque stacked according to the axial coordinates; (b) the magnified region of (A), and (c) showing the reconstructed patient specific 3D plaque model

Figure 6.15 shows the final outcome of combining 3D ultrasound and histology process to generate a high resolution 3D reconstruction of an atherosclerotic plaque. Panel (b) shows the 2D stack of the model and panel (a) shows the model without the 2D stack.

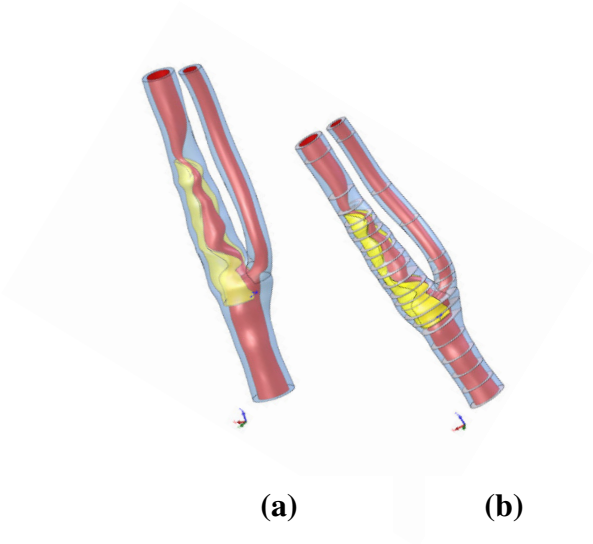

(a) **(b)**

Figure 6.15 The reconstructed 3-D model of the carotid artery, including the arterial wall and lumen. Panel (b) shows the 2D stack used to build the 3D model. Panel (a) shows the same model without the skeleton

6.3.2 Histology Distortion Analysis Result

The histology images shown in this chapter represent significant structural distortions. After FEM based correction, it is possible to compare the corrected image with the un-corrected image for regions such as the fibrous cap, and lipid core etc. If the corrected image represents the original tissue status, then the above comparison result can be treated as a measure for quantifying the tissue distortion for the different plaque components. The results generated from this part of the study may provide a guide to future researchers when interpreting results from histology analysis with regards to the structural uncertainties that samples may be subjected to.

Although the 3D reconstruction of the atherosclerotic plaque was performed on only one case; the quantification of the distortion was performed on three cases. Specimen sample 20, 21, and 24 were selected since they have a general geometry and morphological characteristics. Firstly, the mean and the standard deviation of ε for each parameter of all the samples were evaluated. Geometrical parameters calculated are A: region area; p: region perimeter; a and b: region long and short axis; a.r: aspect ratio; cir: circularity; deg: (A, p, a, b, d_{eg}, a.r, cir) ε value was calculated as:

$$\varepsilon_2 = \frac{X_B - X_A}{X_A} \times 100 \text{ In } \%$$

Where X_A, X_B represent the value of the parameter X after and before the registration procedure respectively. There were 26, 30, and 23 sections analysed for samples 20, 21, and 24 respectively (total n= 79). Samples 20 and 21 were closed specimens (or circumferential intact specimen), whilst sample 24 was an open specimen.

Open specimen: an open specimen has a cut along the longitudinal length of the vessel structure as can be seen in Figure 6.16 (a). **Closed specimen:** a closed specimen has a vascular structure that is circumferentially intact along the longitudinal length of the vessel as can be seen in Figure 6.16 (b).

(a) **(b)**

Figure 6.16 Panel (a) open specimen; and (b) closed specimen

Sample 20 Results (26 Sections)

ε [%]	A	p	a	b	d_{eq}	$a.r.$	cir
Outer Wall	-24.68±49.99 (26 meas.)	-12.96±19.38 (26 meas.)	-10.09±21.71 (26 meas.)	-25.12±17.69 (26 meas.)	-16.66±24.70 (26 meas.)	-15.53±16.08 (26 meas.)	-5.49±41.30 (26 meas.)
Lumen	-59.97±25.81 (31 meas.)	-25.84±19.98 (31 meas.)	-26.65±21.11 (31 meas.)	-36.66±26.74 (31 meas.)	-39.67±19.35 (31 meas.)	-12.35±30.95 (31 meas.)	-29.87±28.34 (31 meas.)
Lipid Core	3.57±85.00 (20 meas.)	-6.90±31.50 (20 meas.)	-17.79±20.38 (20 meas.)	7.91±47.17 (20 meas.)	-6.05±39.87 (20 meas.)	31.25±51.83 (20 meas.)	15.06±64.78 (20 meas.)
Mixed Region	-40.98±26.46 (7 meas.)	-24.34±18.60 (7 meas.)	-22.83±20.46 (7 meas.)	-20.90±21.34 (7 meas.)	-24.60±15.45 (7 meas.)	3.60±17.45 (7 meas.)	2.73±21.85 (7 meas.)
Fibrous Cap	-31.86±63.01 (26 meas.)	-	-	-	-	-	-
Calcification	/	/	/	/	/	/	/

Table 6.4 ε for specimen number 20

ε [%]	A	p	a	b	d_{eq}	$a.r.$	cir
Outer Wall	-29.28±10.07 (30 meas.)	-13.60±5.67 (30 meas.)	-11.25±5.52 (30 meas.)	-17.25±4.97 (30 meas.)	-16.12±5.94 (30 meas.)	-6.65±6.00 (30 meas.)	-5.83±3.88 (30 meas.)
Lumen	-27.55±37.98 (30 meas.)	-7.75±20.35 (30 meas.)	-5.53±21.81 (30 meas.)	-8.65±31.68 (30 meas.)	-17.16±20.14 (30 meas.)	-1.51±32.20 (30 meas.)	-18.20±15.28 (30 meas.)
Lipid Core	-21.03±52.03 (30 meas.)	-18.47±21.73 (30 meas.)	-23.69±14.26 (30 meas.)	3.70±54.07 (30 meas.)	-14.75±25.57 (30 meas.)	-33.45±51.10 (30 meas.)	-10.83±31..26 (30 meas.)
Mixed Region	-26.08±14.91 (31 meas.)	-13.49±17.72 (31 meas.)	-17.43±10.64 (31 meas.)	-7.35±19.72 (31 meas.)	-14.46±8.49 (31 meas.)	13.58±26.56 (31 meas.)	2.54±23.51 (31 meas.)
Fibrous Cap	-27.32±26.39 (30 meas.)	-	-	-	-	-	-
Calcification	-10.07±39.70 (4 meas.)	-8.81±23.32 (4 meas.)	-11.76±23.14 (4 meas.)	1.35±23.97 (4 meas.)	-7.49±23.16 (4 meas.)	-15.52±6.10 (4 meas.)	2.91±2.89 (4 meas.)

Table 6.5 ε for specimen number 21

ε [%]	A	p	a	b	d_{eq}	$a.r.$	cir
Outer Wall	-69.457±6.76 (23 meas.)	-38.01±7.40 (23 meas.)	-49.46±7.40 (23 meas.)	-47.38±5.79 (23 meas.)	-45.09±6.39 (23 meas.)	5.49±14.37 (23 meas.)	-20.09±15.97 (23 meas.)
Lumen	/	/	/	/	/	/	/
Lipid Core	-78.74±-8.00 (22 meas.)	-45.14±8.99 (22 meas.)	-48.37±11.39 (22 meas.)	-49.07±15.47 (22 meas.)	-54.69±8.95 (22 meas.)	4.95±45.80 (22 meas.)	-29.07±23.24 (22 meas.)
Mixed Region	/	/	/	/	/	/	/
Fibrous Cap	-62.80±11.66 (23 meas.)	-	-	-	-	-	-
Calcification	/	/	/	/	/	/	/

Table 6.6 ε for specimen number 24

ε [%]	A	p	a	b	d_{eq}	$a.r.$	cir
Outer Wall	-39.46±35.06 (79meas.)	-20.50±16.60 (79meas.)	-21.99±22.18 (79meas.)	-28.62±16.63 (79meas.)	-24.73±19.81 (79meas.)	-6.04±14.96 (79meas.)	-9.87±25.84 (79meas.)
Lumen	-44.02± 36.02 (61 meas.)	.- 16.94±21.97 (61 meas.)	-16.26±23.79 (61 meas.)	-22.89±32.28 (61 meas.)	-28.60±22.63 (61 meas.)	-7.02±31.78 (61 meas.)	-24.13±23.44 (61 meas.)
Lipid Core	-31.83±64.36 (72 meas.)	-23.40±26.75 (72 meas.)	54.59±47.15 (72 meas.)	-29.59±19.89 (72 meas.)	-24.54±33.68 (72 meas.)	24.13±50.70 (72 meas.)	-0.18±45.35 (72 meas.)
Mixed Region	-28.83±18.11 (38 meas.)	-15.48±18.13 (38 meas.)	-18.43±12.81 (38 meas.)	-9.85±20.43 (38 meas.)	-16.33±10.63 (38 meas.)	11.74±25.24 (38 meas.)	2.58±22.93 (38 meas.)
Fibrous Cap	-38.84±42.67 (30 meas.)	-	-	-	-	-	-
Calcification	-10.07±39.70 (4 meas.)	-8.81±23.32 (4 meas.)	-11.76±23.14 (4 meas.)	1.35±23.97 (4 meas.)	-7.49±23.16 (4 meas.)	15.52±6.10 (4 meas.)	2.91±2.89 (4 meas.)

Table 6.7 ε for all three specimens

Histology Distortion Analysis

The present study assessed the different parameters for shrinkage, including a) the outer wall; b) the fibrous area; c) the luminal area; and d) the perimeter. Investigating the theoretical background of the shrinkage of a cylindrical vessel may help in understanding the results.

Table 6.4 to 6.7 shows the statistical results of the geometric parameter variations before and after the FEM based tissue registration. The outer wall is the overall area defined by the outer wall boundary. The region between the outer wall and the sum of lumen, lipid, mixed and calcification is the fibrous region which has an irregular shape and topology. Thus, only the area result is presented for the fibrous cap. In comparison to all the parameters, the calcified region has the least change, while the luminal area has the largest change in relation to its area and location after histology processing.

The calcified region is the hardest tissue in the plaque, and therefore in the FEM model the material properties were set accordingly so that there is the least change. The findings show that there was 40% shrinkage on average in the overall area for all

three specimens analysed. In addition, specimens in which walls were cut longitudinally (open specimens) as shown in figure 6.16(a), were subjected to 70% shrinkage on average. In comparison, specimens that did not have cuts through the wall (closed specimens) as shown in figure 6.16(b), were subjected to 30% shrinkage on average. The cuts in the walls are caused during plaque excision. The tensile strength of the arterial wall is lost when it is cut, and is therefore subjected to increased shrinkage, compared to intact specimens, which maintains wall tensile strength.

The shrinkage for the internal components of the plaque was found to be case dependent, and is reflected by the large value in the standard deviation (S.D). In addition, no significant difference was found in the shape factor for the outer wall especially for the closed sample case. However, there was a large variation in the shape factor for the internal components of the plaque that includes the lipid core and the mixed region.

Validation of the Shrinkage Results for Sample 21

A test was performed to validate the results that were obtained by comparing a histology cross-section in which only the fibrous tissue is present with a photograph of the same section taken using an optical microscope. Therefore the tissue shrinkage obtained from this calculation represents the true shrinkage of the tissue. Sample 21 was used for the purpose, which was also the one used for the 3D plaque model reconstruction. The test was performed on the first histology section corresponding to a common carotid artery location upstream of the plaque. The two images were compared and the parameters $\varepsilon[\%]$ were calculated on the difference of a) the outer wall; b) the lumen wall; and c) the fibrous tissue. This procedure can be performed

when only the fibrous tissue is present, due to the difficulty in defining the lipid region in the photograph. Results of the measurements are shown in table 6.8.

$\varepsilon_2[\%]$	A	p	a	b	d_{eq}	$a.r.$	cir
Outer Wall	-27.24	-14.51	-15.32	-12.57	-14.70	3.70	-0.46
Lumen	-23.33	-10.42	-13.00	-9.15	-12.52	4.94	-4.17
Fibrous Cap	-32.32	-	-	-	-	-	-

Table 6.8 Results of the comparison between panel (a) and (b)

Assessment of the shrinkage for the fibrous tissue area was found to be 27.4% (mean value) in the FEM analysis (shown in table 6.5); and 32.2% in comparison with the photograph as golden standard shown in table 6.8. In both cases the shrinkage was approximately 30%, and the results was therefore considered to be reliable. The shrinkage of the outer wall for both the FEM and photograph comparison also agreed very well (29% in table 6.5 Vs 27% in table 6.8).

6.4 Discussions

The technique of 3D reconstruction of patient specific plaque has been developed in recent years by using medical images with limited spatial resolution. The present study clearly demonstrates the feasibility of using high resolution histological images for material characterization, combined with the geometrical information provided by ultrasound to reconstruct 3D arterial plaque more accurately.

As mentioned in the introduction section, the major problem with the procedure is: (a) the registration of the sections into 3D; and (b) the structural distortion caused by tissue processing. The study shows that with the proposed procedure it is possible to construct an accurate 3D model of the plaque for stress analysis purposes. In addition,

functional information such as inflammation activities, macrophage distributions obtained from immunohistochemical analysis can be inserted directly in to the model. The direct comparison of the mechanical stress obtained by FEM stress analysis on the model and the biological activities of plaque components will provide critical information on the understanding of the arterial remodelling and plaque rupture. In the current study, we have developed the procedure and have applied it to one case to achieve the 3D reconstructed plaque model. However, the 3D stress analysis was not performed during this PhD project period. It may be performed by other researchers in the group in the future.

Limitations

Firstly, the FEM based deformable image registration protocol requires a landmark near the outer and luminal walls in the evaluation of the displacement vector. In this case study the landmarks were chosen based on visual clues in the image such as calcified regions or abrupt curves in the image, and the experience of the individual performing the registration. However this procedure can be subjective, and inaccurate. The error assessment (appendix A) showed that the registration result is highly sensitive to the uncertainties introduced by a wrongly chosen landmark. Future studies should incorporate external landmarks introduced during the ultrasound scan, and also remain visible in the histology images. It can include the insertion of physical landmarks into the specimen to be identified in both ultrasound and histology sections.

Secondly, the study accounts for the semi-lipid and lipid regions to be as one entity in the 3D model. Simplification was carried out due to the technical difficulties of creating the complex lofting (surfaces of the outer wall, luminal wall, and the lipid

boundary) required in SolidWorks. The calcified regions were not included in the 3D model due to the small area that the region accounted for (<5% of the total area of the vessel). However, future improvements in the ability to loft calcified regions would enable both a more realistic 3D model to be built, and generate accurate stress analysis results.

Thirdly, the study did not perform any investigation using frozen sections (cryosectioning) for comparison purposes. Cryosections are not subjected to structural distortion as found in conventional histology, caused by the dehydration and re-hydration steps of tissue processing, and therefore may provide a more accurate geometry for 3D model reconstruction purposes. Cryosectioning was not performed due to the lack of equipment and expertise available at the time of the study.

Quantitative assessment of the tissue shrinkage caused by histology processing is a novel part of this study. Tissue distortion during dehydration processes has been a problem for many years. It has less impact if the purposes of the histology analysis are purely for tissue recognition and characterization which may be the major outcomes of clinical histology study. However, the shrinkage can be a major problem if the quantitative value of the size of certain regions is the concern, for example, to study the fibrous cap thickness of a vulnerable plaque. Based on our assessment, an approximate 30% area shrinkage can be expected for the fibrous tissue. The shrinkage value is dependent not only on the characteristics of the tissue and its surrounding regions; but is also dependent on the structure of the specimen. A circumferentially intact tubing structure (such as a plaque specimen) will have less influence on shrinkage than an opened specimen. However, the procedure of image restoration is very complex and time consuming and also subject to potential errors. Therefore, it is

not realistic to apply the procedure on every image of histology sections at this stage. To partially compensate for the influence of the shrinkage to the structural assessment result, a region ratio over the section area, which represents a relative value of regional size, will be more accurate than the absolute value of region size. This is the primary reason that most of the results for the histology analysis in this study are presented by the relative values.

Despite the mentioned limitations, the present study shows that it is possible to generate a 3D patient specific plaque model using deformable image registration, and by addressing the above limitations it would prove to be a powerful tool in the assessment of plaque remodelling based on the interaction between biological and mechanical factors.

Chapter 7

Plaque Tissue Characterisation Using Ex-Vivo 2D Ultrasound

7.1 Introduction

Ultrasound is cyclic sound pressure that can penetrate a medium and measure the reflection signature. The reflection signature can provide data about the inner structure of the medium. Therefore, potentially, the ultrasound signal contrast, created by the different plaque components may be able to provide information on tissue characterisation. The velocity of sound can vary between tissues, depending on the health conditions and any mechanical stresses that the tissue may be subjected to.

Due to its non-invasive imaging ability, low cost and easy access, the technique of ultrasound imaging is still the most important tool for assessing patient arterial plaque status, and providing clinical diagnosis. Large numbers of researches have been carried out attempting ultrasound tissue characterization. A study by Altedorneburg et al (2000) investigated the diagnostic precision of non-invasive B-mode ultrasound in predicting histopathological structures. They found that, in mainly echolucent types of plaques, atheromatous debris was most frequently seen, whereas fibrosis was rare. The presence of thrombosis on the plaque surface was often seen in completely echolucent plaque types. The study concluded that carotid B-mode ultrasonography is able to predict the histopathological components and the texture of carotid plaques. However, the study presents no histology image data on the positive correlation that exists between the ultrasound plaque appearance and the histology of the endarterectomy specimen. Another study by Devuyst et al (2005) investigated the feasibility and potential clinical implications of measuring the fibrous cap thickness

(FCT) of internal carotid artery plaques with a new ultrasound system based on boundary detection. They found a strong agreement between ultrasound and histology, and the intra observer disagreement was found to be minimal. They were also able to demonstrate that symptomatic atheromas had thinner fibrous caps compared with asymptomatic plaques, and therefore were able to conclude that fibrous cap thickness measurement of the carotid atheroma with ultrasound is feasible. However, the study was only based on one case image. The problems for the paper were (1) the case image may not be representative of other patients; (2) the definition of the fibrous cap was not reliable based on the figure produced in the paper. After consulting with several practising sonographers within the NHS, none of them accepted that the highlighted region shown in the published figure was fibrous cap. We believed that the paper concluded something which was a step too far from the data presented.

Based on the progress made in the past on the subject, it is generally believed that plaques that demonstrate a homogeneous appearance are stable and are linked with a low risk of subsequent ischemic events. On the contrary, plaques demonstrating either a heterogeneous or an echolucent appearance are associated with a high risk of ischemic neurological events. The typical classification for echogenicity would be a) weak; b) intermediate; c) strong. However this can be very subjective and can result in high inter- and intra-observer variability. In addition to this, visual observation may not be able to extract all the data that is potentially available on a B-mode image.

In in-vivo conditions, the ultrasound signal quality will be influenced by the surrounding tissue, moving artery and blood flow. It is found that in-vivo blood flow generates backscatter signals which can interfere with image quality. Therefore, the

ability to characterise plaque tissue using ultrasound should be better in ex-vivo scans with controlled environments. A good understanding of ultrasound characterisation of plaque component ex-vivo may provide important information on improving in-vivo scan results.

The main objective for this part of the study is to assess ultrasound characterisation of plaque in ex-vivo conditions, compared with histology sections of the corresponding plaque specimen. This chapter is the summary of preliminary results from this study. The study was initiated by the fact that in-vivo ultrasound generally shows poor results for tissue characterisation, while for the same plaque, when scanned with an ex-vivo set up, the plaque regions show heterogeneous character signals. Our research set up allows the patient to be scanned before CEA to gather in-vivo results and after the operation enabling the CEA specimen to be scanned to gather ex-vivo results, including before fixation. The ex-vivo plaque specimen will then be subjected to normal histology analyses. The validation of in-vivo ultrasound versus histology may still have a long way to go; however, the validation of the ex-vivo plaque image against histology sections is achievable. In this chapter some of the comparison results will be demonstrated and analysed.

7.2 Method

To perform this study, the following methods were applied:-

a) 2D Ultrasound scan

b) Histology analysis

c) An in-house designed programme developed using the MATLAB software package for image analysis

7.2.1 Ultrasound Scan and Histology Processing

- The procedure for the ultrasound scan using an ex-vivo set up described in section 6.2.1 was adapted for this study.
- Conventional histology analysis procedure described in section 3.1 and used in Chapter 4 was performed on the specimen.
- The longitudinal registration procedure described in chapter 6 is applied to provide the matching.

7.2.2 Case Studies

Case Study One (Specimen I)

Figure 7.1 shows a CEA specimen that was used for the investigation. Figure 7.1(a), (b) shows the length (22mm) and the width (5mm) of the specimen respectively; Tissue marking dye was applied in the longitudinal direction and was marked at every 5mm interval to maintain the correct circumferential orientation (c); figure 7.1(d) shows the transverse view of the 5mm cut blocks.

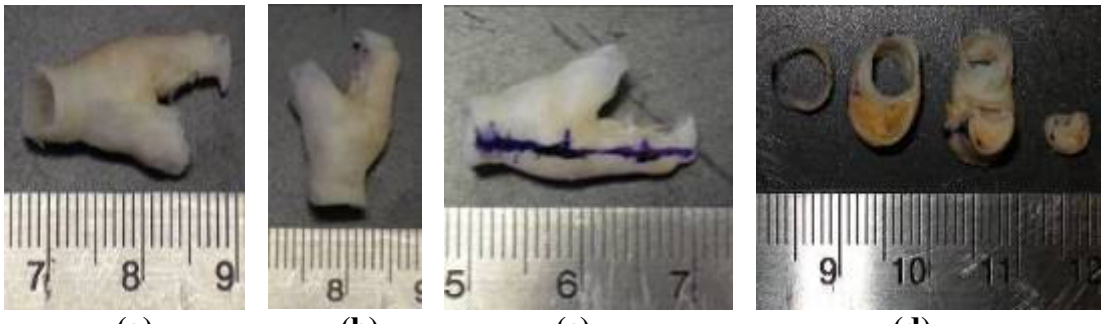

(a) **(b)** **(c)** **(d)**

Figure 7.1 Panel (a) longitudinal length of the CEA specimen; panel (b) the axial width; panel (c) tissue marking dye applied to maintain the correct 3D orientation; panel (d) transverse view of the cut block from the CEA specimen

Figure 7.2 shows the photograph taken of the transverse view of the cut blocks after fixation. Figure 7.2 (a) shows a disease free block taken from the common carotid artery. Figure 7.2 (b) to 7.2 (d) shows the diseased region of the CEA specimen from the common carotid artery (CCA) to the internal carotid artery (ICA). For the purpose of this investigation, the second block was selected for the comparison of US image and histology, as it demonstrated a typical plaque structure.

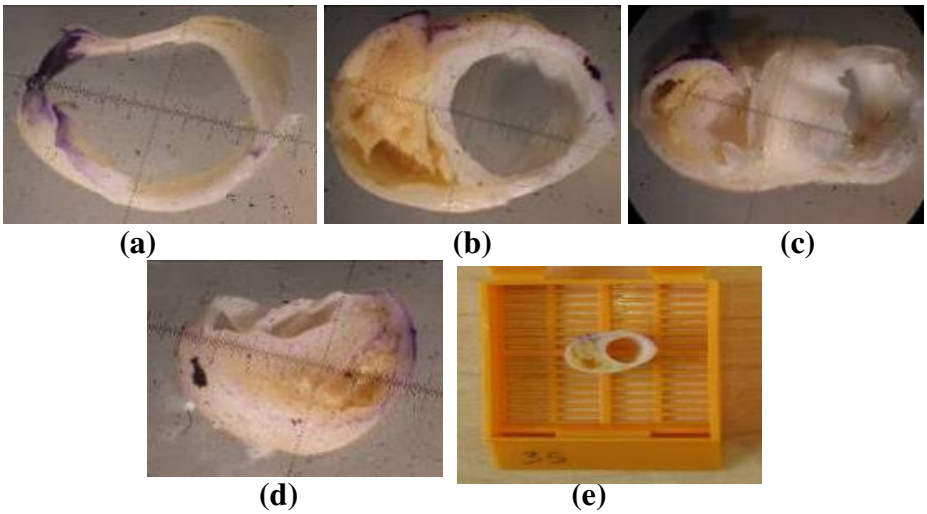

(a) **(b)** **(c)**

(d) **(e)**

Figure 7.2 Panel (a) to (d) shows the transverse view of the cut blocks. Panel (e) shows the block that was used for the histology procedure

Case Study Two (Specimen II)

Figures 7.3 and 7.4 showed another plaque specimen in a similar format as in figures 7.1 and 7.2. The second block was selected for the comparison between ultrasound image and histology, for the same reason as in case I block 2.

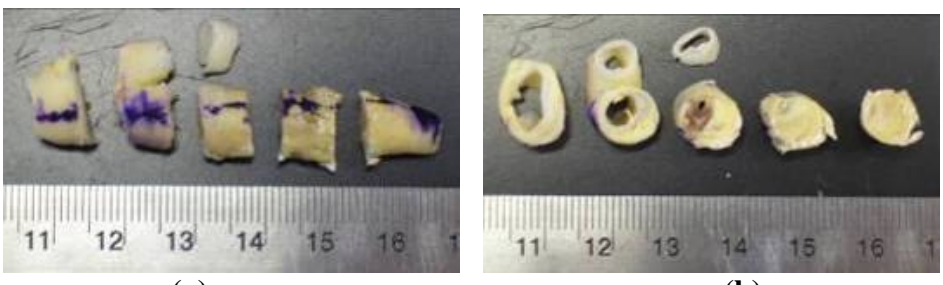

(a) **(b)**

Figure 7.3 Panel (a) longitudinal view of the CEA specimen highlighting the tissue marking dye for 3D orientation purposes; Panel (b) transverse view of the cut blocks from the specimen

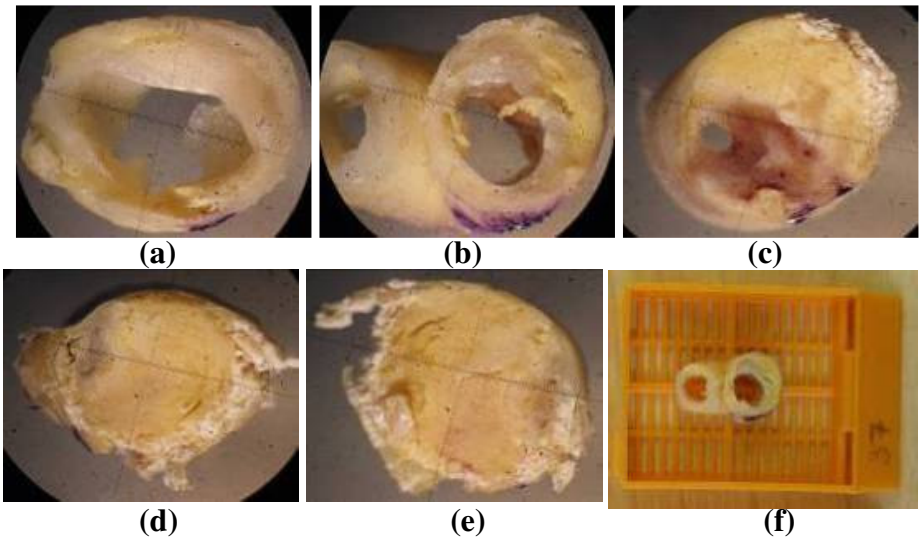

Figure 7.4: Panel (a) to (e) shows the transverse view of the cut blocks. Panel (f) shows the block that was used for the histology procedure

7.2.3 Defining the Plaque Components Using Ultrasound (US)

The tissue characterisation of the plaque components in the US image was carried out by using information found in literature. It was used to define the plaque features in the 2D plane US images. Validation was carried out using photographs of tissue blocks and histology sections to evaluate the feasibility of using ex-vivo US on plaque tissue characterisation.

Calcified Regions- Studies have shown that plaques rich in calcium and fibrous tissue have echogenic properties. Goncalves et al (2004) found that the echogenicity of carotid plaques is mainly determined by their calcium content. This finding was used to define high echogenicity regions as calcifications in the plaque. Figure 7.5(a) shows a region that has a strong white signal which is associated with calcium deposits. Figure 7.5(b) shows the corresponding block photograph highlighting the calcified region that validates the calcified region shown in 7.5(a). No staining procedure was applied to the block photograph shown in 7.5(b), which was captured on the transverse side immediately after cutting the artery into 5mm blocks.

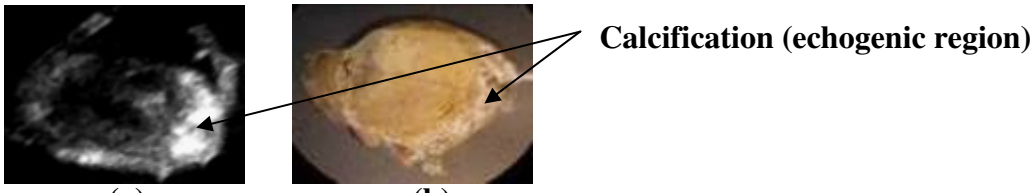

Figure 7.5 Panel (a) 2D plane ultrasound image and panel (b) corresponding transverse view of the carotid tissue block highlighting the calcified region

Lipid Core- A study by El-Barghouty et al (1996) used digital image processing or videodensitometric analysis to characterize B-mode ultrasound images of plaques objectively. Using this method the study found the content of the soft tissue (**lipid** or hemorrhage) in the plaque to be associated with a low gray-scale medium value of the plaque. In contrast the study found that high fibrous tissue content was associated with a high grey-scale value. Figure 7.6 (a) shows a hypoechogenic region (low gray-scale medium) in a 2D plane of an ultrasound image that is associated with the presence of high lipid content. Figure 7.6 (b) is a transverse view of a tissue block that demonstrates the presence of the lipid core (arrowed region). In the same geometrical location for the corresponding 2D ultrasound image (figure 7.6(a), a low grey-scale region is also present (hypoechogenic), confirming the presence of lipid in the ultrasound image.

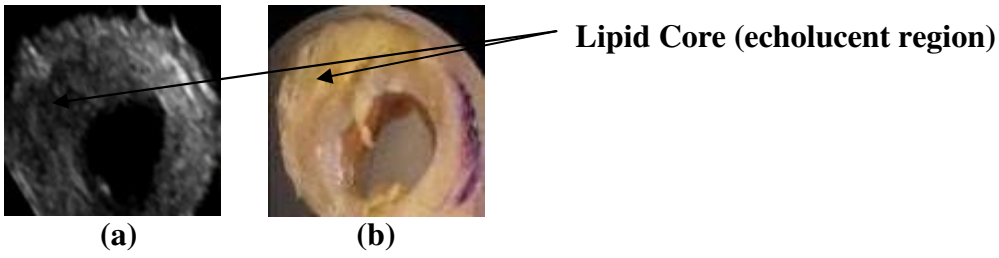

Figure 7.6 Panel (a) 2D plane of an ultrasound image showing a low grey-scale medium region (hypoechogenic); panel (b) showing the corresponding transverse view of the carotid tissue block

Fibrous Cap- A study by Devuyst et al (2005) investigated the feasibility of measuring fibrous cap thickness of internal carotid arteries using ultrasound based on boundary detection by dynamic programming. The study defined the fibrous cap as a hyperechogenic structure that on high-resolution B-mode imaging displayed strong echoes. The fibrous cap covered an area of high echolucency or weaker echoes that corresponded to the accumulation of lipid (lipid core). Figure 7.7(a) is an ultrasound image showing a region of a fibrous cap highlighted by the hyperechogenic region. Figure 7.7(b) is the corresponding histology cross-section validating the hyperechogenic region in figure 7.7(a) is the presence of a fibrous cap. Figure 7.7(c) shows a polarised light image of the histology cross-section in figure 7.7(b,) further validating the presence of the fibrous cap. The difference in the colour and contrast observed do not denote tissue loss, as this is due to differences in collagen types, density, and due to non-collagenous material.

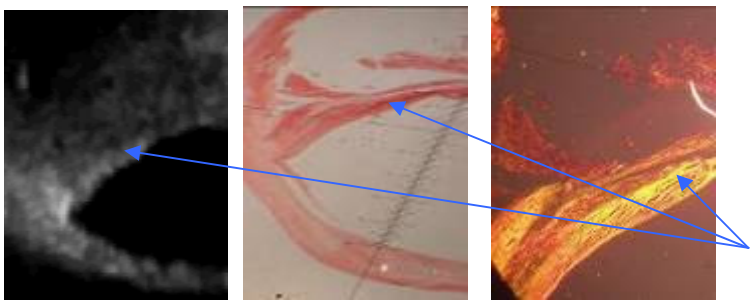

Figure 7.7 Panel (a) 2D ultrasound image highlighting the fibrous cap; panel (b) the corresponding histology cross-section; and panel (c) the corresponding polarised light image

7.2.4 Segmentation of Plaque Components (area calculation)

A manual segmentation procedure of the plaque components was performd to obtain the area data. This procedure was applied to the ultrasound images (figure 7.8) and the histology images (figure 7.9). The programme was developed using MATLAB, and is different to the programme used for the plaque 3D reconstruction in chapter 6

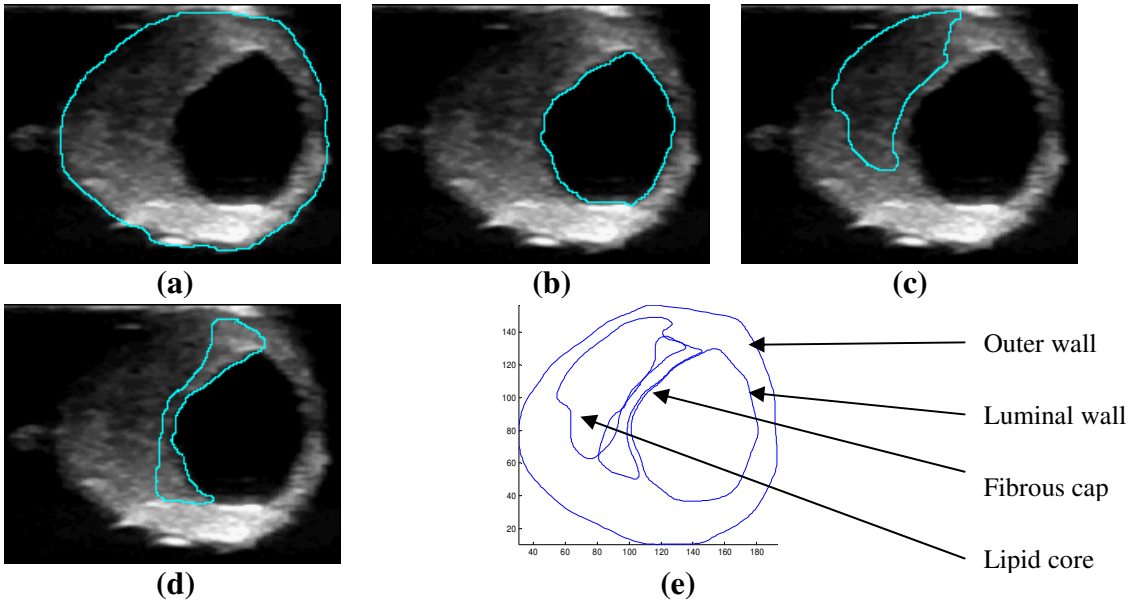

Image 7.8 Manual segmentation of an US image (a) outer wall; (b) luminal wall; (c) lipid core; (d) fibrous cap; and (e) the geometry of all the components

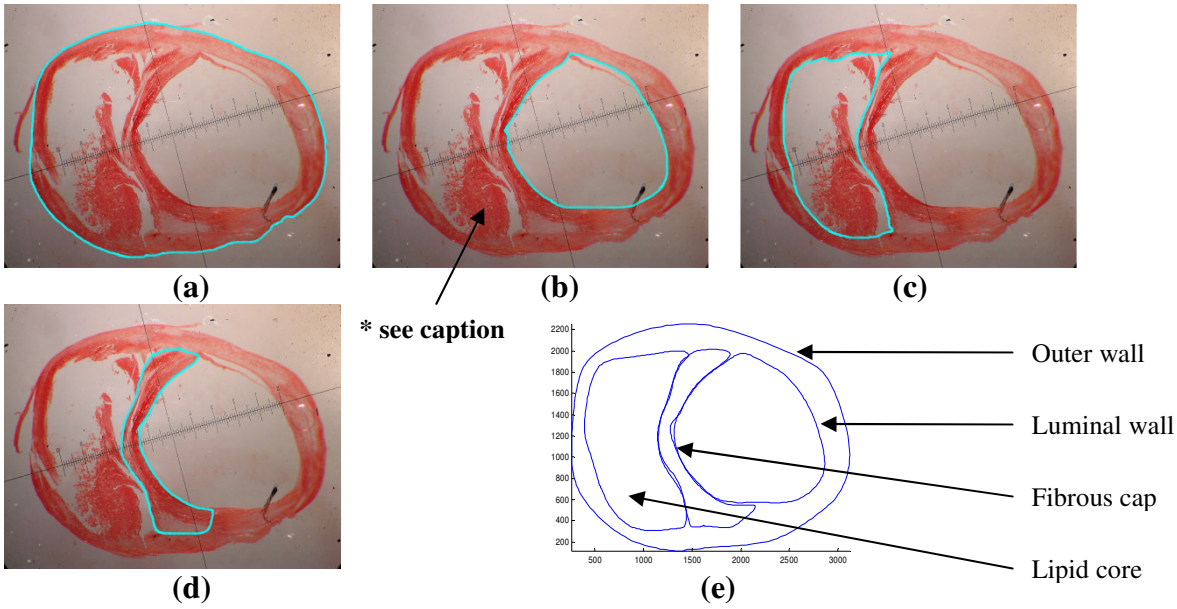

Figure 7.9 Manual segmentation of a histology image (a) outer wall; (b) luminal wall; (c) lipid core; (d) fibrous cap; and (e) the geometry of all the components.

as this is a 2D plane from a 3D structure, it was revealed that this is not part of the lipid core, and was therefore not included in the segmentation

7.2.5 Statistical Analysis

For all statistical analyses, a computer software application using MATLAB to perform independent Mann-Whitney Test (two-tailed) to evaluate the difference

between the methods for each parameter was used. Data were expressed as Mean±SD. The differences in the methods to determine agreement and whether the methods could be used interchangeably were assessed using Bland-Altman plots. A Bland-Altman plot (Difference plot) is a method of data plotting used in analysing the agreement between two different assays. In the clinical field, comparison of a new measuring technique with an established method is often required to see if they agree sufficiently for an existing method to be replaced by the new method. Investigators often use correlation coefficients to compare these methods; however this can be misleading as a high correlation does not mean that the two methods agree, due to the fact that a change in the scale of measurement does not affect the correlation; however it does effect the agreement. The extent of the agreement between the two methods is dependent on the amount of difference there is. If the difference is not sufficient to cause problems in clinical interpretations, then the proposed method can replace an existing technique. In the present study the Bland-Altman plot was used to compare ex-vivo ultrasound and histology to see the level of agreement for plaque tissue characterisation. A probability value of p=<0.05 was considered statistically significant.

The following section compares the area of the plaques tissue components in the 2D ultrasound plane, with the corresponding tissue block image to evaluate the level of agreement for the area of the plaque component in the two sets of image.

7.3 Results

One of the most difficult parts of ultrasound tissue characterization is image segmentation, or how to decide which areas are lipid and others fibrous tissues etc. As described in the methods section, manual segmentation was used in the study to

enhance the accuracy. However, the main problem with manual segmentation is the intra-operator reproducibility. Therefore, segmentation reproducibility is the first to be tested in the study.

7.3.1 Inter-Operator Segmentation Repeatability Test

The present study determined the inter-operator segmentation repeatability of the percentage variation for the components in a plaque tissue from ultrasound images of varying contrast in 4 images (figure 7.10), selected based on the image quality or the level of difficulty, once each by 4 independent observers. The parameters that were measured on the ultrasound (US) image were **a)** the lipid core area; **b)** the fibrous cap area; and **c)** the luminal wall area. The results of ratio of the measured areas against the outer wall area were presented.

	LIPID CORE AREA				**FIBROUS CAP AREA**				**LUMINAL AREA**			
observer	**Image Number**				**Image Number**				**Image Number**			
	1	**2**	**3**	**4**	**1**	**2**	**3**	**4**	**1**	**2**	**3**	**4**
1	23.18	19.84	18.60	18.83	n/a	4.35	4.21	5.83	15.29	12.05	15.52	31.61
2	20.24	30.76	18.64	21.90	n/a	8.53	6.62	8.95	14.57	12.56	15.58	31.80
3	18.98	22.90	18.61	19.99	4.78	4.57	3.78	6.85	17.65	11.15	15.43	31.42
4	11.94	10.97	18.40	20.19	2.48	4.94	5.09	7.19	15.05	10.97	15.62	31.11
Mean ±SD	18.57 ±4.77	24.30 ±4.42	18.56 ±0.11	20.23 ±1.27	3.63 ±1.63	5.60 ±1.97	4.92 ±1.25	7.21 ±1.30	15.64 ±1.37	11.68 ±0.75	15.54 ±0.08	31.48 ±0.29
***SD(SQRT)**	22.75	19.54	0.01	1.61	2.66	3.88	1.56	1.69	1.88	0.56	0.0064	0.0841
***SUM**	43.91				9.79				2.53			
Mean(M)	10.98				2.45				0.63			
(zeta)w (measurement error)	3.31				1.57				0.80			
Repeatability	9.18				4.33				2.20			
Overall Mean	19.62				4.89				18.59			
Repeatability % to Mean	0.47				0.89				0.12			

Table 7.1 Inter-observer repeatability data for the lipid core, fibrous cap, and the luminal area carried out by 4 observers

Table 7.1 shows the inter-operator segmentation repeatability for the area ratio for the lipid core, fibrous cap and luminal area against the plaque area for the four images by four different operators. It can be seen from the table that the measurement error,

(zeta) w ($w = sqrt(\sum \sigma^2 / n)$, where σ is the standard deviation, *n* is the sample size), for the lipid core, fibrous cap, and luminal area is 3.31, 1.57, and 0.80 respectively. Alternatively the measurement error can be presented as the "repeatability" which is defined as 2.77 * the measurement error (Bland J et al 1996). The difference between two measurements by different observers for segmenting the lipid core, fibrous cap and luminal wall for the same image is expected to be less than 9.18%, 4.33%, and 2.20% respectively for 95% of pairs of segmentation.

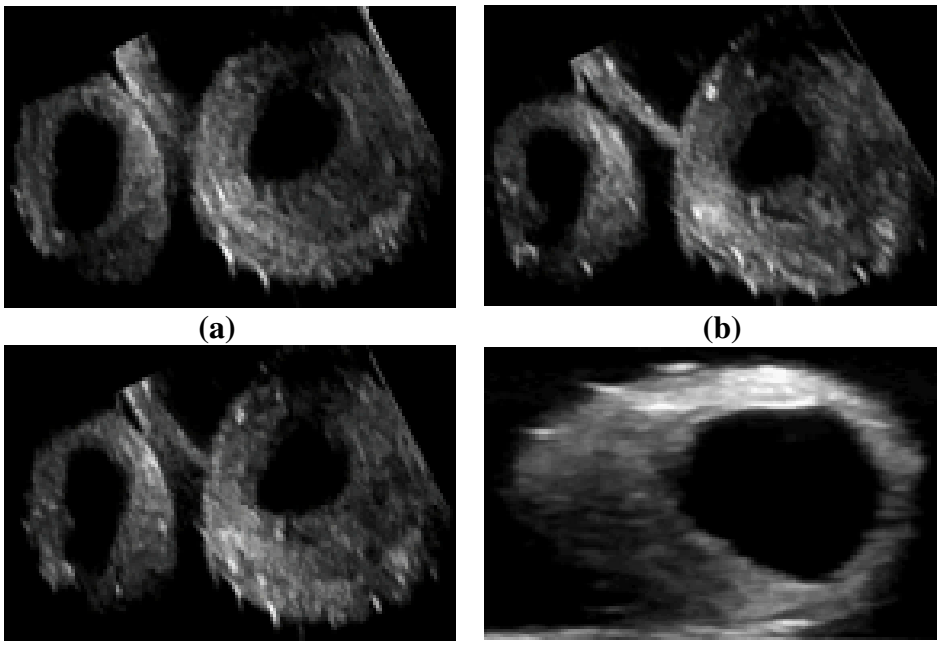

Figure 7.10 Images (a) to (d) shows the 2D Ultrasound Plane Used in Test Number 1-4 for the Reproducibility Test

7.3.2 Comparison of Ultrasound Image and Block Photograph

The photographs of the transverse view of the plaque provide the golden standard of the tissue outer and inner wall since there is no tissue shrinkage at this stage. Due to the tissue residual stress, the tubing structure maybe subjected to buckling when cutting the specimen into 5mm segments which can be seen in figure 7.11 b-1 and b-2. The lipid region may be difficult to derive from photographs without staining. This section presents the result of the comparison between the US image and the block

photograph. Two CEA specimens were studied (case I and II). Photographs were taken in the transverse view for each block and then compared with the corresponding transverse view of 2D ex-vivo ultrasound image (figure 7.12).

Case I

Before tissue processing had taken place, a photograph was taken of the cut block using a 3X table microscope. The block photograph was then compared with the corresponding 2D ultrasound plane image.

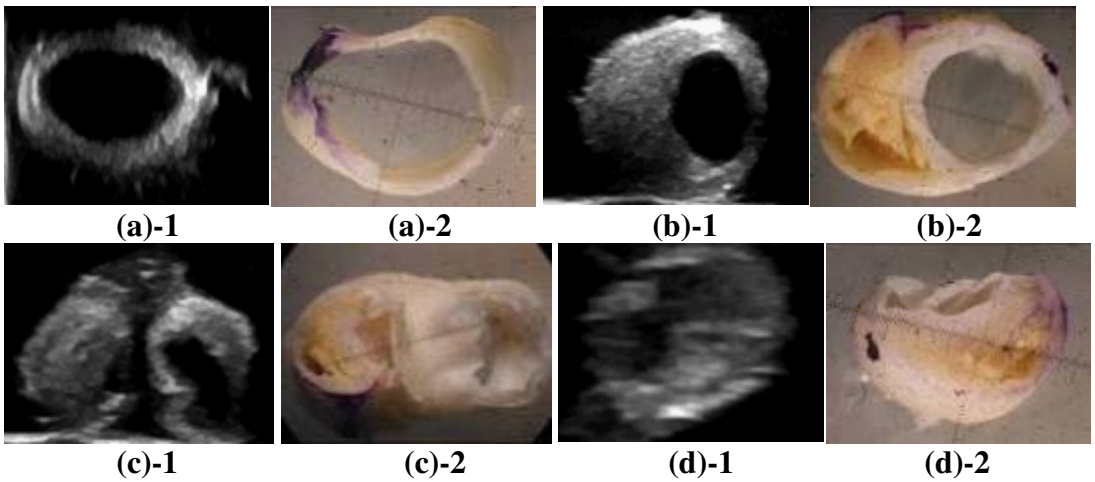

Figure 7.11 2D plane ultrasound images (1) and the corresponding carotid tissue block images (2) (3X magnifications)

Figure 7.11 shows the carotid tissue block (Panel (a)-2 to (d)-2, and the corresponding 2D ultrasound planes (Panel (a)-1 to (d)-1 for all four 5mm block segments. For the purpose of the study the block in panel (b)-2 for the following histology analysis was used, and all four blocks for the ultrasound and block photograph comparison.

Segmentation of Plaque Components for (b)-2

Figure 7.12 shows the region segmentation in which the region boundaries were marked as red for demonstration for both US images and tissue block photos.

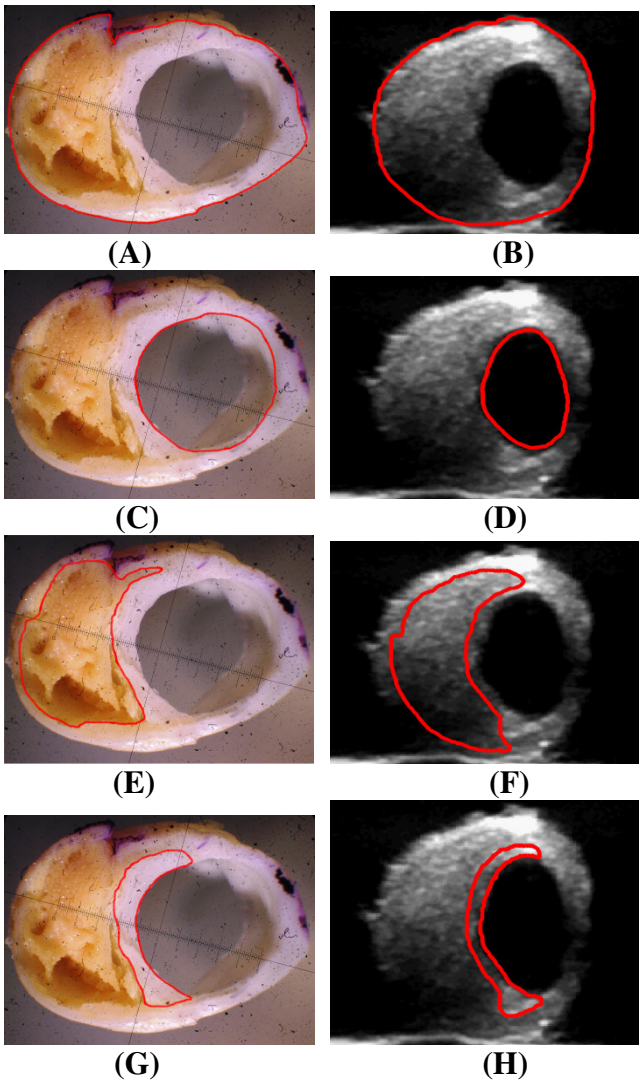

Figure 7.12 Boundary marking of the plaque components in the tissue block and corresponding ultrasound images: Panel (A)-(B) the outer wall; Panel (C)-(D) the lumen; Panel (E)-(F) the lipid core; Panel (G)-(H) the fibrous cap. (3X magnification)

From this figure (7.12), it can be seen that the outer and luminal walls are easily identifiable by their clear boundaries. The lipid core (LC) region for the ultrasound image (F) is identified by the darker signal relative to the surrounding tissue. The soft

material of lipid enables sound waves to pass through it easily giving it its echolucency properties.

The lipid core in the block photograph can be clearly identified as a yellow region corresponding to the ultrasound image dark echolucent region. Figure 7.12(G) demonstrates the fibrous cap which can be identified clearly by the colourless region between the lumen and the lipid core. The ultrasound image in 7.12(H) highlights the corresponding fibrous cap which is identified by a very thin echo-rich layer. The fibrous cap is usually identified by the tissue that is found in-between the segmented luminal wall and the lipid core, which are more readily identifiable. For this case, the fibrous cap lacked sufficient fibrous tissue and therefore this region appeared darker, and was therefore difficult to identify. There are no identifiable calcified regions in any of the blocks studied.

Table 7.2 shows the quantitative assessment of the agreement between the photograph and ultrasound images for the 4 blocks. It gives the measurement results of both methods for the different regions as well as the differences between the two methods. In addition, the mean measurement value of the region, the mean value and standard deviation of the difference between the two method measurement results were also presented.

	Plaque Components								
Block Number	**Luminal Wall**			**Lipid Core**			**Fibrous Cap**		
	Photo	**US**	diff.	**Photo**	**US**	diff.	**Photo**	**US**	diff.
1	81.3	85.9	-4.6	n/a	n/a	n/a	n/a	n/a	n/a
2	31.8	24.4	7.4	30.07	29.17	0.9	9.3	8.18	1.12
3	20.7	24.6	-3.9	39.34	35.17	4.17	12.19	9.41	2.78
4	10.2	12.5	-2.3	49.34	43.47	5.87	8.95	6.23	2.72
***mean**	**36.00**			**39.58**			**10.15**		
****d**			**-0.85**			**3.65**			**2.21**
*****s**			**5.58**			**2.53**			**0.94**

Table 7.2 Comparison of the different plaque component areas (%) using 2D ultrasound and the carotid tissue blocks (case I) *: mean measurement value of both methods; ** mean value of measurement difference; * standard deviation of the measurement difference**

It can be seen from table 7.2 that for the luminal wall data the mean difference and standard deviation of the difference was d=-0.85% and s=5.58% respectively, the range of the difference will be -12% to 10%. According to the *d* and *s* value for the different regions (table 7.2), the range for lipid core, and fibrous cap area are about -1% to 9%, and 0% to 4% respectively. Comparing the mean value and the associated error margin range for the area for lumen, lipid core, and fibrous cap area as: lumen: 36.00% (-12% to 10%); lipid core: 39.58% (-1% to 9%); and fibrous cap: 10.15% (0% to 4%); it is clear that the agreement for fibrous cap region is not acceptable. The error ranges are slightly larger than half of the measurement value for luminal area and about a quarter for lipid core region.

The Bland-Altman plots in figure 7.13 show distributions of the difference between the two methods with the measurement value of (a) luminal wall area; (b) lipid core; and (c) the fibrous cap area. It can be seen that there is no obvious relationship between the differences and the mean measurement values for the three results but

these may be more obvious with an increased sample number. Under these circumstances the lack of agreement can be analysed by calculating the bias, estimated by the mean difference "*d*", and the standard deviation of the differences "s" for each parameter. If the differences are normally distributed (Gaussian), 95% of measurement differences will lie between the limits of *d - 2s* and *d + 2s* according to the sample size and t value table.

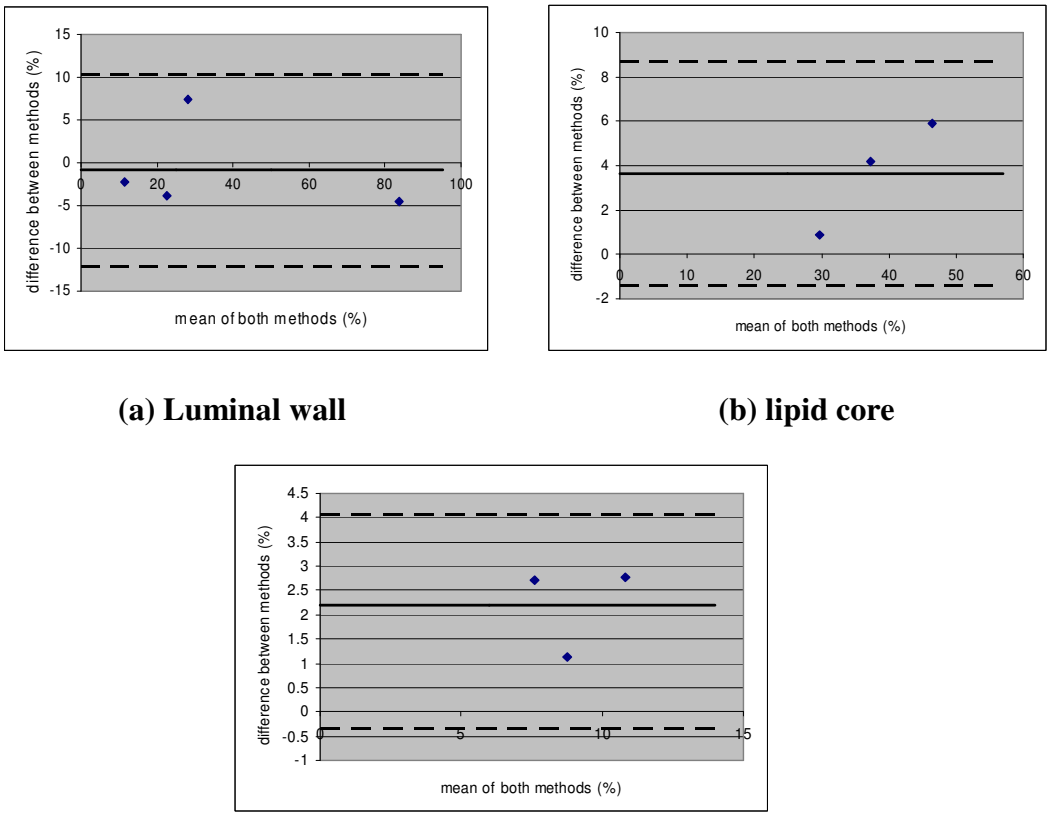

(a) Luminal wall **(b) lipid core**

(c) Fibrous cap

Figure 7.13: Bland and Altman Plot obtained from 4 paired samples of case I analyzed from block photo and ultrasound images of (a) the luminal wall; (b) the lipid core; and (c) the fibrous cap area. The solid line represents the mean bias, with 95% CI defined by the dotted lines

Case II

Figure 7.14 (a)-2 to (c)-2) shows the carotid tissue block, and the corresponding 2D ultrasound (US) planes (panel (a)-1 to (c)-1) for all three 5mm block segments. As previously mentioned, for the purpose of the study the block in panel ((b)-2) was used for the analysis. Figure 7.15 shows the boundary marking of the plaque components in the tissue block and corresponding ultrasound (US) images.

(a)-1 **(a)-2** **(b)-1** **(b)-2**

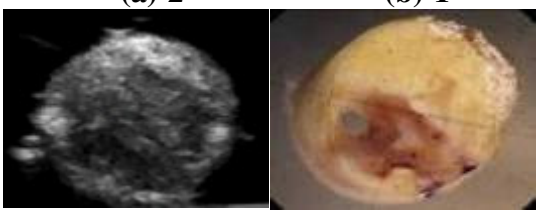

(c)-1 **(c)-2**

Figure 7.14 Images showing the 2D ultrasound plane image (1) and the corresponding carotid tissue block image (2) (5X magnifications)

Segmentation of Plaque Components for (b)-2

The lipid region can be clearly seen in the photograph (Figure 7.15(e)), and the echolucency in the lipid region for the ultrasound image (7.15(f)). The echolucent region was used as a guide to mark the boundaries of the lipid core. Figure 7.15(g) and 7.15(h) show the segmentation of the fibrous cap for the tissue block photograph and ultrasound images respectively. The fibrous cap (fc) in the ultrasound image has a thin strip of echogenic region characterised by the light region found between the echolucent lipid core (dark region) and the lumen. Figure 7.15(b-2) shows a magnified region of 7.15(b) highlighting the boundary between the lipid core (A) and

the fibrous tissue (B). The difference in the grey-scale which defines the two components can be clearly seen. The plane of this section was at the plaque bifurcation region, and is indicated by the red arrow in figure 7.15 (d-2)

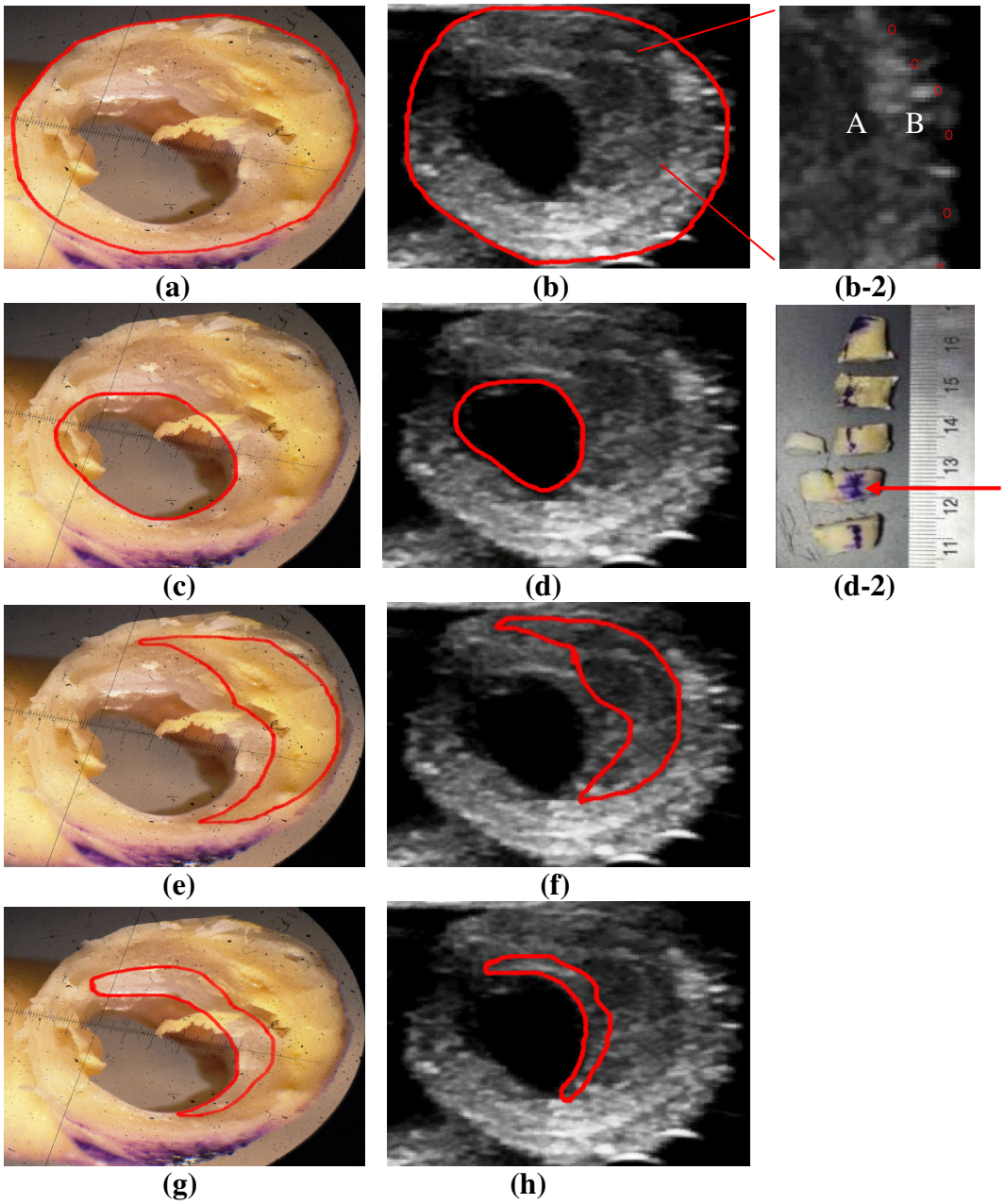

Figure 7.15 Image showing the boundary marking of the plaque components in the tissue block and corresponding ultrasound images: panel (a)-(b) the outer wall; panel (c)-(d) the lumen; panel (e)-(f) the lipid core; panel (g)-(h) the fibrous cap. Panel (b-2) highlights the grey level contrast between fibrous tissue (B) and the lipid content (A) – (3X magnification)

Table 7.3 (below) shows the quantitative assessment of the agreement between the photograph and ultrasound images for the 5 blocks. It gives the measurement results of both methods for different regions as well as the differences between the two methods. In addition, the mean measurement value of the region, the mean value and standard deviation of the difference between the two method measurement results were also presented.

	PLAQUE COMPONENTS											
Block Number	**Luminal Wall**			**Lipid Core**			**Fibrous Cap**			**Calcification**		
	Photo	**US**	**diff**	**Photo**	**US**	**diff**	**Photo**	**US**	**diff**	**Photo**	**US**	**diff**
1	36.6	32.2	4.4	12.1	10.6	1.5	13.9	8.9	5	n/a	n/a	n/a
2	27.9	24.1	3.8	25.5	19.4	6.1	12.0	10.5	1.5	n/a	n/a	n/a
3	2.7	2.2	0.5	31.7	36.2	-4.5	13.5	9.7	3.8	10.1	12.81	-2.7
4	3.0	2.7	0.3	51.7	43.8	7.9	3.9	4.0	-0.1	21.6	28.8	-7.2
5	2.1	1.9	0.2	61.2	51.6	9.6	2.9	3.5	-0.6	20.2	26.5	-6.3
***Mean**	**13.54**			**34.4**			**8.3**			**20**		
** ** d**			**1.84**			**4.12**			**1.92**			**-5.4**
***** ***s***			**2.07**			**5.69**			**2.43**			**2.38**

Table 7.3 Comparison of the different plaque component areas (%) using 2D ultrasound and carotid tissue blocks (case II) *: mean measurement value of both methods; ** mean value of measurement difference; * standard deviation of the measurement difference**

It can be seen from table 7.3 that for the luminal wall data the mean difference and standard deviation of the difference was d=1.83% and s=2.05% respectively, the range of the difference will be -2% to 6%. According to the *d* and *s* value for the different regions (table 7.3), the range for lipid core, fibrous cap and calcified area are about -7% to 16%, -3% to 7% and -10% to 0.7% respectively. Comparing the mean value and the associated error margin range for the area for lumen, lipid core, fibrous cap and calcification area as: lumen: 13.6% (-2% to 6%); lipid core: 34.4% (-7% to 16%); fibrous cap: 8.3% (-3% to 7%); calcification: 20% (-10% to 0.7%), it is clear that the disagreement between the two methods for fibrous cap region was large,

while for the other regions, the agreement for the two measurements were very similar. The error ranges were slightly larger than half of the measurement values.

The Bland-Altman plots in figure 7.16 show distributions of the difference between the two methods with the measurement value of (a) luminal wall area; (b) lipid core; (c) the fibrous cap and (d) the calcified area. It can be seen that there is no obvious relationship between the differences and the mean measurement values for the four results. Similar analysis of the lack of agreement test as used in case I can be carried out.

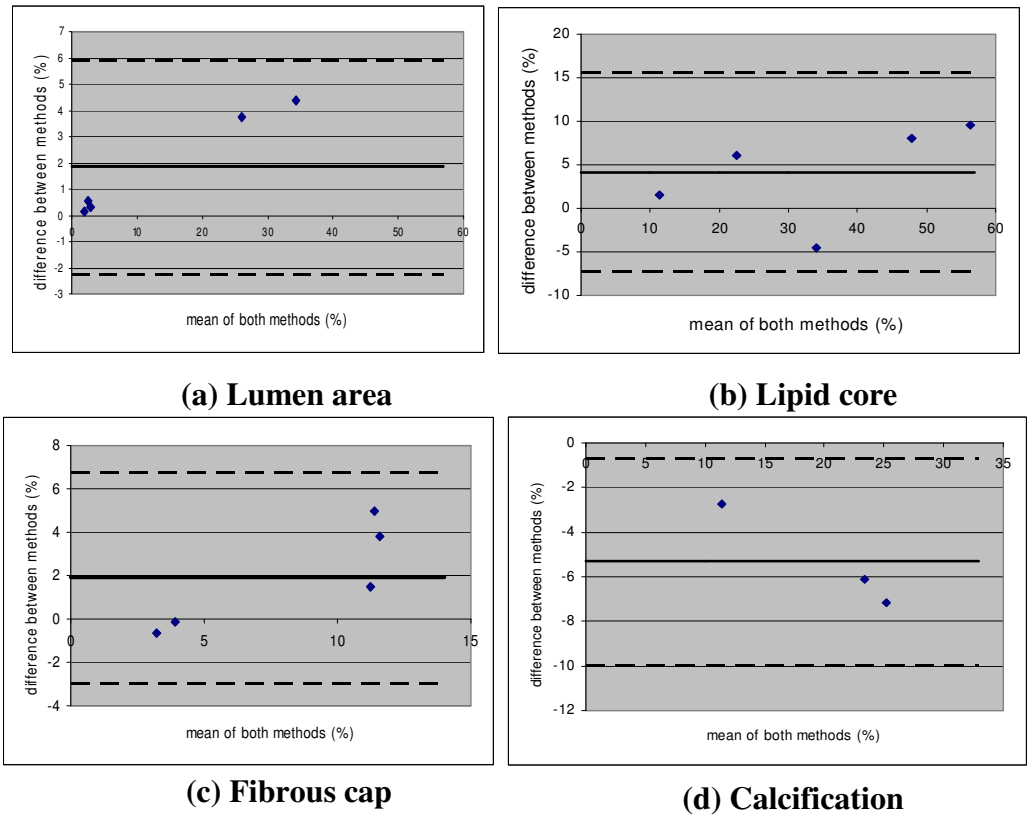

Figure 7.16 Bland and Altman Plots obtained from 4 paired samples of case II analyzed from block photo and ultrasound images of (a) the luminal wall; (b) the lipid core; (c) the fibrous cap area; and (d) the calcified area

7.3.3 Comparison of Ultrasound and Histology Image

A visual assessment was conducted on the US images using the corresponding histology sections as the gold standard to characterise the different plaque components. For the lipid core the observations carried out demonstrate that there is a very good qualitative agreement in characterising the lipid core based on ex-vivo 2D US imaging, confirmed by histological analysis. The lipid core is easily identifiable as an echolucent structure surrounded by fibrous tissue which is echogenic. For the fibrous cap there is also a qualitative agreement, however in comparison to the lipid core the agreement is much lower. The fibrous cap is an echogenic structure that can be visually observed between the echolucent lipid core and the lumen. However, due to the resolution which can be currently achieved using US, the qualitative characterisation of the relatively thin fibrous cap is difficult. In the following section, a detailed quantitative analysis will demonstrate the agreement of the geometric sizes for plaque components between ultrasound and corresponding histology images.

The figure below (figure 7.17) presents the paired images of the US (left panels) and the histology images (right panels) including both the segmentation results. The first set of images relates to case I and the second set of image relate to case II.

Case I

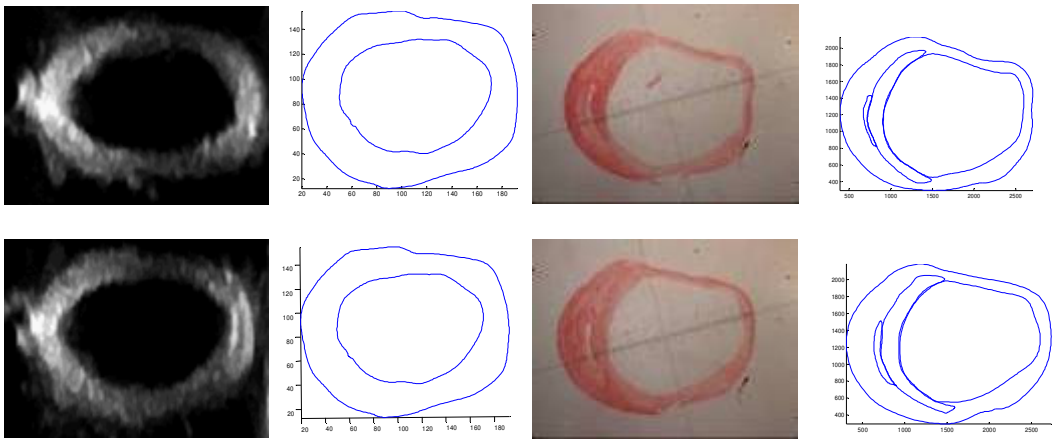

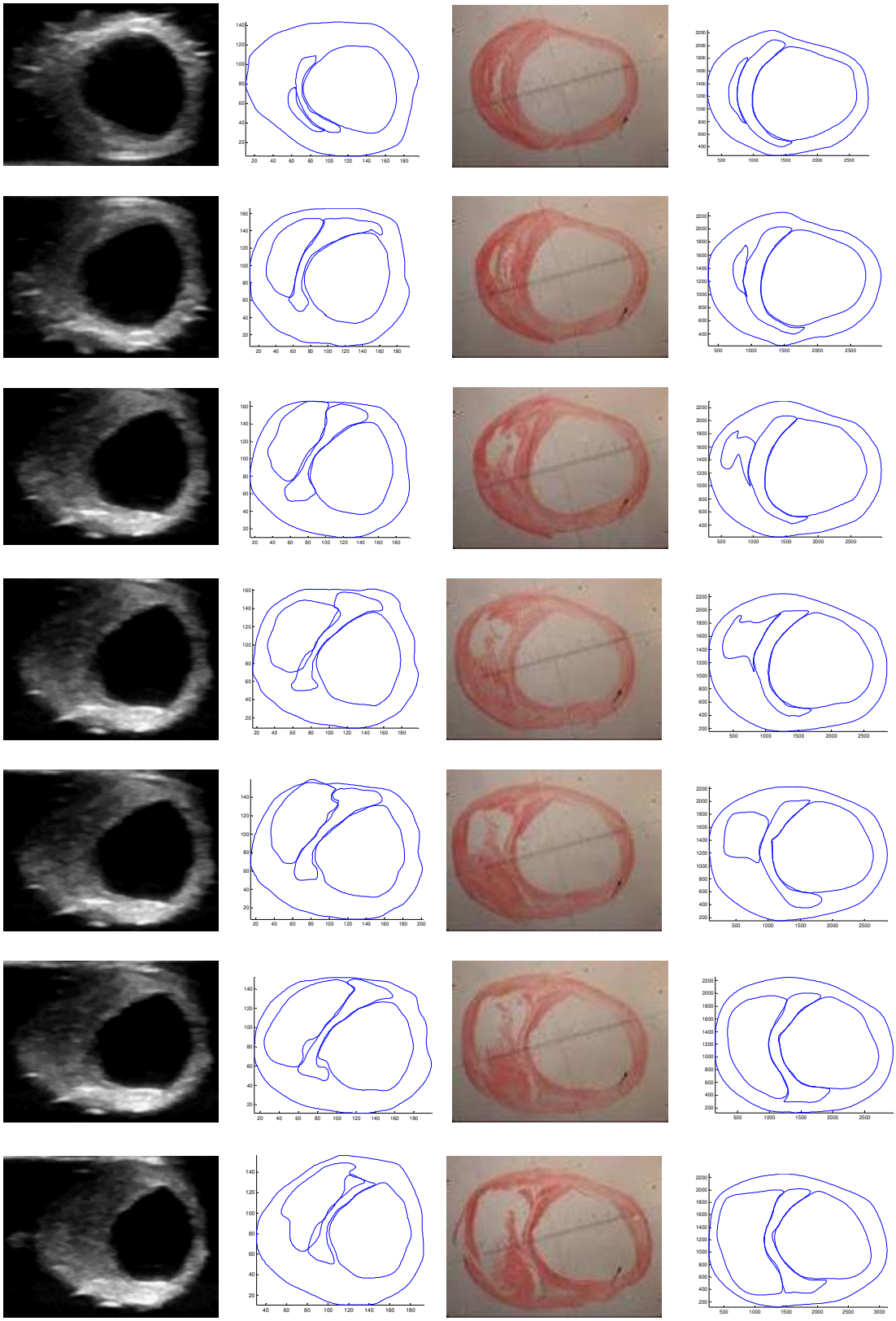

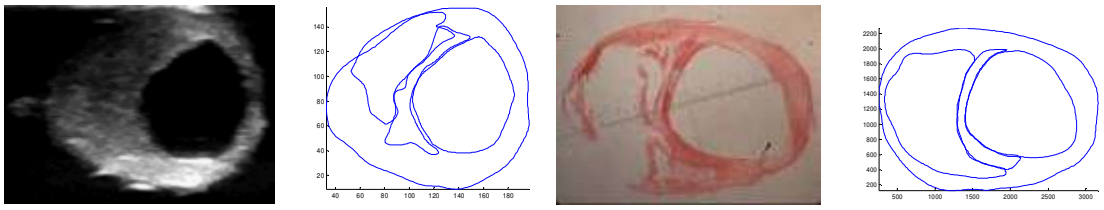

Panel (a) **Panel (b)** **Panel (c)** **Panel (d)**

Figure 7.17 Panels (a) and (c) shows images of the 2D serial ultrasound (US) and corresponding histology planes respectively, and panels (b) and (d) show the geometries of the two sets of images respectively

Table 7.4 presents the quantitative measurement results of the regional area from both methods for the 10 sections. It gives the measurement results of both methods for different regions as well as the differences between the two methods. In addition, the mean measurement value of the region, the mean value and standard deviation of the difference between the two method measurement results are also presented.

Section Number	Lipid Core			Fibrous Cap			Luminal Wall		
	US	His		US	His		US	His	
1	18.81	29.19	-10.38	8.87	6.05	2.82	30.94	31.83	-0.89
2	17.81	25.55	-7.74	6.89	9.23	-2.34	29.45	32.87	-3.42
3	16.83	20.93	-4.1	9.91	9.92	-0.01	31.31	34.90	-3.59
4	17.78	8.93	8.85	10.12	9.37	0.75	31.81	37.20	-5.39
5	17.24	7.16	10.08	10.01	9.04	0.97	30.93	39.02	-8.09
6	11.75	4.80	6.95	10.23	10.01	0.22	31.96	41.50	-9.54
7	13.27	2.52	10.75	9.75	10.96	-1.21	32.22	44.11	-11.89
8	2.56	2.78	-0.22	4.62	11.31	-6.69	33.98	48.51	-14.53
9	0	1.64	-1.64	0	10.30	-10.3	44.32	51.63	-7.31
***mean**	12.2			8.7			36.6		
***P*=value**	*p*=0.72			*p*=0.27			*p*=0.0078		
Mean±SD	12.9± 6.99	10.43± 10.68		7.82± 3.49	9.51± 1.45	20.3±2 1	32.99 ±4.42	41.84± 8.36	
****d**			1.39			-1.75			-7.18
*****s**			8.01			4.18			4.36

Table 7.4: Comparison between 2D ultrasound and corresponding histology images for characterising the lipid core, fibrous cap, and luminal wall, *mean measurement value of both methods; **mean value of measurement difference; ***standard deviation of the measurement difference. All figures in %

For the luminal wall data (table 7.4), the mean difference and standard deviation of the difference was d=-7.18% and s=4.36% respectively, the range of the difference will be -16% to 2%. According to the *d* and *s* value for the different regions (table 7.4), the range for lipid core, and fibrous cap area are about -15% to 17%, and -10% to 7% respectively. Comparing the mean value and the associated error margin range for the area for lumen, lipid core, and fibrous cap area as: lumen: 36.6% (-16% to 2%); lipid core: 12.2% (-15% to 17%); fibrous cap: 8.7% (-10% to 7%); the agreement for both lipid core and fibrous cap region are very poor, while for luminal region, the error range is slightly larger than half of the measurement values.

The Bland-Altman plots in figure 7.18 show distributions of the difference between the two methods with the measurement value of (a) lipid core area; (b) fibrous cap area; and (c) the luminal wall area. Again, the relationship between the differences and the mean measurement values for the three results were weak. The present study adapted the same statistics analysis procedure used in previous section to determine the range of agreement between the two measurement methods.

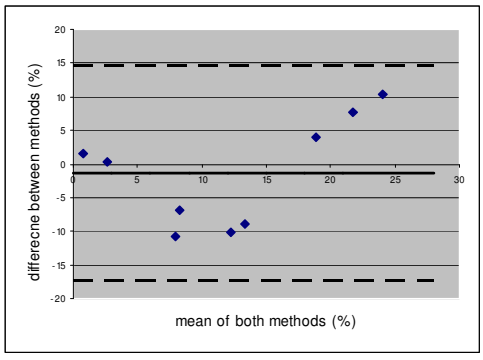

(a) **Lipid core**

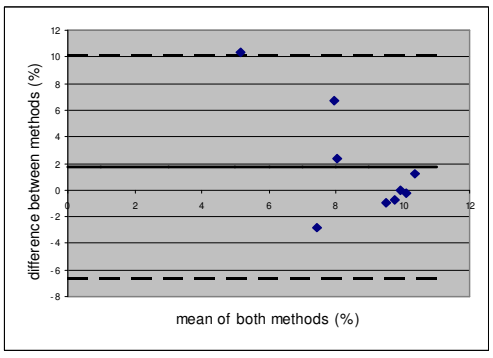

(b) **fibrous cap**

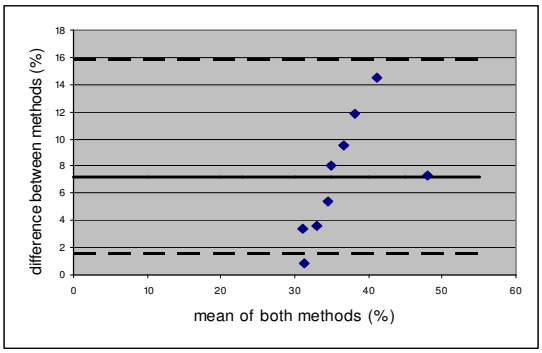

(c) **Luminal wall**

Figure 7.18: Bland and Altman Plots obtained from 9 paired samples of case I analyzed from histology and ultrasound images of (a) the lipid core area; (b) the fibrous cap area; and (c) the luminal wall area. The solid line represents the mean bias, with 95% CI defined by the dotted lines

The mean difference (d) between the two methods (histology and ultrasound) for the lipid core, fibrous cap, and luminal wall is 1.39%, -1.75% and -7.18% respectively. The luminal wall has the largest mean difference (7.18%) between the two methods because it is subjected to an enlargement as a result of tissue shrinkage caused by tissue processing during histology. The fibrous cap has the poorest agreement or largest difference range between the two method measurements. Although it is an echogenic structure, the grey-medium contrast it generates is not clearly visible as it is a relatively thin structure, which the resolution on ultrasound is unable to resolve. The difference range for lipid core measurement between the two methods is also very large, although visual examination shows very good qualitative agreement between the US and histology for lipid core. In all the US images (100%) which have an echolucent region, there is also a lipid core confirmed in the corresponding histology image. Conversely, most of the lipid core regions found in histology images shows echolucent regions in the corresponding US image, except a few images which have very small lipid core regions shown by histology. This is because it is an

echolucent structure that is larger in size (7 out of the 10 sections analysed consisted of a large lipid core), and therefore the resolution on the ultrasound did not inhibit the image quality. As a result it generated a clearer grey-scale contrast enabling a more accurate tissue characterisation. Nonetheless, the range of the difference for the lipid core region measurement between the two methods was very large. Quantitative ultrasound plaque region detection is not accepted based on this case study. However, the qualitative agreements between the two methods were good for lipid core detection. In addition, it must be noted that although the histology sections are subjected to shrinkage, it was not important for this study as the area data calculated for the plaque components was a ratio of the overall plaque area as a percentage (%).

Case II

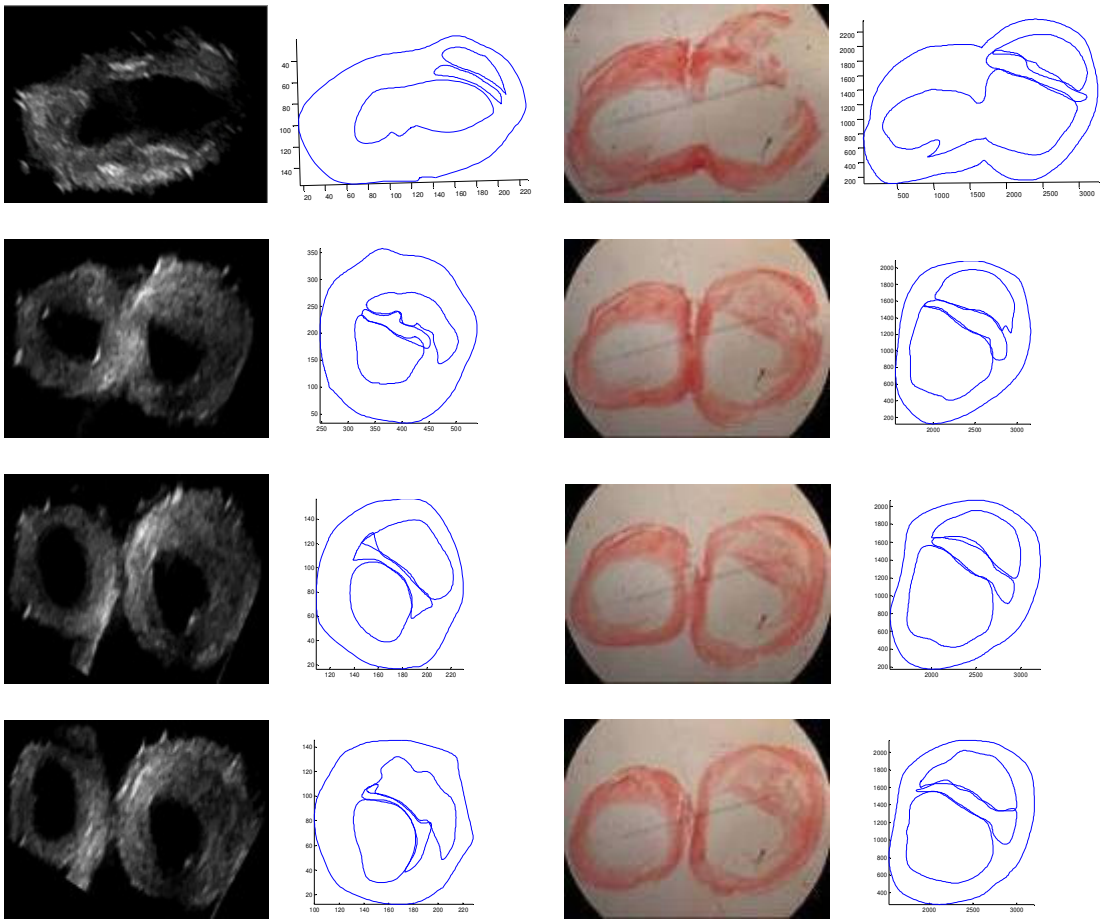

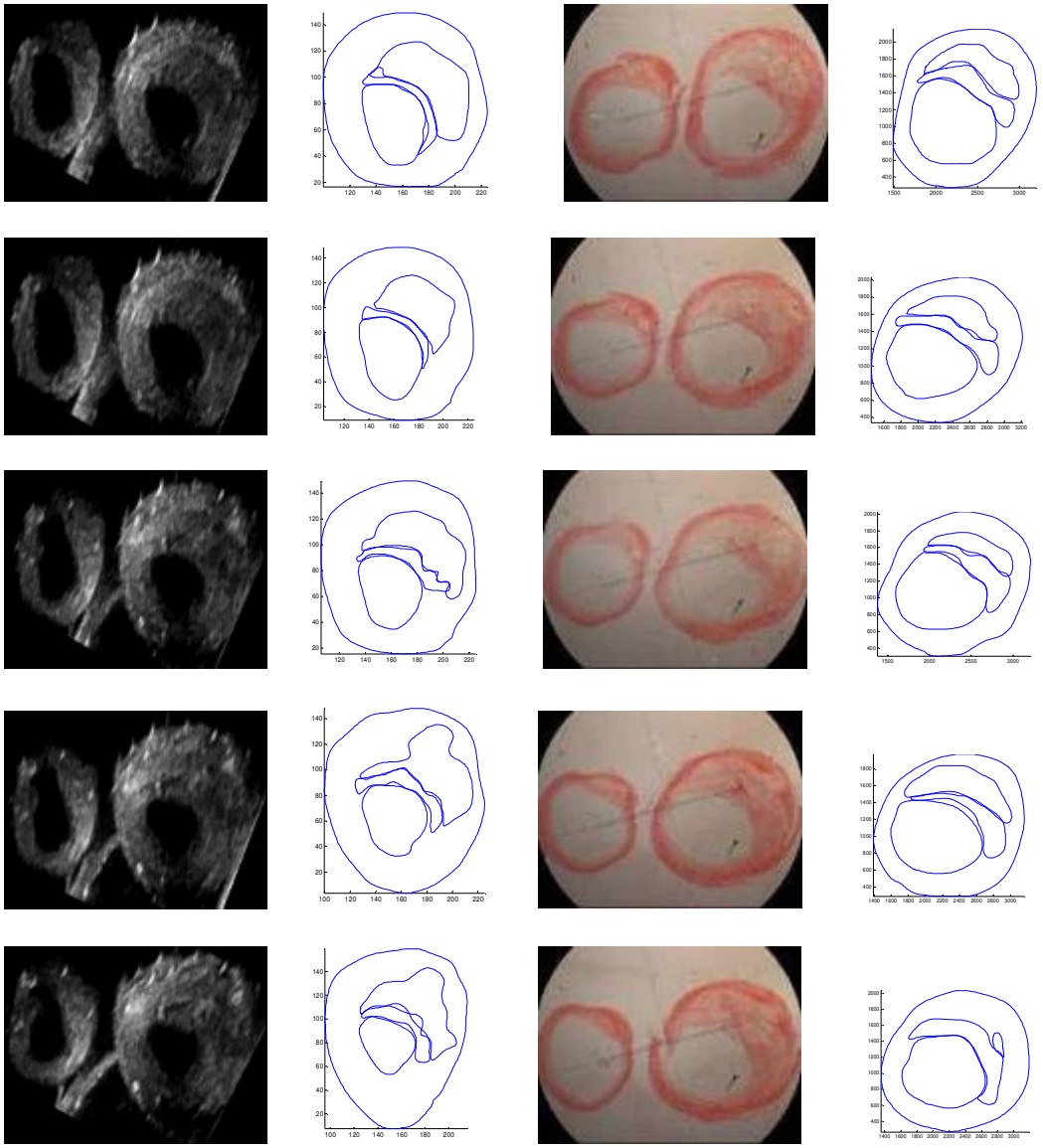

Panel (a) **Panel (b)** **Panel (c)** **Panel (d)**

Figure 7.19 panels (a) and (c) shows images of the 2D serial ultrasound (US) and corresponding histology planes respectively, and panels (b) and (d) show the geometries of the two sets of images respectively

Table 7.5 shows the quantitative assessment of the agreement between the histology and ultrasound images for the 10 transverse sections. It gives the area measurement (%) results of both methods for different regions as well as the differences between the two methods. In addition, the mean percentage value of the region, the mean

value and standard deviation of the difference between the two methods were also presented.

Section Number	Lipid Core			Fibrous Cap			Luminal Wall		
	US	His	diff	US	His	diff	US	His	diff
3	12.29	16.04	-3.75	4.48	8.64	-4.16	19.42	32.06	-12.64
4	19.05	15.54	3.51	6.07	8.57	-2.5	19.06	32.67	-13.61
5	19.66	17.23	2.43	4.33	8.96	-4.63	19.40	31.82	-12.42
6	11.54	14.57	-3.03	4.61	9.96	-5.35	17.34	32.87	-15.53
7	14.99	15.45	-0.46	3.11	9.52	-6.41	17.30	29.47	-12.17
8	10.99	14.48	-3.49	4.87	9.84	-4.97	17.98	31.80	-13.82
9	18.80	15.64	3.16	5.59	8.79	-3.2	16.04	30.78	-14.74
10	17.76	15.65	2.11	5.40	10.16	-4.76	11.16	29.00	-17.84
***mean**	15.635			4.8075			17.2125		
***p*=value**	*p*=0.87848			*p*=0.0001554			*p*=0.0001554		
Mean±SD	**15.63** ±3.63	**15.58** ±0.86		**4.81** ±0.91	**9.31** ±0.64		**16.46** ±2.72	**31.31** ±1.43	
****d**			0.06			-4.50			-14.10
*****s**			3.12			1.22			1.91

***All figures shown are expressed as percentages (%)**

Table 7.5 Comparison between 2D ultrasound and corresponding histology images for characterising the lipid core, fibrous cap, and luminal wall (case II) *mean measurement value of both methods; **mean value of measurement difference; ***standard deviation of the measurement difference

For the luminal wall (table 7.5) data, the mean difference and standard deviation of the difference was d=-14.10% and s=1.91% respectively, the range of the difference will be -18% to -10%. According to the *d* and *s* value for the different regions (table 7.5), the range for lipid core, and fibrous cap area are about -6% to 6%, and -7% to -2% respectively. Comparing the mean value and the associated error margin range for the area for lumen, lipid core, and fibrous cap area as: lumen: 17.21% (-18% to -10%); lipid core: 15.64% (-6% to 6%); fibrous cap: 4.81% (-7% to -2%); it is clear that the agreement for fibrous cap and luminal region are not acceptable, while the agreement between the two measurements for the lipid core region, is marginally

improved. Although the difference ranges are smaller than case I study, it is clear that the two methods cannot be interchangeable.

The Bland-Altman plots in figure 7.20 show distributions of the difference between the two methods with the measurement value of (a) lipid core area; (b) fibrous cap area; and (c) the luminal wall area. It can be seen that there is no obvious relationship between the differences and the mean measurement values for the three results. Therefore, the same statistical analysis used in case study one for photograph comparisons (Table 7.2 and Figure 7.13) is adapted to analyse the difference ranges for different regions.

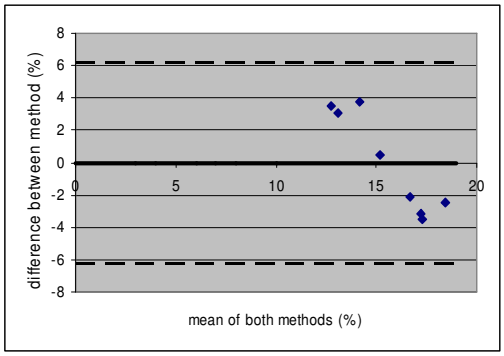

(a) **Lipid core area**

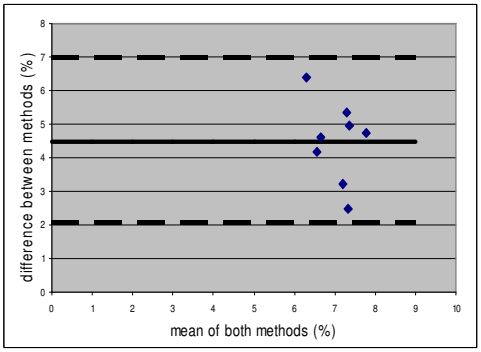

(b) **fibrous cap area**

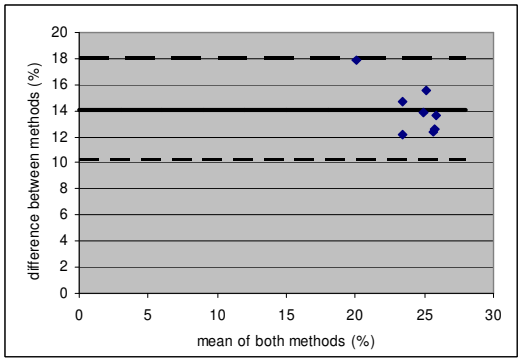

(c) **Luminal wall area**

Figure 7.20: Bland and Altman Plots obtained from 9 paired samples of case II analyzed from histology and ultrasound images of (a) the lipid core area; (b) the fibrous cap area; and (c) the luminal wall area. The solid line represents the mean bias, with 95% CI defined by the dotted lines

7.3.4 Image Segmentation Repeatability Study

The findings on the repeatability suggest that the luminal wall can be characterised well, with a 2.20% difference between measurements by different observers for the same image. This is because the texture of the fibrous tissue and lumen which borders the luminal wall are significantly different, resulting in the ultrasound signal generating a clear boundary to distinguish the luminal wall. The measurement repeatability for the fibrous varied by 4.44%, which can be considered to be reasonably good. However, between the three regions that were investigated, the lipid core showed the greatest difference between the two sets of segmentation measurements (9.18%), nonetheless it may still be considered good for tissue characterising purposes. The large measurement error (9.18%) may be caused by the fact that although the lipid core is an echolucent structure, the boundary of the lipid core is less well defined. The boundary region has overlapping lipid (echolucent) and fibrous tissue (echogenic) which generates a blurred signal. This makes it difficult to characterise the lipid core accurately.

7.4 Discussion & Conclusion

The risk of cerebral ischemia is strongly related to the degree of stenosis in the internal carotid artery. Other additional factors which are indicative of an increased likelihood of stroke are evidence of a thin fibrous cap shown by an echogenic region, as well as low echogenicity caused by the presence of a lipid core (De Bray JM et al 1997). In previous investigations, the primary focus was aimed at comparing sonographic and pathoanatomic findings related to intraplaque haemorrhage and plaque ulceration (Imparato AM et al 1983, Droste DW et al 1997). The ability of ultrasound to image other important pathological features of atherosclerotic plaques has not been investigated systematically or in a complete way. In this chapter,

comparison of ex-vivo ultrasound images of carotid plaques with the corresponding histology images was performed to assess if the difference in the image contrast has any meaningful result in relation to plaque tissue characterisation.

Based on the four cases studied (two cases for photograph (pre-tissue processing) and two cases for the histology), it was found that the agreement of ultrasound with the corresponding photograph is better than the agreement with histology. The reason for this is because the block photograph of the plaque and the ultrasound image was taken before tissue processing and it therefore did not encounter structural distortion caused by the histology procedure.

The results from this study have shown that ex-vivo ultrasound plaque tissue characterisation can be achieved qualitatively for certain components. In all (100%) of the cases in which an echolucent region was found in the ultrasound images, a lipid region can be confirmed at the same location by the corresponding histology sections. Tissue characterisation of the fibrous cap can also be performed qualitatively, however with a certain level of difficulty. Further to this, the outer wall can be characterised quantitatively as can the luminal wall despite the disparity that is caused by the tissue processing. The lipid core and the calcified regions of the plaque can be semi-quantitatively characterised, with a certain degree of accuracy. This may be partially explained by the fact that at the boundary of the lipid region, a mixed fibrous and lipid tissue region may exist. At this mixed region, the echo signal is neither echogenic (associated with non-fibrous tissue), nor echolucent (associated with fibrous tissue). Therefore the grey-scale contrast between the regions can not be clearly defined. However, the fibrous cap cannot be characterised quantitatively due

to its small size and the arbitrary angle between the fibrous cap layer and the ultrasound scan beam.

Based on the visual examination, the echolucent region is present in most of the lipid region which is the key factor that drives this part of the study further. However, the unclear boundary of the echolucent region causes a major problem during image segmentation. The results from this chapter suggested that the image segmentation used for detecting lipid region boundaries may be subjected to errors depending on the character of the mixed region, although a reasonably good inter-operator repeatability was obtained. Further investigation of the signal character for the region boundaries may improve segmentation accuracy and generate better ultrasound tissue characterization results. The ultrasound scan parameters could also be optimized in the future.

Chapter 8

Discussion and Conclusions

The main objectives of this study were the following:

- To study the morphological differences in the atherosclerotic carotid plaque between the ruptured and non-ruptured plaque groups.
- To study the differences in the macrophage content and distribution pattern between the two patients groups (ruptured and non-ruptured).
- To develop a procedure to generate a high resolution 3-D reconstruction of a patient-specific plaque based on histology sections and ex-vivo ultrasound.
- To perform a feasibility study investigating the use of ex-vivo 2D ultrasound images for plaque tissue characterisation, using corresponding histology sections as the "gold standard".

Current MRI technology has been demonstrated by our group to provide sufficient information to perform plaque structure characterisation (Hao et al 2008). This finding has also been supported in other similar studies (Bazot et al 2010). By implementing the use of fluid structure interaction (FSI), on patients who were recently subjected to plaque ruptures, the correlation between local stress concentrations and fibrous cap rupture sites was demonstrated. In addition, the study showed that there is a significant difference in stress levels found between symptomatic and asymptomatic patients, indicating that plaque stress could be used as a factor to determine plaque vulnerability. Since macro-level stress analysis does not include the influence of local material property and strength variations, the results of such studies may be inaccurate. To improve our understanding of plaque rupture

mechanisms, further details are necessary regarding plaque morphology at the micro-level. The present study therefore aimed to improve the current knowledge on the 3D plaque structure at the microscopic level, and investigate any possible relationship between plaque structure and rupture.

Hypothesis: - It was hypothesized that "there is a morphological difference in atherosclerotic carotid plaques between ruptured and non-ruptured groups". It was further hypothesized that "these difference are correlated with differences in the macrophage content and distribution pattern between the two patient groups".

Based on the techniques developed in the present study, attempts were carried out to develop a procedure to generate a high resolution 3-D reconstruction of a patient-specific plaque based on histology sections and ex-vivo ultrasound for possible further stress analysis at the micro-level. Finally, a feasibility study was performed investigating the use of ex-vivo 2D ultrasound images for plaque tissue characterisation using corresponding histology sections as the "gold standard".

To accomplish these, standard histological procedures were applied to analyse carotid endarterectomy specimens. Antibody staining of CD68 inflammatory marker was used on transverse sections generated from histology for identifying macrophage cells. Furthermore, a finite element method (FEM) was used to perform tissue registration to correct the non-linear tissue distortion caused by tissue processing during histology. The corrected 2-D section images were then used to generate high resolution 3-D reconstructions of patient-specific plaques.

Chapter 8 Discussion and Conclusion

8.1 Plaque Morphology Analysis

The rupture of an unstable atherosclerotic carotid plaque can lead in many cases to a thrombus–mediated acute cardiovascular event. The necrotic core fibroatheroma (NCFA) is a type of atherosclerotic plaque that comprises the vast majority of carotid lesions which are implicated in acute cardiovascular events. This type of lesion consists of a fibrous cap, which shields an underlying necrotic lipid pool from contact with the flowing blood in the lumen. Numerous studies have demonstrated that the characteristics of an unstable plaque which is prone to rupture, are a thin fibrous cap (Gao et al 2008), a large compliant necrotic core, and activated macrophages which can be found near the fibrous cap. When the fibrous cap ruptures, the thrombogenic contents of the lipid pool (Sovrshaev et al 2010) become exposed to the blood, resulting in an occlusive thrombus that initiates the onset of an acute cardiovascular event.

8.1.1 Mean value Difference between the Two Patient Groups

Collagen Contents

The invasion of inflammatory cells into the intima results in monocyte/macrophages engulfing lipids found within plaques. These cells form foam cells and then ultimately die, leaving debris which contributes towards the enlargement of the lipid core. Inflammatory cells can send molecular messages such as interferons to smooth muscle cells that inhibit their ability to synthesise new collagen molecules. In addition, the inflammatory cells release proteolytic enzymes that degrade collagen in the fibrous cap. Since collagen is responsible for the structural integrity of the fibrous cap, it is important to be able to quantify its collagen content. Currently, the quantification of collagen in-vivo in the fibrous cap has been difficult due to the low resolution of imaging modalities. However, recent studies have attempted to quantify

the collagen content in plaque indirectly by measuring alternative parameters that are correlated to collagen. Goncalves et al (2008) demonstrated a positive correlation between cystatin C levels and collagen levels (r=0.50, p=0.004) in plaques. Hector et al (2010) found greater collagen deposition, increased presence of CD68 positive cells, and an increased pyridinoline (Pyd): deoxypyridinoline (Dpd) ratio, covalent intermolecular cross-links required for collagen maturation, in plaques versus normal vascular tissue. Differences in these cross-links may have relevance to the mechanisms underlying the rupture of vulnerable plaques. Future improvements in techniques may enable the quantification of these parameters to indirectly measure the collagen content, and distinguish between vulnerable and stable plaques.

Results from the present study show that the collagen content in the fibrous cap in general is significantly lower in ruptured plaques compared with non-ruptured plaques, (40.1±13.11% and 49.31±10.09% respectively, p=0.08). This result is in agreement with a study performed by Fagerberg (2010), which demonstrated that low collagen content in the upstream region of the plaque coincided with the majority of ruptures. Fagerberg et al (2010) only used a limited number of sections throughout the entire plaque, while up to 30 sections were used in the present study. Furthermore, our results have been categorised into ruptured and non-ruptured patient groups, which has not been performed by previous studies.

Lipid core size

Plaques that have small lipid cores generally remain clinically silent (Davis M J et al 1990), whilst plaques that are characterised by large lipid cores are considered to have an increased likelihood of having larger stress and are more prone to rupture (Gao et al 2008). A larger lipid core may result in a higher accumulation of macrophage cells,

therefore causing increased collagen degradation. The size of the lipid core may therefore indicate the macrophage content in plaque, which would indirectly determine the collagen content. If this assumption is correct, the diagnosis of vulnerable plaques can be made easier as ultrasound and MRI can reliably reveal lipid core size. Investigating the lipid cores in plaques has therefore been central for many groups working on plaque vulnerability and rupture (Abdel-Karim et al 2011, Gardner et al 2008, Cappendijk et al 2008). It is widely believed that ruptured plaques are more likely to be associated with large lipid cores (Wasserman et al 2008).

In this study, the mean size of the lipid core was quantified for both ruptured and non-ruptured plaques. The results demonstrated that ruptured plaques have significantly larger lipid core sizes than non-ruptured plaques, 904.31±377.04μm and 548.62±207.56μm (p=0.02), respectively. In addition, the results also showed a negative correlation between lipid core size and collagen content in both ruptured and non-ruptured plaques (r = -0.73 and r = -0.84, respectively). Although the present study did not directly stain for proteolytic enzymes released by macrophage cells, it does indirectly suggest this trend by the negative correlations found between the lipid core size and the collagen content in both plaque groups.

Fibrous cap thickness

It is believed that a thicker fibrous cap is associated with a more stable plaque. Studies analysing both plaque specimens and stress have shown that a thin fibrous cap (<65microns) for a coronary plaque will most likely be subject to rupturing (Tavora et al 2010), while for a carotid plaque, this critical value is 200 microns (Redgrave et al 2008). Therefore, a direct measurement of fibrous cap thickness for individual plaques will provide a direct plaque rupture risk index. Previous studies

have reported fibrous cap thickness in either only non-ruptured (Kume et al 2006), or ruptured (Kubo et al 2007) coronary plaques, or in symptomatic carotid plaques (Fagerberg et al 2010). The present study categorised carotid plaques into ruptured and non-ruptured groups, and compared the mean values using sections taken at high frequency in the longitudinal direction of the plaque. The results of the present study showed that ruptured plaques have thinner mean fibrous caps compared with non-ruptured plaques, 302.64±97.08μm and 417.52±139.74μm (p=0.03), respectively. Although the difference was not significant, this difference in characteristics may be explained by the fact that plaques with thin fibrous caps also had large lipid cores (904.31±377.04μm), and plaques that had thicker fibrous caps had smaller sized lipid cores (548.62±207.56μm). It should also be noted that these fibrous cap thickness values are the average value of the minimum fibrous cap thickness per section for the entire plaque, which may be larger than the minimum value of the fibrous cap thickness quoted by Redgrave et al (2008). These findings are in concordance with Yonetsu et al (2011), who also showed that ruptured plaques had thinner fibrous cap thickness than non-ruptured plaques; however, it was performed using coronary plaques, which can differ from carotid plaques in numerous ways, and was carried out using OCT imaging, which can suffer from low resolution and contrast.

8.1.2 Longitudinal Distribution

Hypothesis: - "If there are differences in blood flow variations between the up- and downstream regions of a plaque, which can influence gene expression and cellular function, then plaque morphology may vary longitudinal between ruptured and non-ruptured plaques".

Most studies analysing plaque morphology have only focused on a few sections around the plaque throat region (Fagerberg et al 2010). These studies rarely investigated the 3D distribution variation of plaque morphology longitudinally. Studies have shown that collagen content varies considerably along the length of the plaque (Kratky et al 1998), based on a few specific locations in a plaque. Fagerberg et al (2010) also studied the variations in the plaque components along the longitudinal direction by analysing 7 sections in total, 3 in the upstream region, 1 at the plaque throat, and 3 in the downstream region. The objective of the present study was to also investigate these parameters longitudinally throughout the plaque. Three regions (upstream, throat (maximum stenosis), and downstream) were defined for each plaque in the study, and each section was selected at every 250 micron longitudinal intervals to reveal the detailed structural changes that may occur.

Lipid core:

Although Fagerberg et al (2010) reported on the longitudinal variations in the collagen and macrophage content in plaques, there was no data on lipid core size. The results from the present study showed that the lipid core is generally thinner in the shoulder regions, and thicker in the throat regions. The ruptured plaque group had a significantly larger lipid core thickness than the non-ruptured plaque group in the upstream (p=0.009) and throat (p=0.04) regions. In the downstream region, although the ruptured plaques continued to have a larger lipid core than the non-ruptured plaque group, the difference was not significant (p=0.12). Nevertheless, the results demonstrate a significant morphological difference that exists between the longitudinal lipid core thickness for ruptured and non-ruptured plaques.

Fibrous cap thickness:

In the present study, the mean fibrous cap thickness was calculated for each of the three longitudinal regions. The results showed that the ruptured plaque group had a significantly thinner fibrous cap than the non-ruptured plaque group in the upstream (p=0.004) and throat (p=0.015) regions, although the difference between the two groups were not significant in the downstream region (p=0.8), despite a thinner cap being evident for the ruptured group (307±115 μm versus 332±66 μm). To the author's knowledge there are no known studies in the literature which have quantified the longitudinal cap thickness in such detail.

Collagen content

Although previous studies have reported variations in the collagen content in plaques (Kratky et al 1998), the present study demonstrated quantitatively the collagen content distribution for ruptured and non-ruptured plaque groups at high resolution along the longitudinal aspect of the plaque. The collagen content in the non-ruptured plaque group is at its lowest in the upstream region, highest in the throat region, with a slight decline in the downstream region. In contrast, collagen content in ruptured plaques is at its peak in the upstream region and gradually declines towards the downstream region. This finding is on partial agreement with Fagerberg et al (2010), who also demonstrated a gradual decrease in collagen content along the longitudinal aspect of the symptomatic plaque. In comparing the collagen content difference between the two patient groups, in the upstream region, the collagen content value is slightly lower in the non-ruptured group than the ruptured group, whereas the value is significantly higher for the non-ruptured plaques compared with the ruptured plaques in the throat region.

It is interesting to note that the results of the fibrous cap and lipid core thickness are both indicative that the upstream region is more vulnerable to rupture than the other regions in a plaque, which is in agreement with clinical evidences that indicate that the majority of ruptures occur in the upstream region of the plaque. The higher collagen content occurring at the upstream shoulder for ruptured plaques may be due to arterial remodelling.

3D distribution of the plaque components

The 3D collagen distribution for 18 specimens was studied and demonstrated the distribution for a ruptured and a non-ruptured case. A common feature in most ruptured plaques studied was that ruptured regions generally correlated with regions of low collagen content. From figure 4.10(a), it can be seen that in section 10, along the longitudinal aspect of the plaque (throat region) there is very low collagen. Histological assessment revealed that this region has a fibrous cap with a clear sign of rupture. This finding is in agreement with Bury et al (2001) who showed that low collagen content correlated with a decrease in fibrous cap mechanical strength causing it to be more prone to rupture. This study has shown that by investigating the 3D collagen distribution pattern in high resolution, it is possible to identify and present the longitudinal location/region of a plaque rupture site clearly. It can also be used to improve our understanding of the morphological difference between ruptured and non-ruptured plaques.

8.1.3 Structure at the Rupture Sites:

Although it was found that the collagen content was higher in the upstream region, conferring stability; studies have shown the upstream region to also contain a higher frequency of thin fibrous caps (Fagerberg et al 2010), allowing instability, it is

therefore important to conduct a detailed investigation into the morphology at the rupture site itself to improve our understanding of the actual morphometric of plaque rupture. Lendon et al (1991) demonstrated that in human aortic plaques, fibrous caps of ruptured plaques are locally weakened by significant increases in macrophage density. Although the study does not directly quantify the collagen content, it did quantify the macrophage density, which weakens the caps of plaques by degradation of the collagen.

In the present study, the collagen content at sites circumferentially adjacent to the rupture site was analysed. The mean collagen content in the adjacent region to the rupture site for all the specimens was found to be 15.06±8.58%, compared with 37.76±22.47% for the surrounding circumferential regions (p=0.04). Longitudinally (regions located 0.5mm upstream and downstream of the rupture site), the mean collagen content was found to be significantly lower for the rupture site (15.06±8.58%) compared with the immediate upstream sections (53.58±34.72%, p=0.008). The collagen content in the rupture site was found to be lower than the non ruptured region at the downstream sections (28.40±19.30%, p=0.24026), however, the difference was not significant. These findings suggest that a local event within the fibrous cap may occur resulting in a general decrease in the collagen content, causing the weakening, potentially leading to the eventual rupturing of the fibrous cap. It is generally believed that low collagen content can be the result of a local accumulation of macrophages and the consequent ECM degradation. However, it is not known why they may accumulate more in certain areas of the cap than others. There have been a few recent studies which have focused on investigating factors that may influence such occurrences. Howarth et al (2007) demonstrated that the location of macrophage cells correlated to maximum predicted stresses on the plaque. However, it is very

difficult to prove the possible relationship between macrophage migration and accumulation in a plaque with local stress.

The findings from this part of the study led to the investigation of the lipid core size, located directly behind the rupture site. It was hypothesised that a large lipid core would contain higher densities of macrophage cells. The macrophage cells would release proteolytic enzymes that would degrade the collagen in the nearby fibrous cap. This may explain the significantly lower collagen contents found at the rupture site.

The results showed that the mean thickness in this region was 2045.79±120.66μm, while the mean thickness of the lipid core in the surrounding circumferentially adjacent regions was 1539.21±258.70μm (p=0.004). The difference was significant. The result also showed that in the immediate upstream section (250 microns upstream), the lipid core thickness reduced to 1237.19±860.44μm. In the immediate downstream section (250 microns downstream), the lipid core thickness was found to be significantly lower than the rupture site with a value of 1206.88±626.37μm and p=0.009. These findings indirectly support the hypothesis that the lower collagen content demonstrated at the rupture site may be due to the higher accumulation of macrophage cells, which was initially manifested by the large sized lipid core. The macrophage cells would release proteolytic enzymes that would act to degrade the collagen in the nearby fibrous cap causing it to rupture as was observed.

The differences in the lipid core size and collagen contents between the rupture sites and the adjacent regions are significant; however, the fibrous cap thickness does not vary significantly between the regions, although the fibrous cap is generally thinner at

the rupture site. This may be due to the small sample size available for the present study. Fibrous cap thickness has been generally studied between symptomatic and non-symptomatic plaques in published literature. There are very few studies which have reported results around the rupture sites. Based on this study, it seems that local collagen fibrous density is more predictive of the occurrence of a rupture; this has not previously been reported.

Macrophage Distribution

Hypothesis: - "If macrophages release proteolytic enzymes which act to degrade collagen causing them to be more prone to rupture, and if there are blood flow variations in the up- and downstream regions, then ruptured plaques may have a higher frequency of macrophages compared to non-ruptured plaques, and there may be variations in the different regions between the two groups".

Inflammation plays an important role in the initiation and development of atherosclerosis in human carotid arteries. Macrophages are the key cells that drive the inflammatory process in atherosclerotic plaques. The presence of macrophages in carotid plaques is a result of monocytes entering the vessel wall in response to cell adhesion molecules being expressed on the surface of endothelial cells. Upon entering the arterial wall, monocytes differentiate into macrophage cells and function to engulf the lipid in the plaque. A study by Potteaux et al (2011) demonstrated this process by inhibiting monocyte recruitment into plaques, coupled with a stable rate of apoptosis, there was a reduction in macrophage content. In addition, as already mentioned, macrophage cells release proteolytic enzymes that degrade collagen in plaques. The study of macrophage cells in atherosclerotic plaques is therefore fundamental in

assessing the progression of plaques as well as in the risk assessment of plaque rupture.

Many studies have also focussed on macrophage-collagen interaction to improve current risk assessment strategies. Barascuk et al (2010) showed that human macrophage foam cells degrade the extracellular matrix (ECM) of atherosclerotic plaques by cathepsin K mediated processes. Fagerberg et al (2010) reported that in sixty eight percent of plaques that were studied, macrophages were found to be more prevalent upstream of maximum stenosis compared with the downstream region, based on approximately 7 sections taken from the entire plaque length. Correspondingly, Fagerberg et al (2010) also found that collagen content was higher in the upstream region compared to the downstream region. Although only the cap shoulder regions were examined, Dirksen et al (1998) and Yilmaz et al (2007) also demonstrated that macrophage content is higher in the upstream region than in the downstream region.

In the present study, transverse sections were stained for macrophage cells at 250μm intervals along the longitudinal aspect of the plaque to ensure local variations in macrophage contents were identified. The results showed that in both ruptured and non-ruptured groups, macrophage cells were found to occupy a larger area in the upstream region of the plaque throat compared with the downstream region. These results further confirm the findings from previous studies, however, in the present investigation the results were based on an increased frequency of sections along the longitudinal aspect of the plaque to take into account any local variations. In addition, the 3D localization analysis showed that macrophage cells were found localised at close proximity to the luminal wall in ruptured plaques compared with non-ruptured

plaques. Attempts have been previously made by other groups demonstrating macrophage cell distributions in vulnerable plaques ((Barascuk et al 2010), Hyafil et al (2009) Korosoglou et al (2008)), however, they have seldom been used to correlate these macrophage localisations with the rupture site.

The findings of this study have suggested that macrophage cell content is greater in ruptured plaques compared with non-ruptured plaques. It has also demonstrated that ruptured plaques have larger lipid core sizes than non-ruptured plaques. Gronholdt et al (2002) observed that increases in macrophage density in carotid plaques were associated with increased lipid content, and plaque echolucency. However, the detection of macrophage cells was performed by identifying specific histological sections with the largest area of macrophages, which is subjective. In addition, their study harvested only 3 sections from each specimen to generate the mean value for the analysis, which may not be accurate. Results from the present study show that there is a strong correlation between the mean lipid core area and the mean macrophage area for both the ruptured (r=0.76) and non-ruptured plaques (r=0.98). For the longitudinal comparisons, results showed that in the upstream region, for both ruptured and non-ruptured plaques, the correlation between lipid core size and macrophage area is much stronger (r=0.92 and r=0.90, respectively), compared with the downstream region (r=0.72 and r=0.68, respectively). These findings are in agreement with previous studies performed by Gronholdt et al (2002), and Kuroiwa et al (2010); however the present study has shown this in much greater detail and has categorised the data into two patient groups, unlike previous studies.

The significance of this finding is that it could aid in the clinical diagnosis of patients with vulnerable plaques. Although it is currently not possible to detect macrophage

accumulation clinically, ultrasound is able to detect lipid cores of atherosclerotic plaques due to their echolucent properties and it could therefore be used to indirectly indicate local accumulations of macrophage cells and the consequent low local collagen contents.

8.2 High Resolution 3D Reconstruction of Plaque

Hypothesis: - "A combination of histology, ultrasound, FEM, and 3D modelling techniques may provide a solution to using high resolution analysis of plaque morphology to improve the clinical assessment of vulnerable plaques".

Further analysis of plaque stability using methods such as stress analysis relies on accurate reconstruction of the plaque 3D structure. MRI images are generally used for mechanical model generation. (Tang et al 2009, Gao et al 2011) However, the limited spatial resolution of MRI is not capable of resolving detailed plaque features. In addition, the contrasts between plaque features are also difficult to distinguish and can be subjective. However, histology sections of plaque specimens can provide not only high resolution images of the plaque, but also accurate tissue definitions of plaque components, and provide an ideal solution for accurate model generation. Vengrenyuk et al (2010) used histology based finite element analysis to evaluate peak circumferential stresses in aortic and brachelocephalic arteries However, there are many potential problems in applying the method to 3D plaque model reconstruction such as **(a)** registration of the sections into 3D; **(b)** studies have shown that the fixation, tissue processing, and the wax embedding steps during histology can cause significant tissue distortion; (Dobrin et al 1995, Lowder et al 2007) which was also demonstrated in the present study (Luppi et al 2009).

Chapter 8 Discussion and Conclusion

The idea of reconstructing 3D tissue structure from high resolution images such as histological sections using micro CT, has previously been performed, and is therefore not novel. Investigators have previously developed algorithms for generating 3D tissue micro-structure (Requena R et al 2007). Groen et al (2010) performed three-dimensional registration of histology sections from human atherosclerotic carotid plaques to in-vivo images with section intervals of 1mm. The study showed the feasibility of the procedure. However, the 3D reconstruction of the present study has the specific aim of performing plaque stress analysis in an accurate model. It is a cross-scale reconstruction with certain fine details (at the micron level in-plane resolution) but performed on a large longitudinal axis (>5cm in general), and was therefore very difficult to perform, as it required the registration of the orientations for all the sections. The present study clearly demonstrated the feasibility of generating high resolution plaque 3D structure throughout the entire length. The study showed that with the proposed procedure using ex-vivo ultrasound, it is possible to construct an accurate 3D model of plaques for stress analysis purposes. In addition, the proposed procedure enables functional information such as inflammation activities obtained from immunohistochemical analysis to be inserted directly in to the model in the future. This has not been reported or proposed in any other previous reports, and it may provide a framework for advanced 3D registration of plaque histological sections to ex-vivo ultrasound with molecular level accuracy. The direct comparison of the mechanical stress and the biological activities of plaque components will provide critical information on the understanding of arterial remodelling and plaque rupture.

This part of the study also performed an indirect assessment of the tissue shrinkage of histological sections by a FEM registration modelling process. The quantification of

the shrinkage rate for the different arterial plaque components is novel. It was found that the shrinkage varied significantly for the different plaque components, and the overall shrinkage is also morphology dependent. Large shrinkages generally occurred during the tissue processing step of the histology procedure. An opened plaque specimen (incision made through the lumen) was found to have a much larger shrinkage than a circumferentially intact specimen after the histology procedure. This result indicates that care must be taken when analysing results from histology analysis.

8.3 Application of the Morphology Study Results to Clinical Diagnosis

The plaque morphology results discussed in this chapter focused on the lipid content, the collagen content and the macrophage content of atherosclerotic carotid plaques in ruptured and non-ruptured patient groups. These have been investigated and discussed in detail in relation to the plaques longitudinal direction, and the correlations between the different components. The aim of this part of the present study was to apply the results of the morphological analysis to aid clinical practises.

Ultrasound imaging is the front line technique for assessing patient arterial plaque in clinical practices due to its low cost, easy access, and non-invasive nature. However, the information that clinicians can use from ultrasound assessment of a plaque is generally limited to the degree of stenosis (or luminal narrowing). Luminal narrowing is not an ideal parameter to use for estimating plaque size, and may even underestimate the atherosclerotic burden. Glagov et al (1987) demonstrated that due to compensatory enlargement of the adventitial wall, vessels can suffer large increases in atherosclerotic plaque mass without luminal narrowing. Ultrasound tissue characterization of plaque assessment became a major research focus for many years.

Based on the fact that different plaque components have significantly different mechanical properties, a varied contrast is generated between components to provide an accurate diagnosis of plaque morphology. However, due to the generally poor image quality caused by many factors, the results for ultrasound tissue characterization is still far from satisfactory (Kern et al (2004). A few studies have attempted to improve the image quality of B-mode scanning for the characterisation of atherosclerotic plaques in carotid arteries by reducing the reverberation artefacts (Liasis et al 2008). Despite the limitations of the image quality in ultrasound, studies have focused on understanding differences in image contrast (grey-scale) to assess plaque vulnerability. Tegos et al (2001) demonstrated that echogenic characteristics and the degree of stenosis are the strongest predictors of carotid plaque behaviour. Gronholdt et al (2001), demonstrated that echolucent plaques causing >50% diameter stenosis by Doppler ultrasound are associated with the risk of future strokes in symptomatic patients. Although encouraging, the studies showed no evidence of validating the echolucent region correlation to the corresponding plaque features. Denzel et al (2003) investigated whether ultrasonography could characterise plaque morphology and surfaces independent of the observer. The study showed that analysis of the internal structure on the basis of the grey-scale showed only vague agreement with the histological findings. Droste et al (2000) compared preoperative B-mode ultrasound plaque appearance with the histology of carotid endarterectomy specimens, and found that carotid B-mode ultrasonography is able to predict the histopathological components and the texture of carotid plaques. However, the preoperative B-mode ultrasound images were compared to corresponding histology images without the consideration of the tissue distortions caused by histology processes. In the present study, ultrasound images were compared not only with

associated histology sections, but also with cross-sectional photographs, which were not subjected to structural distortions.

The research setup in our group at Brunel University enables us to perform in-vivo ultrasound scans for patients before CEA, and ex-vivo scans on the same plaque specimens. It provides an ideal opportunity to assess the ability of ultrasound tissue characterization, by comparing ultrasound images of a plaque at in vivo condition, ex vivo condition (ideal scan condition), and with histology results. A major difficulty of assessing plaque in vivo by ultrasound was that the outer arterial wall cannot be defined accurately. As a consequence, the varied image intensity in the plaque regions cannot be defined accurately. An ex vivo ultrasound scan is not subjected to this problem. The preliminary results of this study were presented in this thesis.

The results of the current study indicated that ultrasound images can accurately demonstrate the appearance of the lipid core. An echolucent region in an ultrasound image can always be identified as a lipid core in the corresponding histology sections for all tested sections. Conversely, for most of the histology images which have a lipid core, an echolucent region can be found on the corresponding ultrasound image. In certain cases, ultrasound images which did not show echolucent regions were contradicted by histology images, and in these certain cases, the lipid regions were generally found to be very small in size.

The agreement for the fibrous cap size measurements from the ultrasound image with either photograph or histology was very poor. This was primarily as a result of the small size of the fibrous cap, which the resolution of the ultrasound was unable to clearly resolve.

As the findings have shown, the macrophage content is closely linked with plaque collagen content, which is a major determinant of fibrous cap quality. Therefore, by assessing the echogenic properties of the plaque using ultrasound, it may provide an indication to the fibrous cap quality. With improvements in ultrasound image quality, and in boundary detection, the ability to characterise and quantify the plaque lipid content would have considerable benefits to clinical practice, as the fibrous cap quality could be determined indirectly.

8.4 Limitation

Firstly, cryosectioning (frozen section) was not adopted in the present study. Unlike wax histology, frozen sections would preserve the lipid core of plaques, providing increased accuracy in the morphology assessment. As shown in the study, paraffin wax histology can introduce upto 30% tissue shrinkage, a problem which could be eliminated by using frozen sections. In addition, 3D plaque geometry reconstruction for stress analysis purposes requires accurate plaque geometry; the use of frozen section would have enabled this without the requirement of image registration using finite element method, which was used for the current study.

Secondly, MMP distributions were not directly measured. Although the study did show an indirect link between macrophage distribution and collagen degradation, using MMP staining would have enabled the demonstration of a more direct link between the two factors, since macrophages release MMP's which act to degrade collagen. Furthermore, elastin distribution was not measured; therefore the internal elastic lamina could not be defined in plaque tissue, which is believed to have significant influence on macrophage cell migration. Staining for elastin would have provided important information that may have given us a better understanding of the

mode of entry for macrophage cells, i. e. whether they enter from the adventitia by local microcirculation or via the luminal wall.

Thirdly, we did not use sufficient landmarks in the ultrasound scan for the registration process. In the present study only an ink landmark was used to perform the registration process. Increasing the number of physical landmarks would significantly increase the accuracy of the registration result.

Fourthly, the use of pressure-fixation would be desirable to obtain physiological accurate model geometries. In the present study, the vessel lumen was subjected to buckling as it was without the presence of any internal pressure, and which is evident in the ultrasound images.

8.5 Conclusion

The vulnerability of a plaque to rupture has been shown to be largely determined by its morphological characteristics. Plaques with large lipid cores and thin fibrous caps are more prone to rupture than plaques with a small lipid core and a thick fibrous cap. The study of plaque morphology is therefore important in determining a plaques vulnerability to rupture. In the present study, it has been shown that that there is a morphological difference in atherosclerotic carotid plaques between the ruptured and non-ruptured groups.

It was further demonstrated that these differences are correlated with differences in the macrophage content and distribution patterns between the two patient groups. Macrophages are known to release proteolytic enzymes that act to degrade the collagen in plaques, rendering them susceptible to rupture. Ruptured plaques have higher macrophage contents than non-ruptured plaques. Using the results obtained

from these studies (chapters 4 and 5); a procedure was developed to generate a high resolution 3-D reconstruction of a patient-specific plaque, based on histological sections and ex-vivo ultrasound for accurate stress analysis to study biomechanical interactions. The latter study led us to perform a feasibility study investigating the use of ex-vivo 2D ultrasound images for plaque tissue characterisation, using corresponding histological sections as the "gold standard".

The current limitations of ultrasound are that its resolution is not sufficiently high to resolve and distinguish small sized plaque structures. Other limitations of ultrasound are that it is not possible to distinguish between tissues with similar echolucent or echorich properties.

The present study has demonstrated that quantifying the thickness of the fibrous cap using ultrasound is clearly not attainable. In addition, other parameters such as the collagen density and macrophage activity are not possible to quantify using ultrasound. The development of molecular imaging technology in the future may enable macrophage activity to be quantified. This study has shown that although it is not possible to derive the thickness of the fibrous cap in atherosclerotic plaques using ultrasound, it is possible to reliably show the size of the lipid core (discussed in detail in chapter seven). The study showed us qualitatively that the lipid core in ex-vivo ultrasound is clearly definable. The study has also demonstrated that the size of the lipid core is correlated to the plaques macrophage content, which is negatively correlated to the collagen content. Therefore, by investigating the lipid core using ultrasound, it should be possible to reveal the quality of the fibrous cap indirectly based on its collagen content and in a manner that may facilitate better clinical diagnosis and prognosis.

Chapter 8 Discussion and Conclusion

Based on the research results the main conclusions which can be derived from this research are:

- Ruptured plaques have a significantly thinner mean minimum **fibrous cap** compared with the non-ruptured plaque group (p=0.03).
- The **lipid core** thickness is significantly larger in the ruptured plaque group, compared with the non-ruptured plaque group.
- The mean **collagen density** (ratio of collagen and non-collagen material) in the fibrous cap of ruptured plaques is significantly lower compared with the non-ruptured plaques.
- The collagen content decreases along the longitudinal length of the plaque in ruptured plaques from the upstream to the downstream regions.
- In both the upstream and downstream regions for all the specimens studied, the fibrous cap thickness is significantly greater in the non-ruptured plaque group compared with ruptured plaques.
- Collagen content in the fibrous cap at the site of the rupture is significantly lower compared with the mean in the surrounding region. Also the lipid core thickness behind the rupture site is significantly larger in size compared with the mean thickness in the rest of the surrounding region.
- The thickness of the fibrous cap at the rupture site is thinner than the mean thickness of the fibrous cap in the adjacent regions but the difference is not significant. The presence of a large lipid core and active collagen degradation (therefore a low content), may therefore be more important than a thin cap as a feature of plaque stability.

- In both upstream and downstream regions, the ruptured plaque group has a higher macrophage area in each transverse section compared with the non-ruptured plaque group.
- The area occupied by macrophage cells is positively correlated to the size of the lipid rich necrotic core, and negatively correlated with the collagen content for most sections.
- There is a difference in the 3-D macrophage distribution pattern between ruptured and non-ruptured plaques. In ruptured plaques, macrophage cells are located nearer to the boundary of the luminal wall, compared with non-ruptured plaques.
- The macrophage area is larger in the upstream region, than in the downstream region for both plaque groups.
- The study demonstrates the feasibility of using histological images, combined with the plaque outline geometry provided by US images, to reconstruct 3D arterial plaque at a microscopical-level for stress analysis purposes.
- Ex-vivo 2D US has shown good potential for plaque tissue characterisation based on 2 plaque specimen blocks. However, the quantitative agreement between the US tissue characterization results and associated histology results are still not satisfactory. More studies should be carried out to improve ultrasound image quality and image segmentation accuracy.

8.6 Future Research Directions

There is currently a gap in the knowledge between abnormal biological activity, such as macrophage accumulation, and the final result of structural change. The distribution pattern of enzymes such as MMP's that are produced by macrophage

cells and which may modify plaque collagen distribution is an important area for future studies. A detailed study of MMP involvement in plaque stability and remodelling may provide a clearer understanding of plaque pathogenesis.

Immediate future work on the application of the 3D plaque model could be a FEM stress analysis, using models of patient-specific plaques. The stress distribution results could be analysed together with inflammatory information about the plaque. Furthermore, to improve the accuracy of FEM based image restoration, more physical landmarks are required to be introduced to the ultrasound scans. The application of cryosection could generate sections that are not subjected to tissue shrinkage; therefore validation of the corrected image with frozen section images may be performed to assess the accuracy of the corrected image in the current study.

Ultrasound tissue characterization is an ongoing project in the group. More specimens will be analysed using similar procedures as described in Chapter 7. Improvements to the ultrasound scan procedure, as well as in image segmentation techniques, will be important tasks for the future.

References

Agardh HE, Folkersen L, Ekstrand J, Marcus D, Swedenborg J, Hedin U, Gabrielsen A, Paulsson-Berne G Expression of fatty acid–binding protein 4/aP2 is correlated with plaque instability in carotid atherosclerosis, J Intern Med 2011; 269: 200–210

Amano T, Matsubara T, Uetani T, Kato M, Kato B, Yoshida T, Harada K, Murohara T, Lipid-rich plaques predict non-target-lesion ischemic events in patients undergoing percutaneous coronary intervention insights from integrated backscatter intravascular ultrasound, Circulation Journal 75 (1), 2011 pp. 158-166

Aqel N, Ball R, Waldmann H, Mitchinson J, Identification of macrophages and smooth muscle cells in human atherosclerosis using monoclonal antibodies, Volume 146, Issue 3, pages 197-204, July 1984

Arauz A, Hoyos L, Zenteno M, Mendoza R, Alexanderson E, Carotid plaque inflammation detected by 18F-fluorodeoxyglucose-positron emission tomography Pilot study, Clinical Neurology and Neurosurgery 109 (2007) 409-412

Ball RY, Stowers EC, Burton JH, Cary NR, Skepper JN, Mitchinson MJ, Evidence that the death of macrophage foam cells contributes to the lipid core of atheroma, Atherosclerosis 1995 April 7;114(1):45-54

Baldewsing R A. , Mastik F , Schaar J A. , Serruys P W. , Steen A F W, Young's modulus reconstruction of vulnerable atherosclerotic plaque components using deformable curves, Ultrasound in Medicine & Biology, Volume 32, Issue 2, February 2006, Pages 201-210

Barascuk N, Skjot-Arkil H, Register T C, Larsen L, Byrjalsen I, Christiansen C, Karsdal M A, Human macrophage foam cells degrade atherosclerotic plaques through cathepsin K mediated processes, 2010, BMC Cardiovascular Disorders 10, art. No 19

Barascuk N, Vassiliadis E, Larsen L, Wang J, Zheng Q, Xing R, Cao Y, Crespo C, Lapret I, Sabatini M, Villeneuve N, Vilaine J, Rasmussen L M, Register T C, Karsdal M A, Development and validation of an enzyme-linked immunosorbent assay for the quantification of a specific MMP-9 mediated degradation fragment of type III collagen - A novel biomarker of atherosclerotic plaque remodelling, Clinical Biochemistry xxx (2011) xxx–xxx

Baroncini L, Nakao L S, Ramos S G, Filho A P, Murta L O, Ingberman M, Tefé-Silva C, Précoma D B, Assessment of MMP-9, TIMP-1, and COX-2 in normal tissue and in advanced symptomatic and asymptomatic carotid plaques, Thrombosis Journal 2011, 9:6

Burke, A.P., Farb, A., Malcom, G.T., Liang, Y., Smialek, J.E., Virmani, R., 1999. Plaque rupture and sudden death related to exertion in men with coronary artery disease. JAMA 281, 921–926.

Cappendijk VC, Kessels AG, Heeneman S, Cleutjens KB, Schurink GW, Welten RJ, Mess WH, van Suylen RJ, Leiner T, Daemen MJ, van Engelshoven JM, Kooi ME. Comparison of lipid-rich necrotic core size in symptomatic and asymptomatic carotid

atherosclerotic plaque: Initial results. J Magn Reson Imaging. 2008 Jun;27(6):1356-61.

Casscells W. Thermal detection of cellular infiltrates in living atherosclerotic plaques: possible implications for plaque rupture and thrombosis. Lancet 1996; 347(9013):1447-9

Chandran KB, Mun JH, Choi KK, Chen JS, Hamilton A, Nagaraj A, McPherson DD. "A Method for In-vivo Analysis for Regional Arterial Wall Material Property Alterations with Atherosclerosis: Preliminary Results," Med Eng Phys 2003; 25:289–298. [PubMed: 12649013]

Chaturvedi S, Madhavan R, Santha kumar S, Mehri Bash M, high risk factor burden and worse outcomes in urban carotid endarterectomy pateints, 2008;39:2966-2968

Cheng C, Tempel D, Haperen R, Damme L, Algür M, Krams R, Crom R, Activation of MMP8 and MMP13 by angiotensin II correlates to severe intra-plaque haemorrhages and collagen breakdown in atherosclerotic lesions with a vulnerable phenotype, Atherosclerosis 204 (2009) 26–33

Cheng G C., AB; Howard M. Loree, PhD; Roger D. Kamm, PhD; Michael C. Fishbein, MD; and Richard T. Lee, MD, Distribution of Circumferential Stress in Ruptured and Stable Atherosclerotic Lesions a Structural Analysis with Histopathological Correlation, Circulation 1993; 87:1179-1187

Chi Z, Melendez A, Role of Cell Adhesion Molecules and Immune-Cell Migration in the Initiation, Onset and Development of Atherosclerosis, Cell Adh Migr. 2007 Oct-Dec; 1(4): 171-175

Choudhury A, Long Q, Das S, High resolution 3-D Reconstruction of an Atherosclerotic Plaque using a Combination of Histology and Ultrasound (2009)

Choudhury A. Macrophage Distribution in Human Ruptured and Non-Ruptured Atherosclerotic plaques, (2009).

Cicha L, Worner A, Urschel K, Klein M, Raithel D, Daniel W. G, Fibrous cap thinning and plaque vulnerability at the proximal region are associated with increased levels of Cathepsin L, Atherosclerosis Supplements 11, no. 2 (2010) 17–108

Coombs B, Rapp J, Ursell P, Reilly L, Saloner D, Structure of plaque at carotid bifurcation – High-Resolution MRI with Histological Correlation, Stroke, 2001.32:2516-2521

Coons AH, Creech HJ, Jones RN: Immunological properties of an antibody containing a fluorescent group. Proc Soc Exp Biol Med 1941; 47: 200-202.

Croons V, Martinet W, Herman A G, Timmermans J, De Meyer G R Y, The Protein Synthesis Inhibitor Anisomycin Induces Macrophage Apoptosis in Rabbit Atherosclerotic Plaques through p38 Mitogen-Activated Protein Kinase, The journal of pharmacology and experimental therapeutics, 329:856–864, 2009

Dai D, Ding Y H, Kadirvel R, Danielson M A, Lewis D A, Cloft H J, Kallmes D F, A longitudinal immunohistochemical study of the healing of experimental aneurysms after embolization with platinum coils AJNR April 2006 27: 736-741

References

Dandapat A, Hu C P, Chen J, Liu Y, Khan J A, Remeo F, Carey R M, Hermonat P L, Mehta J L, Over-expression of angiotensin II type 2 receptor (agtr2) decreases collagen accumulation in atherosclerotic plaque, Biochemical and Biophysical Research Communications 366 (2008) 871–877

De Bray J M, Baud J M, Dauzat M on behalf of the Consensus Conference Consensus concerning the morphology and the risk of carotid plaques. Cerebrovasc Dis 1997; 7; 289-96

De Meyer I, Martinet W, Hove C E V, Schrijvers D M, Hoymans V Y, Vaeck L V, Fransen P, Bult H, De Meyer G, Inhibition of inositol monophosphatase by lithium chloride induces selective macrophage apoptosis in atherosclerotic plaques, British Journal of Pharmacology, Volume 162, Issue 6, pages 1410–1423, March 2011

Denzel C, Fellner F, Wutke R, Bazler K, Muller K, Lang W Ultrasonographic analysis of atherosclerotic plaques in the internal carotid artery, European Journal of Ultrasound, Volume 16, Issue 3, February 2003, pages 161-167

Devuyst G, Ruchat P, Karapanayiotides T, Jonasson L, Cuisinaire O, Lobrinus J, Pusztaszeri M, Kalangos A, Despland P A, Thiran J P, Kalangos A, Ultrasound Measurement of the Fibrous Cap in Symptomatic and Asymptomatic Atheromatous Carotid Plaques. Circulation 2005; 111; 2776-2782

Dirksen, M.T., van der Wal, A.C., van den Berg, F.M., van der Loos, C.M., Becker, A.E., 1998. Distribution of inflammatory cells in atherosclerotic plaques relates to the direction of flow. Circulation 1998, pages 2000–2003.

Dobrin P, Effect of histologic preparation on the cross-sectional area of arterial ring, Journal of surgical research 61, 413-415 (1995)

Djuric T, Zivkovic M, Stankovic A, Radak Dj, Radak S, Alavantic D, MMP-8 Gene Expression In Human Carotid Plaques, Atherosclerosis Supplements, Volume 9, Issue 1, May 2008, Page 236

Driessen, N.J.B., Wilson, W., Bouten, C.V.C., Baaijens, F.P.T., 2004. A computational model for collagen fibre remodelling in the arterial wall. J. Theor. Biol. 226, 53–64.

Droste DW, Karl M, Bohle RM, Kaps M Comparison of ultrasonic and histopathological features of carotid artery stenosis. Neurol Res 1997;19:380±4.

Droste D. W., N. Haas, V. Kemeny, D. G. Nabavi, L. Fuzesi, E. B. Ringelstein. Preoperative B-mode ultrasound plaque appearance compared with carotid endarterectomy specimen histology. Acta Neurol Scand 2000: 101: 188-194.

El-Barghouty N.M, Levine T, Ladva S, Flanagan A, Nicolaides A. Histological Verification of Computerised Carotid Plaque Characterisation. (1996)

El-Barghouty N.M, Geroulakos G, Nicolaides A, Androulakis A, Bahal V. Computer assisted carotid plaque characterization. Eur. J. Vasc. Endovasc. Surg. 1996; 9:389 393.

Erbel C, Dengler T J, Wangler S, Lasitschka F, Bea F, Wambsganss N, Hakimi M, Bockler D, Katus H A, Gleissner C A, Expression of IL-17A in human atherosclerotic

lesions is associated with increased inflammation and plaque vulnerability, Basic Res Cardiol (2011) 106:125–134

Fagerberg B, Ryndel M, Kjelldahl J, Akyürek L M, Rosengren L, Karlström L, Bergström G, Olson F J, Differences in Lesion Severity and Cellular Composition between in vivo Assessed Upstream and Downstream Sides of Human Symptomatic Carotid Atherosclerotic Plaques J Vasc Res 2010;47:221–230

Fayad ZA, Fuster V. Clinical imaging of the high-risk or vulnerable atherosclerotic plaque. Circ Res 2001;89(4): 305e16.

Feldkamp LA, Goldstein SA, Parfitt AM, Jesion G, Kleerekoper M. The direct examination of three-dimensional bone architecture in vitro by computed tomography J Bone Miner Res 2004; 4:3-11.

Felton C V, Crook D, Davies M J, Oliver M F, Relation of plaque lipid composition and morphology to the stability of human aortic plaques, Arteriosclerosis, Thrombosis, and Vascular Biology 17 (7), pp.1337-1345 1997

Furukawa S, Uchino E, Azetsu T, Suetake N, Hiro T, Matsuzaki M, Plaque classification using sparse features of IVUS RF signal for the diagnosis of arteriosclerosis, 10th WSEAS International Conference on Applied Computer and Applied Computational Science, ACACOS, 2011, page. 99-103

Galis Z, Muszynski M, Sukhova GK, Simon-Morrissey E, Libby P. Enhanced expression of vascular matrix metalloproteinases induced in vitro by cytokines and in regions of human atherosclerotic lesions. Ann NY Acad Sci 1995;748:501–507.

Galis ZS, Sukhova GK, Lark MW, Increased expression of matrix metalloproteinase's and matrix degrading activity in vulnerable regions of human atherosclerotic plaques. *J Clin Invest*. 1994;94:2493–2503

Gao H, Long Q, Choudhury A. Macrophage Deformation in Plaque with Finite Element Analysis 2008

Gao H, Long Q, Effects of varied lipid core volume and fibrous cap thickness on stress distribution in carotid arterial plaques, Journal of Biomechanics 41 (2008) 3053–3059

Gao H, Long Q, Sadat U, Graves M, Gillard J H, Li Z Y, Stress analysis of carotid atheroma in a transient ischaemic attack patient using the MRI-based fluid –structure interaction method, British Journal of Radiology (2009) 82, S46-S54

Gao H, Long Q, Graves M, Gillard J H, Li Z, Carotid arterial plaque stress analysis using fluid–structure interactive simulation based on in-vivo magnetic resonance images of four patients, Journal of Biomechanics 42 (2009) 1416–1423

Gao H, Long Q, Kumar Das S, Halls J, Graves M, Gillard J H, Li Z-Y, Study of carotid arterial plaque stress for symptomatic and asymptomatic patients, Journal of Biomechanics 44 (14), pp. 2551-2557

Gojova A, Brun V, Bruno E, et al. Specific abrogation of transforming growth factor beta signalling in T cells alters atherosclerotic lesion size and composition in mice. Blood 2003;102:4052–8.

References

Gonçalves I, Ares M P.S, Moberg A, Moses J, To F, Montan J, Pedro L M, Dias N, Fernandes J F, Fredrikson G N, Nilsson J, Jovinge S, Bengtsson E, Elastin- and Collagen-Rich Human Carotid Plaques Have Increased Levels of the Cysteine Protease Inhibitor Cystatin C, J Vasc Res 2008;45:395–401

Goncalves I, Lindholm M W, Pedro L M, Dias N, Fernandes J, Fredrikson G N, Nilsson J, Moses J, Ares Mikko P S, Elastin and calcium rather than collagen or lipid content are associated with echogenicity of human carotid plaques. Stroke 2004;35;2795-2800

Groen H C, Walsum T V, Rozie S, Klein S, Gaalen K V, Gijsen F J H, Wielopolski P A, Beusekom H, Crom R, Verhagen H, Steen A, Lugh A, Wentzel J, Niessen W, Three-dimensional registration of histology of human atherosclerotic carotid plaques to in-vivo imaging, Journal of Biomechanics 43 (2010) 2087–2092

Gronholdt ML, Nordestgaard BG, Wiebe BM, et al. Echo-lucency of computerized ultrasound images of carotid atherosclerotic plaques are associated with increased levels of triglyceride-rich lipoproteins as well as increased plaque lipid content. *Circulation*. 1998; 97:34–40.

Gronholdt Marie-Louise M., Borge G. Nordestgaard, Torben V. Schroeder, Sissel Vorstrup and Henrik Sillesen. Ultrasonic Echolucent Carotid Plaques Predict Future Strokes. Circulation 2001;104;68-73

Gronholdt M L J, Nordestgaard B G, Schroeder T V, Vorstrup S, Sillesen H, Ultrasonic Echolucent Carotid Plaques Predict Future Strokes. Circulation 2002;104;68-73

Guyton JR, Klemp KF, Development of the lipid-rich core in human atherosclerosis, Arterioscler Thromb Vasc Biol. 1996 Jan;16(1):4-11

Hackett D, Davies G, Chierchia S, et al. Intermittent coronary occlusion in acute myocardial infarction: value of combined thrombolytic and vasodilator therapy. N Engl J Med. 1987; 317:1055–1059.

Hallow K M, Taylor W R, Rachev A, Vito R P, Markers of inflammation collocate with increased wall stress in human coronary arterial plaque, Biomech Model Mechanobiol (2009) 8:473–486

Hao H, Iihara K, Ishibashi-Ueda H, Saito F, Hirota S, Correlation of thin fibrous cap possessing adipophilin-positive macrophages and intraplaque hemorrhage with high clinical risk for carotid endarterectomy: Clinical article**,** 2011 Journal of Neurosurgery 114 (4), pp. 1080-1087

Hariton, I, de Botton, G, Gasser, T.C, Holzapfel, G.A. Stress driven collagen fiber remodelling in arterial walls. Biomec. Model. Mechanobio. DOI: 10.1007/s10237-006-0049-7 2006

Hariton I, DeBotton G, Gasser T.C, Holzapfel G.A, Stress-modulated collagen fibre remodelling in a human a human carotid bifurcation, Journal of Theoretical Biology 248 (2007) 460–470

References

Hector E, Robins S, Mercer D, Brittenden J, Wainwright C, Quantitative measurement of mature collagen cross-links in human carotid artery plaques, Atherosclerosis 211 (2010) 471-474

Heft G, Worthley SG, Fuster V, Fayad ZA, Zaman AG, Corti R, Fallon JT, Badimon JJ (2002) Progression and regression of atherosclerotic lesions—monitoring with serial non-invasive magnetic resonance imaging. Circulation 105:993–998

Hiltawsky KM, Wiegratz A, Enderle MD, Ermert H. Real-time detection of vessel diameters with ultrasound. Biomed Technik 2003;48(5):141e6.

Hockings P, Roberts T, Galloway G, Reid D, Harris D, Hart M, Groot P, Suckling K, Benson M, Repeated three-dimensional magnetic resonance imaging of atherosclerosis development in innominate arteries of low density lipoprotein receptor-knockout mice, Circulation. 2002;106:1716-1721

Hoeks APG, Brands PJ, Smeets F, Reneman R, Assessment of the dispensability of superficial arteries. Ultrasound Med Biol 1990;16(2):121e8.
Hollander M, Hak AE, Koudstaal PJ, Bots ML, Grobbee DE, Hofman A, et al. Comparison between measures of atherosclerosis and risk of stroke e The Rotterdam Study. Stroke 2003; 34(10):2367e72.

Honda O, Sugiyama S, Kugiyama K, Fukushima H, Nakamura S, Koide S, Kojima S, Hirai N, Kawano H, Soejima H, Sakamoto T, Yoshimura M, Ogawa H, Echolucent carotid plaques predicts future coronary events in patients with coronary artery disease, J Am Coll Cardiol, 2004; 43:1177-1184, doi:10.1016/j.jacc.2003.09.063

Howarth S, Li ZY, R. A. Trivedi, J. M. U-King-Im, M. J. Graves, P. J. Kirkpatrick & J. H. Gillard, Correlation of macrophage location and plaque stress distribution using USPIO-enhanced MRI in a patient with symptomatic severe carotid stenosis: a new insight into risk stratification British Journal of Neurosurgery, August 2007; 21(4): 396 – 398

Huang H, Virmani R, Younis H, et al. The impact of calcification on the biomechanical stability of atherosclerotic plaques. Circulation 2001;103:1051–6.

Hussain T, Abbots C R, Scott J A, Gough M J. Macrophage accumulation within the cap of carotid atherosclerotic plaques is associated with the onset of cerebral ischemic events J Vasc Surg 1999;30:269-76

Hyafil F, Cornily J C, Rudd J H F, Machac J, Feldman L J, Fayad Z A, Quantification of inflammation within rabbit atherosclerotic plaques using the macrophage specific CT contrast agen N1177: A comparison with 18F-FDG PET/CT and histology, Journal of Nuclear Medicine 50 (6), pp. 959-965, 2009

Imoto K, Hiro T, Fujii T, Murashige A, Fukumoto Y, Hashimoto G, Okamura T, Yamada J, Mori K, Matsuzaki M. Longitudinal structural determinants of atherosclerotic plaque vulnerability: a computational analysis of stress distribution using vessel models and three-dimensional intravascular ultrasound imaging. *J Am Coll Cardiol* 46: 1507–1515, 2005.

Imparato AM. The importance of hemorrhage in the relationship between gross morphologic characteristics and cerebral symptoms in 376 carotid artery plaques Ann Surg 1983; 197: 195-203

References

Ionita M G, Dijke A, Laman J D, Peeters W, Kraak P, Moll F L, Vries J, Pasterkamp G, Kleijn D P V, High Levels of Myeloid-Related Protein 14 in Human Atherosclerotic Plaques Correlate With the Characteristics of Rupture-Prone Lesions, Arterioscler Thromb Vasc Biol 2009;29;1220-1227

Ivan E, Khatri J, Johnson C, Magid R, Godwin D, Nandi S, Lessner S, Galis Z, Expansive arterial remodelling is associated with increased neo-intimal macrophage foam cell content. Circulation, 2002;105:2686-2691

Johnstone MT, Botnar RM, Perez AS, Stewart R, Quist WC, Hamilton JA,Manning WJ (2002) In vivo magnetic resonance imaging of experimental thrombosis in a rabbit model Arterioscler Thromb Vasc Biol 21:1556–1560

Junqueira L. C. U, G. Bignolas and R. R. Brentani, Picrosirius staining plus polarization microscopy, a specific method for collagen detection in tissue sections, Histochemical Journal, 11 (1979), 447-455

Karim A, Intercatheter reproducibility of near-infrared spectroscopy for the *in vivo* detection of coronary lipid core plaques, Volume 77, Issue 5, pages 657-661, 1 April 2011

Kitakaze M, Myoish M i, Tsukamoto O, Minamino T, Fujita M, Tomoike H, Hashimoto N, Roles of Inflammation and Endoplasmic Reticulum Stress In the Progression and Rapture of Atherosclerotic Plaques, Atherosclerosis Supplement 2009, Vol. 10, Issue 2

Kobayashi T, Ito T, Hirayama N, Yamada S, Shiomi M, Macrophage Accumulation and Expression of Matrix Metalloproteinases Relate to Plaque Vulnerability and Arterial Outward Remodelling, Atherosclerosis Supplement 2009, Vol. 10, Issue 2

Kolodgie F D, Narula J, Burke A P, Haider N, Farb A, Hui-Liang Y, Smialek J, Virmani. Localization of Apoptotic Macrophages at the Site of Plaque Rupture in Sudden Coronary Death American Journal of Pathology, Vol. 157, No. 4, October 2000

Kolodgie F D, Gold HK, Burke AP, et al. Intraplaque hemorrhage and progression of atheroma. N Engl J Med. 2003;349:2316–25.

Korosoglou G, Weiss R G, Kedziorek D A, Walczak P, Gilson W D, Schar M, Sosnovik D E, Stuber M, Non-invasive detection of macrophage rich atherosclerotic plaque in hyperlipidemic rabbits using positive contrast magnetic resonance imaging, Journal of the American College of Cardiology 52 (6), pp. 483-491, 2008

Kovanen PT. Mast cells: multipotent local effecter cells in atherothrombosis. Immunol Rev. 2007;217:105–22.

Kratky R G, Ivey J, Roach M R. Local changes in collagen content in rabbit aortic atherosclerotic lesions with time. Atherosclerosis 143 (1999) 7-14

Kristanto W, van Ooijen PM, Groen JM, Vliegenthart R, Oudkerk M, Small calcified coronary atherosclerotic plaque simulation model: minimal size and attenuation detectable by 64-MDCT and MicroCT, Int J Cardiovasc Imaging. 2011 Apr 21.

References

Ku, D.N., Giddens, D.P., Zarins, C.K., Glagov, S., 1985. Pulsatile flow and atherosclerosis in the human carotid bifurcation, positive correlation between plaque location and low and oscillating shear stress. Artherios 5, 293–302.

Kume T, Akasaka T, Kawamoto T, Okura H, Watanabe N, Toyota E, Neishi Y, Sukmawan R, Sadahira Y, Yoshida K, Measurement of the thickness of the fibrous cap by optical coherence tomography, American Heart Journal, Volume 152, Issue 4, October 2006, Pages 755.e1-755.e4

Kunte H, Kuntea G, Buschb M A, Weichertc W, Rückertd R, Harmsa L, Differences in carotid plaque content of macrophages, T cells and MMP-9 between patients with embolic and hemodynamic cerebral ischemia due to symptomatic carotid stenosis, Atherosclerosis 211 (2010) 456–460

Kuroiwa Y, Yamashita A, Miyati T, Furukoji E, Takahashi M, Azuma T, Sugimura H, Asada Y, Atherosclerotic lesions rich in macrophages or smooth muscle cells discriminated in rabbit liliac arteries based on T1 relaxation time and lipid content, 2010, Academic Radiology 17 (2), pp.230-238

Landini L, Santarelli MF, Pingitore A, Positano V. New technological developments in the clinical imaging of atherosclerotic plaque. Curr Pharm Des 2003;9 (29):2403e15

Langheinrich AC, Atherosclerotic Lesions at Micro CT: Feasibility for Analysis of Coronary Artery Wall in Autopsy Specimens October 2010, 257 (1)
Lee RT, Kamm RD.Vascular mechanics for the cardiologists. J Am Coll Cardiol 1994;23:1289–1295.

Lendon CL, Davies MJ, Born GVR, Richardson PD. Atherosclerotic plaque caps are locally weakened when macrophage density is increased. *Atherosclerosis*. 1991; 87:87–91.

Lessner S M, Prado H L, Waller E K, Galis Z S, Atherosclerotic lesions grow through recruitment and proliferation of circulating monocytes in a murine model, Am J Pathol. 2002 Jun;160(6):2145-55

Liasis N, Klonaris C, Katsargyris A, Georgopoulos S, Labropoulos N, Tsigris C, Giannopoulos A, Bastounis E, The use of Speckle Reduction Imaging (SRI) Ultrasound in the characterisation of carotid artery plaques, European Journal of Radiology 65 (2008) 427-433

Li Zhi-Yong, Simon Howarth, Rikin A. Trivedi, Jean M. U-King-Im, Martin J. Graves, Andrew Brown, Liqun Wang, Jonathan H. Gillard Stress analysis of carotid plaque rupture based on in vivo high resolution MRI Journal of Biomechanics 39 (2006) 2611–2622

Li Zhi-Yong, Simon P.S. Howarth; Tjun Tang; Jonathan H. Gillard, How Critical Is Fibrous Cap Thickness to Carotid Plaque Stability Stroke. 2006; 37:1195-1199

Libby P. Inflammation in atherosclerosis. Nature 2002; 420: 868–74.

Lillian Rich, Collagen and picrosirius red staining: a polarised light assessment of fibrillar hue and spatial distribution. Braz. J, morphol. Sci. (2005) 22(2), 97-104

References

Madjid M, Willerson JT, Casscells SW. Intracoronary thermography for detection of high-risk vulnerable plaques. J Am Coll Cardiol 2006 Apr 18; 47 (Suppl. 8):C80e5.

Matthias G Friedrich, Oliver Strohm, Jeanette Schulz-Menger, Heinz Marciniak, Friedrich C Luft and Rainer Dietz, Contrast Enhanced Magnetic Resonance Imaging Visualizes Myocardial Changes in the Course of Viral Myocarditis Circulation 1998;97;1802-1809

McConnell MV, Aikawa M, Maier SE, Ganz P, Libby P, Lee RT (1998) MRI of rabbit atherosclerosis in response to dietary cholesterol lowering. Arterioscler Thromb Vasc Biol 19:1956–1959

McKnight, A.J. and Gordon, S. (1998) Membrane molecules as differentiation antigens of murine macrophages. Adv Immunol 68, 271-314, PubMed ID: 98165990

MacNeil B, Intravascular Modalities for Detection of Vulnerable Plaques (current status) Arterioscler Thromb Vasc Biol. 2003;23:1333-1342

Meese TM, Lisauskas JB, Doucet CM, Clark NV, Gardner CM, HulEL l, Sum ST, Madden SP, Caplan JD, Goldstein JA, Muller JE, Spectroscopic identification of lipid-rich plaques causing intermediate stenosis: a study in coronary autopsy specimens, Cardiovascular Revascularization Medicine 9 (2008) 101–129

Megan R, Egbrink M, Cleutjens J, Kuijpers M, Schiffers P, Merkx M, Slaaf D, Zandvoort M, Imaging collagen in intact viable healthy and atherosclerotic arteries using fluorescently labelled CNA35 and two-photon laser scanning microscopy, Molecular Imaging, Vol 6, No 4 (July-August 2007): pp 247-260

Miyata K, Nakayama M, Mizuta S, Hokimoto S, Sugamura K, Oshima S, Oike Y, Sugiyama S, Ogawa H, Yamamura K, Elevated mature macrophage expression of human ABHD2 gene in vulnerable plaque, Biochemical and Biophysical Research Communications 365 (2008) 207–213

Nadkarni S K, Pierce M C, Park B. H, De Boer J F, Whittaker P, Bouma B E, Bressner J E, Halpern E, Houser S L, Tearney G J, Measurement of Collagen and Smooth Muscle Cell Content in Atherosclerotic Plaques Using Polarization-Sensitive Optical Coherence Tomography, (J Am Coll Cardiol 2007;49:1474–81)

Nederkoorn PJ, van der Graaf Y, Hunink M. Duplex ultrasound and magnetic resonance angiography compared with digital subtraction angiography in carotid artery stenosis e a systematic review. Stroke 2003; 34(5):1324e31.

Nelson K L, Runge V M, Basic Principles of MR contrast, Top. Magn. Reson, Imag, 7, 124-136 (1995)

Nissen SE, Yuck P: Intravascular ultrasound: novel path physiological insights and current clinical applications. *Circulation* 2001, 103:604–616.

O'Leary DH, Polak JF, Kronmal RA, Manolio TA, Burke GL, Wolfson SK. Carotid artery intima and media thickness as a risk factor for myocardial infarction and stroke in older adults. N Engl J Med 1999;340(1):14e22.

Ogawa M, Ishino S, Mukai T, Asano D, Teramoto N, Watabe H, Kudomi N, Shiomi M, Magata Y, Iida H, Saji H, 18F-FDG Accumulation in Atherosclerotic Plaques: Immunohistochemical and PET Imaging Study, J Nucl Med 2004; 45:1245-1250

References

Ohayon J, Teppaz Pierre, Finet G, Rioufol G. "In-vivo Prediction of Human Coronary Plaque Rupture Location using Intravascular Ultrasound and the Finite Element Method,". Coron Artery Disease 2001; 12:655–663. [PubMed: 11811331]

Ohayon J, Finet G, Treyve F, Rioufol G, Dubreuil O. A three-dimensional finite element analysis of stress distribution in a coronary atherosclerotic plaque: In vivo predictions of plaque rupture location. In: *Biomechanics Applied to Computer Assisted Surgery*, edited by Payan Y. Trivandrum, India: Research Signpost Publisher, 2004.

Ota H, Yu W, Underhill H R, Oikawa M, Dong L, Zhao X, Polissar N L, Neradilek B, Gao T, Zhang Z, Yan Z, Guo M, Zhang Z, Hatsukami T S, Yuan C, Hemorrhage and Large Lipid-Rich Necrotic Cores Are Independently Associated With Thin or Ruptured Fibrous Caps: An In vivo 3T MRI Study, *Arterioscler Thromb Vasc Biol* 2009;29;1696-1701

Pedersen, P. C., Chakareski, J., and Lara-Montalvo, R., 2003, "Ultrasound Characterization of Arterial Wall Structures based on Integrated Backscatter Profiles," Proc. for the 2003 SPIE Med Imaging Symposium, San Diego, pp. 115–126.

Philan G A, Purohit A, Wallace J, Knecht H, Woda B, Quesenberry P, Doxsey S, Centrosome defects and genetic instability in malignant tumors, Cancer research 58, 3974-3985, September 1, 1998

Potteaux S, Gautier E L, Hutchinson S B, Van Rooijen N, Rader D J, Thomas M J, Sorci-Thomas M G, Randolph G H, Suppressed monocyte recruitment drives macrophage removal from atherosclerotic plaques of Apoe-/- mice during disease regression, 2011, Journal of Clinical Investigation 121 (5), pp. 2025-2036

Radj A. Baldewsing, Frits Mastik, Johannes A. Schaar, Patrick W. Serruys, and Antonius F.W. van der Steen. Young's modulus reconstruction of vulnerable atherosclerotic plaque components using deformable curves. Ultrasound in medicine & biology, volume 32, issue 2, February 2006, pages 201-210.

Redgrave J N, Gallagher P, Lovett J K, Rothwell P M, Critical cap thickness and rupture in symptomatic carotid plaques, Stroke, 2008;39:1722-1729

Rekhter M, Gordon D. Cell proliferation and collagen synthesis are two independent events in human atherosclerotic plaques. J Vasc Res 1994;31:280–286.

Rekhter M Type I collagen gene expression in human atherosclerosis. Localization to specific plaque regions, American Journal of Pathology, Vol. 143, No. 6 December 1993

Rekhter M, Collagen Synthesis in Atherosclerosis: too much and not enough Cardiovascular Research 41 (1999) 376-384

Requena R S, Moratal D, Garcia-Sanchez D, Bodi V, Rieta J, Sanchis J, Automatic segmentation and 3D reconstruction of intravascular ultrasound images for a fast preliminary evaluation of vessel pathologies, Computerized Medical Imaging and Graphics 31 (2007) 71-80

Richardson PD, Davies MJ, Born GV. Influence of plaque configuration and stress distribution on fissuring of coronary atherosclerotic plaques. Lancet 1989;2:941–4.

References

Rikin A. Trivedi, Jean-Marie U-King-Im, Martin J. Graves, Jo Horsley, Martin Goddard, Peter J. Kirkpatrick, Jonathan H. Gillard. MRI-derived measurements of fibrous cap and lipid core thickness: the potential for identifying vulnerable carotid plaques in vivo. Neuroradiology (2004) 46: 738-743

Ross R, Atherosclerosis – An inflammatory disease. N Engl J Med 340; 115-126 1999

Rudd J, Myers K, Bansilal S, Machac J, Rafique A, Farkouh M, Fuster V, Fayad Z, 18Fluorodeoxyglucose Positron Emission Tomography Imaging of Atherosclerotic Plaque Inflammation Is Highly Reproducible, J Am Coll Cardiol 2007;50:892–6)

Sadat U, Teng Z, Young V E, Zhu C, Tang T Y, Graves M J, Gillard JH, Impact of plaque haemorrhage and its age on structural stresses in atherosclerotic plaques of patients with carotid artery disease: An MR imaging-based finite element simulation study. 2011. International Journal of Cardiovascular Imaging 27 (3), page 397-402

Schulte-Altedorneburg G, Droste DW, Haas N, Kemeny V, Nabavi DG, Fuzesi L, Ringelstein EB. Preoperative B-mode ultrasound plaque appearance compared with carotid endarterectomy specimen histology. Acta Neurol Scand 2000: 101: 188-194.

Schwartz, S.M., Virmani, R., Rosenfeld, M.E., 2000. The good smooth muscle cells in atherosclerosis. Curr. Atheroscler. Rep. 2, 422–429.

Seemantini K. Nadkarni, Measurement of Collagen and Smooth Muscle Cell Content in Atherosclerotic Plaques Using Polarization-Sensitive Optical Coherence Tomography. Journal of the American College of Cardiology Vol. 49 No. 13 2007

Seemantini K. Nadkarni, Brett E. Bouma, Johannes de Boer, Guillermo J. Tearney. Evaluation of collagen in atherosclerotic plaques: the use of two coherent laser-based imaging methods. Laser Med Sci (2009) 24:439-445

Seimon T A, Wang Y, Han S, Senokuchi T, Schrijvers D M, Kuriakose G, Tall A R, Tabas I A, Macrophage deficiency of p38α MAPK promotes apoptosis and plaque necrosis in advanced atherosclerotic lesions in mice, J. Clin. Invest. 119:886–898 (2009)

Shinnar M, Fallon J T, Wehrli S, Levin Ml, Dalmacy D, Fayad Z A, Badimon J J, Harrington M, Harrington E, Measurement of the Fibrous Cap in Symptomatic and Asymptomatic Atheromatous Carotid Plaques *Circulation* 2005;111; 2776-2782

Shiomi M, Ito T, Hirouchi Y, Enomoto M. Fibromuscular cap composition is important for the stability of established atherosclerotic plaques in mature WHHL rabbits treated with statins. Atherosclerosis 2001;157:75-84

Shi Z-D, Wang H, Tarbell J M, Heparan sulphate proteoglycans mediate interstitial flow mechanotransduction regulating MMP-13 expression and cell motility via FAK-ERK in 3D collagen, PLoS ONE 6(1): e15956. doi:10.1371/journal.pone.0015956,

Shah PK. Mechanisms of plaque vulnerability and rupture. J Am Coll Cardiol. 2003;41:15S–22S.

Shah PK. Molecular mechanisms of plaque instability. Curr Opin Lipidol. 2007;18:492–9.

References

Slager, C.J., Wentzel, J.J., Gijsen, F.J., Thury, A., van der Wal, A.C., Schaar, J.A., Serruys, P.W., 2005. The role of shear stress in the destabilization of vulnerable plaques and related therapeutic implications. Nat. Clin. Pract. Cardiovasc. Med. 2, 456–464.

Smedby, O., 1997. Do plaques grow upstream or downstream?: an angiographic study in the femoral artery. *Arterioscler Thromb Vasc Biol*, 17 (1997), pp. 912–918.

Smith EB. The influence of age and atherosclerosis on the chemistry of aortic intima. J Atheroscler Res 1965;5:241–248.

Sovershaev MA, Egorina EM, Bogdanov VY, Seredkina N, Fallon JT, Valkov AY, Østerud B, Hansen JB, Bone morphogenetic protein -7 increases thrombogenicity of lipid-rich atherosclerotic plaques via activation of tissue factor. Thromb Res. 2010 Oct;126(4):306-10

Stary H, Chandler A, Dinsmore R, et al. A definition of advanced types of atherosclerotic lesions and a histological classification of atherosclerosis. A report from the Committee on Vascular Lesions of the Council on Atherosclerosis, American Heart Association. Arterioscler Thromb Vasc Biol 1995;15:1512–1531.

Stefanadis C, Vavuranakis M, Toutouzas P. Vulnerable plaque: the challenge to identify and treat it. J Interv Cardiol 2003 Jun;16(3):273e80.

Stefanadis C, Toutouzas K, Tsiamis E, Stratos C, Vavuranakis M, Kallikazaros I, et al. Increased local temperature in human coronary atherosclerotic plaques: an independent predictor of clinical outcome in patients undergoing a percutaneous coronary intervention. J Am Coll Cardiol 2001;37(5): 1277e83.

Stone P H, Coskun A U, Kinlay S, Popma J J, Sonka M, Wahle A, Yeghiazarians Y, Maynard C, Kuntz R E, Feldman C L, Regions of low endothelial shear stress are the sites where coronary plaque progresses and vascular remodelling occurs in humans: an in vivo serial study, European Heart Journal (2007) 28, 705–710

Synetos A, Toutouzas K, Karanasos A, Riga M, Tsioufis C, Tousoulis D, Stefanadi E, Stefanadis C, Culprit Lesions Located In The Proximal Segments of the Coronary Arteries Have Thinner Fibrous Cap and Greater Incidence of Plaque Rupture. An Optical Coherence Tomography Study the American Journal of Cardiology, September 21-25, 2009, TCT-47

Tang D, Teng Z, Canton G, Hatsukami T S, Dong L, Huang X, Yuan C, Local critical stress correlates better than global maximum stress with plaque morphological features linked to atherosclerotic plaque vulnerability: an in vivo multi-patient study, Biomedical Engineering Online 2009, 8:15

Tang D, Teng Z, Canton G, Yang C, Furguson M, Huang X, Zheng J, Woodard P K, Yuan C, Sites of rupture in human atherosclerotic carotid plaques are associated with high structural stresses: An in Vivo MRI-based 3D fluid-structure interaction study, stroke 40 (10), pp. 3258-3263

Tang T.Y, Howarth S.P.S, Li Z.Y, Miller S.R, Graves M.J, U-King-Im J.M,Trivedi R.A, Walsh S.R, Brown A.P, Kirkpatrick P.J, Gaunt M.E, Gillard J.H, Correlation of carotid atheromatous plaque inflammation with biomechanical stress: Utility of USPIO enhanced MR imaging and finite element analysis, Atherosclerosis 196 (2008) 879–887

References

Tang T Y, Howarth S P S, Miller S R, Graves M J, U-King-Im J M, Li Zhi Y, Walsh S R, Patterson A J, Kirkpatrick P J, Warburton E A, Varty K, Gaunt M E, Gillard J H, Correlation of Carotid Atheromatous Plaque Inflammation Using USPIO-Enhanced MR Imaging With Degree of Luminal Stenosis, Stroke. 2008; 39:2144-2147

Taranto D, Morgante A, Bracale U.M, Guercio L. D, Carbone F, D'Armiento F.P, Porcellini M, Bracale G, Salvatore F, Fortunato G, Expression of Inflammation-Related Genes in Human Atherosclerotic Plaques, Atherosclerosis Supplements 11, no. 2 (2010) 17–108

Tavora F, Cresswell N, Li L, Fowler D, Burke A: Frequency of acute plaque ruptures and thin cap atheromas at sites of maximal stenosis, Arq. Bras. Cardiol. Vol.94 no.2 Sao Paulo Feb. 2010

Tearney G J, Quantification of Macrophage content in atherosclerotic plaque by optical coherence tomography. Circulation.2003: 107:113-119

Tearney G J, Measurement of Collagen and Smooth Muscle Cell Content in Atherosclerotic Plaques Using Polarization-Sensitive Optical Coherence Tomography. Journal of the American College of Cardiology Vol. 49, No. 13, 2007

Tegos T, Kalomiris K, Sebetai M, Kalodiki E, Nicolaides A, Significance of sonographic tissue and surface characteristics of carotid plaques, American Journal of Neuroradiology 22:1605-1612 (9 2001)

Trivedi R A, Mallawarachi C, U-King-Im, J M, Graves M J, Horsley J, Goddard M J, Brown A, Gillard J H, Identifying inflamed carotid plaques using in vivo USPIO enhanced MR imaging to label plaque macrophages, arteriosclerosis, Thrombosis, and Vascular Biology 26 (7), 2004 pp. 1601-1606

Vaina S, Stefanadis C. Detection of the vulnerable coronary atheromatous plaque. Where are we now? Int J Cardiovasc intervent 2005; 7(2):75-78

Van der Wall E E, de Graaf F R, van Velzen J E, Jukema J W, Bax J J, Schuijf J D, IVUS detects more coronary calcifications than MSCT; matter of both resolution and cross-sectional assessment? Int J Cardiovasc Imaging (2011) 27:1011–1014 DOI 10.1007/s10554-010-9668-2

Vengrenyuk Y, Carlier S, Xanthos S, et al. A hypothesis for vulnerable plaque rupture due to stress-induced debonding around cellular microcalcifications in thin fibrous caps. Proc Natl Acad Sci USA. 2006;103:14678–83.

Waldo S, Li Y, Buono C, Zhao B, Billings E, Chang J, Kruth H, Heterogeneity of human macrophages in culture and in atherosclerotic plaques. The American Journal of Pathology (2008), Volume: 172, Issue: 4, Publisher: American Society for Investigative Pathology, Pages: 1112-1126

Wasserman B A, Sharrett A R, Lai S, Gomes A S, Cushman M, Folsom A R, Bild D E, Kronmal R A., Sinha S, Bluemke D A. Risk Factor Associations with the Presence of a Lipid Core in Carotid Plaque of Asymptomatic Individuals Using High-Resolution MRI: The Multi-Ethnic Study of Atherosclerosis (MESA) *Stroke* 2008;39;329-335

References

Weitkamp, B., Cullen, P., Plenz, G., Robenek, H., Rauterberg, J. Human macrophages synthesize type VIII collagen *in vitro* and in the atherosclerotic plaque. *FASEB J.* 13, 1445–1457 (1999)

Werner, Martin M.D.; Chott, Andreas M.D.; Fabiano, Alfredo M.D; Battifora, Hector M.D., Effect of Formalin Tissue Fixation and Processing on Immunohistochemistry, The American Journal of Surgical Pathology July 2000, Volume 24, Issue 7, page 1016-1019

Whittaker P, R A Kloner, D R Boughner, and J G Pickering; Quantitative assessment of myocardial collagen with picrosirius red staining and circularly polarised light. Basic Res Cardiol 89:397-410 (1994)

Winter P M, Morawski A M, Caruthers S D, Fuhrhop R W, Zhang H, Williams T A, Allen J S, Lacy E K, Robertson D, Lanza G M, Wickline S A, Molecular Imaging of Angiogenesis in Early-Stage Atherosclerosis With $\alpha_v\beta_3$-targeted nano-particles Circulation. 2003; 108

Xie D, Qiu B, Zhang J, Yang X, Visualization and Characterisation of Atherosclerotic Plaques by Micro-MRI at 4.7 T In Vivo and 11.7 T Ex Vivo, Applied Magnetic Resonance, Volume 39, Issue 4, December 2010, Pages 373-380.

Yang C, Canton G, Yuan C, Ferguson M, Hatsukami T S, Tang D, Advanced human carotid plaque progression correlates positively with flow shear stress using follow-up scan data: An in vivo MRI multi-patient 3D FSI study, Journal of Biomechanics, Volume 43, Issue 13, September 2010, Pages 2530-2538

Yehuda H, Szuchman-Sapir A, Khatib S, Musa S, Tamir S, Human atherosclerotic plaque lipid extract promotes expression of proinflammatory factors in human monocytes and macrophage-like cells, Atherosclerosis, Volume 218, Issue 2, October 2011, Pages 339-342

Yilmaz A, Bettina Lipfert, Iwona Cicha, Katja Schubert, Michael Klein, Dieter Raithel, Werner G. Daniel, Christopher D. Garlichs, Accumulation of immune cells and high expression of chemokines/chemokine receptors in the upstream shoulder of atherosclerotic carotid plaques, Experimental and Molecular Pathology 82 (2007) 245-255

Yim P, J. Cebral, R. Mullick, H. Marcos, and P. Choyke, "Vessel surface reconstruction with a tubular deformable model," *IEEE Trans. Med. Imag.*, vol. 20, pp. 1411–1421, 2001.

Yonetsu T, Fakuta T, Lee T, Takahashi K, Kawaguchi N, Yamamoto G, Koura K, Hishikari K, Lesaka Y, Fujiwara H, Isobe M, In vivo critical fibrous cap thickness for rupture-prone coronary plaques assessed by optical coherence tomography, Eur Heat J, (2011) 32 (10): 1251-1259

Yuan C, Mitsumori LM, Beach KW, Maravilla KR. "Special Review: Carotid Atherosclerotic Plaque: Non-invasive MR Characterization and Identification of Vulnerable Lesions," Radiology 2001; 221:285–299. [PubMed: 11687667]

Yuan C, Mitsumori LM, Ferguson MS, Polissar NL, Echelard DE, Ortiz G, Small R, Davies JW, Kerwin WS, Hatsukami TS. "In Vivo Accuracy of Multispectral MR

Zhi-Yong Li, Simon P.S Howarth, Tjun Tang, Jonathon H. Gillard. How Critical Is Fibrous Cap Thickness to Carotid Plaque Stability. Stroke. 2006;37:1195-119

Appendix 1 FEM Based Image Restoration Error Analysis

1.0 APPENDIX: FEM Based Image Restoration Error Analysis

1.1 Axial Registration Errors

Axial registration uncertainties can have a significant impact on the accuracy of the overall registration. Two major sources which contributes to axial registration errors. They are as follows; **(a)** US scan error; and **(b)** non-uniform longitudinal shrinkage of the specimen.

In 3D ultrasound acquisition, sound waves are strongly reflected by calcified regions resulting in strong signals, which makes the specimen appear longer then its actual length. The identification of the first section is difficult in this type of specimen. Furthermore, micro bubbles can attach to the surface of the specimen, caused by temperature differences between the specimen and the water in the tank, and can result in over-estimation of the specimen size. Ultrasound images are considered as the "gold standard" for the reconstruction of plaque specimens, errors introduced at this stage may affect the results of the entire registration procedure. To overcome these problems, a specially designed mechanical arm attached to the US scan probe was developed. The image longitudinal location is able to be accurately defined in the set of 2D images without pre-processing; therefore the 2D US scan attached to the mechanical arm will increase accuracy. In addition, the 2D scans will limit the effects of the signal reflection that occurs in calcification regions.

The longitudinal non-uniform shrinkage in plaque specimens is partially corrected by measuring the longitudinal length of each tissue segment after tissue processing, and therefore the shrinkage encountered by each segment will not influence the registration of other segments, and eliminating potential errors.

1.2 Influence of Assuming First Point during Contour Definition

The location of the contour starting point for the outer and luminal walls is a crucial parameter in the registration procedure. Starting points selected incorrectly can have profound influences on the outcome of the FEM registration. The first point selected is required to be a recognizable landmark feature in both histology and ultrasound images. This point provides the basis of the wall registration between the source and target images. However, in certain cases, there can be difficulties in finding a landmark which appears in both source and target images. For these certain cases, assumptions are made in defining the contour starting point. A test was performed to assess the registration uncertainties caused by an inaccurately chosen starting point, by altering the locations of the starting point to see the affects on the registration results (figure A1-1).

In Figure A-1, the upper panels demonstrate the normal registration, with the first point chosen on the left side of the source image. In the lower panels, the first point was chosen marginally above the initial first point. The results for the registration, for the lower panel, clearly show an inaccurate configuration of the colour region caused by distortion. In relation to histology images, where the plaque geometry is irregular, and the different plaque components are characterized by different material properties, registration errors caused by an inaccurate first point, can result in increased levels of uncertainties. Therefore it can be seen that a more reliable landmark system needs to be developed in future studies for accurate registration results.

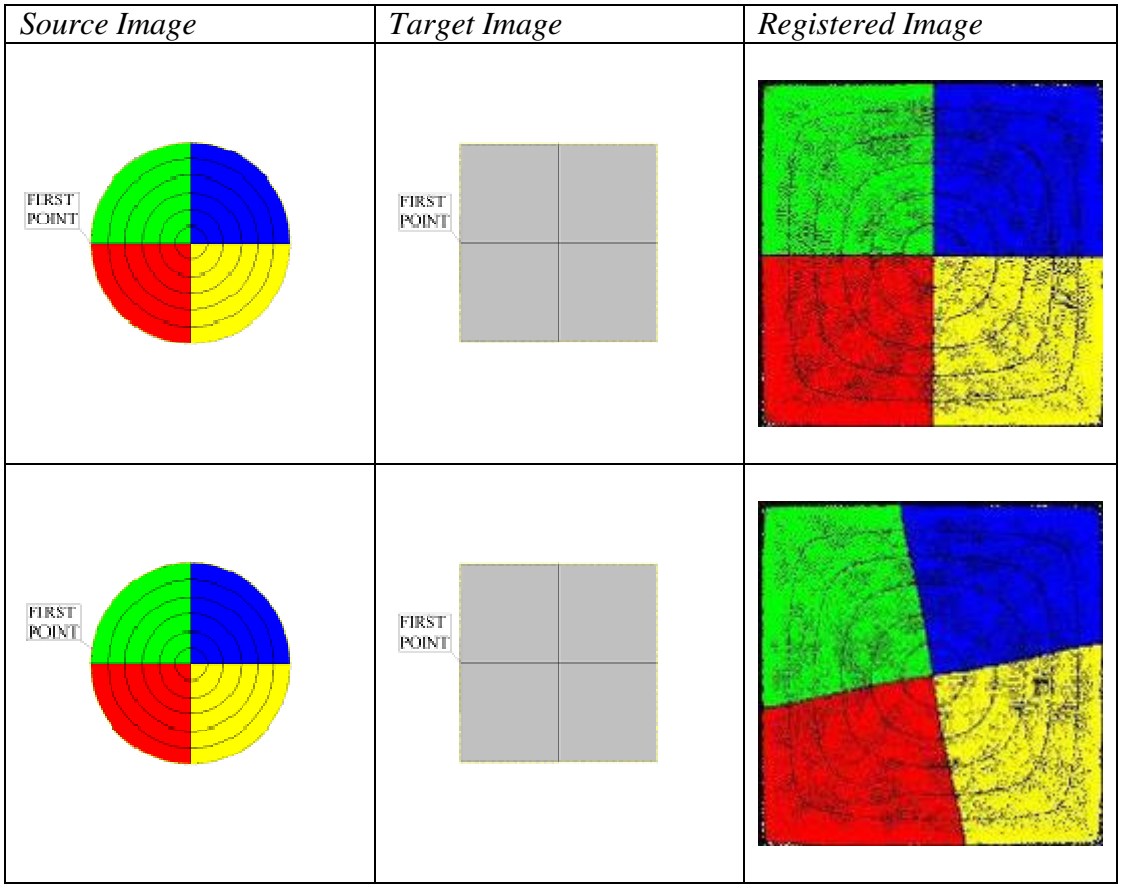

Figure A1-1: Highlighting an Error in the First Point Assumption

1.3 Sensitivity Test: Influence of the Material Properties

The values assigned to the material properties for the different components will influence the displacement of the internal points. For example, calcified regions are of a hard nature, and therefore its shape and position will alter marginally during the FEM registration, whilst the geometric shape and position of the lipid region will change significantly. A uniform set of material property values were implemented for each case, and therefore it is important to assess the sensitivity of the FEM predicted displacement of the internal points, by altering the material properties to see the affects.

Appendix 1 FEM Based Image Restoration Error Analysis

A set of FEM simulations was performed to assess the sensitivity, as shown in Figure A1-2. Six models of arterial plaque section were constructed. The original geometry is maintained for all the models. The young's modulus of the fibrous region, and the mixed region (lipid and fibrous tissue) are more likely to have inconsistency in there values, and therefore both parameters were varied from 1Kpa to 100Mpa, and 1Pa to 10KPa for the fibrous and lipid regions respectively, for the six models.

	I	**II**	**III**	**IV**	**V**	**VI**
E Fibrous [Pa]	10^3	10^4	10^5	10^6	10^7	10^8
ν Fibrous	0.5	0.5	0.5	0.5	0.5	0.5
E Lipid [Pa]	10^3	10^3	10^3	10^3	10^3	10^3
ν Lipid	0.3	0.3	0.3	0.3	0.3	0.3
E Mixed [Pa]	1	10	10^2	10^3	10^4	10^5
ν Mixed	0.3	0.3	0.3	0.3	0.3	0.3
E Calcified [Pa]	10^9	10^9	10^9	10^9	10^9	10^9
ν Calcified	0.5	0.5	0.5	0.5	0.5	0.5

Figure A1-2: mechanical properties applied to the sensitivity test

The results of the FEM registration can be seen in figure A1-3 for one section as an example. It can be seen that the results for the first three cases (I to III) were very similar. However, in the last three cases (IV to VI), the plaque **components** can be seen to have changes in their size and position, especially the lipid and mixed regions. The registered images for cases I to VI are shown in figure A1-3.

Appendix 1 FEM Based Image Restoration Error Analysis

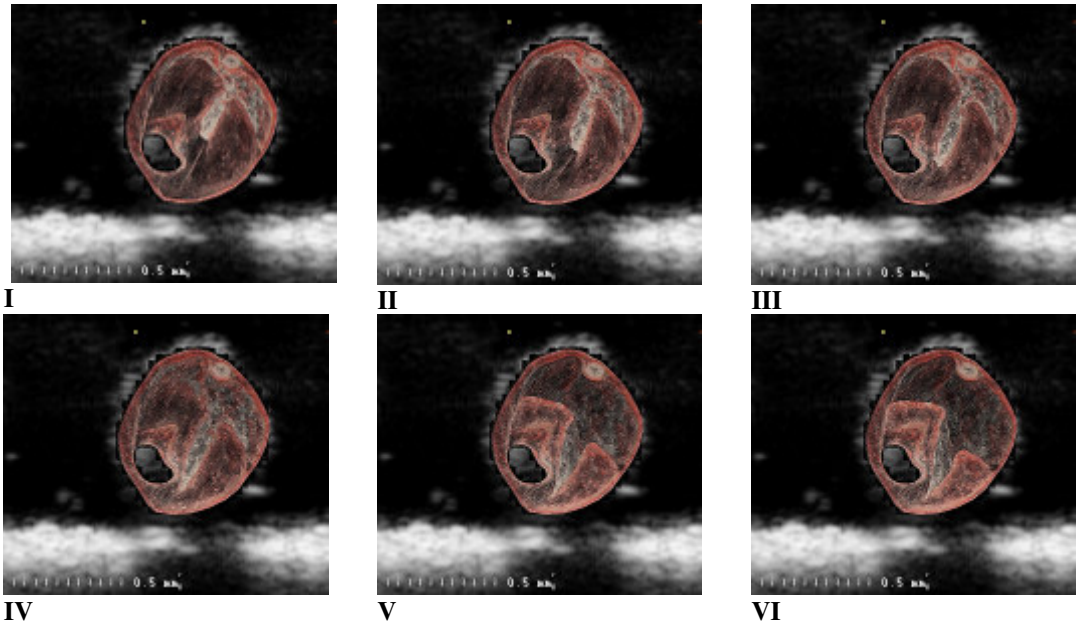

Figure A1-3: Registered section for the sensitivity test

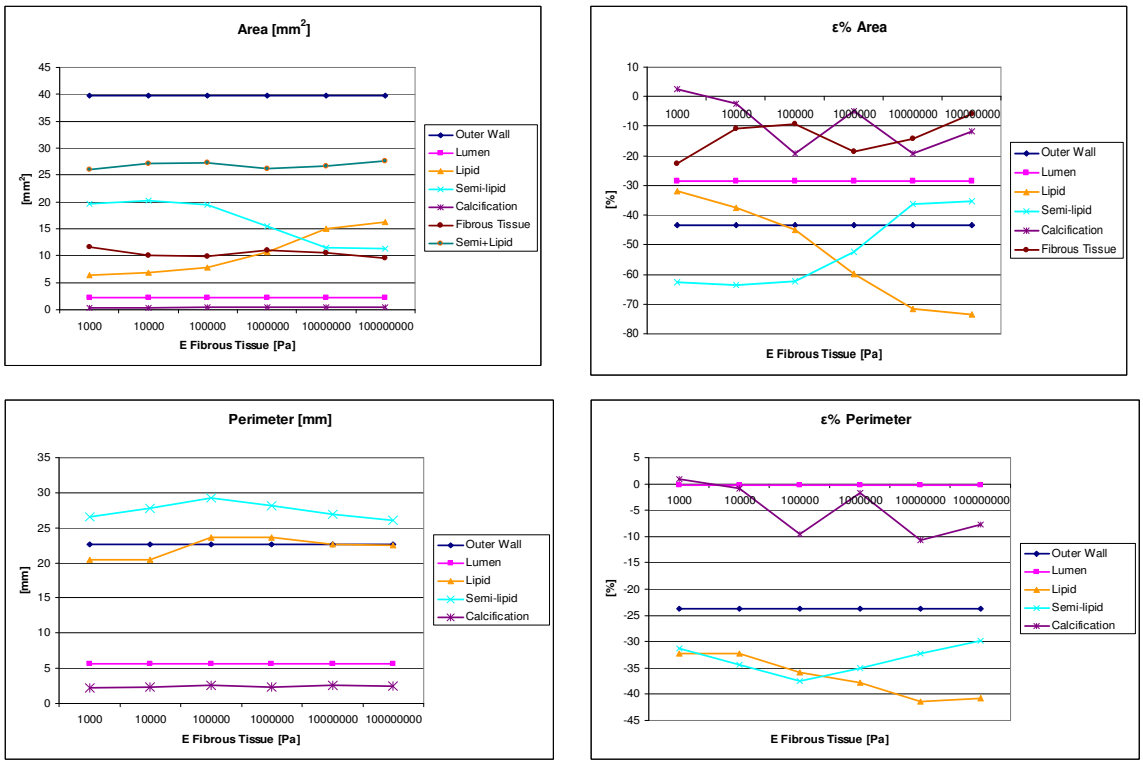

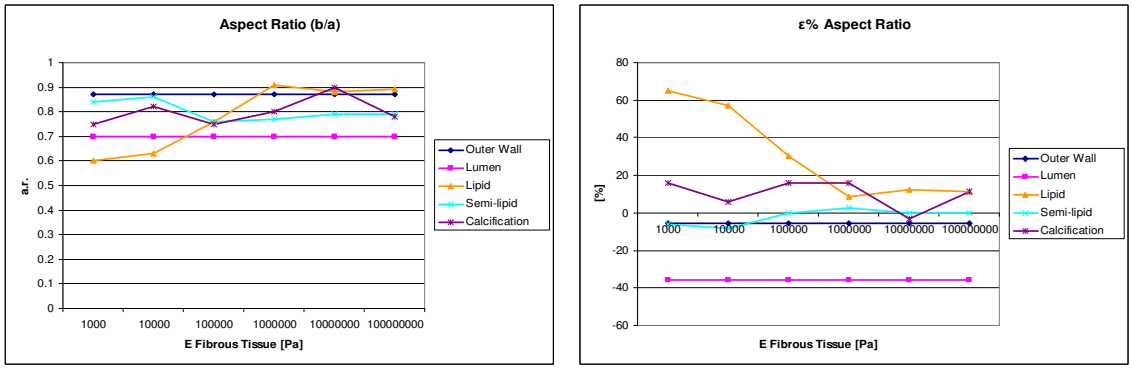

Figure A1-4: Results for the measurements of area (a, b), perimeter (c, d) and aspect ratio (e, f)

The calculated values of "ε" are based on values of areas; perimeters and aspect ratio (a.r), and are shown in figure A1-4.

	Outer Wall	Lumen	Lipid	Semi-lipid	Calcification	Fibrous Tissue
Area [mm^2]	22.55	1.55	4.29	7.36	0.38	8.97
Perimeter [mm]	17.28	5.6	13.83	18.26	2.27	/
Aspect Ratio	0.82	0.45	0.99	0.79	0.87	/

Figure A1-5: Values of A, p and a.r. for the source image (before the registration)

The area of the calcified and fibrous tissue region was virtually unaltered because of the incompressibility of the material properties that was applied. The lipid core area increased from 6.31 to 16.36mm^2 as the rigidity of the fibrous cap was also increased from the lowest to the highest values. On the contrary, the area of the semi-lipid region (mixed region) decreased from 19.67 to 11.36mm^2. The sum of the area for the lipid core and the semi-lipid regions remained constant. Figure A-4 (second column)

demonstrates that depending on the material properties implemented, there can be a significant affect on the results of the distortion quantification that occurs due to the histology procedure. For example, when the material property of the fibrous tissue is altered to be of a softer nature, the shrinkage of the lipid core is 32%, however, when the material property is altered to be more rigid, there is 73% shrinkage of the lipid core. The results demonstrate that the selection of material properties can have a significant influence on the results for both the distortion quantification, and also the 3D reconstruction of the model. Therefore, requires the material properties selected to perform deformable registration is required to be kept constant for every FEM model built.

Appendix 2 Effects of Temperature of Paraffin Wax Sections

2.0 APPENDIX: Testing the Effects of Temperature Variations on Paraffin Wax Sections

2.1 Background: Histology is the study of the microscopic anatomy of cells and tissues of plants and animals. The accurate diagnosis of diseases requires tissues to be preserved in its natural state when viewing under a microscope. In conventional wax histology, a microtome is used to section wax blocks. Paraffin was sections are placed into a water bath to remove the presence of any wrinkles, caused by the surface tension of the water, and to also enable the sections to be mounted onto the microscope slide. However, if the sections are subjected to excess levels of stretch, then this process may influence the sections negatively by causing tissue ruptures and other artefacts

The primary factors that control the extent of the stretching, is the contents of the water bath, and its temperature. Sections with large thicknesses may require increased levels of stretching compared to thinner sections to generate a flattened section. Increased levels of stretch can be generated by the addition of alcohol to the water bath. Placing thin sections in an alcohol/water mixture can cause over-stretching, and damage the tissue. The temperature of the water bath is another factor which may influence the extent of the stretching, as excess temperatures can cause sections to be overstretched. Different studies have reported using different temperatures for the water bath to stretch sections. Dai et al (2006) performed histology analysis on aneurysm tissue by floating tissue sections on a water bath at 42ºC to remove wrinkles (5-6 µm thick sections). Pihan et al (1998) investigated centrosome defects in tumor tissues, which are required for correct cell division, and used a water bath temperature set at 37ºC. Both studies reported no tissue damage caused by these temperatures.

Appendix 2 Effects of Temperature of Paraffin Wax Sections

2.2 The primary objective of this study is to analyse the detailed morphological differences between ruptured and non-ruptured plaques. It is therefore important to distinguish between genuine ruptures, and ruptured caused by artefacts. Evidence of a break in the fibrous cap is the main characteristic of a ruptured plaque. Therefore, any potential artefacts which may cause breaks in the fibrous cap during the histology process should be avoided. The present study is designed to test the possibility of fibrous cap ruptures caused by the water bath at varied temperatures.

2.3 Method: The temperature of the water bath was set and maintained for 1 minute at the following temperature conditions: 34ºC, 37ºC, 42ºC, 44ºC, 47ºC, 49ºC, and 55ºC. Tissue blocks were sectioned at 6µm thickness and placed into the water bath immediately for approximately 1 minute and mounted on APES coated microscope glass slides. A standard picrosirius red staining procedure was applied to all sections. The tissue embedding medium used for the test was Kendall Paraplast.

2.4 Results

Figure A2-1 panels 1-7, shows the result of the tissue structure for the paraffin wax sections when the temperature of the water bath is increased from 34ºC to 55ºC. The overall structure is shown on the left panel (40X magnification). A magnified image (400X magnification), shows the fine details of the collagen structure, and is pointed by the arrow on the left panel. The cut in the wall observed in the left panel was caused during plaque excision.

Appendix 2 Effects of Temperature of Paraffin Wax Sections

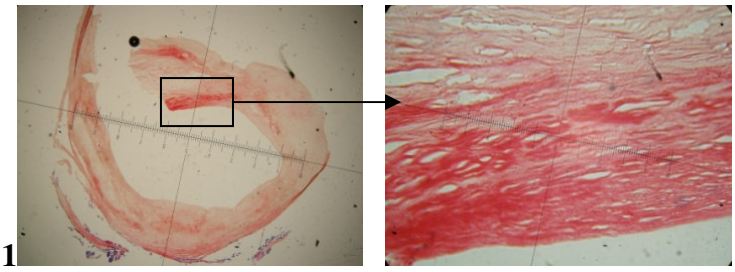

1 34°C

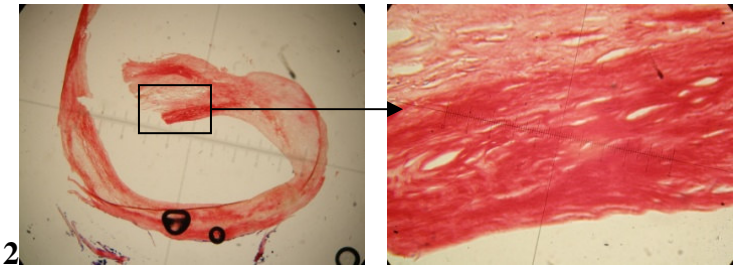

2 37°C

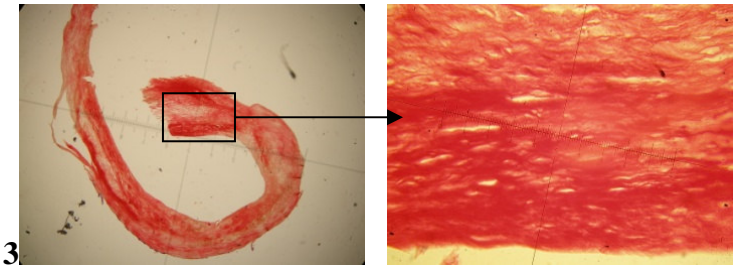

3 42°C

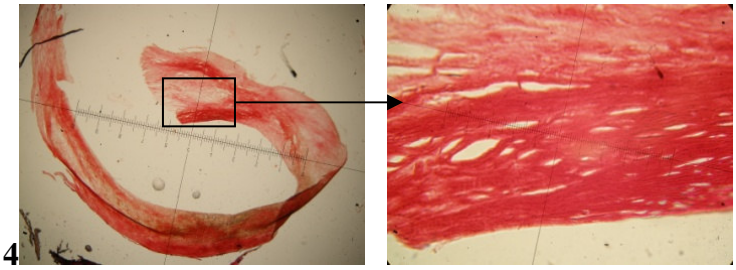

4 44°C

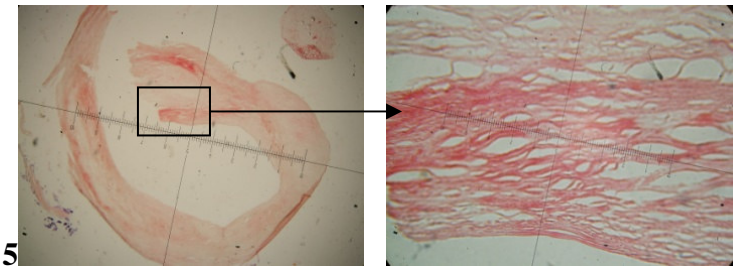

5 47°C

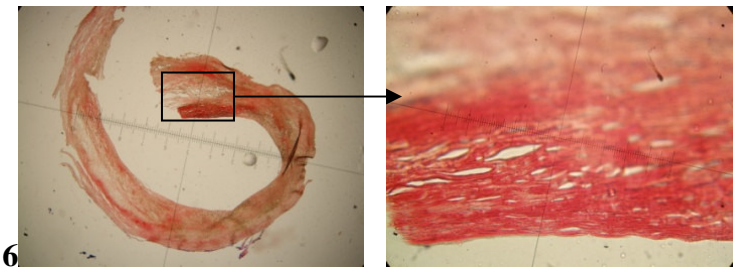

6 49°C

Appendix 2 Effects of Temperature of Paraffin Wax Sections

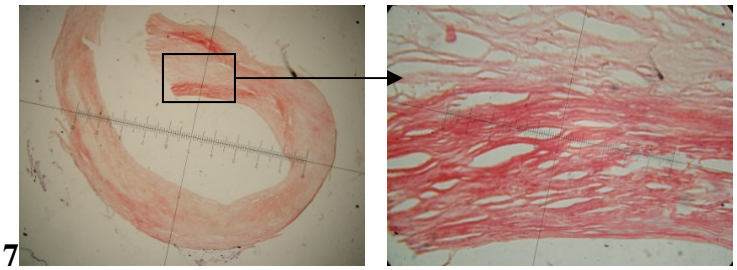

Panel (A) **Panel (B)**

Figure A2-1 Picrosirius red staining of plaque tissue at varied water bath temperatures Panel (A) 40X magnification; Panel (B) 400X magnification. Water bath temperature indicated on right side of panel (B)

From the above figure (A2-1), it can be seen that the tissue sections have no visible tissue distortions. The structure of the fibres was maintained at a large range of water bath temperature conditions.

2.5 Discussion and Conclusion:

It was found that the paraffin wax used for the histology protocol for this study is able to withstand temperatures of up to 55ºC, without causing any visible structural damage to the paraffin wax sections as shown in figure A2-1. The temperature of the water bath that was used for the present study was 37ºC. Results of this test provide support that there is no evidence of tissue structure damage that can be found in the tested temperature range.

A separate test was performed in which a wax block without tissue embedded was sectioned. The wax section (6µm thickness) can hold its intake structure until 57ºC. Further increases in temperature resulted in the wax section to melt and become visibly transparent in appearance. At temperatures above 60ºC, the wax section above 60 ºC. The manufacturer's description for the paraffin wax indicated that the pellet form melting point was 56 degree centigrade (ºC). This may suggest that

increasing the water bath temperature may have limited effects on tissue structure, providing the paraffin wax is structurally reliable to maintain the tissue.

The results of this test are in concordance with other studies found in literature which have also used 37 ºC for the water bath temperature. Fujimoto et al (2008) used 4µm-thick sections with a water bath containing deionised water at 43 ºC in their study of plaque tissue. Baker et al (1999) used fixed atherosclerotic coronary plaque tissue embedded in paraffin blocks to cut serial 3µm sections. The sections were then floated in a water bath set at a temperature of 52ºC. There was no comment on tissue damage stated in their studies.

In conclusions, the results of this test demonstrates that paraffin wax sections can withstand temperatures of up to 55ºC, without causing any structural damage to tissue sections. Water bath temperature of 37 ºC can therefore be considered safe for plaque tissue histology analysis.

3.0 Appendix: List of Publications

Journal Papers

1. **Ahsan R. Choudhury**, Michael Luppi, Warren Hopkins, Hao Gao, Saroj Das, Ian Kill, Michele Pinelli, Quan Long; **High Resolution 3D Reconstruction of an Atherosclerotic Plaque by a Combination of Histology and 3D Ultrasound** Preparation for Journal of Biomechanics
   Submitted

2. **Ahsan R. Choudhury**, Hao Gao, Saroj Das, Ian Kill, Quan Long; **Morphology Analyses of Human Carotid Plaques in Assessing Fibrous Cap Rupture Risk** American Journal of Cardiology college
   Submitted

3. **Ahsan Choudhury** Michael Luppi, Hao Gao, Warren Hopkins, Saroj Das, Michele Pinelli, Quan Long. **Assessment of Structure Distortion of Paraffin Wax Histology Section of Human Carotid Atherosclerotic Plaque Specimen**
   In Preparation for Journal of Biomechanics

4. **Ahsan R. Choudhury,** Warren Hopkins, Hao Gao, Quan Long, **Carotid Plaque Tissue Characterisation using Ex-Vivo 2D Ultrasound for Vulnerability Assessment**
   In Preparation for International Journal of Medical Imaging

Papers - Peer-Reviewed Conference Papers & Oral Presentations

1. **Ahsan R. Choudhury**, Hao Gao, Ian Kill, Quan Long. **Quantification of the 3D Collagen Distribution on the Human Arterial Fibrous Plaque Cap**; 5th World Congress of Biomechanics, Munich, July 29th to August 4th 2006

2. **Ahsan R. Choudhury**, Michael Luppi, Warren Hopkins, Hao Gao, Saroj Das, Ian Kill, Michele Pinelli, Quan Long; **High Resolution 3D Reconstruction of an Atherosclerotic Plaque by a Combination of Histology and 3D Ultrasound.** Proceeding 2009 Summer Bioengineering Conference, ASME, June, 2009, Lake Tahoe, CA, USA

3. **Ahsan R. Choudhury**, Hao Gao, Saroj Das, Ian Kill, Quan Long; **Morphology Analyses of Human Carotid Plaques In Assessing Fibrous Cap Rupture Risk;** 6th World congress of Biomechanics, Singapore, August 1st to 6th 2010

Appendix 3 List of Publications

4. **Ahsan R. Choudhury**, Hao Gao, Saroj Das, Ian Kill, Quan Long; **Morphology Analyses of Human Carotid Plaque in Assessing Fibrous Cap Rupture Risk;** Society of Academic and Research Surgery (SARS) Royal Free Hospital London January 2009

5. Michael Luppi, Hao Gao, **Ahsan Choudhury**, Warren Hopkins, Saroj Das, Michele Pinelli, Quan Long. **Assessment of Structure Distortion of Paraffin Wax Histology Section of Human Carotid Atherosclerotic Plaque Specimen;** Proceeding 2009 Summer Bioengineering Conference, ASME, June, 2009, Lake Tahoe, CA, USA